# In vitro evaluation of asparagine endopeptidase as a candidate biomarker of treatment failure in childhood acute lymphoblastic leukaemia

Krishnan, Shekhar

# *In vitro* evaluation of Asparagine Endopeptidase as a candidate biomarker of treatment failure in childhood acute lymphoblastic leukaemia

Shekhar Krishnan

CRUK Children's Cancer Group
Paterson Institute for Cancer Research
Manchester

Supervisors: Prof. Vaskar Saha and Prof. Andrew Lister

*Submitted towards a Doctor of Philosophy degree, University of London*

April 2011

To Naina Patel

Colleague, lab guide, kin

**CONTENTS**

Acknowledgements iv
Note to Reader vii
Abbreviations viii
Glossary of terms xiii
Synopsis xiv

**Chapter 1: Investigating treatment failure in childhood acute lymphoblastic leukaemia**
Text 1
Figures 5
Tables 24

**Chapter 2: Asparagine endopeptidase – a candidate molecular marker of treatment failure in childhood ALL**
Text 38
Figures 40
Tables 47

**Chapter 3: AEP expression in childhood acute lymphoblastic leukaemia**
Text 56
Figures 62
Tables 83

**Chapter 4: AEP expression and cell motility**
Text 87
Figures 91
Tables 104

**Chapter 5 AEP and Asparaginase**
Text 107
Figures 112
Tables 122

**Chapter 6 Additional lines of investigation**

Text 126

Figures 128

**Chapter 7 Summary and Ongoing Studies**

Text 133

Figures 135

**Chapter 8 Methods**

Section 8.1 Material—non-reagent components 139

Section 8.2 Reagents, buffers and reaction mixes 144

Section 8.3 Selected Methods Outline 163

Section 8.4 Selected Protocol Worksheets 172

Section 8.5 Optimisation-validation procedures 177

Section 8.6 Statistics 189

Section 8.7 Life Science Suppliers 190

Figures 194

Tables 208

**References** 214

**Supplemental**

Supplement to Chapter 3 260

Supplement to Chapter 4 275

Supplement to Chapter 5 277

Supplement to Chapter 6 279

**Appendix A-D** 281

**Publications** 286

**In gratitude**

I am deeply indebted to Naina Patel, colleague, coach, cherished friend. Her scientific ideation, rigour and integrity have been a profound influence.

Vaskar Saha, my supervisor, for the opportunity to pursue a PhD and for allowing me wide latitude in its pursuit;

Prof. Andrew Lister, my adviser, for his unflinching support and wisdom;

Colleagues in the Children's Cancer Group (CCG) past and present, for invaluable instruction and support;

Prof. Colin Watts (Dundee), for serving as intellectual and material resource for all things AEP;

Patients and parents, for generously and readily consenting to participate in these studies;

The Paterson Institute for Cancer Research (PICR, Manchester), for providing a vibrant and stimulating scientific environment; and

Cancer Research UK for funding this work.

## Acknowledgements

My grateful thanks to the following for advice and help on specific aspects of this work

| | |
|---|---|
| Microarray analyses | Frederik van Delft and Naina Patel (CCG) |
| Laboratory techniques | Naina Patel, Olga Yiannikouris, Louise Jones and Seema Alexander (CCG), Sharon James and Sameena Iqbal (Medical Oncology, Institute of Cancer, Barts School of Medicine and Dentistry), Salizawati Salhimi and Delphine Lees (Tumour Biology, Institute of Cancer, Barts School of Medicine and Dentistry) |
| Motility assays | Claire Hart (Genitourinary Cancer Research, PICR), experimental techniques; Ian Hart, John Marshall and Gareth Thomas (Tumour Biology, Barts), advice; Seema Alexander, Mark Holland (CCG) and Fernanda Castro (Immunology, PICR), motility data on leukaemic cell lines; Michael Lie-A-Ling (Stem Cell Biology, PICR), flow cytometry on modified HEK293 cells |
| Immunohistology | Partnership with Hany Ariffin (Paediatrics, University Malaya, Malaysia); support from Andrew Clear and Abigail Lee (Medical Oncology, Barts), Histopathology unit at St. Barts Hospital, Emma Nye and Gordon Stamp (Experimental Pathology, London Research Institute), Margaret Jones and the late Prof. David Mason (Nuffield Department of Clinical Laboratory Sciences, John Radcliffe Hospital, Oxford) |
| AEP reagents | Prof. Colin Watts (Cell Biology and Immunology, University of Dundee), including gifts of the AEP plasmid clone, monoclonal antibodies, recombinant protein, activity assay protocol, mapping of AEP cleavage sites on L-asparaginase (Cathy X Moss); John Roffey (CRUK Cancer Research Technology), synthesis of the AEP inhibitor |

| | |
|---|---|
| Asparaginase | Partnership with Naina Patel (CCG); Paul Bates, Marc Offman, Marcin Krol (Biomolecular Modelling, London Research Institute), asparaginase modelling; Monika Essink (Medac GmbH), asparaginase activity kits; Nick Coe (University of Salford) and Prof Tim Eden (Paediatric and Adolescent Oncology, University of Manchester), data from pilot clinical study of plasma asparaginase activity; Protein Production Laboratory, Department of Biology Technology Facility, University of York, purification of ASNase recombinant proteins; Jizhong Liu (CCG), ASNase cytotoxicity assays |
| Imaging | Steve Bagley (Advanced Imaging Facility, PICR), guidance on microscopy; Matthew Bogyo (Pathology, Stanford University, CA), gift of AEP activity binding probe; Eva Diffner (Breakthrough Breast Cancer Unit, PICR), flow cytometry of cryopreserved primary cells |
| Others | Molecular Biology Core Facility, PICR; Ric Swindell (Medical Statistics, Christie Hospital), statistical advice; Markella Mikkelsen (Oncology Cytogenetics, Christie Hospital), cytogenetic authentication of cell lines |

## Note to reader

For ease of reading, concision has been emphasised in preparation of this work. Thus the text in each chapter is condensed to principally communicate the main lines of argument, supported by comprehensive summary tables, concept drawings, elaborately annotated figures and supplemental material. In places, discussions have been reiterated for clarification or emphasis. The bibliography has been compiled chapter-wise. Experimental methods have been schematically illustrated, written deliberately in condensed active voice for clarity and organised into seven complementary sections, forming part of a Methods chapter that features towards the end of the document. Additionally, each Results chapter contains a brief summary of experimental approaches. It is hoped that these approaches serve to enhance clarity, maintain narrative flow and avoid tedium.

## Abbreviations

| | |
|---|---|
| 2-ME | 2-mercaptoethanol |
| 7-NHMec | 7-amino 4-methyl coumarin |
| AA | Amino acid |
| ABP | Activity Binding Probe |
| AEBSF | 4-(2-Aminoethyl) benzenesulfonyl fluoride hydrochloride |
| AEP | Asparagine endopeptidase |
| AEPi | Selective inhibitor of AEP (MV026630) |
| AEP.293 | Enforced AEP-expressing HEK293 cells stably transfected with a pcDNA3.1 expression plasmid |
| AEP.293GS | Inducible AEP-expressing HEK293 cells stably transfected with dual GeneSwitch plasmids |
| ALL | Acute Lymphoblastic Leukaemia |
| AML | Acute Myeloid Leukaemia |
| ANOVA | Analysis of Variance |
| ASNase | *Escherichia coli* L-asparaginase II |
| ASNS | Asparagine synthetase |
| β2M | Beta 2 Microglobulin |
| BM | Bone Marrow |
| bp | base pair |
| BSA | Bovine serum albumin |
| cDNA | Complementary DNA |
| CD | Cluster of differentiation |
| CI | Confidence Interval |

| | |
|---|---|
| CHAPS | 3-[(3-Cholamidopropyl)dimethylammonio]-1-propanesulfonate |
| CNS | Central Nervous System |
| Ct | Threshold PCR cycle |
| CTSB | Cathepsin B |
| CTSBi | Selective inhibitor of Cathepsin B (CA-074me) |
| CV | Coefficient of Variation |
| DAPI | 4',6-diamidino-2-phenylindole |
| dATP/dCTP/dGTP/dTTP | Deoxy Adenosine /Cytosine /Guanosine / Thymidine triphosphate nucleotides |
| dd | double-distilled (deionised) |
| DEPC | Diethylpyrocarbonate |
| DMEM | Dulbecco's Minimal Essential Medium |
| DMSO | Dimethylsulfoxide |
| DNA | Deoxyribonucleic acid |
| dNTP | Deoxyribonucleotide triphosphate |
| DTT | Dithiotreitol |
| *E. coli* | *Escherichia coli* |
| EBV | Ebstein-Barr virus |
| ECL | Enhanced chemiluminescence |
| ECM | Extracellular matrix |
| EDTA | Ethylenediamine tetraacetic acid |
| EV.293 | Control HEK293 cells stably mock-transfected with insert-free pcDNA3.1 expression plasmid |

| | |
|---|---|
| F-actin | Filamentous actin |
| FBS | Fetal bovine serum |
| FISH | Fluorescent *in situ* hybridisation |
| FRET | Förster resonance energy transfer |
| *g* | Relative centrifugal force |
| GAPDH | Glyceraldehyde-3-phosphate dehydrogenase |
| H&E | Haematoxylin and Eosin |
| HD50 | High hyperdiploidy (also HHD) ALL |
| HEK293 | Human embryonic kidney 293 cells |
| HHD | High hyperdiploidy (also HD50) ALL |
| HRP | Horseradish peroxidase |
| ID | Identification |
| kDa | kiloDalton |
| LAMP1 | Lysosome-associated membrane protein 1 |
| LGMN | Legumain, also known as AEP |
| LyTR | Lysotracker Red DND-99 |
| mAb | Monoclonal antibody |
| MFI | Mean fluorescent intensity |
| MFP or Mfp | Mifepristone |
| MGG | May-Grünwald Giemsa |
| MHC | Major histocompatibility complex |
| MMP | Matrix metalloproteinase |

| | |
|---|---|
| MNC | Mononuclear cells |
| MRD | Minimal residual disease |
| MW | Molecular weight |
| NA | Numerical aperture |
| NBF | Neutral Buffered Formalin |
| NFDM | Non-fat dried milk solution |
| NP-40 | Nonidet P-40 |
| nt | nucleotide |
| NTC | Nil-template control |
| OD | Optical density |
| p | Probability of test statistic given the null hypothesis |
| PAGE | Polyacrylamide gel electrophoresis |
| PBS | Phosphate buffered saline |
| PCR | Polymerase chain reaction |
| Ph+ ALL | Philadelphia chromosome positive ALL |
| PIC | Protease inhibitor cocktail |
| PVDF | Polyvinylidene fluoride |
| qRT-PCR | Quantitative reverse transcription PCR (also RQ-PCR) |
| $r^2$ | Pearson coefficient of determination |
| RNA | Ribonucleic acid |
| RPMI | Roswell Park Memorial Institute cell culture medium |
| RQ-PCR | Quantitative real time PCR (also qRT-PCR) |

| | |
|---|---|
| RT | Reverse transcriptase |
| SD | Standard deviation |
| SDS | Sodium dodecyl sulphate |
| shRNAi | Short hairpin interfering RNA |
| SNP | Single nucleotide polymorphism |
| TAM | Tumour-associated macrophage |
| Tris | Tris(hydroxymethyl)aminomethane |
| UPN | Unique patient number |
| v/v | Volume / volume |
| w/v | Weight / volume |
| WBC | White blood cell count |
| WCL | Whole cell lysate |
| WT | Wild type |

## Glossary: Childhood ALL

| | |
|---|---|
| *BCR-ABL1* ALL | Synonymous with adverse-risk Philadelphia-chromosome positive (Ph+) ALL |
| CNS-directed therapy | Treatment designed primarily to eliminate leukaemic cells in the central nervous system; cranial irradiation was previously a major component but has now been largely replaced by a combination of intra-spinal and CNS-penetrating systemically-administered cytotoxics |
| Early response | Microscopic (or flow-cytometric) assessment of bone marrow response, 8-15 days into treatment; early response is designated Rapid or Slow based on pre-defined criteria |
| Extramedullary disease | Leukaemia in anatomical sites other than the bone marrow |
| Good-risk genotypes | Typically, progenitor-B lymphoblasts with *ETV6-RUNX1* and *TCF3-PBX1* fusion translocations and the high hyperdiploidy genotype |
| MRD | Submicroscopic residual disease; typically estimated in the bone marrow using molecular techniques (quantitative PCR of clonal antigen receptor rearrangements) or flow cytometry (detection of clonal surface markers) |
| Progenitor-B ALL | Haematopoietic neoplasm of early B-lymphocytes. Synonymous but less accurate terminologies include Pre-B (precursor B) and B-lineage ALL |
| Poor-risk genotypes | Synonymous with adverse-risk genotypes. Typically, progenitor-B lymphoblasts with *BCR-ABL1* fusion, *MLL* rearrangements, the iAMP21 abnormality and hypodiploidy |
| Induction phase | Refers to the initial block of ALL treatment; treatment during this phase usually spans 4-5 weeks, typically includes a combination of 4-5 cytotoxic drugs and culminates in bone marrow tests to assess response |
| Treatment failure | Recurrence of disease (relapse) or unresponsive (refractory) disease |
| Risk | Relates to the probability of treatment failure |

# Synopsis

*Background*

Although cure rates in childhood acute lymphoblastic leukaemia (ALL) approach 90%, relapses, particularly central nervous system (CNS) relapses, pose a significant therapeutic challenge. Prevention of relapses requires better predictive biomarkers. Towards this end, global gene-expression microarray screens of primary ALL samples were performed. Overexpression of the lysosomal cysteine protease, asparagine endopeptidase (AEP) was identified in adverse-risk progenitor-B ALL genotypes. AEP overexpression in adult human epithelial cancers has been linked to metastasis and adverse prognosis.

*Hypothesis*

AEP overexpression promotes leukaemic cell infiltration of the CNS and other extramedullary sites. AEP degrades the bacterial protein, *E*. *coli* L-asparaginase (ASNase) and potentially mediates lymphoblast resistance to this key antileukaemic drug.

*Summary of findings*

Quantitative AEP transcript estimation validated microarray findings in the discovery cohort. Sample availability precluded conclusive demonstration of protein overexpression. Intracellular expression in SD1 cells, a model AEP-overepressing ALL cell line, was strikingly heterogeneous and included aberrant peripheral localisation in endolysosomal macrovesicles. Similar findings were observed anecdotally in primary lymphoblasts. In SD1 cells, precursor AEP protein was shed in microvesicles.

AEP's role in cell motility was examined in human embryonic kidney (HEK293) cells. Contrary to published reports, ectopic AEP overexpression in HEK293 cells was not associated with enhanced motility.

ASNase was consistently degraded when incubated with ALL cell lysates. In overexpressing disease, ASNase degradation is potentially accelerated by AEP, resulting in inadequate drug activity during early treatment. AEP-cleaved ASNase

fragments retain known sensitising epitopes, suggesting that AEP cleavage could also potentiate formation of neutralising ASNase antibodies, compounding ASNase treatment failure. Sole substitution at an AEP cleavage site generated an AEP-resistant ASNase variant. Computational protein modelling enabled identification of an appropriate substituting amino acid that best retains drug activity.

*Conclusions*

AEP is a candidate marker of poor treatment response in childhood ALL and is presently the subject of a prospective nationwide clinical biomarker study. Its postulated role in cell motility appears to be cell-specific and dependent on the concomitant upstream expression of additional candidate pro-motility molecules. The protease also appears to be a marker of aberrant lymphoblast vesicle phenotype, an observation that is currently the focus of further studies.

# 1

# Investigating treatment failure in childhood acute lymphoblastic leukaemia

*See Box 'Childhood acute lymphoblastic leukaemia: a summary' (Pages 3-4)*

Acute lymphoblastic leukaemia (ALL) is a clonal neoplasm of progenitor lymphocytes. It is the commonest childhood malignancy (**Figure 1.1**). Once a uniformly fatal disease in the 1950s, cure rates in economically-advanced countries are now approaching 90% (**Figure 1.2**). This remarkable progress has been achieved through a combination of serendipity, astute clinical observations and steady refinements in treatment as a result of large-scale collaborative studies (**Figure 1.6**, **Table 1.1**). In tandem, cytologic and molecular genetic studies have underscored the biological heterogeneity of disease (**Figure 1.5**, **Table 1.2**). Collectively, these insights and incremental advances have enabled the characterisation of key treatment elements (**Figure 1.8**, **Table 1.1**) and the adaptation of treatment intensity to the risk of relapse (**Figure 1.7**).

These approaches have successfully driven down the incidence of treatment failure in childhood ALL (**Figure 1.1**, **Figure 1.6**). Treatment failure, a term that collectively refers to relapsed and refractory disease, is a major adverse event that is consistently associated with poor outcome (**Figure 1.9**). Relapsed ALL is second only to brain neoplasms as the commonest cause of childhood cancer-related mortality in the UK and USA [116]. Thus, prevention of relapses is a key objective.

Risk stratification of treatment is designed to specifically achieve this goal. The intention is to avoid overtreatment in children at low risk of relapse while escalating treatment intensity in those at highest risk of treatment failure. Although broadly successful, estimates of risk of relapse still remain imprecise.

Thus relapses continue to occur across all risk categories and numerically predominate in the population of children with apparent good risk disease (**Figure 1.11**). Equally, the imprecision in risk estimate potentially subjects a significant proportion of children to overtreatment and the attendant complications of short- and long-term treatment toxicities. Thus, adequately addressing the risk of relapse necessarily requires an enhanced understanding of disease biology (**Figures 1.12, 1.13 and 1.14**, **Table 1.3**).

**The biology of central nervous system (CNS) leukaemia**

One well-recognised but still poorly understood aspect of disease biology is the singular propensity for leukaemic cells to infiltrate the central nervous system (CNS). During the early evolution of treatment in childhood ALL, disease relapse in the CNS was a common cause of treatment failure. The structural and functional peculiarities of the CNS microvasculature render it impervious to standard therapies and require the administration of specific CNS-directed treatments to eliminate leukaemic cells in this anatomical compartment (**Figure 1.15**).

The contemporary combination of intensified systemic and CNS-directed therapies has considerably decreased the risk of CNS relapse but has not eliminated it [128]. Importantly in modern treatment protocols, the proportionate incidence of CNS relapses appears to be rising (**Figure 1.16**). Although there is room for additional refinement, current treatments have probably been near-maximally intensified. Tackling CNS relapses thus requires novel approaches and new therapies. Designing such strategies requires insight into the fundamental molecular and cellular mechanisms that drive leukaemic infiltration of the CNS (**Figure 1.17**, **Table 1.4**). To this end, a global gene expression microarray screen was performed to identify candidate molecules potentially contributing to the pathogenesis of CNS disease. As will be discussed in the next chapter, the lysosomal cysteine protease, asparagine endopeptidase (AEP) was identified as one such molecule.

**Childhood acute lymphoblastic leukaemia (childhood ALL): a summary**

- Malignancy of lymphoid progenitor cells
- Commonest childhood cancer (**Figure 1.1**); peak incidence 2-5 years
- Cure rates in industrialised world approach 90% (**Figure 1.2, Table 1.1**)
- Pathogenetic mechanisms are incompletely understood (**Figure 1.3**)
- Diagnostic tests are prompted by characteristic clinical symptoms and are based on a suite of complementary bone marrow tests (microscopy, flow cytometry and cytogenetics) (**Figure 1.4, Figure 1.5, Table 1.2**)
- Treatment is based on a complex schedule of multiagent chemotherapy (**Table 1.1**). Most drugs used in contemporary treatment were introduced in the 1950s-1970s. Major gains in survival have largely been achieved by progressive refinements in the use of these drugs, informed by large-scale collaborative clinical trials (**Figure 1.6**).
- Treatment intensity is adapted to the estimated risk of relapse. This risk assessment is based on clinical and biological variables at diagnosis and the response to therapy (**Figure 1.7**).
- Assessment of response to therapy is based on serial submicroscopic evaluation of marrow disease burden using sensitive quantitative PCR or flow cytometry tests (**Figure 1.7**). Optimal response is characteristically observed early in treatment (1-2 weeks by microscopy, 4 weeks by submicroscopic testing).
- Fundamental treatment elements include a Remission Induction phase, a Delayed Intensification phase, a Continuation phase and Central Nervous System-directed treatment. Additional treatment phases are administered in patients with adverse presentation features or unsatisfactory response to treatment (**Figure 1.8**). In contemporary management of childhood ALL, a risk-adapted, response-driven strategy has meant that (appropriate) treatment is currently the most powerful determinant of outcome [22].
- As corollary, the incidence of treatment failure (typically relapse, less commonly treatment-refractory disease) has fallen. This is important since outcomes following relapse have been consistently poor by comparison (**Figure 1.9**)
- Relapses can occur at variable time-points from diagnosis. A peculiar feature of relapsed ALL is the propensity to recur at anatomical sites other than the bone marrow (extramedullary sites). Timing and site of relapse together with lymphoblast lineage influence treatment outcomes (**Figure 1.10**)

**Childhood acute lymphoblastic leukaemia: a summary** (continued)

- The predilection for central nervous system (CNS) relapse has been well-recognised since the 1970s. The biological basis for this is incompletely understood. Part of the reason is attributable to the relatively impermeable blood-brain barrier which restricts access of cytotoxics to the CNS. Thus, frontline treatment protocols as a rule include treatment elements designed to eliminate leukaemic cells in the CNS compartment. These treatment components typically include intra-cerebrospinal fluid drug administration and CNS-penetrating systemic agents (**Figure 1.15**)
- Achieving comprehensive cure in childhood ALL requires a deeper understanding of the mechanisms contributing to treatment failure. This includes understanding the predilection for recurrence at extramedullary sites. As cure rates steadily improve, attention is increasingly focused on decreasing treatment toxicity without compromising cure (**Table 1.1**). The long-term goal is to customise therapy to the individual patient so as to avoid over- or under-treatment as well as short- and long-term treatment toxicities.
- Overlapping strategies to achieve this goal include
  (a) Improving prognostication

  Despite increasing sophistication, current estimates of relapse risk are still imprecise and additional biomarkers are required (**Figure 1.11**). Global microarray discovery screens have been instructive in this regard (for instance, by uncovering prognostically significant cryptic somatic lesions including gene deletions, mutations and deregulated expression [**Table 1.2**]).

  (b) Investigating lymphoblast biology

  Recent studies indicate that durable cure requires elimination of both leukaemic and pre-leukaemic clones (**Figures 1.12 – 1.13**). As intrinsic drug sensitivity is determined by biological features of leukaemic cells and interactions with the stromal microenvironment, investigations exploring these mechanisms are required to advance cure (**Figure 1.14**).

  (c) Investigating host pharmacogenomics

  Treatment safety and response is powerfully influenced by host pharmacogenomics that govern drug toxicity and pharmacodynamics.

  (d) Investigating new therapies, including further optimising current therapies as well as examining biologically-targeted agents that have the potential to improve cure and reduce toxicity (e.g. the ABL tyrosine kinase inhibitor Imatinib in Ph+ ALL).

**Figure 1.1** ALL is the most common childhood malignancy

Annual incidence of cancers in the UK among children <15 years old. ALL is the most common childhood neoplasm (25% of all cancers). The declining incidence of relapsed ALL places this disease category as the 9th most common form of childhood cancer in the UK. Importantly, after central nervous system tumours, relapsed ALL is the commonest cause of cancer-related mortality in young children.

*ML, acute myeloid leukaemia; Bone Tmrs, bone tumours; Germ cell, germ cell neoplasms; Liver, paediatric liver tumours (hepatoblastomas); Neural crest, tumours derived from neural-crest precursors (neuroblastomas); NOS, not otherwise specified; Renal, paediatric renal tumours (Wilms tumours); Retinal, retina-based tumours (retinoblastomas); Soft tissue sarc, soft tissue sarcomas (rhadomyosarcoma and Ewing/primitive neuroectodermal family tumors).*

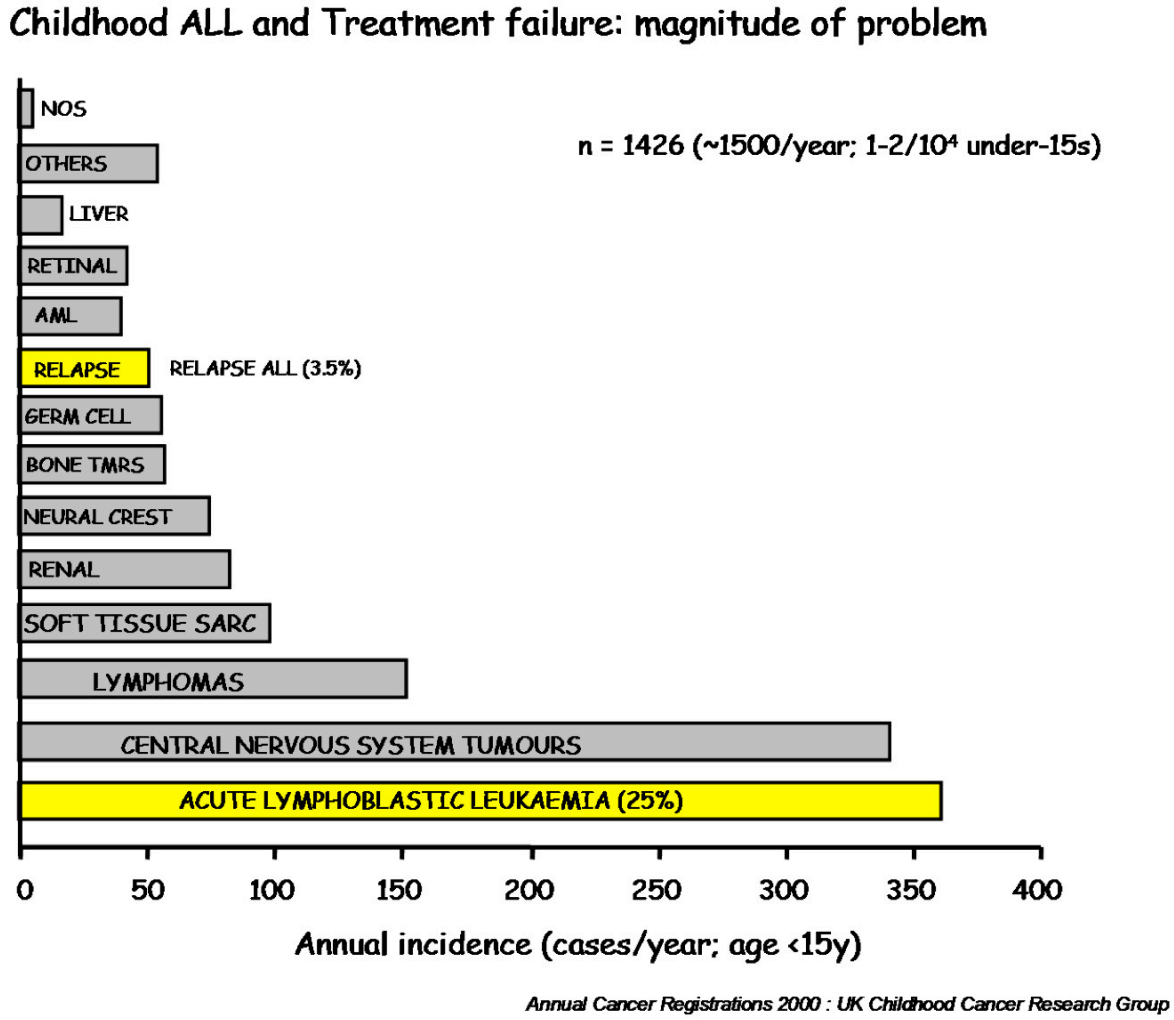

**Figure 1.2** The average cure rate for childhood ALL in the developed world is ~85%

Cumulative continuous probability distribution of overall survival in childhood ALL plotted against time. Survival increased steeply in the two decades between 1980 and 2000 and is now approaching 90%. The plateau in cure rates suggests that contemporary treatment has probably been maximally intensified and new agents and novel treatment approaches are now required.

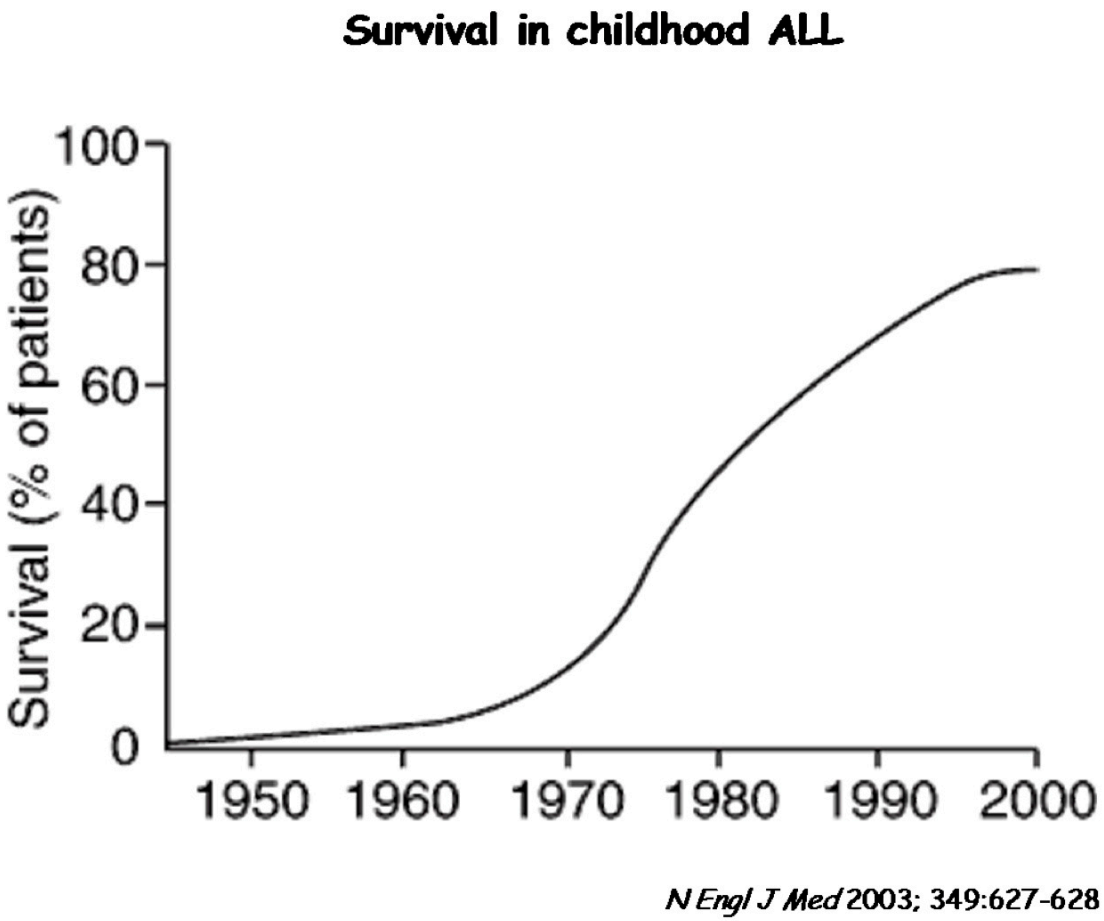

**Figure 1.3**: The aetiopathogenesis of childhood ALL is unclear in most cases. A two-hit transformation event is postulated in progenitor-B ALL.

*Upper panel* A predisposing cause is identified only in a minority of cases and typically involves constitutional or acquired abnormalities of germline DNA. Trisomy 21 (Down syndrome, DS) is a well-recognised risk factor with a 10-20 fold increased risk [89]. Unlike DS-related AML, ALL in DS has an intermediate prognosis, does not co-associate with known favourable or unfavourable chromosome lesions, is linked with aberrant kinase activation (e.g., Janus family kinases) and is characterised by increased mucosal sensitivity to cytotoxics such as methotrexate [90]. Genome-wide association studies identified predisposing germline polymorphisms in IKZF1 (Ikaros family zinc finger 1, 7p12.2), ARID5B (AT-rich interactive domain-containing protein 5B, 10q21.2), and CEBPE (CCAAT enhancer binding protein epsilon, 14q11.2)

*Lower panel* The pathogenesis of childhood progenitor-B ALL is attributed to a two-hit transformation event. The first hit refers to the *in utero* occurrence of somatic gene fusions, as revealed by analysis of dried neonatal blood spot cards [91]. This in itself is insufficient for leukaemogenesis. A second hit results in acquisition of additional (driver) genomic lesions in key lymphocyte differentiation and proliferation pathways, eventually resulting in overt leukaemia. An infection-driven immune-mediated transformation event is believed to represent this second-hit and is postulated to account for the rising incidence of childhood ALL (1.5% increase in annual incidence) in the industrialised world [92, 93]. Immunological insulation in infancy (lowered herd immunity, 'hygiene hypothesis') followed by delayed exposure in later childhood (for instance due to population-mixing, [94]), synchronous with the period of maximal lymphoid proliferation and expansion, confers adverse 'immunological stress' and drives neoplastic transformation of pre-leukaemic lymphocytes. This two-hit theory accounts for the peak incidence of childhood ALL in children aged 2-5 years; population-mixing additionally explains the occurrence of case clusters, for instance due to mass emigration to areas of low herd immunity. These theories probably do not apply to the origin of childhood progenitor-T lymphocyte ALL.

*ETV6-RUNX1, chromosome fusion translocation of chromosome segments 12p13.1 and 21q22.3, resulting in a chimaeric gene fusion; PAX5, paired box gene 5 (chromosome locus 9p13); CDKN2A/B, gene locus encoding cyclin dependent kinase inhibitor 2A and the alternating reading frame product, cyclin dependent kinase inhibitor 2B*

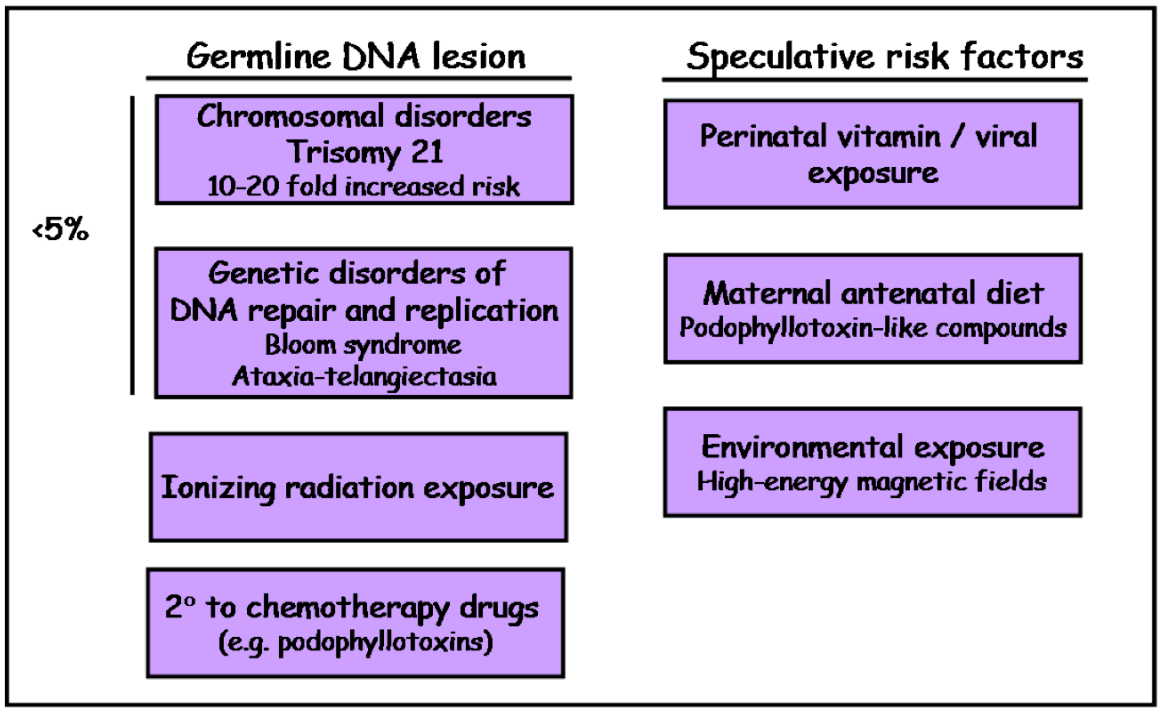


Postulated pathogenesis of childhood ALL

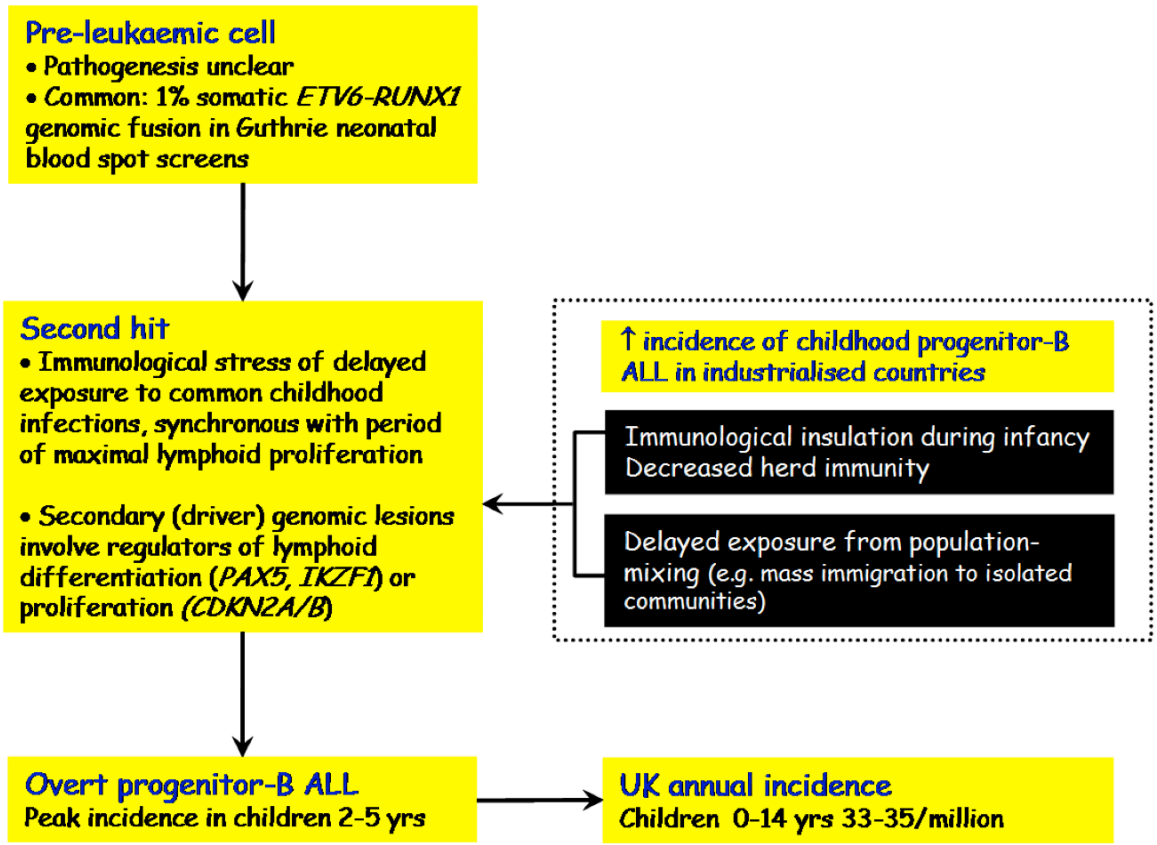

**Figure 1.4**: Clinical presentation and routine diagnostics in childhood ALL

Most children present with a short history of symptoms (*Upper panel*). Diagnosis is established by a complement of tests performed typically on bone marrow samples. This starts with microscopy examination of stained bone marrow aspirates (*Middle panel*). Normal haematopoietic elements in the bone marrow are near-completely replaced by characteristic large cells with scanty agranular cytoplasm (occasionally with cytoplasmic projections [uropod] forming hand-mirror morphological forms) and round-to-oval nuclei with homogenous-staining finely dispersed chromatin (lymphoblasts, morphological forms L1 and L2). Diagnosis and lineage is established by flow cytometry immunophenotyping of CD45+ cells (*Lower panel*). Immunophenotyping and morphology (typically, basophilic vacuolated blast cytoplasm) additionally distinguish mature-B ALL from progenitor-B disease; the former is a distinct disease entity characterised by rapid tumour expansion and excellent response to intensive short-term cycling multiagent cytotoxic therapy.

*CD, cluster of differentiation markers; cy, cytoplasmic; Ig, immunoglobulin; s, surface; TdT, terminal deoxynucleotidyl transferase*

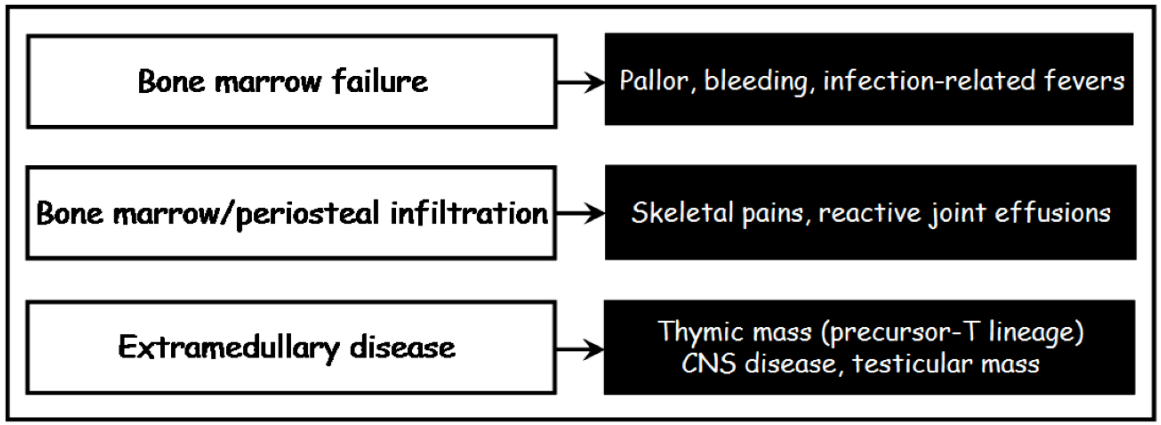

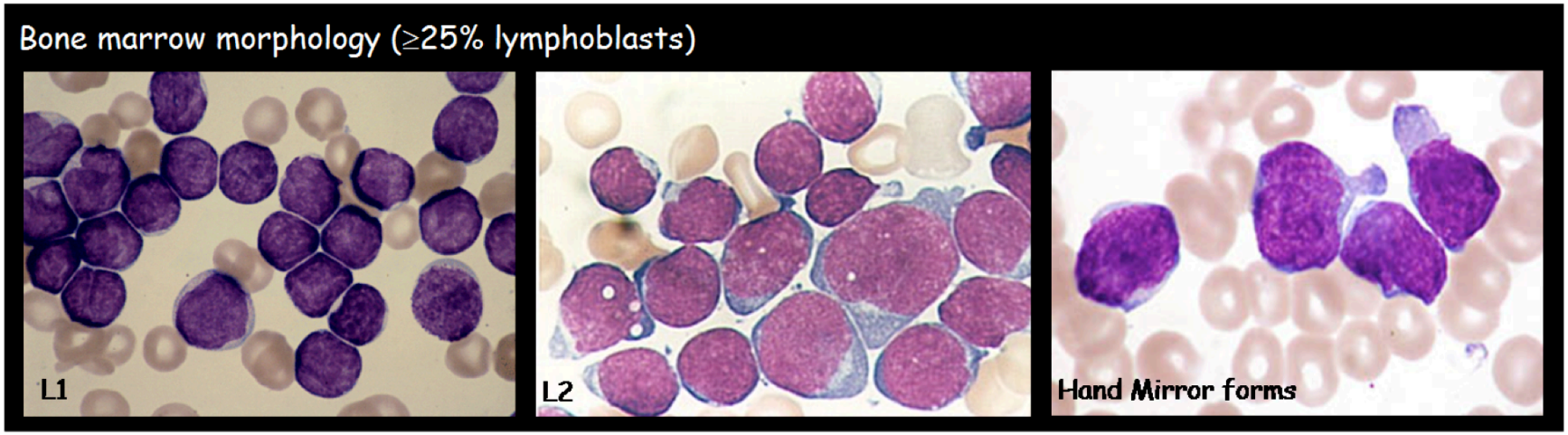
Bone marrow morphology (≥25% lymphoblasts)
L1
L2
Hand Mirror forms

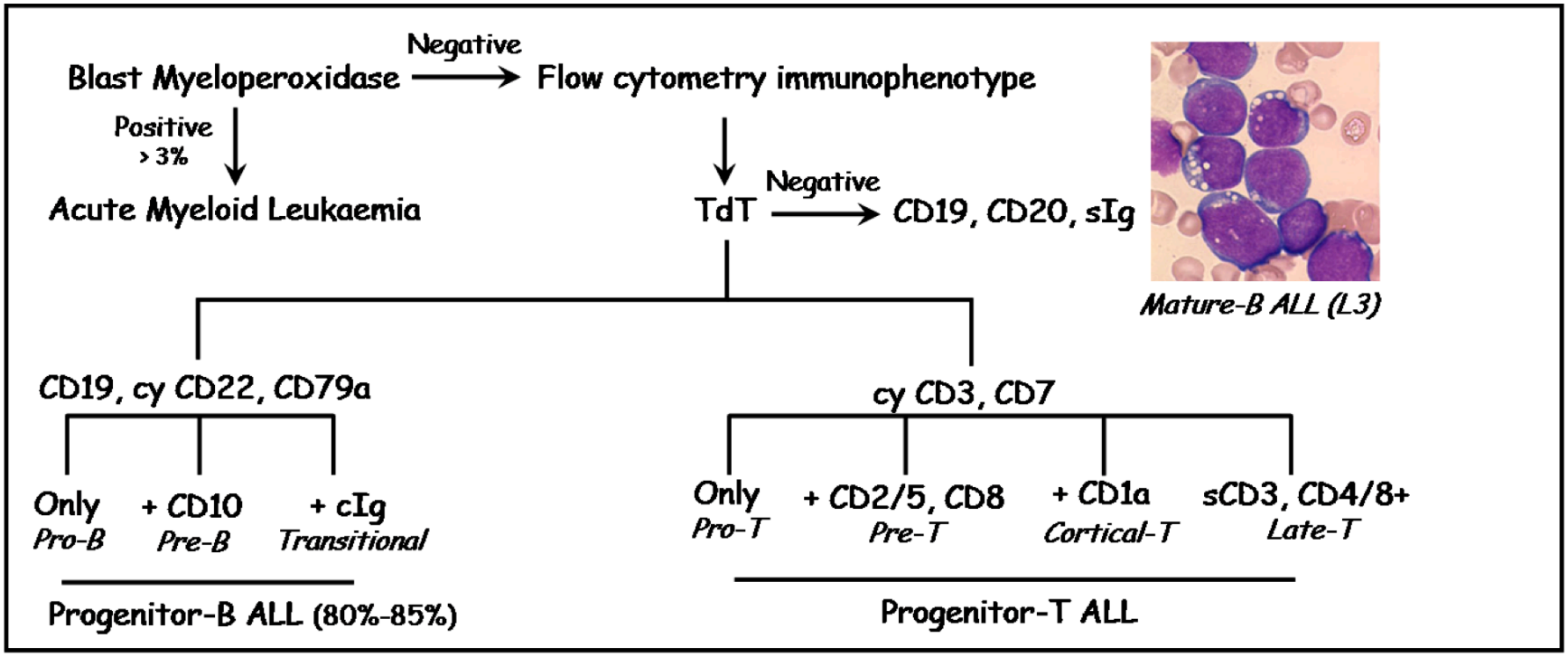
Blast Myeloperoxidase
Negative
Flow cytometry immunophenotype
Positive
> 3%
Acute Myeloid Leukaemia
TdT
Negative
CD19, CD20, sIg
Mature-B ALL (L3)
CD19, cy CD22, CD79a
cy CD3, CD7
Only
Pro-B
+ CD10
Pre-B
+ cIg
Transitional
Only
Pro-T
+ CD2/5, CD8
Pre-T
+ CD1a
Cortical-T
sCD3, CD4/8+
Late-T
Progenitor-B ALL (80%-85%)
Progenitor-T ALL

**Figure 1.5**: Childhood ALL is characterised by non-random somatic genetic lesions

Typical recurring lymphoblast genetic abnormalities detected by conventional cytogenetic testing (G-banded karyotyping and FISH) in childhood ALL. Structural somatic lesions include non-random gene fusions that either encode hybrid proteins or result in enhanced expression of proto-oncogenes. These lesions are well-characterised in progenitor-B ALL and influence prognosis. By contrast, the impact of genetic abnormalities on treatment outcomes in progenitor-T ALL is incompletely understood.

*ABL1, Abelson murine leukaemia viral oncogene homolog-1 (chromosome locus 9q34.1); AF10, mixed-lineage leukemia (Drosophila trithorax homolog) translocated to 10 (10p12); BCR, breakpoint cluster region (22q11.2); CALM, clathrin assembly lymphoid myeloid leukaemia gene (11q14-21); CEBP, CCAAT enhancer binding protein gene family; CRLF2, cytokine receptor-like factor 2 (pseudoautosomal region, Xp22.3, Yp11.3); ETV6, ETS (E-26 transforming specific) variant gene 6 (12p13.1); HOX11, T-cell leukaemia homeobox 1 (TLX1, 10q24.31); HOX11L2, T-cell leukaemia homeobox 3 (TLX3, 5q35.1); iAMP21, intrachromosomal amplification of chromosome 21; IgH, immunoglobulin heavy chain locus; LMO1 and LMO2, LIM domain only 1 (11p15.4) and 2 (11p13); MLL, mixed lineage leukaemia gene (11q23); NUP214, nucleoporin 214 kiloDalton (9q34.3); PBX1, pre-B leukaemia homeobox 1 (1q23); RUNX1, runt related transcription factor 1 (21q22.3); TAL1 and TAL2, T-cell acute lymphoblastic leukaemia 1 (1p32) and 2 (9q31); TCF3, transcription factor family 3 (E2A, 19p13.3); TCR, T-cell receptor loci.*

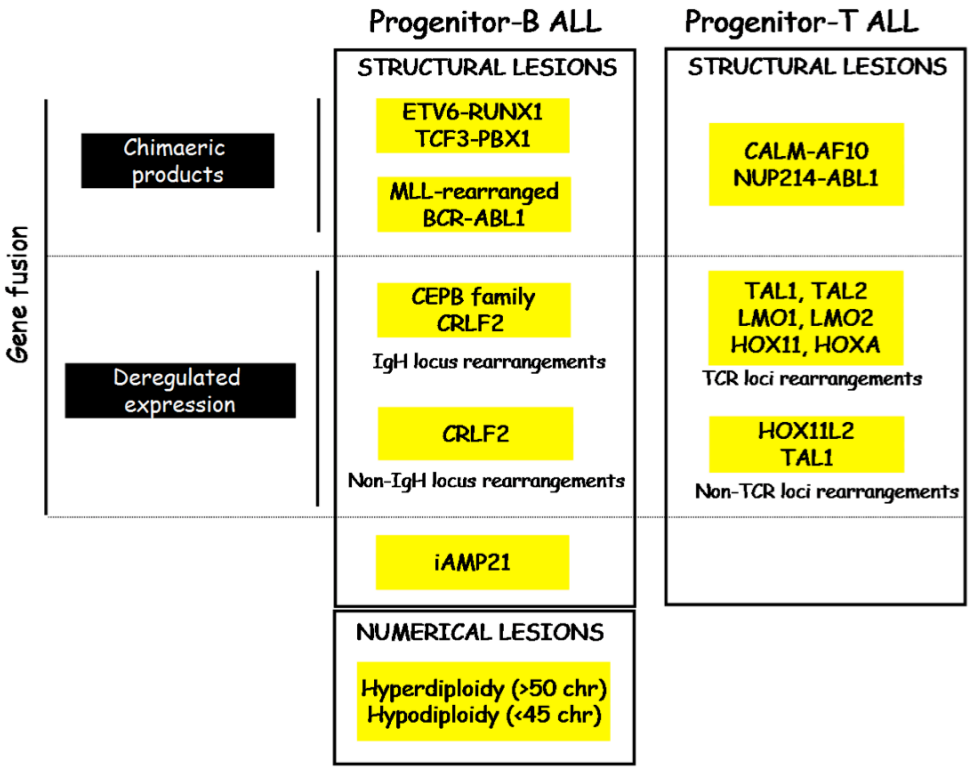

**Figure 1.6** Incremental refinements in therapy rather than introduction of new drugs, accounted for the steep improvement in childhood ALL cure rates between the 1980s and 2000s

*Left panel*: Timeline schematic indicating chronology of introduction of key cytotoxic agents and treatment strategies in childhood ALL.

*Right panel*: Kaplan-Meier analysis of event (relapse or death)-free survival indicates steady improvement with successive UK childhood ALL treatment protocols

*6-MP, 6-mercaptopurine; Ara-C, cytosine arabinoside; ASNase, E.coli L-asparaginase; CNS, central nervous system; Cyclo, cylophosphamide; Dauno, daunorubicin; MTX, methotrexate; PEG, polyethylene glycol; RT, XRT, radiotherapy; VCR, vincristine*

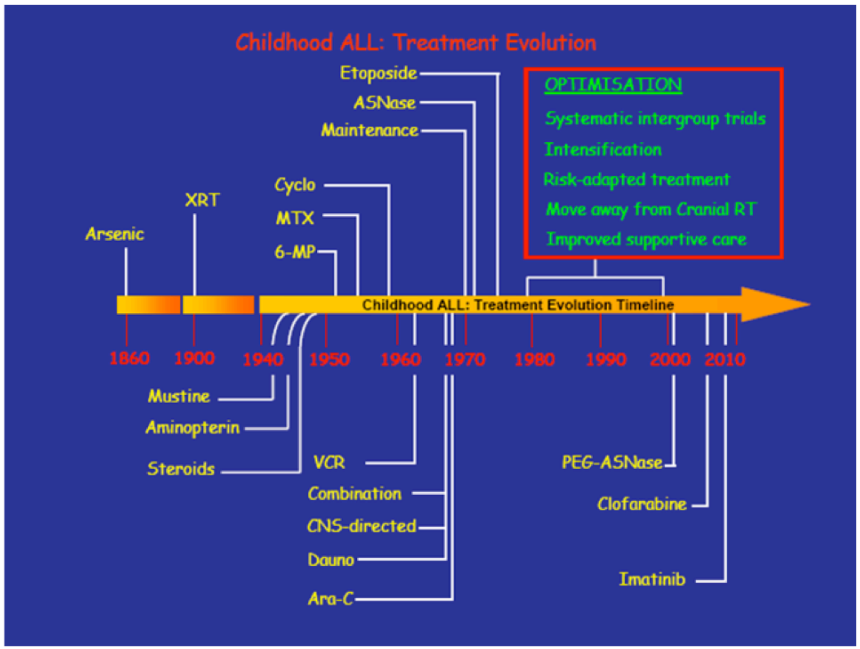


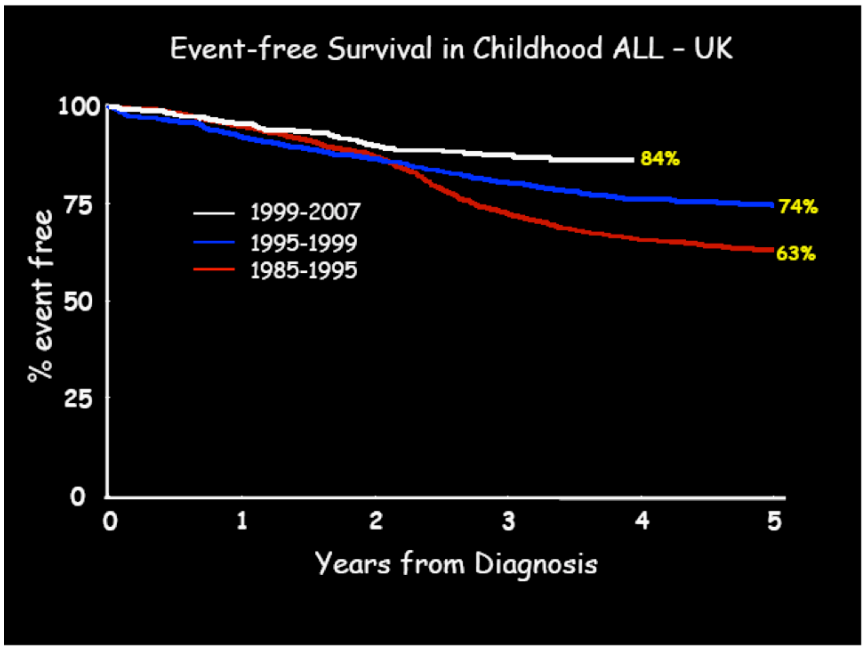

**Figure 1.7** A general approach to risk stratification in childhood ALL.

Risk estimate is based on probability of relapse. Clinical features, Somatic genetic characteristics and Response to therapy are combined to generate a three-tier risk stratification approach. In contemporary treatment protocols, appropriate treatment intensity and satisfactory (submicrosopic) response to therapy supersede all other prognostic variables.

*D8/15, day 8 or 15 of ALL treatment; WBC, white blood cell*

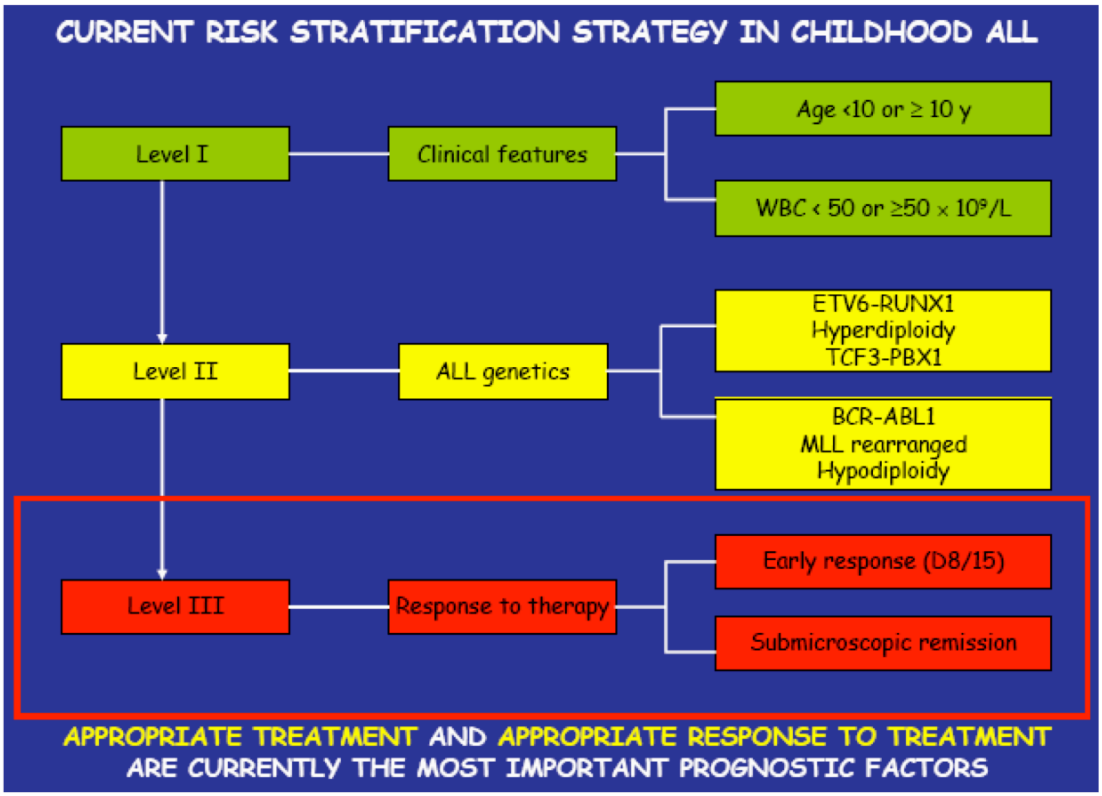

**Figure 1.8** Contemporary risk-adapted treatment design in childhood ALL

Integral treatment elements comprise the Induction, Delayed Intensification and Maintenance phases and central nervous system (CNS)-directed therapy. Intermediate-risk patients typically receive additional treatment during induction (Ext. Indn) and delayed intensification phases. Treatment is further intensified in patients at high risk of relapse (Augmented Intensification treatment blocks) and is sometimes consolidated by allogeneic haematopoietic stem cell transplant (allo-SCT). CNS-directed therapy typically consists of a combination of CNS-penetrating systemic and intra-spinal fluid (intrathecal, IT) cytotoxics; cranial irradiation (RT) is generally reserved for children with overt CNS leukaemia. Treatment intensity is directed by early and serial submicroscopic assessment of response.

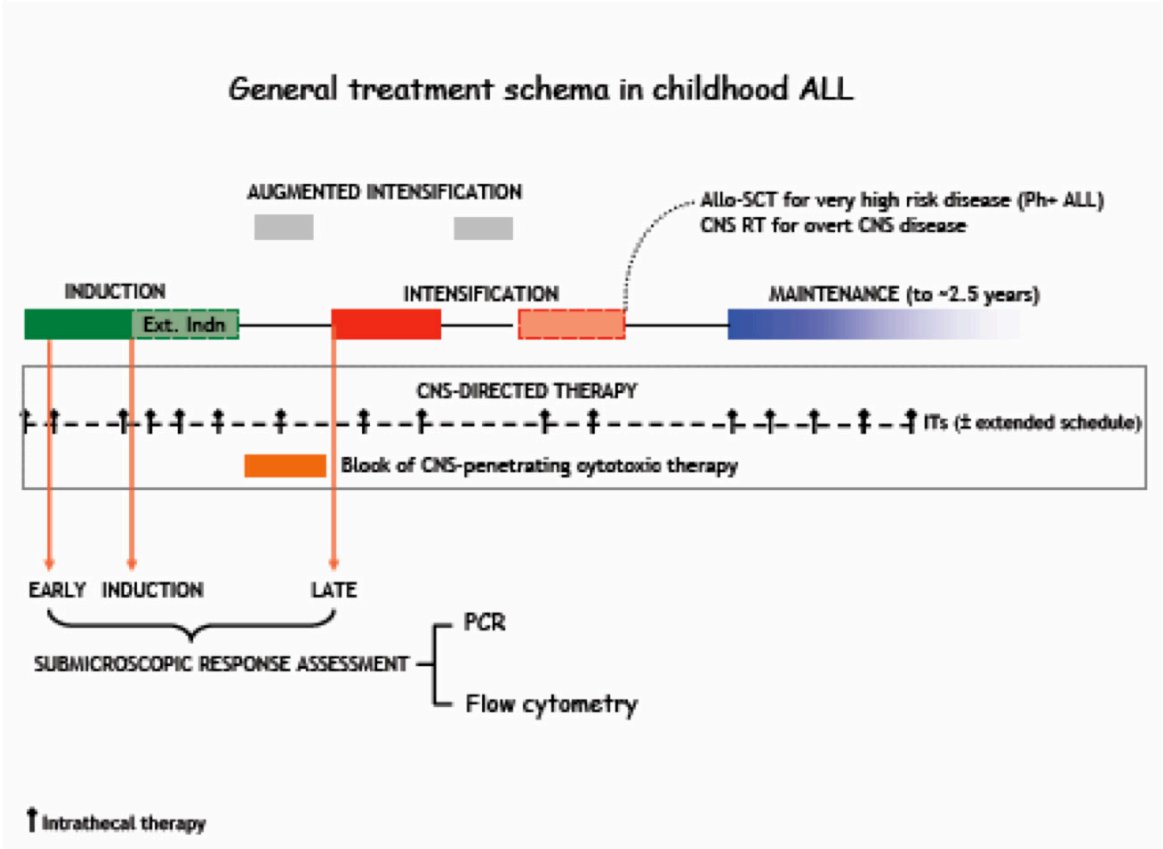

**Figure 1.9** Childhood ALL relapses are best prevented.

Kaplan-Meier estimates of survival probabilities in children enrolled on CCG trials for relapsed ALL. Survival outcomes in all three categories of relapse (early, intermediate and late) have remained static over successive trial eras, spanning a period of 15 years [115].

*CCG, North American Children's Cancer Group*

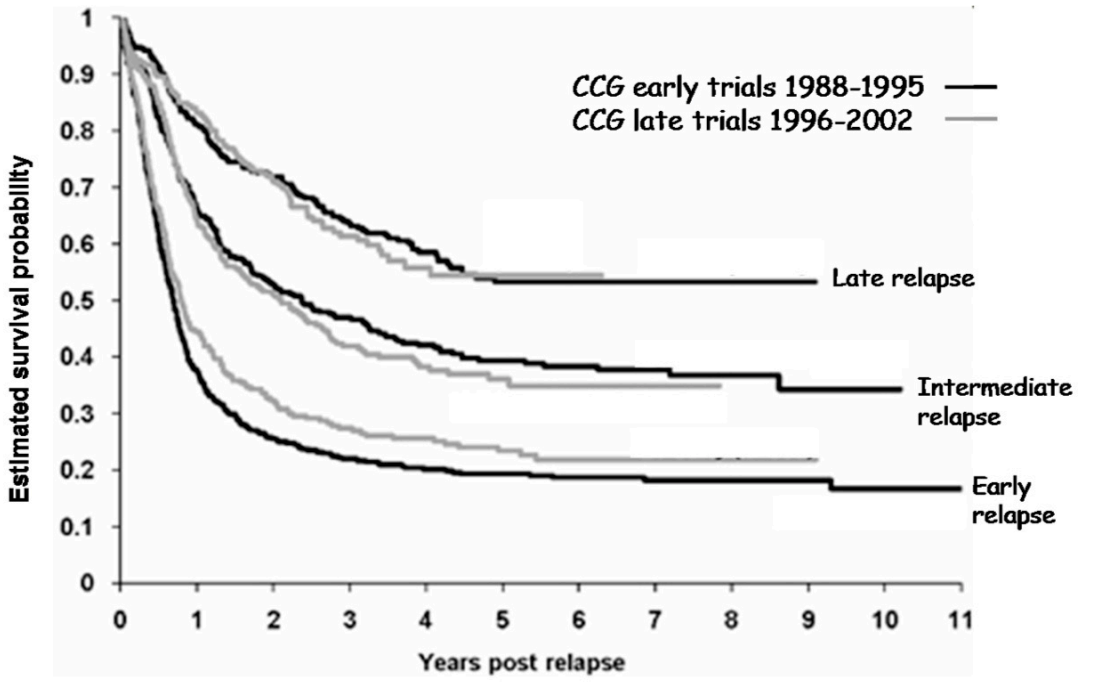


Leukemia 2008 22:2142-2150

**Figure 1.10** A risk-adapted approach is also used in the contemporary management of relapsed childhood ALL

*Upper panel*: Treatment outcomes following relapse are strongly influenced by timing and site of relapse and disease lineage. *Lower panel*: All three variables are typically incorporated in the design of risk-adapted treatment strategies for relapsed disease.

*BM, bone marrow disease; EM, extramedullary disease sites; EOT, end of therapy*

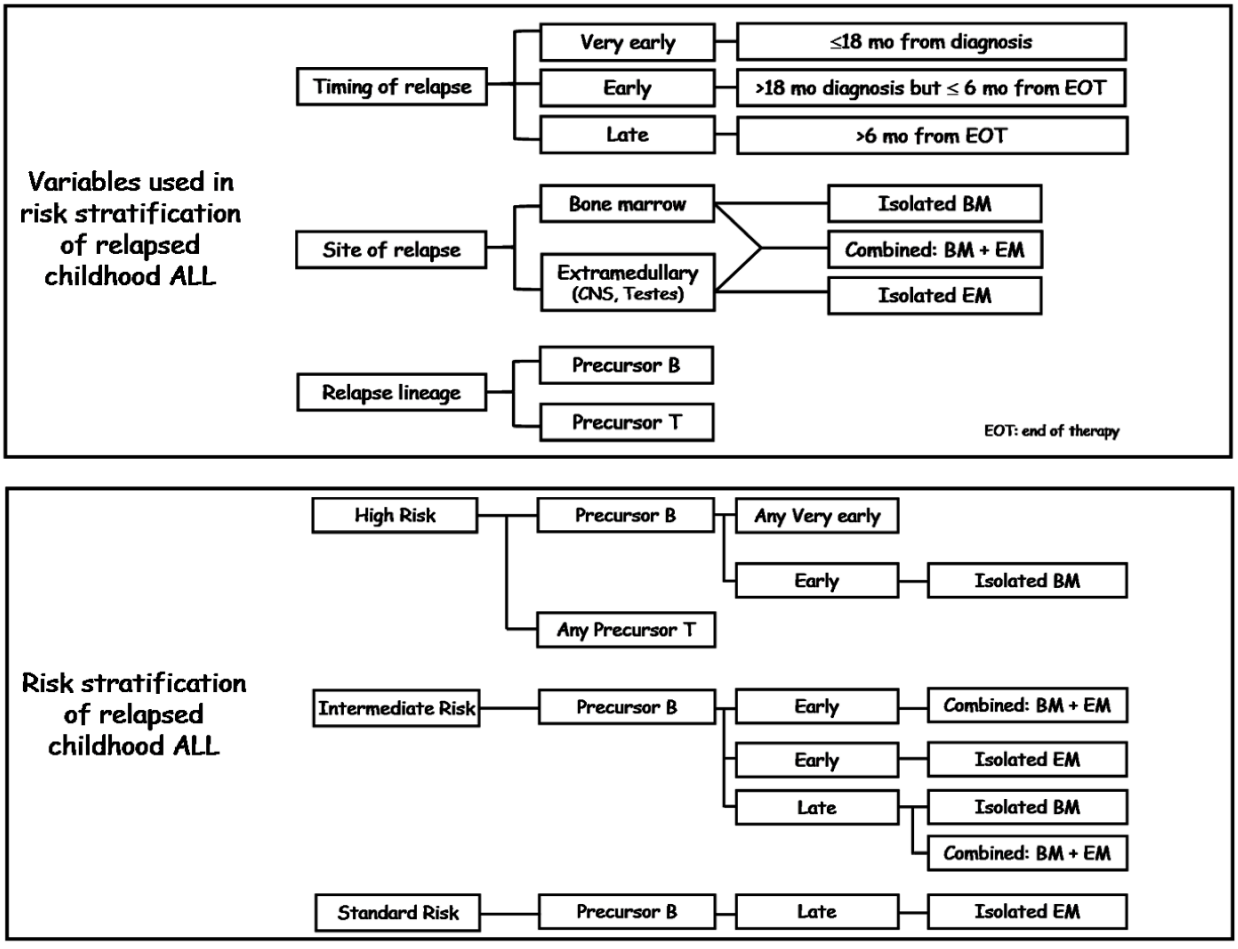

**Figure 1.11** Current strategy of relapse risk stratification in childhood ALL is still imprecise

Proportion of childhood ALL disease subtypes at diagnosis and relapse. The majority of relapses still occur in children with apparent 'good-risk' progenitor-B ALL.

Pre-B Good Risk refers to progenitor-B ALL with favorable risk cytogenetics (*ETV6-RUNX1*, high hyperdiploidy, *TCF3-PBX1*, normal karyotype disease and other non-recurrent cytogenetic lesions); Pre-B Poor Risk refers to progenitor-B ALL with adverse risk cytogenetics (Ph+ALL, *MLL* rearranged, hypodiploidy); Pre-T refers to any progenitor-T ALL

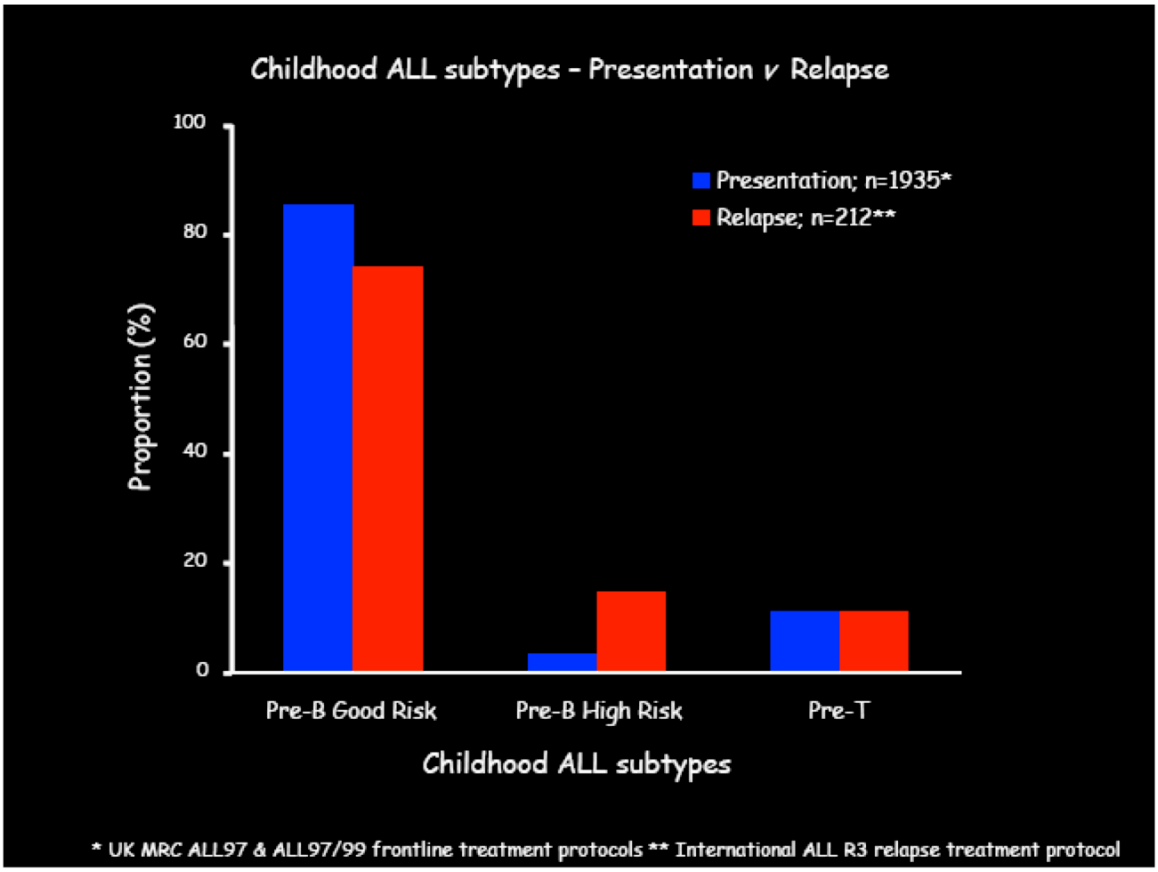

**Figure 1.12**: Ancestral pre-leukaemic clones are responsible for childhood ALL relapse

Cartoon representation of the origins of the relapse clone in childhood ALL based on results of high-resolution DNA copy number analyses in matched diagnosis-relapse samples from children with ALL; alphabets indicate somatic genomic lesions. In ~40% of cases, relapse clones are either identical to or clonally evolved from diagnosis clones. Instructively, in more than half the cases, the relapse clone is genomically related to an ancestral pre-leukaemic clone. In both situations, relapse clone cells are often identified as minor subpopulations at diagnosis, suggesting that cytotoxic treatment more likely favours clonal selection rather than progression. Thus durable cure requires elimination of both leukaemic and pre-leukaemic disease clones [117].

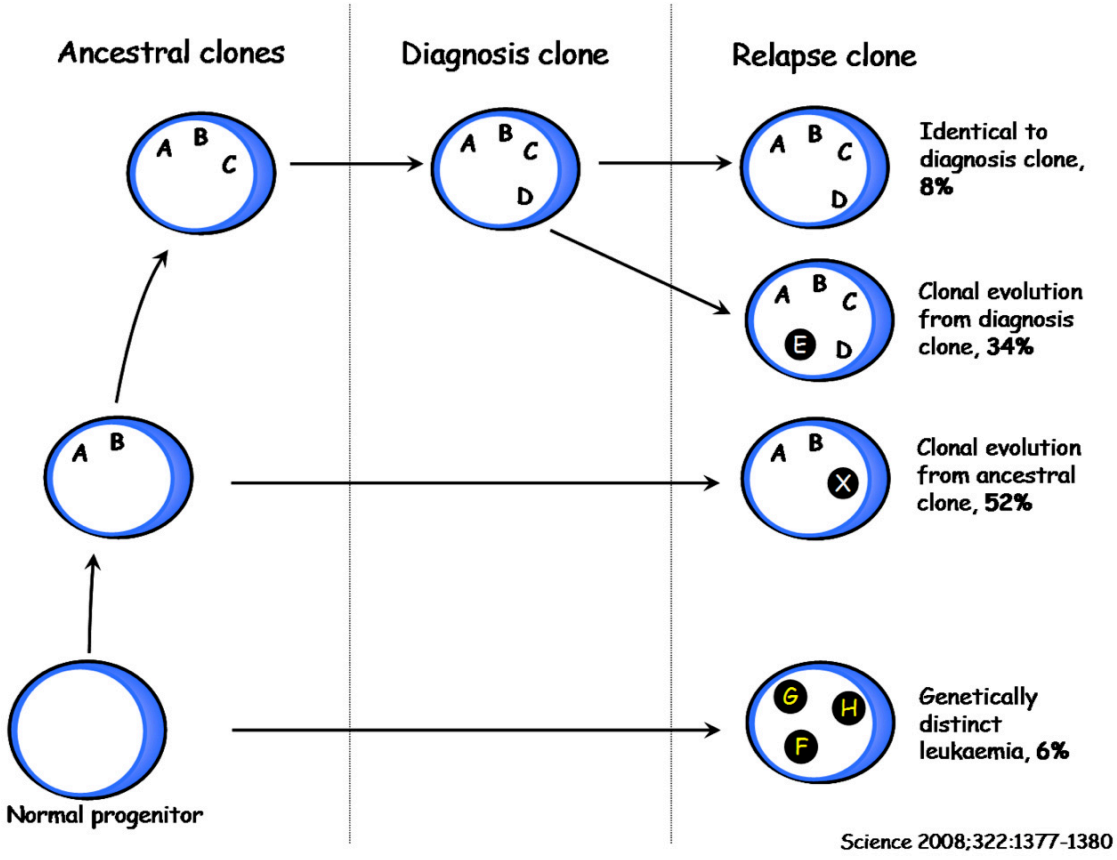

**Figure 1.13** A biological paradigm of disease origin and relapse in childhood progenitor-B ALL

A pre-leukaemic clone arises *in utero* and acquires secondary driver genetic lesions to give rise to overt leukaemia [91]. Leukaemia-initiating clones responsible for disease relapse are similarly related to an ancestral pre-leukaemic clone [117]. Persistence of the ancestral clone is probably a result of both autonomous (autocrine-paracrine signalling and stromal remodulation, e.g. Ph+ALL) and stromal-dependent (adhesion or non-adhesive interaction) mechanisms. Some extramedullary sites additionally serve as pharmacological sanctuaries (e.g. central nervous system). A*dapted from* [100].

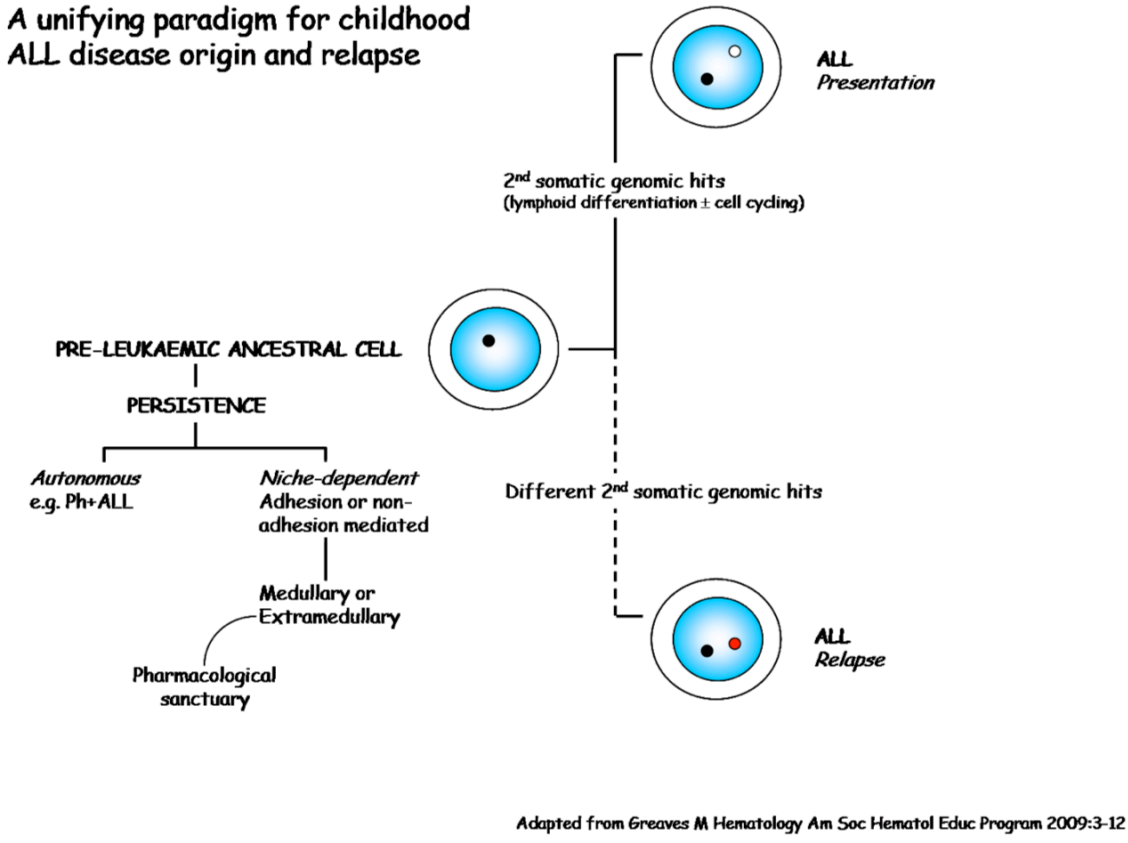

**Figure 1.14** Postulated mechanisms contributing to disease relapse

Intrinsic tumour characteristics and tumour stromal properties can interact to enhance lymphoblast survival. This when coupled with unfavorable drug-handling host germline polymorphisms can lead to persistence of leukaemia-initiating subclones and eventual disease relapse.

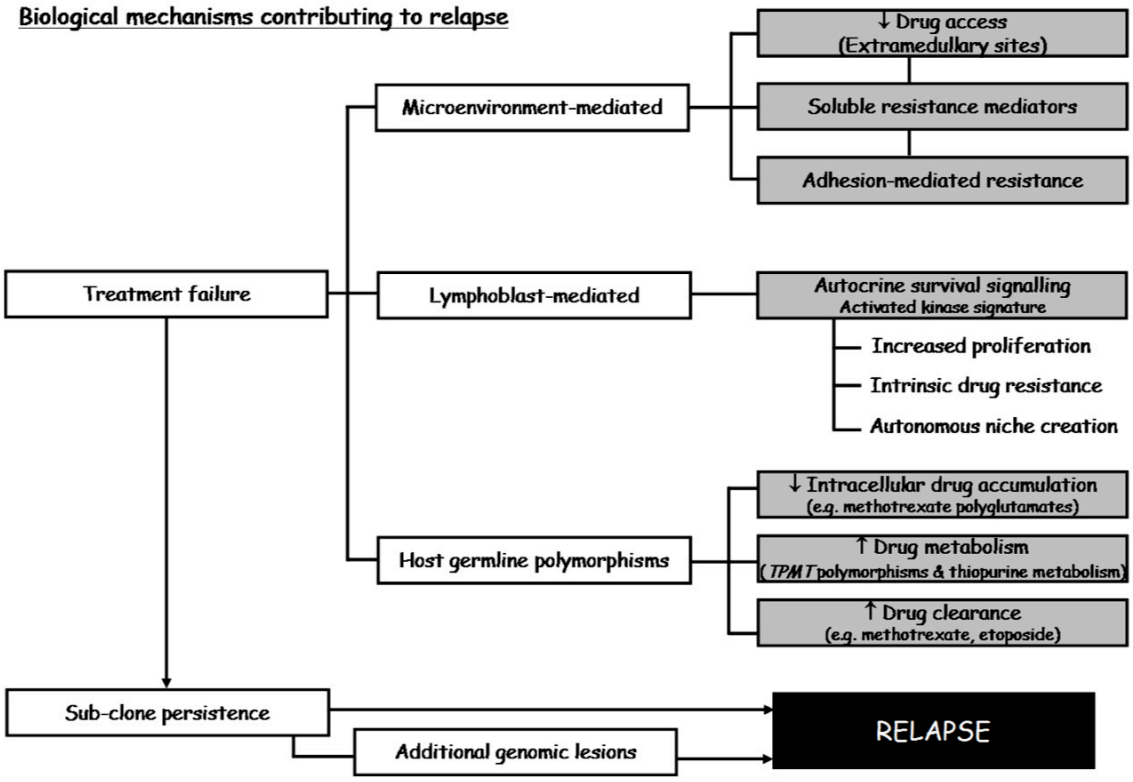

**Figure 1.15** Persistence of brain-seeking lymphoblasts results in CNS relapse

The unique neurotropism of lymphoblasts results in infiltration of the central nervous system (CNS). Systemic chemotherapy limits meningeal seeding while directed therapy eliminates blasts already resident in the CNS. These measures complement each other, and are integral to the success of therapy. These treatments have probably been maximally intensified. Notwithstanding, CNS leukaemia is a recurring feature of relapsed ALL, accounting for up to a third of all relapses. Thus tackling CNS leukaemia requires new treatment strategies, which can only arise from a deeper understanding of the mechanisms that drive leukaemic neuroinfiltration.

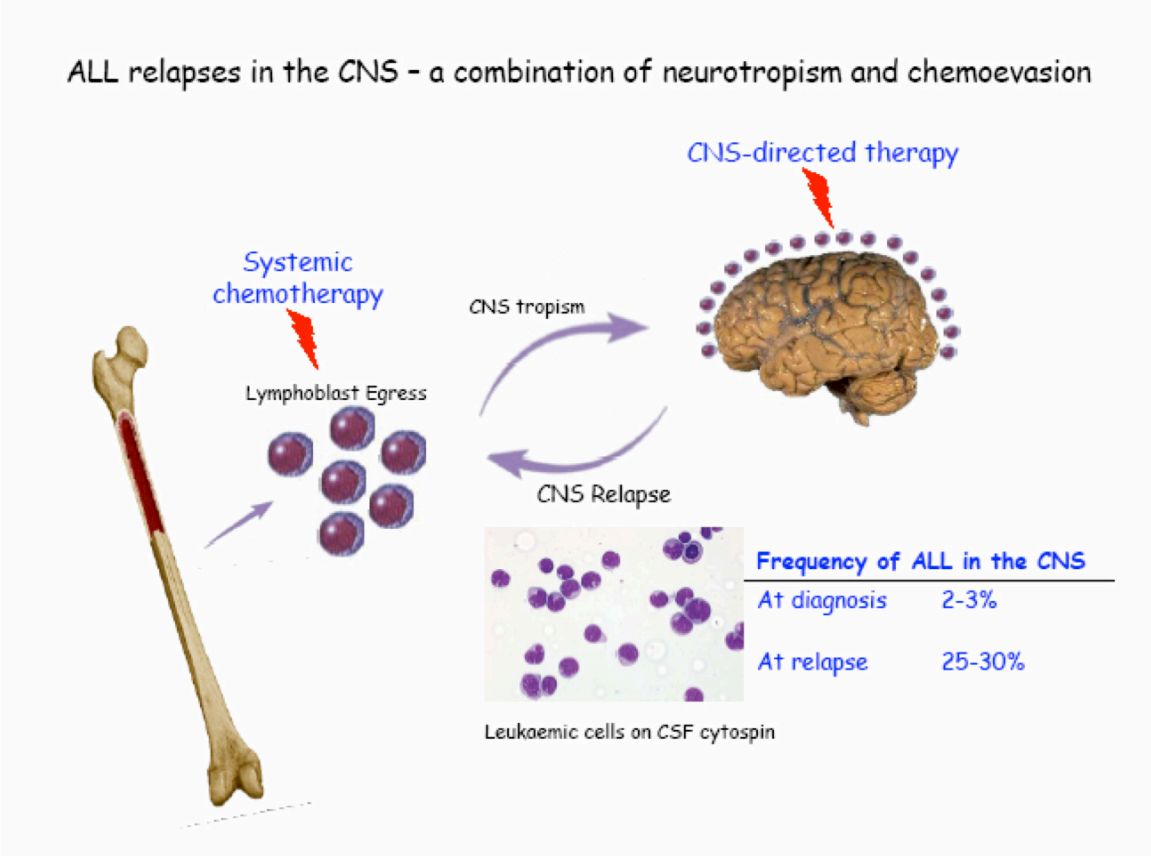

**Figure 1.16** The proportional frequency of CNS relapses is increasing

Data from the UK Medical Research Council (MRC) childhood ALL trials (x-axis). While the frequency of ALL relapse (as a proportion of the total diagnosed) has near-steadily declined to now under 10%, the proportion of relapses occurring in the central nervous system (CNS) has increased. Tailoring treatment intensity to residual disease burden in the bone marrow appears to have successfully decreased isolated marrow relapses and in the process, unmasked the discordance in the dynamics of disease clearance between medullary and extramedullary compartments.

*'CNS relapses' refers to both isolated and combined (bone marrow & CNS) relapses*

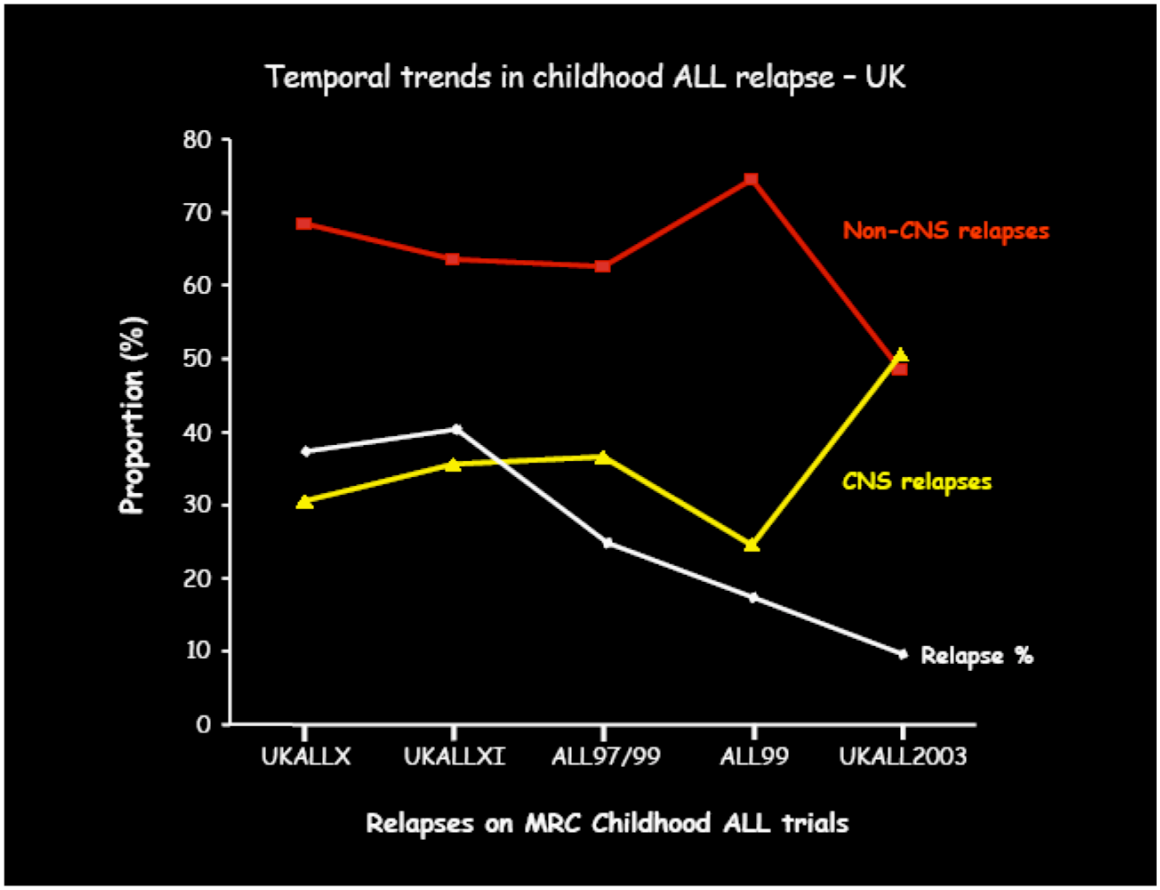

**Figure 1.17** Putative cellular and molecular events involved in extramedullary infiltration by lymphoblasts

Chemokine signals drive the egress and homing of lymphoblasts from bone marrow to extramedullary sites. Circulating lymphoblasts probe the endothelial surface by deploying podosomes, specialised actin-based structures enriched in matrix-degrading enzymes, including matrix metalloproteases (MMP) and lysosomal hydrolases. Selectin-mediated endothelial rolling and integrin-based interactive endothelial adhesion trigger reciprocal lymphoblast-endothelial cytoskeletal reorganization and exocytosis of matrix-degrading enzymes, resulting in basement and stromal matrix degradation and lymphoblast extravasation by paracellular diapedesis or transendothelial migration. Adhesive and non-adhesive interactions with stromal component cells contribute to lymphoblast persistence at extramedullary sites.

*CXCR4 chemokine (CXC motif) receptor 4; CXCL12 chemokine (CXC motif) ligand 12; ECM, extracellular matrix; ICAM, intercellular adhesion family of molecules; VEGF/VEGFR vascular endothelial growth factor/receptor*

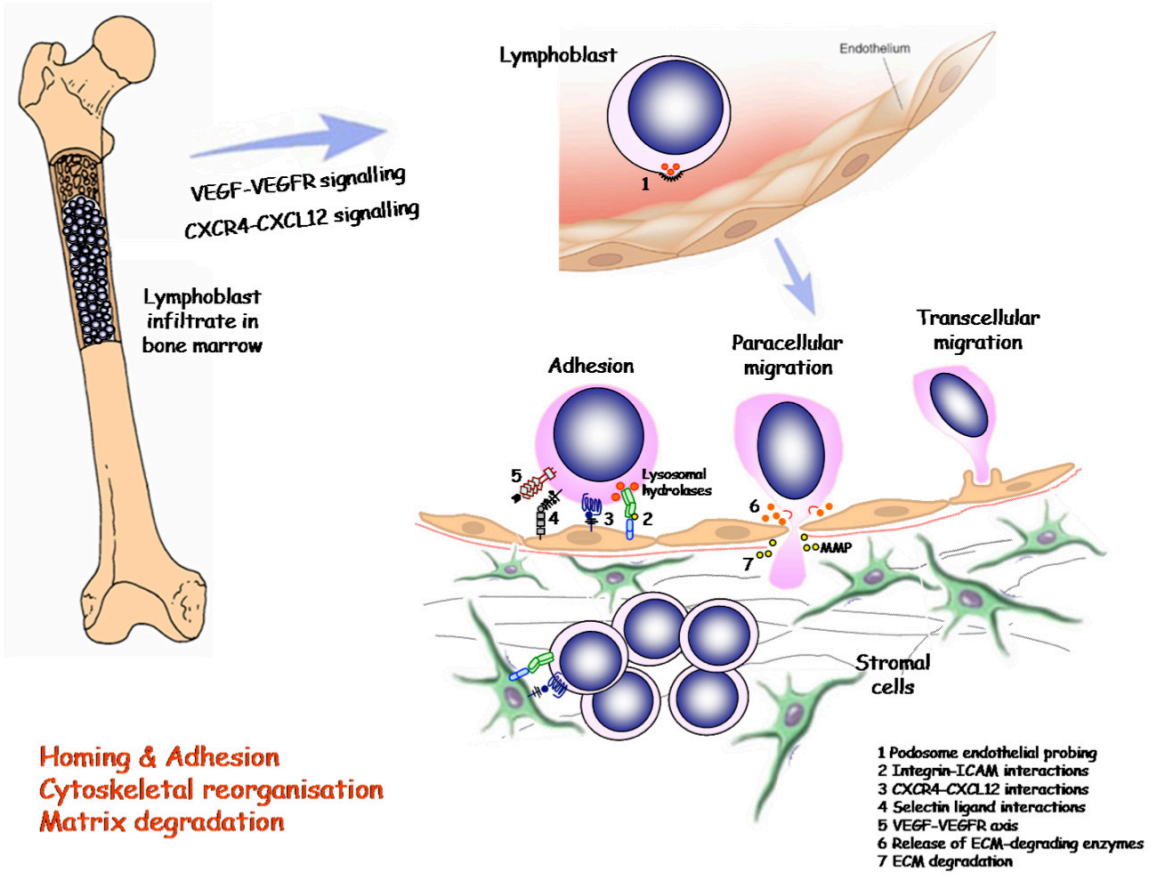

**Table 1.1 Milestones in the evolution of treatment of childhood ALL**

| Elements | Year / decade introduced | Opening remarks | Perspective/Current status | Relevance / Refinements / Modifications | Key references |
|---|---|---|---|---|---|
| DIAGNOSIS | | | | | |
| Bone marrow morphology | First attempts in the mid-1960s; systematic guidelines since 1981 | Bone marrow morphology and cytochemistry used for diagnosis, differentiation from AML and determination of adverse-risk morphological subtypes | Still remains the primary diagnostic technique. The FAB classification is useful only insofar as identifying mature B-lineage ALL (vacuolated L3 blasts). Cytochemistry is no longer used. | Morphological adverse-risk variants such as granular blasts and hand-mirror forms are no longer relevant in the contemporary era | [1], [2], [3] |
| Blast immunological phenotype | Mid 1980s | Monoclonal antibody detection of surface and intracytoplasmic lineage- and differentiation-specific antigens | Important diagnostic tool. Allows rapid and reliable diagnosis of leukaemia type (lymphoid *v* myeloid), lineage (T- or B-) and differentiation (early progenitor *v* precursor) | Prognostic relevance of antigen markers largely obviated by current therapy. CD10-positive B-lineage disease in infants is a good-risk feature while immature T-cell immunophenotype is associated with inferior outcomes. Aberrant myeloid antigen expression (15-20% cases) is no longer relevant | [4], [5], [6], [7] |
| Blast cytogenetics | Late 1980s | Metaphase G-banded karyotyping and FISH to detect recurrent translocations and aneuploidy | Important diagnostic, risk-stratification and discovery tool | Extremely relevant in contemporary classification and treatment schemes. Growing significance with biologically-directed therapies. Enhanced resolution using high-resolution whole-genome arrays and now, whole-genome sequencing | [8], [9], [10] |

| | | | | | |
|---|---|---|---|---|---|
| PROGNOSIS | | | | | |
| Presentation risk factors | | | | | |
| Clinical risk factors | Mid 1980s | Several clinical risk factors have been serially examined, including age, presenting white cell count, sex, blast lineage and extramedullary disease | Two powerful clinical features continue to inform risk assignation and constitute the NCI-Rome risk criteria - age (<10 or ≥10 years) and presenting WBC count (<50 or $\geq 50 \times 10^9$/L) | Contemporary treatment has rendered redundant several previously relevant disease features. The biological basis for the persistent prognostic significance of age and leucocyte count is not fully understood | [11], [12] |
| Genetic risk factors | Late 1980s | Blast genotype influences outcome | Contemporary treatment consistently recognises three adverse-risk genotypes - Philadelphia-chromosome positive ALL (Ph+ ALL), *MLL*-rearranged ALL and blast hypodiploidy (<45 chromosomes) | Intensified therapy including allogeneic stem cell transplant in adverse-risk genotypes. Relapses still occur in the numerically-larger good-risk genotypes suggesting that current genotype-based stratification is still imprecise | [13], [14] |
| Response to therapy | | Bone marrow remission (blasts <5%) by light microscopy is seen in ~98% of patients after 4-weeks of treatment and is therefore a poor discriminating measure of response | | | [15] |
| Early prednisolone response | 1983 | A simple measure of early *in vivo* sensitivity to a key agent in therapy, first introduced in ALL-BFM 83 | Circulating blast cell count following a prednisolone prophase still used to stratify risk on the AIEOP-BFM protocols | Still remains a powerful and widely-adopted prognostic determinant in risk stratification; biological basis uncertain and relevance may change in the era of molecular monitoring | [16] |
| Early bone marrow response | 1983 | A measure of early response to therapy based on initial observations in the late 1970s that early response mattered | Residual marrow blast % following 1-2 weeks of therapy still used to stratify risk groups in the CCG and MRC ALL trials | Poor early microscopic marrow blast clearance remains an adverse-risk feature - likely to be supplanted by more sensitive measures of early response such as flow cytometry | [17], [18], [19] |

| | | | | | |
|---|---|---|---|---|---|
| Minimal residual disease monitoring | 1998 | Marrow blast burden post-induction estimated using somatic clonal genomic (immunoglobulin or T-cell receptor rearrangements) or immunophenotypic lymphoblast markers | Genomic clonal marker determination is currently cumbersome and resource-intensive. Flow cytometry detection is at least as sensitive, has higher throughput and may be more widely available | Powerful prognostic determinant. Used as risk-stratification determinant in contemporary MRC and BFM-based protocols. Probable surrogate marker of *in vivo* drug sensitivity. Current sensitivity detection threshold at 1 blast/10,000 cells may need to be enhanced. Does not estimate extramedullary blast clearance | [20], [21], [22], [23] |
| TREATMENT MILESTONES | | Uniformly fatal disease before the 1960s. Combination chemotherapy modelled on efficacy in treatment of tuberculosis and experimental findings in non-human leukaemic cell lines | Remarkable combination of trial-and-error and serendipity. Intrinsic disease chemosensitivity was fortuitous and propelled early advances in therapy. Probability of cure mooted in early 1970 (Simone J Cancer 1972 30:1488-1494) | Success of combination chemotherapy accords with the Goldie-Coldman hypothesis. Efficacy of post-induction intensification complies with the Norton-Simon model of Gompertzian tumour growth characteristics. | [24], [25], [26], [27], [28] |
| | Early 1950s-early 1960s | Initial drugs | Efficacy of folate antagonists and antimetabolites initially demonstrated in a murine leukemia cell line and later as single agents in patients | Folate antagonists and antimetabolites continue to feature as key drugs in contemporary therapy | [29], [30], [31] |
| | Late 1950s-early 1960s | Combination chemotherapy | Folate antagonists, purine anti-metabolites and steroids followed by continuation treatment | Rotating, iterative schedules of intensive therapy followed by the maintenance phase continues to remain the feature of contemporary therapy | [32], [33] |

| | | | | | |
|---|---|---|---|---|---|
| TREATMENT MILESTONES | Mid 1960s-early 1970s | Several key drugs introduced in therapy | Vincristine, L-asparaginase, Daunorubicin, Cytarabine and Cyclophosphamide | These agents remain key components of contemporary treatment protocols. Asparaginase has a singular mechanism of action and is unique and vital in ALL therapy. Cytarabine is chiefly used in treatment of high-risk/refractory disease or as part of intrathecal triple therapy. | [34], [35], [36], [37], [38] |
| | Since late 1960s | Supportive care to manage complications of cytotoxic therapy | Platelet transfusion, management of febrile neutropenia, prophylaxis of Pneumocystis *jirovecii* pneumonia, recognition of varicella zoster risk, recognition and management of vascular thrombosis | Septic death secondary to neutropenia is an important cause of remission mortality (2-5%). Vigilance, institutional protocols, early empirical institution of broad-spectrum antimicrobials, appropriate radioimaging and adaptation of antimicrobial therapy to microbiological investigations form key elements of management. Judicious use of growth factors to accelerate haematopoietic recovery | [39], [40], [41], summarised in [42], [43] |
| | Mid 1980s | Etoposide | Introduced as a non-crossresistant agent | Risk of epipodophyllotoxin-related secondary myeloid leukaemia relegated use of drug in relapse-refractory disease | [44], [45] |
| | 1980s-2000s | No new agents but steady improvement in outcomes following progressive refinements in therapy | Optimisation of key treatment elements and improvements in supportive care | Advances driven by systematic clinical trials conducted by multicentre trial consortia (the BFM and CCG) and large treatment centres (St Jude Children's Research Hospital, the Dana-Farber Cancer Institute) | Reports from several large trial groups summarised in [46] |

| | | | | | |
|---|---|---|---|---|---|
| TREATMENT MILESTONES | Late 1980s | Allogeneic hematopoietic stem cell transplantation (allo-SCT) - systematic evidence of benefit in the mid-1990s | Ablative chemoradiotherapy conditioning followed by infusion of allograft from genotypically HLA-matched related or unrelated donors; stem cell source may include bone marrow, peripherally mobilised or umbilical cord stem cells | Contemporary risk-adapted intensification of therapy has largely confined use of allo-SCT to very high-risk (e.g., subsets of Ph+ ALL), refractory or early-relapse disease subsets. Further restricted utility envisaged in line with future advances in chemotherapy. Long-term complications adversely impact overall survival. | [47], summarised in [48] and [49] |
| | Mid-2000s | Rationally-designed new generation of purine nucleoside analogues - clofarabine and nelarabine | First new agents in childhood ALL therapy after nearly two decades | Use chiefly in relapsed-refractory disease - nelarabine has specific activity in T-lineage disease | [50], [51] |
| | Late 2000s | Targeted therapies exemplified by the tyrosine-kinase inhibitor, Imatinib mesylate | Biological therapies targeting cell survival pathways, enhancing cell death mechanisms or accelerating leukaemic cell clearance | Potential role in high-risk or relapsed/refractory disease as adjuvant to chemotherapy and/or allo-SCT | [52] |
| <u>RISK-ADAPTED THERAPY</u> | | | | | |
| Risk stratification | Late 1980s | Risk-adapted therapy enabling tailored intensity of treatment | Current risk stratification based on presentation and response characteristics (see above). Maximally intensive treatment reserved for patients deemed at highest risk of relapse | Risk characteristics are still imprecise. Sensitive measures of early response and additional biological characteristics (including germline pharmacogenomics) likely to result in further fine-tuning and probable individualisation of therapy | [12], [53], [54], [55] |

| | | | | | |
|---|---|---|---|---|---|
| Minimising toxicity from overtreatment | 1990s | As cure rates improved, therapy refined to prevent overtreatment and minimise acute (sepsis) and long-term (organ dysfunction, growth and cognitive deficits, second neoplasms) treatment-related complications | Risk-adapted therapy and refinements in treatment elements (next column) minimises overtreatment in standard-risk patients at lowest risk of relapse | Elimination of cranial irradiation (below), cumulative anthracycline dose reduction, pulsed dosing to decrease risk of dexamethasone-related avascular osteonecrosis, long-term monitoring | [56], [57], [58], [59] |
| <u>TREATMENT COMPONENTS</u> | | | | | |
| Induction (also referred to as remission-induction) | 1960s | Arguably the most important phase of treatment; timely administration is critical and early response to this phase is a powerful prognostic determinant of outcome | 4-week induction phase with a steroid, vincristine, L-asparaginase backbone, intrathecal therapy ± an anthracycline | The now widely-adopted BFM-pioneered intensified induction (otherwise called Induction-Consolidation or Protocol IA/IB) using non-cross-resistant drugs in an 8-week schedule for intermediate- and high-risk disease groups | |
| Central Nervous System (CNS)-directed treatment (less accurately referred to as CNS prophylaxis) | Early 1970s | The CNS is a sanctuary site for ALL blasts from a combination of CNS tropism of lymphoblasts and poor CNS penetration of chemotherapy. Non-inclusion of this phase of therapy is inevitably attended by disease recurrence in the CNS [60] | Intensified systemic and extended intrathecal therapy has largely superseded cranial irradiation | Craniospinal radiotherapy (RT) initially, later replaced by combination of cranial RT and intrathecal therapy (IT) | [61], [62], [63], [64], [65] |

| | | | | | |
|---|---|---|---|---|---|
| CNS-directed treatment | | | Use of CNS-penetrating systemic agents, specifically methotrexate, either as a dedicated CNS treatment block (BFM protocols) or in high-risk disease, as a component of augmented post-induction intensification; beneficial effect of dexamethasone | Serial reduction of cranial RT dose - from 24Gy to 18Gy, then 18Gy to 12Gy - while intensifying systemic and intrathecal therapies; later restricting cranial RT only to those at high-risk of recurrent CNS leukaemia (overt CNS leukaemia at presentation, T-lineage high-risk disease) | [57], [66], [67], [68], [69] |
| | | | Significant cognitive and neuroendocrine sequelae (growth and pituitary gonadal failure) and importantly, second malignant neoplasms (gliomas) with cranial RT | Systemic and intrathecal methotrexate therapy also associated with complications (acute-stroke like syndromes, cerebral white matter changes, arachnoiditis); dexamethasone associated with osteonecrosis and increased susceptibility to invasive fungal infections | [70], [71], [72] |
| Post-induction intensification (less commonly described as re-induction) | Early 1980s | Agents used during induction therapy are re-administered in hybrid schedules during this phase | Intensification improves outcomes in all risk categories and is in keeping with the Norton-Simon model | Double-delayed intensification for all patients other than those with standard-risk disease; augmentation with Capizzi schedules (in sequence, high-dose antimetabolite followed by L-asparaginase) and intensified L-asparaginase schedules in high-risk disease | [73], [74], [75], [76], [77], [78], [79] |

| | | | | | |
|---|---|---|---|---|---|
| Maintenance or Continuation therapy | 1960s | 18-24 months of low-dose antimetabolites (a thiopurine and methotrexate) ± pulses of vincristine and steroid. Unique treatment phase, now adopted in other haematological cancers (acute promyelocytic leukaemia, multiple myeloma, follicular non-Hodgkin lymphoma) | Metronomic therapy with dosing of antimetabolites to haematological tolerance; important phase of contemporary therapy but biological basis poorly understood and may include direct cytotoxicity of residual quiescent blasts, activation of immune clearance or promoting differentiation of residual blasts | In the context of current treatment intensity, antimetabolite-based maintenance alone may be sufficient; shortening duration below 18 months attended by increased recurrence while lengthening therapy beyond 3 years confers little additional benefit. Concern over antimetabolite-related second neoplasms [85] | [80], [81], [82], [83], [84], [85], [86] |
| Adjuvant targeted therapy | Late 2000s | Targeted therapies will increasingly feature in future treatment protocols | Biological targets suggested by global microarray technologies and by extrapolation of experience in other haematological malignancies | Impressive early event-free survival when a continuous Imatinib dosing schedule was combined with conventional chemotherapy in childhood Ph+ ALL | [87], [88] |

Collaborative childhood ALL study groups: AEIOP, Associazonie Italiana Ematologia Oncologica Pediatrica; BFM, Berlin-Frankfurt-Münster consortium (Germany-Austria-Hungary); CCG, North American Children's Cancer Group; UK MRC, UK Medical Research Council; FAB, French-American-British; Gy, gray (100 Rad); HLA, human leucocyte antigen; NCI, National Cancer Institute

**Table 1.2 Somatic genetic lesions in childhood acute lymphoblastic leukaemia** (also see **Fig 1.5**)

| | | | |
|---|---|---|---|
| Progenitor-B ALL | | | |
| Numerical abnormalities | Good Risk | Hyperdiploidy (modal chromosome number >46), particularly high hyperdiploidy (51-65 chromosomes), arising from somatic non-disjunction in an early committed progenitor. Most common genetic subtype (25-30%). Early pre-B immunophenotype. Typically extra copies of chromosomes 4, 6, 10, 14, 17, 18, 21, X. Subset with trisomies of chromosomes 4, 10, 17 experience especially good outcome. Associated FLT3-mutations (of the activating loop or internal tandem duplications) in 20-25%, uncertain significance. Methotrexate sensitive. | [95], [96], [97], [98] |
| | Poor Risk | Low hypodiploidy (35-45 chromosomes) and near-haploidy (24-34 chromosomes). Rare (2-3%). Arise from unbalanced translocation, single chromosome losses or dicentric chromosome formation. | [99] |
| Fusion translocations | | Aberrant recombinase-activating-gene activity during the course of immunoglobulin (Ig) loci rearrangements in maturing progenitor B cells, resulting in illegitimate in-frame fusion rearrangements of gene segments clustered topologically in nuclear transcription hubs. Most occur *in utero* and require second hits for leukaemogenesis | [100] |
| | Good Risk | *ETV6-RUNX1* [t(12;21)(p13;q22)]. 20-25%, typically in children 2-6 years. Early pre-B immunophenotype. Cryptic lesion, detected by FISH. Helix-loop-helix domain of *ETV6* fused to DNA-binding and transactivation domains of *RUNX1*. Well-established *in utero* origin, second-hit lesions include deletion of wild-type *ETV6* allele. Asparaginase-sensitive | [101], [102], [103] |
| | | *TCF3-PBX1* (also *E2A-PBX1*) [t(1;19)(q23;p13)]. 4-6%, probable post-natal origin, often (25%) in late pre-B cells expressing cytoplasmic Ig. Transactivation domains of TCF3 fused to homeodomains of PBX1. Associated with high presenting WBC count and propensity for CNS relapse. Contemporary therapy has nullified previous adverse prognosis. | [104], [105], [106] |
| | Poor Risk | *BCR-ABL1* [t(9;22)(q34;q11)] associated with the Philadelphia chromosome (Ph+). 3-5%, early pre-B immunophenotype. The typical e1-a2 *BCR-ABL1* fusion encodes a cytoplasm-localised chimaeric 185-190 kDa molecule with aberrant ABL1 kinase activity. Associated with older age, high WBC count, overt CNS disease and slow early response. Imatinib-responsive. | [107] |

**Table 1.2 (continued)**

| | | | |
|---|---|---|---|
| Progenitor-B ALL; Fusion translocations | Poor Risk | *MLL* gene (11q23) rearrangements. Typically associated with infant leukaemias (>70%), often biphenotypic. Multiple partner genes. Chimaeric proteins with amino-terminal MLL elements. *MLL-AF4* most common [t(4;11)(q21;q23)] in ALL. Occur *in utero*, sufficient for leukaemogenesis, pro-B (often CD10 negative) immunophenotype. FLT3 overexpressing. Associated with high WBC count, CNS disease and poor response to treatment. | [108], [109] |
| | | *TCF3-HLF* [t(17;19)(q22;p13)]. Rare (<1%). Pro-B immunophenotype, chimaera containing amino-terminal of TCF3 transactivation domain fused to the basic leucine zipper domain of HLF. Often presents with disseminated intravascular coagulopathy. Impaired lymphoblast apoptosis in vitro. Particularly poorly responsive. | [110] |
| Segmental amplifications | Poor Risk | Intrachromosomal amplification of (the long-arm segment of) chromosome 21 (iAMP21), probably from chromosome breakage-fusion-bridge cycles. Typically detected by observing clustered *RUNX1* signals (>3) on interphase FISH. 2-3%. Early pre-B immunophenotype, older age, low WBC count. Probably responsive to intensified methotrexate therapy. | [9] |
| Recurrent submicroscopic lesions | | Whole-genome single nucleotide polymorphism analyses, both in diagnostic material and paired diagnosis-relapse material indicate (a) a limited number of highly focal lesions (mean of six per case) (b) lesions are typically, deletions (c) deletions often involve genes encoding lymphoid transcription factors (40%, e.g. *PAX5*) or cell-cycle regulators (e.g. *CDKN2A/B*) (d) both diagnosis and relapse blasts demonstrate common clonal origins | [10] |
| | Poor Risk | Deletions of Ikaros (*IKZF1*) noted in 80-85% Ph+ALL. On directed sequencing, activating mutations of Janus family kinases (JAK) in ~10% BCR-ABL1 negative ALL, frequently associated with *IKZF1* deletion and with gene-expression profiles similar to Ph+ ALL. Recently reported overexpression of the cytokine CRLF2, either due to intrachromosomal deletion or Ig heavy-chain rearrangements, also co-associates with *IKZF1* and Janus family kinase mutations and specifies a poor-prognosis subgroup | [88], [118], [119], [120], [121] |
| Precursor T ALL | | Genetic risk-based stratification not fully characterised in T-lineage disease. Genetic lesion is linked to maturational stage and the latter may be a more important determinant of outcome in T-lineage disease. | [111], [112], [113], [114] |
| Fusion translocations | | Result in aberrant activation of structurally intact proto-oncogenes (*TAL1*, *TAL2*, LIM-only domain proteins *LMO1* and *LMO2, TLX1 [HOX11], TLX3 [HOX11L2], LYL1, MYB, BHLHB1, LCK, NOTCH1, CKND2* ) | |

**Table 1.2 (continued)**

| | | |
|---|---|---|
| Precursor T Cell; Fusion translocations (continued) | | Protooncogene activation following fusion with promoter-enhancer elements of T cell receptor (TCR) genes on 14q11 (*TCRA/D*) or 7q34 (*TCRB/G*) - one example is the *TLX1-TCRA/D* fusion [t(10;14)(q24;q11)] in 4-7% childhood ALL associated with cortical pre-T (CD1a+) immunophenotype and a favourable outcome |
| | | Non-TCR gene fusions, e.g. *NUP214-ABL1* fusion (rare, episomal localisation, Imatinib-sensitive); *CALM-AF10* fusion (10%, gamma-delta T-lineage blasts, poor outcome) |
| Amplifications and deletions | Variable risk | Examples include (1) Intrachromosomal deletions resulting in overexpression of LMO2; *SIL-TAL1 (*or *SIL-SCL)* in 1p32, fusing the promoter of *SIL* with the coding region of *TAL1*, 25% T-lineage ALL, male predominance, conflicting prognostic impact (2) *MYB* amplification (amplified 6q22.3) |
| Recurrent submicroscopic features | Uncertain risk | Spanning the spectrum of chromosomal lesions is activated intracellular Notch1 activity, primarily due to mutations in component molecules (>50%) or rarely, due to the t(7;9) (q34;q34.3)] translocation. Targeting aberrant Notch signalling has therapeutic potential in T-lineage disease |
| | Secondary driver lesion | Deletion in the *CDKN2A/B* tumour suppressor locus (75%) |

CNS, central nervous system; CRLF2, cytokine receptor-like factor 2; FLT3, fms-like (receptor) tyrosine kinase 3; FISH, fluorescent in-situ hybridisation

**Table 1.3 Biology of ALL Relapse**

| | | |
|---|---|---|
| Investigations | Global somatic and germline genome and transcriptome microarrays investigating paired (± lymphoblast-enriched) diagnosis-relapse samples; correlation of gene-expression profiles in diagnostic lymphoblasts with designated outcome endpoints such as relapse-free survival or end-induction minimal residual disease (MRD) burden | |
| Clonal origin of relapse | A significant proportion arise from pre-leukaemic ancestral clones that have acquired second-hit somatic lesions | [117]; **Figure 1.12** |
| Lymphoblast characteristics | An aberrant activated kinase expression signature associated with autocrine survival signalling, probably resulting in accelerated blast proliferation, chemoresistance and creation of autonomous tumour niches; traditional cancer resistance mechanisms such as exaggerated drug-efflux (e.g. through P-glycoprotein overexpression) or somatic *TP53* tumour suppressor gene mutations are not typically observed in relapse lymphoblasts | [118], [88], [119], [120], [121], [122], [123] |
| Host germline polymorphisms | Associated with variations in drug metabolism (Thiopurine Methyl Transferase [*TPMT]* polymorphisms and thiopurine metabolism), drug clearance (methotrexate, etoposide) and intracellular drug accumulation (methotrexate polyglutamates) | [124], [125] |
| Role of the tumour microenvironment | By restricting drug access (extramedullary sanctuary sites) and by pro-survival paracrine interactions mediated by adhesion-dependent or -independent mechanisms | [126], [127] |

**Table 1.4 Extramedullary disease in ALL: putative molecular and cellular mechanisms**

| *Event* | *Probable Mechanisms* | *References* |
|---|---|---|
| Bone marrow egress and extramedullary tropism | Subversion of the physiological trafficking behaviour of lymphocytes | [129], [130] |
| Candidate chemokine signalling mechanisms | VEGF-VEGFR1 axis | [131], [132] |
| | CXCR4-CXCL12 axis | [133], [134], [135] |
| | The homing-adhesion molecule CD44 and its variant CD44v6 | [136], [137], [138] |
| | Other chemokine molecules: CCR7 and IL-15 | [139], [140], [141] |
| Stromal-endothelial adhesion | Reciprocal interactions of blast cell VLA-4/VLA-5 integrins with stromal-endothelial cell adhesion molecules and extracellular matrix components; integrin activation and signalling triggers cytoskeletal reorganisation | [142], [143], [144], [145], [146] |
| Lymphoblast extravasation | Deployment of probing podosomes followed by paraendothelial / transendothelial diapedesis | [147], [148], [149] |
| Extracellular matrix degradation | The gelatinase family of matrix metalloproteases (MMP), MMP2 and MMP9; may be integrin-anchored (forming a supramolecular complex capable of outside-in signalling and localised degradation) or released as soluble enzyme | [150], [151], [152], [153] |
| | Lysosomal cysteine proteases | [154], [155] |
| Extramedullary nests | Haematopoietic cells capable of creating novel extramedullary niches | [156], [157], [123] |
| | Egressed VEGFR1-positive cells may establish precursor extramedullary niches | [158] |

**Table 1.4 (continued)**

| *Event* | *Probable Mechanisms* | *References* |
|---|---|---|
| Persistence in extramedullary niches through chemoevasion and autocrine-paracrine survival signalling | Prosurvival ligand-independent or ligand-hypersensitive kinase signalling - VEGF; CD44-CXCR4-CXCL12-p38MAPK; JAK-STAT | [159], [160], [161] |
| | Stroma-induced chemoprotection and survival signalling - adhesion-dependent and independent mechanisms | [162], [163], [164], [165] |
| | Tumour dormancy | [166], [167] |

CCR7, chemokine (C-C) motif receptor 7; CLL, chronic lymphocytic leukaemia; CXCR4, chemokine (CXC motif) receptor 4; CXCL12, chemokine (CXC motif) ligand 12 (also known as stromal-derived factor 1 (SDF-1); JAK, Janus family kinases; p38MAPK, p38 mitogen-activated protein kinase; STAT, signal transduction and activator of transcription family of transcription factors; VEGF, vascular endothelial growth factor; VEGFR1, vascular endothelial growth factor receptor 1; VLA-4, very late antigen 4, integrin heterodimer of $\alpha$4(CD49d)-$\beta$1(CD29); VLA-5, very late antigen 5, integrin heterodimer of $\alpha$5(CD49e)-$\beta$1

# 2

# Asparagine endopeptidase – a candidate molecular marker of treatment failure in childhood ALL

Relapses in the CNS are a recurring and increasingly more prominent feature of treatment failure in childhood ALL. In an attempt to identify candidate molecular markers associated with this adverse disease characteristic, oligonucleotide microarrays were employed as discovery tools.

As a first step, microarrays were used to examine the global transcript signature of a distinct adverse-risk genetic subtype of progenitor-B ALL [1]. This recently recognised genotype is characterised by intrachromosomal amplification of chromosome 21 (iAMP21 ALL) [2]. Adverse-risk progenitor-B childhood ALL genotypes are typically associated with poor early treatment response and a higher incidence of relapse, including high-risk relapses (Chapter 1, [95]). Thus, the relative risk of relapse is six-fold higher in iAMP21 ALL (Chapter 1, [95]) and includes a disproportionate high incidence of early CNS relapses [2].

Microarray analysis was later extended to include examination of global transcript profiles of primary leukaemic cells across genetic and risk categories of childhood ALL (n=89, [1]). Comparative gene expression profiling identified unique overexpression of the gene encoding the lysosomal cysteine protease, asparagine endopeptidase (AEP), in iAMP21 ALL (**Figure 2.1**). Extended analysis indicated that the gene was similarly overexpressed in the archetypal adverse-risk B-lineage disease, Philadelphia-chromosome positive ALL (Ph+ ALL) (**Figure 2.2**).

### AEP, the invasive cancer phenotype and ALL treatment failure

AEP is a distinct and evolutionarily conserved lysosomal cysteine protease. The enzyme, along with other cysteine proteases, is a well-recognised mediator of

host tissue invasion by parasites (**Table 2.1**). AEP is characterised by its singular cleavage specificity, typical acid pH-activated maturation sequence and restricted tissue expression in humans (**Figure 2.3**, **Table 2.2**) Expression is physiologically bimodal in B lymphocytes and occurs at the extremes of B-cell ontogeny, in early progenitor cells (**Figure 2.4)** and mature plasma cells [25].

AEP overexpression is a feature of several adult human epithelial cancers (**Figure 2.5**, **Table 2.3**). Overexpression is associated with metastatic disease and adverse prognosis (**Table 2.4**) and analogous to observations in parasite pathogens, ectopic AEP expression confers human cells with a motile phenotype (**Figure 2.6**).

Aberrant expression and activity of lysosomal hydrolases is well-recognised in cancers and putatively operates through several mechanisms to promote cancer cell motility and tissue invasion (**Table 2.5**). Overexpressed AEP in progenitor-B lymphoblasts could conceivably promote leukaemic infiltration of the CNS as well as dissemination to other extramedullary sites, where persistence of disease eventually manifests as relapse.

Adverse-risk progenitor-B ALL genotypes are also characterised by poor response to conventional treatment (Chapter 1, [95]). Intrinsic drug resistance may in part account for this. In this context, AEP, a proteolytic enzyme, is potentially capable of degrading the bacterial protein drug, *E. coli* L-asparaginase (ASNase). ASNase is a critical component of childhood ALL therapy and its accelerated inactivation by AEP-overexpressing leukaemic cells could possibly contribute to inferior treatment response.

AEP is thus a plausible candidate biomarker of treatment failure in childhood progenitor-B ALL (**Figure 2.7**). The subsequent chapters discuss results of *in vitro* studies investigating this hypothesis.

**Figure 2.1** Serial comparison of microarray gene expression signatures identified unique overexpression of AEP in the adverse-risk progenitor-B ALL subtype, iAMP21

Schematic outline of analysis workflow. To identify genes uniquely overexpressed in the adverse-risk ALL subtype iAMP21, step-wise comparisons of gene expression signatures were performed. The initial assessment was a comparison of iAMP21 expression profile against that of all other ALL subtypes as a group. Like iAMP21, the genetic subtypes *ETV6-RUNX1* and high-hyperdiploidy also demonstrate somatic aberrations of chromosome 21 but unlike iAMP21, both subtypes are associated with good outcome. Thus, comparative analysis of expression profiles with *ETV6-RUNX1* and high-hyperdiploidy helped define both a unique and biologically pertinent iAMP21 overexpression signature. This stepwise approach identified AEP as the top uniquely overexpressed gene in iAMP21 ALL. Adapted from [1].

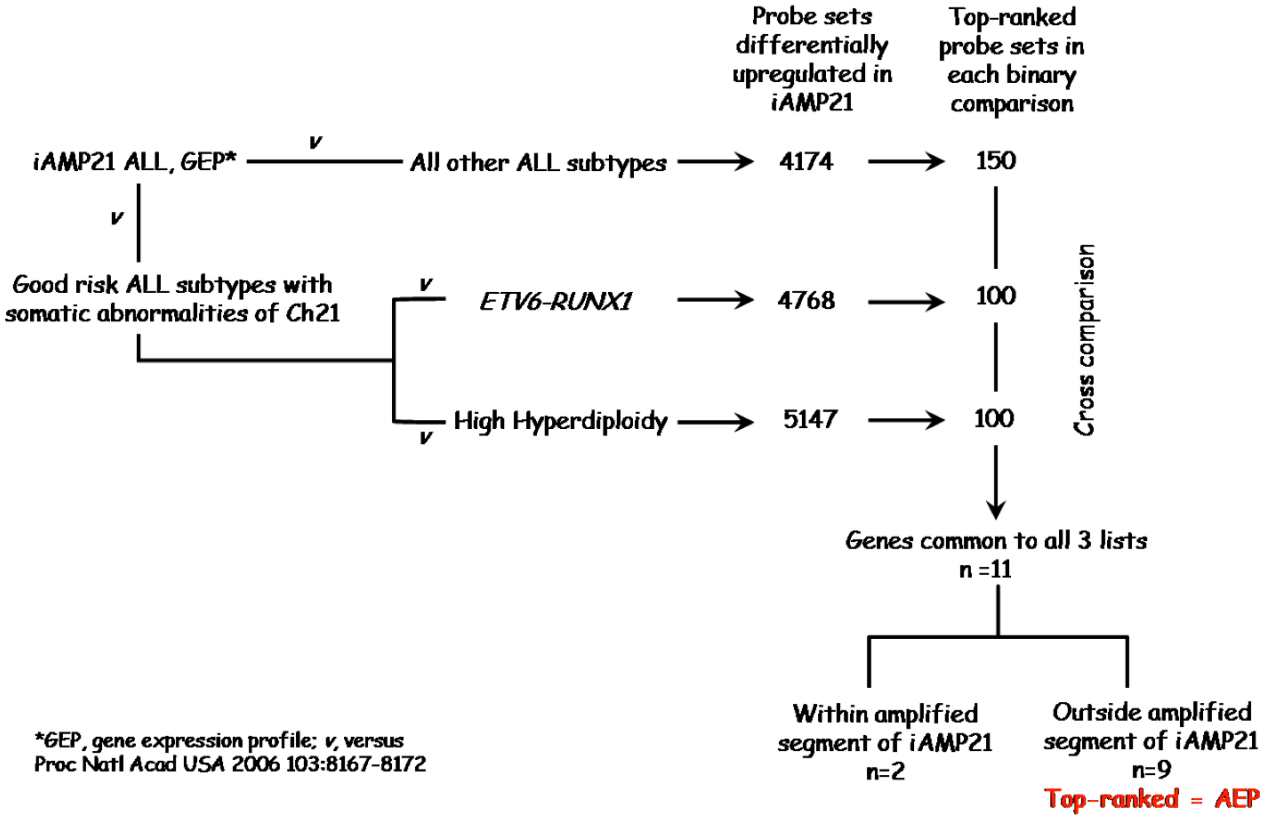

**Figure 2.2** AEP is relatively overexpressed in adverse-risk progenitor-B ALL

Boxplot representation of microarray analyses of AEP transcript expression in childhood ALL (n=89). Median relative AEP expression is higher in the adverse-risk progenitor-B disease subtypes, Philadelphia-chromosome positive ALL (BCR-ABL) and iAMP21, although there is considerable overlap in expression. Of note, these adverse-risk ALL subtypes are associated with a higher incidence of central nervous system (CNS) leukaemia at relapse. *Data courtesy of Frederik van Delft and Olga Yiannikouris, CRUK Children's Cancer Group;* reported in [1]

The fusions translocations (BCR-ABL [or Ph+ALL], E2A-PBX1 [or TCF3-PBX1] and ETV6-RUNX1 [or TEL-AML1]), high hyperdiploidy (HD50), intrachromosomal amplification of chromosome 21 (iAMP21) and the 'Others' category represent genetically distinct subsets of progenitor-B ALL. Boxes encompass the interquartile (IQR, 25$^{th}$-75$^{th}$ percentile) ranges, horizontal bars within boxes represent median values, '+' values indicate means, whiskers denote values 1.5× IQR, outlier values are represented by asterisks, dashed lines demarcate off-scale outlier values.

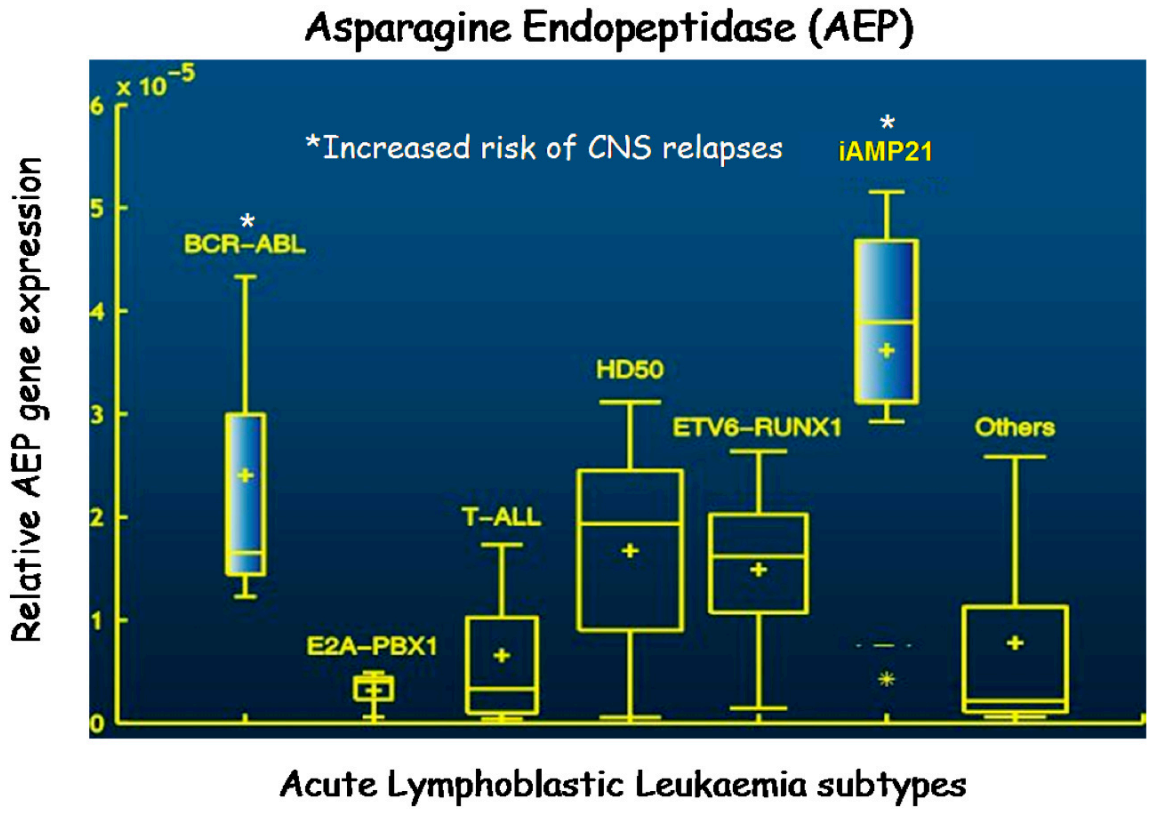

**Figure 2.3**: Asparagine endopeptidase (AEP) is a lysosomal cysteine protease distinct from the papain family cathepsin enzymes. The protease is activated by increasing endolysosomal acidification and demonstrates strict cleavage specificity.

(A) Cartoon representation indicating role of lysosomal proteases in antigen-presenting cells. AEP, like other lysosomal cysteine proteases, processes exogenous microbial peptide antigens and the invariant chain to facilitate MHC Class II molecule loading towards T-cell presentation (B) AEP differs from the papain family of cathepsin (CTS) lysosomal cysteine proteases in terms of its strict cleavage specificity and resistance to the pan-cathepsin inhibitors E-64 and Leupeptin. (C) As with other lysosomal cysteine proteases, the mature active enzyme is generated *in vivo* by a combination of acidification-triggered autocleavage and additional processing by extrinsic proteases. The initial unimolecular activation involves sequential autocleavage at carboxyl- (asparagine residue [N] at position 323) and amino-terminal (aspartate residue [D] at position 25) amino acid (AA) residues. Additional processing involves carboxyl-terminal trimming by as-yet unidentified proteases. (D) AEP demonstrates strict carboxyl-terminal endoproteolytic cleavage specificity for selected asparagine and (to a lesser extent) aspartate residues [3]

*C ter, carboxyl terminal; N ter, amino terminal; Xaa, any amino acid residue*

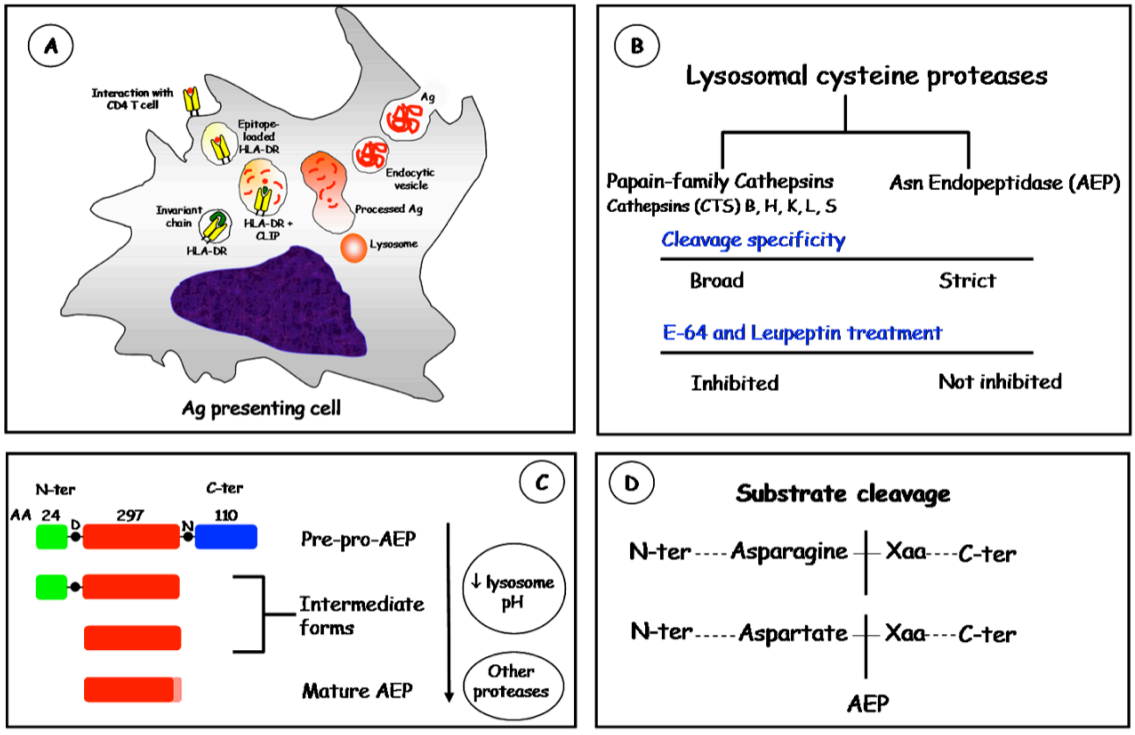

**Figure 2.4** Serial AEP expression across early B cell ontogeny

AEP transcript expression at various stages of early B cell maturation, as determined by microarray analyses of purified isolates from human placental blood. *Upper panel*: Distinct stages of early B-cell maturation, identified by typical expression profiles of surface CD (cluster of differentiation) antigens and nuclear TdT expression. Differentation is sequentially characterised by immunoglobulin heavy chain (IgH) locus rearrangements, surface pre-B cell receptor (BCR) expression, immunoglobulin light chain locus rearrangements (rIgL) and surface IgM expression. *Lower panel*: A sharp peak in AEP expression is observed in pro-B cells, possibly suggesting a role for AEP as proteolytic mediator of adhesive interactions with bone marrow stromal cells, a key feature at this stage of early B-cell maturation [51]. (Created from data in [52]).

*CD34/Lin-, connotes putative lineage-negative haematopoeitic stem cells; cIgμ, cytoplasmic Ig μ heavy chain; cIg, cytoplasmic immunoglobulin M; cy, cytoplasmic; $D_H$-$J_H$, rearrangements of diversity and joining regions of IgH gene locus; TdT, terminal deoxynucleotidyl transferase; $V_H$-$D_H$, rearrangements of variable and diversity regions of IgH gene locus; $VDJ_H$, completed VDJ rearrangement at IgH gene locus*

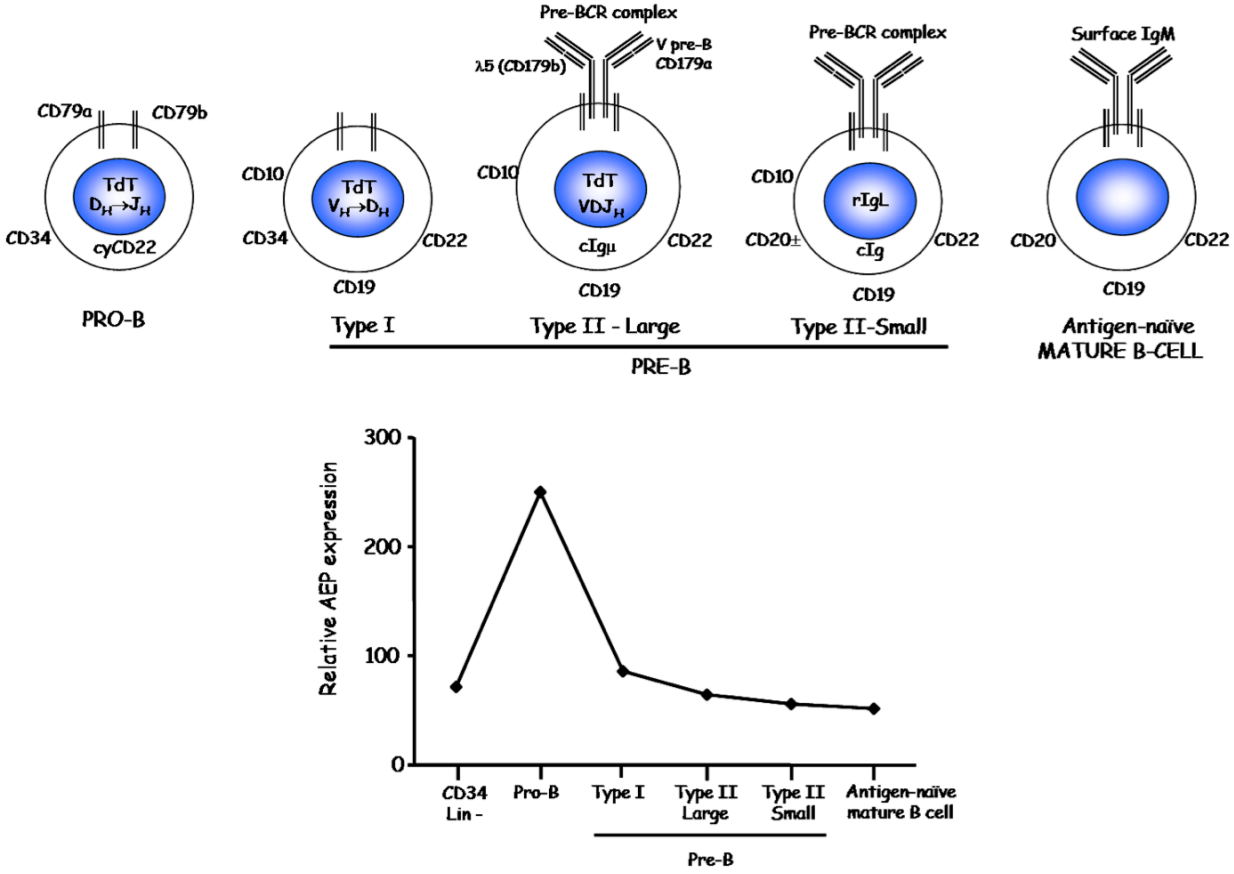

**Figure 2.5** Asparagine endopeptidase (AEP) in solid human cancers

Select data from published reports [24, 61]. AEP overexpression has been reported to be a feature of many adult epithelial cancers (table). Experiments using a cell-impermeable doxorubicin prodrug provide surrogate evidence of extracellular AEP release. The red fluorescent anthracycline doxorubicin (Doxo) was tagged to an AEP-substrate linker sequence to create a cell-impermeable compound. Presumed cleavage of the substrate linker by extracellular AEP enabled free Doxo to penetrate cells, as evidenced by bright red fluorescent staining in AEP-expressing 293 cells (AEP+293) compared to wild-type controls (293-WT). A molecular basis for AEP's role in cell invasion is suggested by immunofluorescence staining showing colocalised expression of AEP and the β1-integrin cell adhesion subunit in AEP+293 cells.

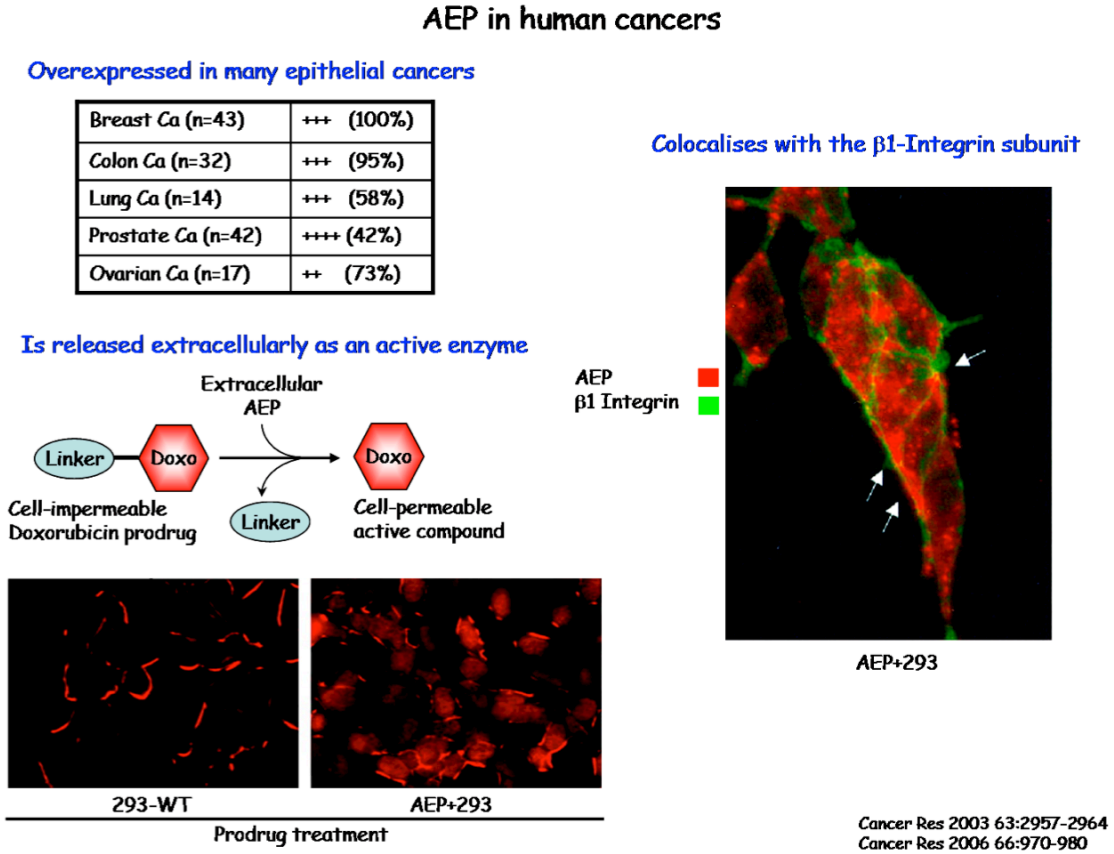

**Figure 2.6** Enforced expression of AEP in HEK293 cells results in a motile phenotype – results reported by the Scripps Institute Immunology group [24]

Results of Boyden chamber assays using (A) uncoated and (B) Matrigel-coated cell inserts. AEP-overexpressing HEK293 cells (AEP-293) migrated briskly across both uncoated and Matrigel-coated 8μm-pore cell culture inserts. By contrast, native HEK293 control cells were essentially immotile. Motility was attenuated by nearly 50% when cells were treated with the non-selective AEP inhibitor (AEPi) cystatin. Treatment with the non-selective MMP-2 (matrix metalloprotease 2) inhibitor (MMPi), TIMP-2 also modestly decreased trans-Matrigel motility, suggesting that at least part of the invasive phenotype could be attributed to (AEP-activated) MMP-2. The motile phenotype of AEP-293 cells was not modified by the broad-spectrum inhibitor of the papain family Cathepsins, E64 (CTSi).

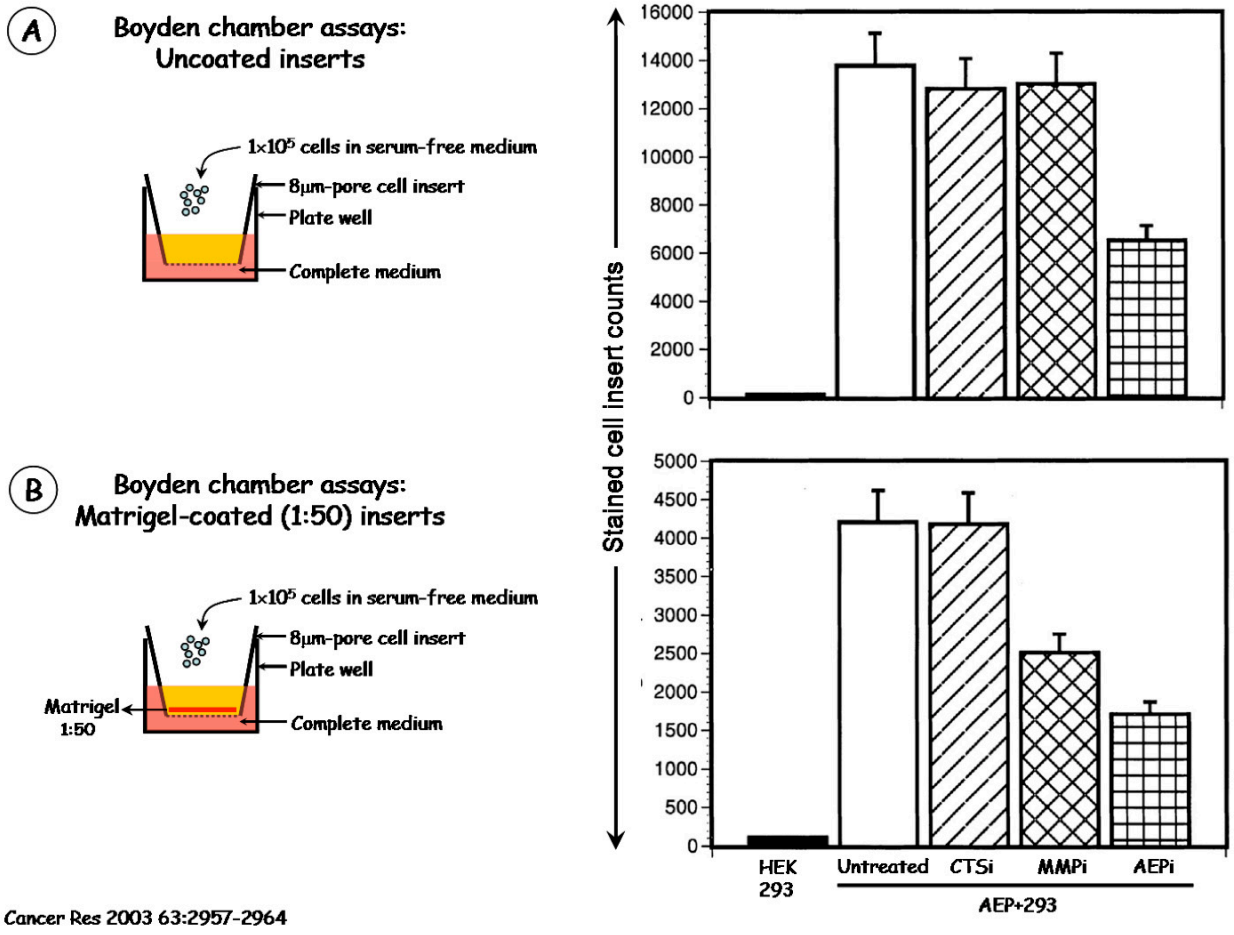

**Figure 2.7** *In vitro* studies investigating AEP as a candidate biomarker of treatment failure in childhood progenitor-B ALL

Schematic outline; proposed *in vitro* studies are represented in blue. Global gene-expression microarray studies in childhood acute leukaemia identified AEP overexpression in the adverse-risk progenitor-B ALL genotypes, Philadephia-chromosome positive ALL (Ph+ ALL) and intrachromosomal amplification of chromosome 21 (iAMP21). These observations shall be validated by transcript quantitation, protein expression and imaging studies. Both Ph+ ALL and iAMP21 ALL are associated with an increased incidence of relapse, including CNS relapse. AEP overexpression in leukaemic blasts of these subtypes is postulated to augment cell motility and contribute to extramedullary infiltration and recurrence. This pro-motility role of AEP would be investigated by examining the effect of ectopic AEP expression on the motility phenotype of human embryonic kidney fibroblasts. Another feature of adverse-risk disease is poor response to treatment. Both slow early response and sluggish clearance of minimal residual disease (MRD) result in disease persistence and relapse. Innate drug resistance may in part account for poor response to treatment and AEP is postulated to be a molecular mediator of this phenotype, possibly by degrading and inactivating the bacterial enzyme *E. coli* L-asparaginase (ASNase), a vital component of ALL treatment.

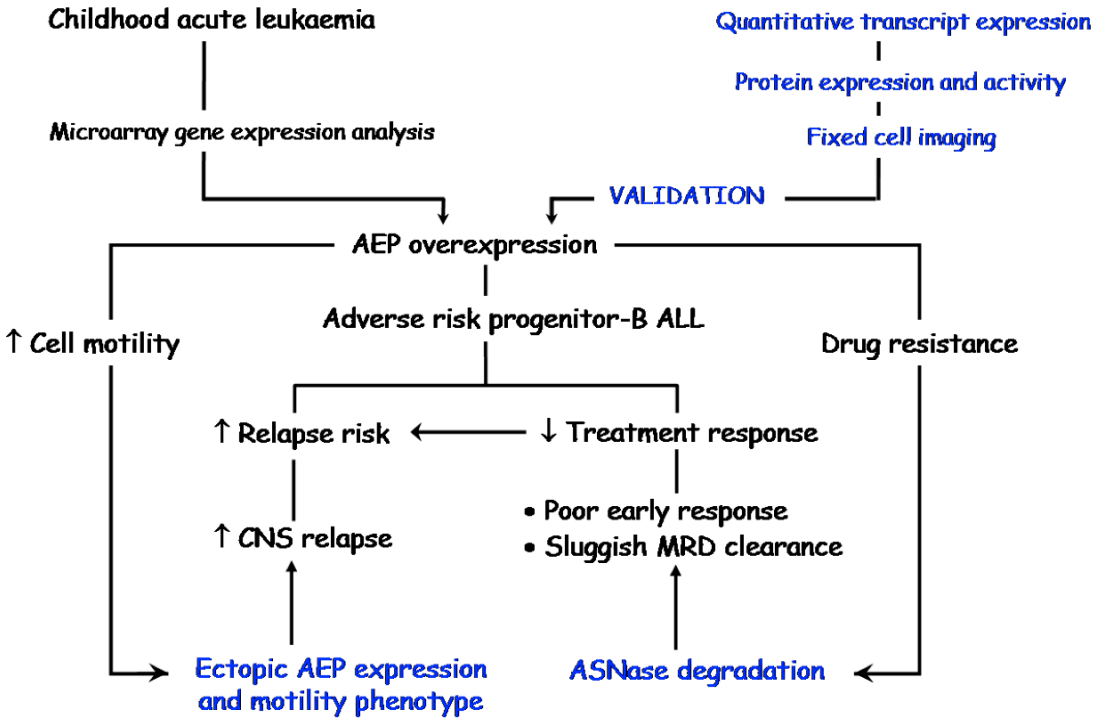

**Table 2.1 AEP in parasites**

| | | | | |
|---|---|---|---|---|
| Activation of other cysteine proteases, host tissue digestion/penetration, excystment/encystment, immune evasion, programmed cell death | | | | [4] |
| *Parasite* | *Species* | *Human pathology* | *Significance of AEP homolog* | *Reference* |
| Protozoa | Trichomonas *vaginalis* | Trichomoniasis | Serological marker of infection and potential candidate for vaccine targeting | [5], [6] |
| | Blastocystis *hominis* | Uncertain human pathology | Antibody targeting of surface-localised homolog activates programmed death | [7] |
| Trematodes | Schistosoma *mansoni* | Human Schistosomiasis | AEP homolog Sm32 in gastrodermal cells of adult worms and head glands of cercariae. Role in enteral digestion of host haemoglobin. Sm32 DNA vaccine protective against cercarial challenge *in vivo* | [8], [9], [10], [11] |
| | Schistosoma *japonicum* | Human Schistosomiasis | Serological marker of infection. DNA vaccine targeting AEP homolog Sj32 protective against cercarial challenge in vivo | [12] |
| | Opisthorchis *viverrini* | Cholangitis and cholangiocarcinoma in humans | AEP homolog Ov-AEP-1 - serological marker of infection and candidate target for therapy | [13] |
| | Fasciola *hepatica* | Human Fascioliasis | Identified in excysted juveline stage of parasite | [14] |
| | Clonorchis *sinensis* | Cholangitis, cholangiocarcinoma | Serodiagnostic antigen | [15] |
| Nematodes | B *malayi* | Lymphatic filariasis | Bm-CPI-2 cysteine protease inhibitor targets human AEP | [16] |
| Arachnids | Ixodes *ricinus* | Vector for Lyme Disease (Borreliosis) | Homolog IrAE in gut digests host blood meal | [17], [18], [19] |
| | Haemophysalis *longicornis* | Vector for Lyme Disease (Borreliosis) | Homolog HlLgm2 in tick midgut | [20], [21], [22] |

**Table 2.2 Known physiological functions of mammalian AEP and implicated role in non-neoplastic disease**

| *Context* | *Comments* | *References* |
|---|---|---|
| Restricted tissue expression | Proximal tubular epithelial cells of the kidney, placental trophoblast, antigen-presenting cells (activated B lymphocytes and mature plasma cells, macrophages, dendritic cells) and monocyte-macrophage derived cells (osteoclasts in bone, Kupffer cells in liver) | [23], [24], [25] |
| Adaptive immune response | Redundant and context-specific role | |
| Antigen-presenting cells | Invariant chain cleavage to facilitate MHC Class II loading | [26] |
| | Redundant but preferential proteolytic processing of microbial antigen (Tetanus toxin C fragment) for MHC Class II loading towards T cell presentation | [27], [28], [29] |
| | Destructive processing of Myelin Basic Protein epitope may limit central tolerance to the immunogenic protein; redundancy with cathepsins S and G | [30] |
| | Lysosomal activation of other cysteine proteases, e.g. cathepsin L | [31] |
| | Facilitating Toll-like receptor 9 signalling by activating cleavage in antigen-presenting cells; endotoxin tolerance in monocytes associated with AEP downregulation | [32], [33] |
| Regulatory T cells | Molecular marker of *in vitro* generated CD4+CD25$^{high}$ FOXP3-positive regulatory T cells; uncertain role | [34] |
| Epidermal cornification | In combination with the inhibitory Cystatin M/E, forms a protease-antiprotease functional dyad that coordinates epidermal and hair follicle cornification through regulation of transglutaminase 3 activity | [35], [36], [37] |
| Bone mass regulation | Negative regulator of osteoclast differentiation, possibly acting through its C-terminal fragment; upregulated with mechanical bone loading and osteoclast stimulation possibly as a feedback mechanism (murine) | [38], [39], [40] |
| Embryogenesis | Implicated as one of the molecules involved in restricted trophoblast invasion during early placentation (bovine). Also observed in murine yolk sac lining, possibly with yolk sac haematopoiesis | [41], [42] |

**Table 2.2 AEP in physiology and non-neoplastic pathology** (continued)

| | | |
|---|---|---|
| *Non-neoplastic disease* | | |
| Vascular disease | Overexpressed in macrophages infiltrating unstable atheromatous plaques; role in activating cleavage of Cathepsin L | [43], [44], [45] |
| Neuronal death | Overexpressed in astrocytes and microglial cells in the peri-infarct zone following experimental middle cerebral artery occlusion; promotes apoptosis following induction of neuronal death by inactivating cleavage of the DNase inhibitor SET | [46], [47] |
| Atopy | Upregulated in monocytes in atopic dermatitis, associated with eosinophilia, raised IgE and mite-specific IgE levels | [48] |
| *aep*-null mouse model | Late reduction in body weight, normal fertility, normal anatomy and morphology, giant lysosomes in proximal renal tubular epithelial cells with reduced two-chain forms of cathepsins B, H, L. Insidiously progressive haemophagocytic lymphohistiocytosis associated with extramedullary haematopoiesis and decreased NK cell numbers | [49], [50] |

**Table 2.3 AEP in human cancers**

| | | | |
|---|---|---|---|
| *Expression* | | | |
| Gene expression arrays | Acute lymphoblastic leukaemia | Overexpression in the adverse-risk progenitor-B genetic subtype *BCR-ABL1* (ranked 18th of 40 top-ranked genes) | [53] (Table 11, Supp.) |
| | | Overexpressed in heterogeneous adverse-risk adult progenitor-B disease where expression profile matches the BCR-ABL transcription signature in paediatric ALL | [54] |
| | | Significant overexpression in the adverse-risk progenitor-B genetic subtype iAMP21 | [1] |
| | Multiple myeloma | Twelve-fold overexpression (primary and cell line samples) compared to non-malignant *in vitro* differentiated polyclonal plasmablastic cells | [55] |
| | Follicular non-Hodgkin lymphoma | Top-ranked gene as part of the expression signature of monocyte-macrophage tumour-infiltrating cells (designated immune-response 2) | [56] |
| *Immuno-histochemistry* | Colorectal cancer | AEP expressed in primary tumours (95/164 [58%] strong staining) and in metastases (22/33 [67%] strong staining) | [57] |
| | | Significantly associated with adverse histological features | [57] |
| | Breast cancer | Strong expression in 43/43 (100%) breast carcinomas | [24] |
| | | Strong macrogranular or vesicular expression pattern in 24% (of 432) tumours | [58] |
| | Prostate cancer | Very strong expression in 42/56 (75%) prostate carcinomas | [24] |
| | Lung cancer | Strong expression in 14/24 (58%) tumours; details of histological subtypes not reported | [24] |
| | Ovarian cancer | Moderate-intensity expression in 17/23 (73%) tumours | [24] |
| | CNS tumour | Moderate intensity expression in 8/8 (100%) tumours | [24] |

**Table 2.3 AEP in human cancers** (continued)

| | | | |
|---|---|---|---|
| *Association with prognosis* | | | |
| Primary tumour | Colorectal cancer | Stromal or tumour AEP expression in colorectal cancer was significantly associated with poorer outcome (5-year estimate 40-45% *v* 70-75%). Prognostic significance retained in multivariate analysis | [57] |
| | Breast cancer | Vesicular expression pattern associated with poorer outcome (5 year disease-free estimate 45% *v* 80%) | [58] |
| *Tumour stroma* | Follicular non-Hodgkin lymphoma | Significantly poorer outcome with the immune-response 2 macrophage expression signature | [56] |
| *Indirect associations* | | | |
| Correlation with other adverse-risk biomarkers | Colorectal cancer | Immunohistochemistry expression of the cell growth regulator MAC30 and the transmembrane ion regulator FXYD3 | [59], [60] |

**Table 2.4 AEP and invasion - summary of supporting observations in human cancer**

| | | |
|---|---|---|
| *Molecular trafficking* | | |
| Subcellular localisation | Within membranous vesicles clustered at invadopodia of migrating cells | [24] |
| | Induction of expression *in vivo* in cancer cell line xenografts associated with surface localisation, as demonstrated by flow cytometry; surface localisation abrogated by *ex vivo* collagenase treatment of overexpressing tumour cells. | [61] |
| Colocalisation | With cortical actin in the murine brain endothelial cell line b.End.3 | [24] |
| | With β1 integrin subunit at cell surface in enforced-expression cells | [24] |
| | With β2 integrin in transduced monocytes; colocalisation not altered by modifying the integrin interaction sequence motif Arg-Gly-Asp | [43] |
| Extracellular release | Extracellular release of AEP by overexpressing tumours results in cleavage of a substrate-tagged cell-impermeable prodrug to locally generate active cell permeable cytotoxic compound, resulting in selective tumour kill | [61] |
| | AEP from intact overexpressing murine proximal renal tubular epithelial cells cleaves human fibronectin in culture | [62] |
| *Substrates* | | |
| Protease activation | Activation of Cathepsin L | [43] |
| | Redundant activation of Cathepsins B, L and H (from single chain to double-chain mature forms; observations in *aep*-null mice) | [49] |
| | Activation of matrix metalloproteinase 2 | [63], [24] |
| Extracellular matrix degradation | Fibronectin degradation | [62] |
| Apoptosis inhibition | Inactivating cleavage of Caspase 9 and inhibition of Cathepsin B-mediated cleavage of the proapoptotic Bid molecule | [64] |
| | Cleavage of Prothymosin α, potentially inhibiting Prothymosin α-regulated apoptosis induction; thymosin-α1 generated from cleavage is a putative growth factor and immune modulator | [65], [66], [67] |

**Table 2.4 AEP and invasion** (continued*)*

| | | |
|---|---|---|
| *In vitro studies* | | |
| Enforced expression | Ectopic AEP-expressing human embryonic kidney 293 (HEK293) cells demonstrate enhanced motility and Matrigel invasion; motility blocked by the non-selective AEP inhibitor Cystatin but not by the pan-cathepsin inhibitor E-64 | [24] |
| *In vivo studies* | | |
| Mouse models | Disseminated disease (50%, lung and liver metastases) and locally infiltrative masses associated with subcutaneous xenografts of AEP-overexpressing HEK293 cells in athymic mice | [24] |
| | An AEP DNA vaccination strategy targeting AEP-overexpressing tumour-associated macrophages generates potent cytotoxic T cell response and protects against fatal tumour challenge (75%), tumour dissemination (62%) and angiogenesis | [68], [69], [70] |
| *Inverse correlation studies* | Cystatin E/M silencing in an oral squamous carcinoma cell line results in enhanced AEP and CTSB expression and increased motility | [71] |
| | Cystatin E/M expression inversely related to AEP and CTSB expression in primary human melanoma and metastatic cells; forced expression of Cystatin E/M associated with specific decline in AEP expression and cell motility | [72] |

**Table 2.5 Aberrant lysosome biology and role of lysosome hydrolases in human cancer**

| | | |
|---|---|---|
| **Overexpression** | | |
| *Tumour* | Gene amplification (Cathepsin B) | [73], [74] |
| | Aberrant translation<br>• Variant transcript: exon skipping (Cathepsin B) or use of alternative promoters (Cathepsins B and L) | [75], [76], [77], [78], [79] |
| | • Altered transcript stability | [80] |
| *Tumour microenvironment* | Typically observed in stromal macrophages but also noted in endothelial cells, pericytes, fibroblasts and myofibroblasts | [81], [82], [83], [84], [85], [86] |
| | Paracrine (cytokine-mediated) induction of lysosomal protease expression in tumour cells | [87], [88] |
| **Aberrant lysosomal trafficking** | Widely observed in epithelial cancers; altered lysosome dynamics associated with aberrant peripheral localisation, as opposed to typical perinuclear situs; implicated in exaggerated cell motility or enhanced extracellular discharge of lysosomal contents | [89], [90], [91], [92], [93] |
| **Enhanced cell motility** | Widely reported in cancer cell lines - Osteosarcoma (Cathepsins B and L), Glioblastoma (Cathepsin B), T-cells (Cathepsin X); experimental evidence variably includes enforced expression and inhibition/depletion studies | [94], [95], [96], (Chapter 1, [154]) |
| *Clustering in motility-associated plasma membrane microdomains* | In caveolae (pro- and mature Cathepsin B in close proximity to β1 integrin and the Annexin II-tetramer complex); in podosomes (localisation directed by a Src family kinase, p61 Haematopoeitic Cell Kinase); in CD63-enriched tetraspannin domains as in the case of Cathepsin L (CD63 is an integral lysosomal membrane protein) | [97], [98], [99], [100], [101], [102] |
| *Plasma membrane remodelling* | Pre-formed plasma membrane fragments from endocytic process re-used to rapidly generate membranes at extending cell front | [103], [104], [105], [106] |
| *Cell adhesion/de-adhesion sequence* | Integrin-activation and signalling ($\beta_2$ integrin heterodimers [$\alpha_L\beta_2$ in lymphocytes; $\alpha_M\beta_2$ in monocyte-macrophages] and Cathepsin X) | (Chapter 1, [154]), [107] |
| | Aberrant Rho kinase signalling implicated in disrupted lysosomal translocation | [108], [109], [110] |
| *Activating cleavage of promotility zymogens* | Lysosomal cysteine proteases often cleave to activate other related zymogens or non-family proproteins (e.g. the pro-urokinase plasminogen receptor) | [111], [112] |

**Table 2.5 Aberrant lysosomal biology and role of lysosomal hydrolases in human cancers** *(continued)*

| | | |
|---|---|---|
| *Exocytosis* | Exocytosis- a key mechanism in cell motility regulation | [113], [114] |
| | Results in extracellular release of active proteases | [100], [115] |
| | The stroma helps activate and stabilise extracellular proteases | |
| | • Inactive precursor proteases released by tumour cells (Cathepsins B, C, L, X) | [109], [116] |
| | • Low pH of tumour microenvironment (including in the bone marrow) facilitates both release and extracellular activation of lysosomal proteases | [117], [118], [119], [120] |
| | • Stromal glycosaminoglycans also help activate and stabilise extracellular proteases | [121], [122] |
| | Discharged proteases degrade structural components of extracellular matrix | [123], [124], [125] |
| **Altered cell signalling** | | |
| *Exocytosis* | Release of bioactive molecules tethered to extracellular matrix; once liberated, these molecules participate in a multitude of pro-oncogenic signalling processes, including cell proliferation and angiogenesis (akin to the wound healing response) | [112], [126] |
| *Intracellular substrate cleavage* | Degradation following endocytosis | |
| | • Extracellular matrix components (e.g. CTSB and collagen) | [127] |
| | • Surface signalling receptors (e.g. C-terminal inactivating cleavage of human epidermal growth factor receptor 2 in breast cancer cells) | [128] |
| **Drug resistance** | Aberrant lysosome trafficking links with accelerated exosome export to contribute to cisplatin drug resistance in an ovarian carcinoma cell line | [129] |

# 3

# AEP expression in childhood acute lymphoblastic leukaemia

Microarray gene expression analysis indicated predominant overexpression of AEP in adverse-risk progenitor-B ALL. This chapter discusses results of studies to validate and extend these findings. Validation studies were performed on the microarray discovery cohort.

## Experimental methods

*Full details of all procedures, including materials, reagents, protocols and optimisation-validation steps are available in the Methods chapter. The following account is a summary*.

*Primary samples*

Mononuclear cells were isolated from diagnostic bone marrow samples by density-separation. Isolated cells were either directly lysed in TRIzol reagent towards RNA isolation or cryopreserved in liquid nitrogen (**Figure 3.1**). All research samples were obtained from patients treated on national protocols and processed after explicit patient/parental consent for sampling, storage and use of material for ethically-approved research (**Supplementary Table 3.1**). The studies were approved by the Tameside and Glossop Local Research Ethics Committee, Manchester, UK (Reference 07/Q1402/56).

*Cell lines*

Full details are available in the companion Supplemental section (**Appendix A**, **Supplementary Table S3.2**). Unless otherwise specified, cells were washed in PBS and pelleted by centrifugation at 300*g* for 5 minutes at room temperature. In all experiments, low-passage cells (typically, less than 15) were used and cell counts and viability (Trypan blue staining exclusion) were strictly determined.

*Two-step quantitative real-time PCR for estimation of AEP transcript expression*

RNA was isolated from cells lysed in TRIzol using the one-step guanidinium thiocyanate-phenol-chloroform phase extraction procedure [1]. Five hundred nanogram RNA was used as template for first-strand cDNA synthesis. AEP transcript expression was quantitated using on-demand *Taqman* (hydrolysis probe) gene expression assays (**Supplementary Table S3.3**, **Appendix B**) and the ABI Prism 7700HT instrument system. The delta-delta CT approximation method was used to estimate relative normalised AEP transcript expression, using β2M expression as endogenous reference and normalised expression of the HRC57 cell line as calibrator.

*Protein immunoblotting*

Total protein was extracted by whole cell lysis in NP40- or acidified citrate-based lysis buffers and quantitated using a modified Lowry assay. Uniform quantities of denatured whole cell protein lysates were resolved by discontinuous SDS-PAGE and transferred semi-dry to PVDF membranes. Following blocking, membranes were serially probed with primary and HRP-conjugated secondary antibodies. Protein bands were detected by chemiluminescence. (**Figure 3.2**) Membranes were subsequently stripped and probed for estimation of loading control or for detection of alternative proteins.

*AEP activity assay*

Pre-quantitated whole cell lysates in acidified NP40-citrate lysis buffers were incubated with a synthetic fluorogenic aminomethyl coumarin conjugated-peptide substrate, without or in the presence of the selective AEP inhibitor, MV026630 (AEPi). Enzyme activity corresponded to the net intensity of fluorescence generated following substrate cleavage and was read off a standard curve.

*Cytofluorescence staining*

Formalin-fixed cell cytospins were permeabilised, blocked, probed serially with primary and secondary antibodies and mounted with DAPI as nucleus

counterstain (**Figure 3.3**). In some experiments, cells were live-labelled with the fluorescent acidotropic probe, LysoTracker Red DND-99 or with the BODIPY fluorophore-conjugated azaepoxy-asparagine peptidyl AEP activity-based probe (**Figure 3.4**; [2]) prior to fixation. All experiments included parallel negative controls (**Chapter 8**, **Figures 8.6-8.9**). Image acquisition details are provided in the figure annotations. The Adobe Photoshop software package was used to process images.

*AEP immunohistochemistry*

Formalin-fixed paraffin tissue sections were deparaffinised, rehydrated, treated to quench endogenous peroxidase and biotin activity, serially probed with primary and secondary antibodies, counterstained, dehydrated and DPX-mounted. Photomicrograph acquisition details are provided in the figure annotations. All experiments included parallel negative controls (**Chapter 8, Figure 8.10**). Images were processed using the Adobe Photoshop software package.

*SD1 microvesicle isolation*

Microvesicles were isolated from cell-free supernatants of near 100%-viable SD1 cells cultured in serum-unsupplemented growth medium, using serial standard and high-velocity centrifugation steps (**Figure 3.14A**).

## Results

*Quantitative PCR validates microarray analysis of AEP transcript expression*

As shown in Figure 3.5, relative quantitation of AEP transcript expression parallels microarray findings (**Supplementary Table S3.4**). Although median AEP transcript expression is highest in poor-risk progenitor-B ALL, there is considerable overlap in expression with good-risk progenitor-B disease. This is in part due to smaller sample numbers in the poor-risk B-lineage category. Part of the overlap is also attributable to AEP overexpression being largely restricted to the adverse-risk progenitor-B ALL genotypes, Ph+ ALL and iAMP21 ALL. AEP

overexpression is essentially not a feature of progenitor-T ALL and acute myeloid leukaemia.

*AEP protein expression imperfectly matches transcript expression*

Figures 3.6 and 3.7 discuss these findings. The observations are clearly limited by inadequate sample sizes. In cell lines and primary cells, estimated AEP activity matched immunoblot protein expression and suggested expression of fully functional protease. Relative AEP transcript expression and enzyme activity however correlated imperfectly (**Figure 3.7**, **Supplementary Table S3.5**, **Appendix D**).

*Progenitor-B lymphoblasts demonstrate heterogeneous intracellular AEP expression, including localisation in peripherally-sited macrovesicular endolysosomal compartments*

SD1 cells

Intracellular expression was investigated in SD1 cells, a model AEP-overexpressing poor-risk genotype (Ph+) progenitor-B ALL cell line. Labelling, using both an antibody and the activity-binding probe, indicated remarkable heterogeneity of expression of intracellular AEP. Stippled perinuclear staining suggested typical lysosomal distribution (**Figure 3.8**, **upper panel**). Additionally, some cells strikingly demonstrated peripherally localised macrovesicular AEP staining (**Figure 3.8**, **middle and lower panels**). Dual staining with lysosomal markers, LysoTracker Red and antibody to LAMP1, characterised these peripherally-localised AEP+ macrovesicles as endolysosomal organelles (**Figure 3.9**).

Primary cells

Tissue section immunostaining localised AEP expression to lymphoblasts (**Figure 3.10**). Cytofluorescence staining in iAMP21 primary lymphobasts mirrored observations in SD1 cells; distinct peripherally-localised acidified AEP+ vesicles were similarly observed (**Figure 3.11**)

*SD1 cells shed preproAEP in microvesicles*

Microscopy observations of peripheral AEP localisation suggested extracellular lysosomal discharge of mature active AEP. Fixed-cell imaging supported this probability (**Figure 3.12**). AEP immunoblotting and enzyme activity studies however consistently failed to detect active AEP in SD1 cell supernatants. Instead, AEP immunoblotting detected preproAEP in cell-free SD1 supernatants. Despite stringent measures to avoid cell contamination, preproAEP detection in cell supernatants was invariably associated with trace detection of β-actin (**Chapter 8**, **Figure 8.15**). Phase-contrast microscopy provided an explanation. In culture, SD1 cells were associated with apparent granular 'debris' that on higher magnification, were membranous microparticles characteristic of microvesicles (**Figure 3.13**). AEP immunoblots of microvesicles harvested from cell-free SD1 supernatants similarly detected preproAEP, suggesting extracellular release of the zymogen in microvesicles (**Figure 3.14B**). Confirmation of preproAEP detection was provided by AEP immunoblot of microvesicle isolates lysed in acid citrate buffer; low pH of the buffer triggered autoactivating cleavage of preproAEP in the lysate, resulting in the additional detection of the intermediate proAEP precursor (**Figure 3.14C**).

## Discussion

Global gene-expression microarray was used as a discovery tool for novel prognostic biomarkers in childhood ALL. AEP was identified as one such candidate. AEP was overexpressed in adverse-risk progenitor-B ALL genotypes, predominantly in the iAMP21 and Ph+ ALL subsets, and this observation was corroborated by quantitative PCR on the same sample cohort. The wide range and overlap of expression may in part be due to inadequate sample numbers but the variability in expression may also be a reflection of the current imprecision of cytogenetic stratification as an estimate of risk and prognosis. Indeed, restricted overexpression in poor-risk genotypes would have raised doubts over the usefulness of AEP as an independent risk variable. The question of concomitant AEP protein overexpression remains an open one and will need to await results

of an ongoing prospective biomarker study. Related issues are highlighted in **Tables 3.1** and **3.2**.

**Table 3.3** sets out the limitations of microscopy studies. Importantly, the observations are largely based on findings in the model high-risk SD1 cell line, with only anecdotal corroboration in primary cells. Despite the acknowledged limitations, microscopy observations demonstrate striking heterogeneity of intracellular AEP expression, including localisation to atypically distributed peripheral macrovesicular endolysosomes. Taken together with the observation of preproAEP exocytosis in SD1 microvesicles, the findings suggest that poor-risk ALL is potentially characterised by perturbed lysosome homeostasis, involving aberrant antegrade lysosome trafficking and extracellular discharge (**Figure 3.15**). This phenotype could conceivably be mechanistically implicated in many of the adverse-risk characteristics of lymphoblasts, including exaggerated transvascular motility and drug resistance (Chapter 2, [129]). Targeting lysosomes may therefore be a feasible therapeutic option in childhood ALL. Indeed, in the case of mature-B lymphoid neoplasms, the therapeutic effect of a subset of anti-CD20 monoclonal antibodies is directly attributable to lysosomal disruption and downstream activation of non-apoptotic cell death [5].

**Figure 3.1** Schematic outline of mononuclear cell isolation from bone marrow/peripheral blood by density gradient centrifugation

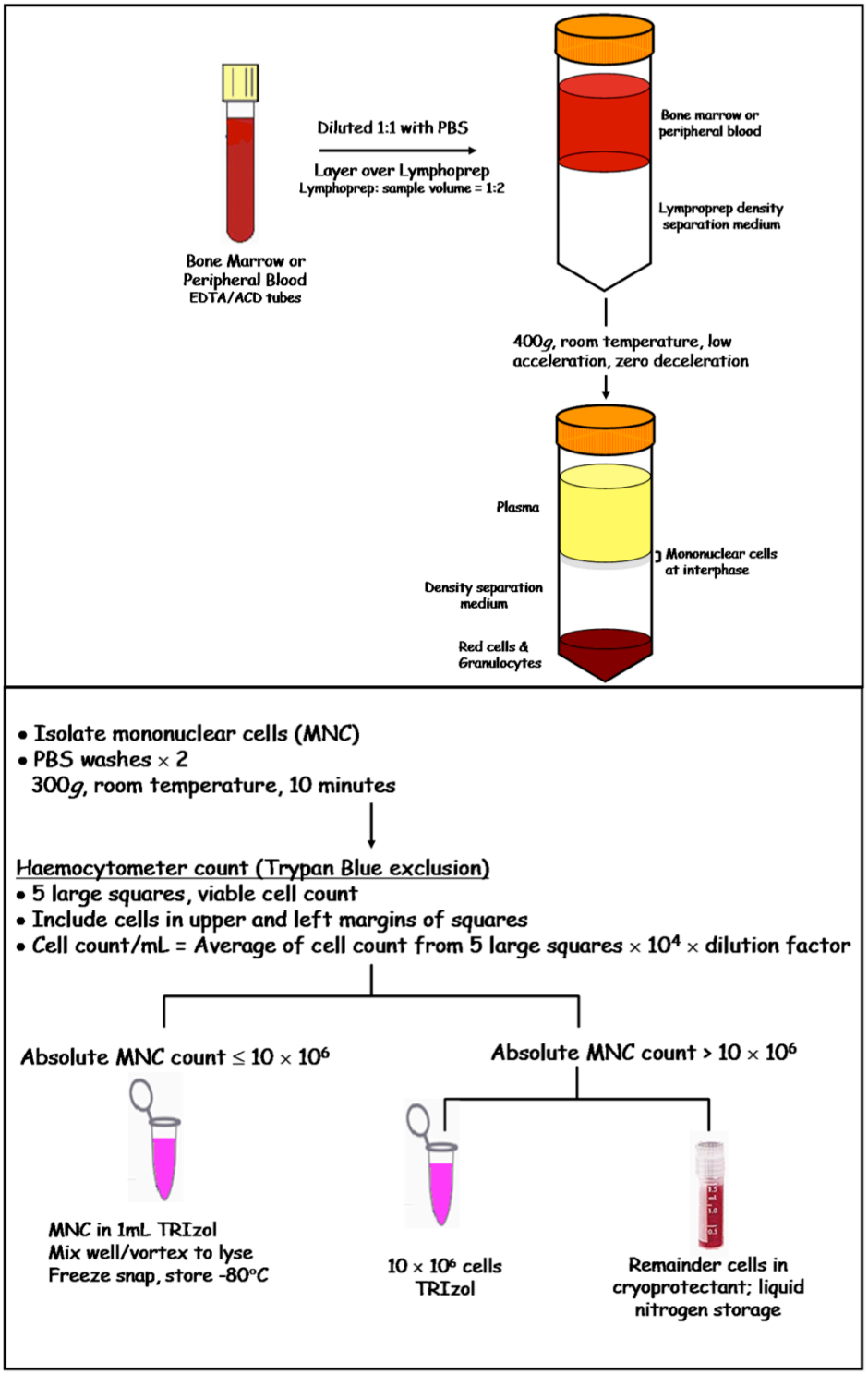

**Figure 3.2** Schematic outline of protein immunoblotting using discontinuous reducing SDS-PAGE

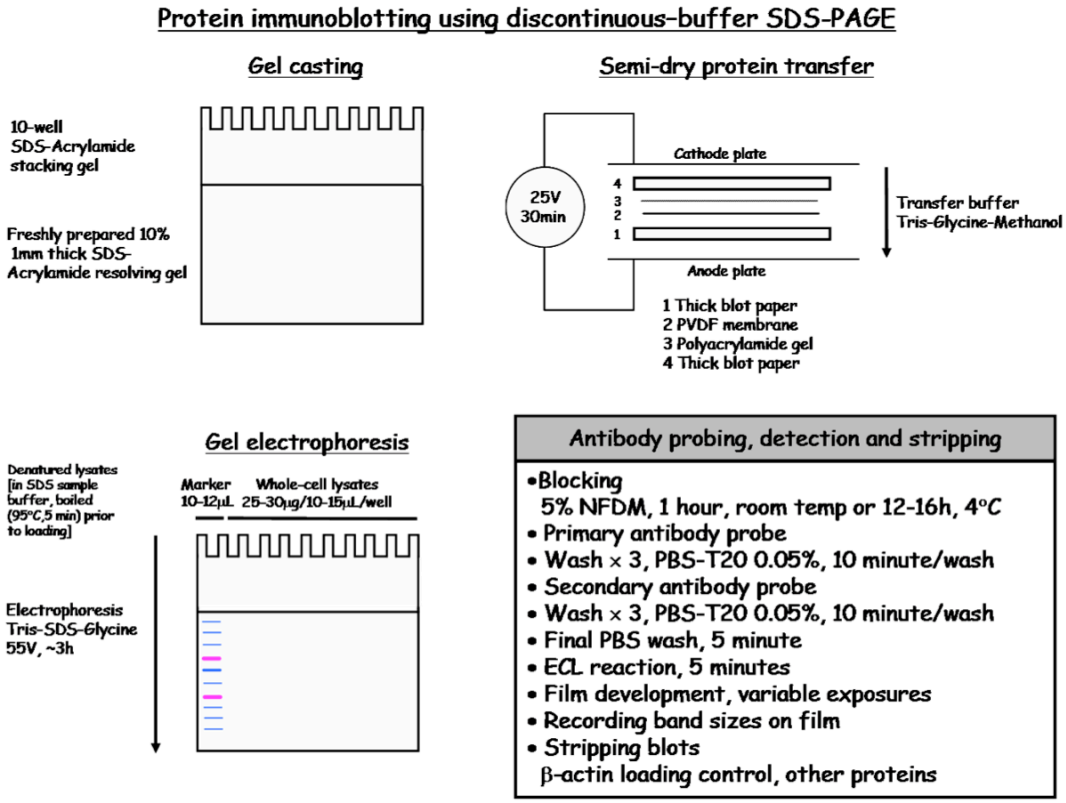


**Figure 3.3** Schematic outline of cytospin immunostaining procedure

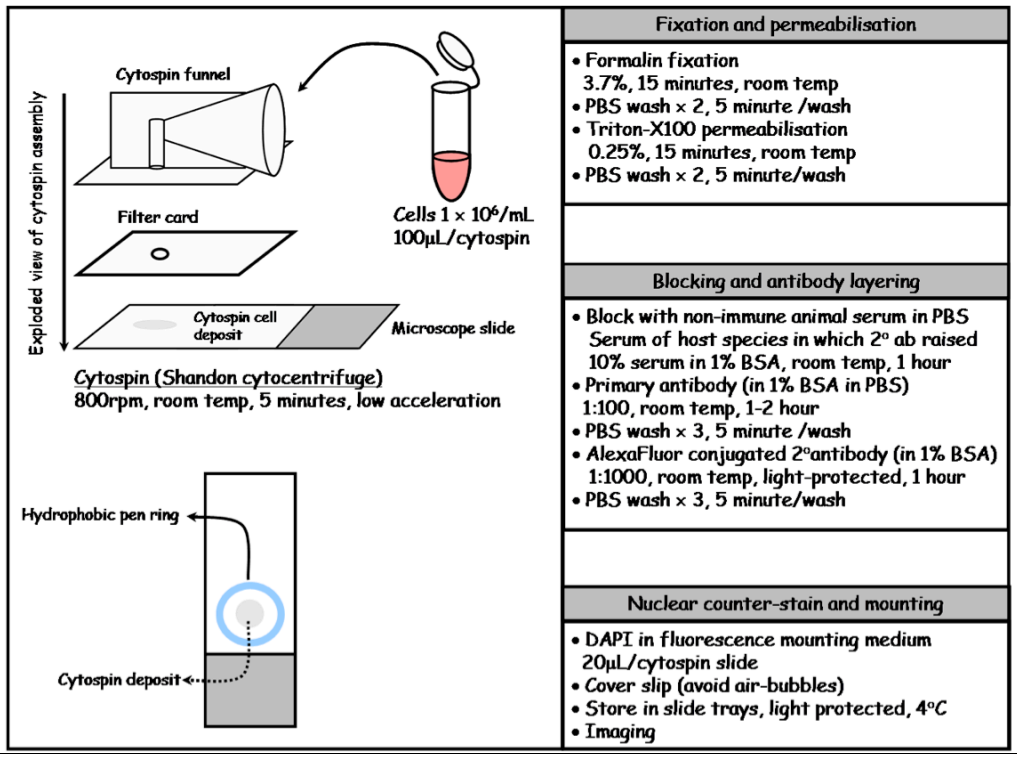

**Figure 3.4** Cartoon representation of fluorescent *in vivo* labelling of mature active AEP by the AEP activity-binding probe (AEP-ABP)

Sequential carboxyl- and amino- termini cleavages during the process of AEP maturation (Appendix C) preclude labelling of the active AEP protease using traditional terminal-tagged fluorescent reporters. The AEP-ABP circumvents this problem by binding directly to the catalytic site of mature AEP. The probe, a gift from Dr. Matthew Bogyo's lab at Stanford University in California, is a fluorophore-conjugated cell-permeable compound and its azaepoxy-dipeptidyl warhead sequence determines its reactivity as well as binding specificity.

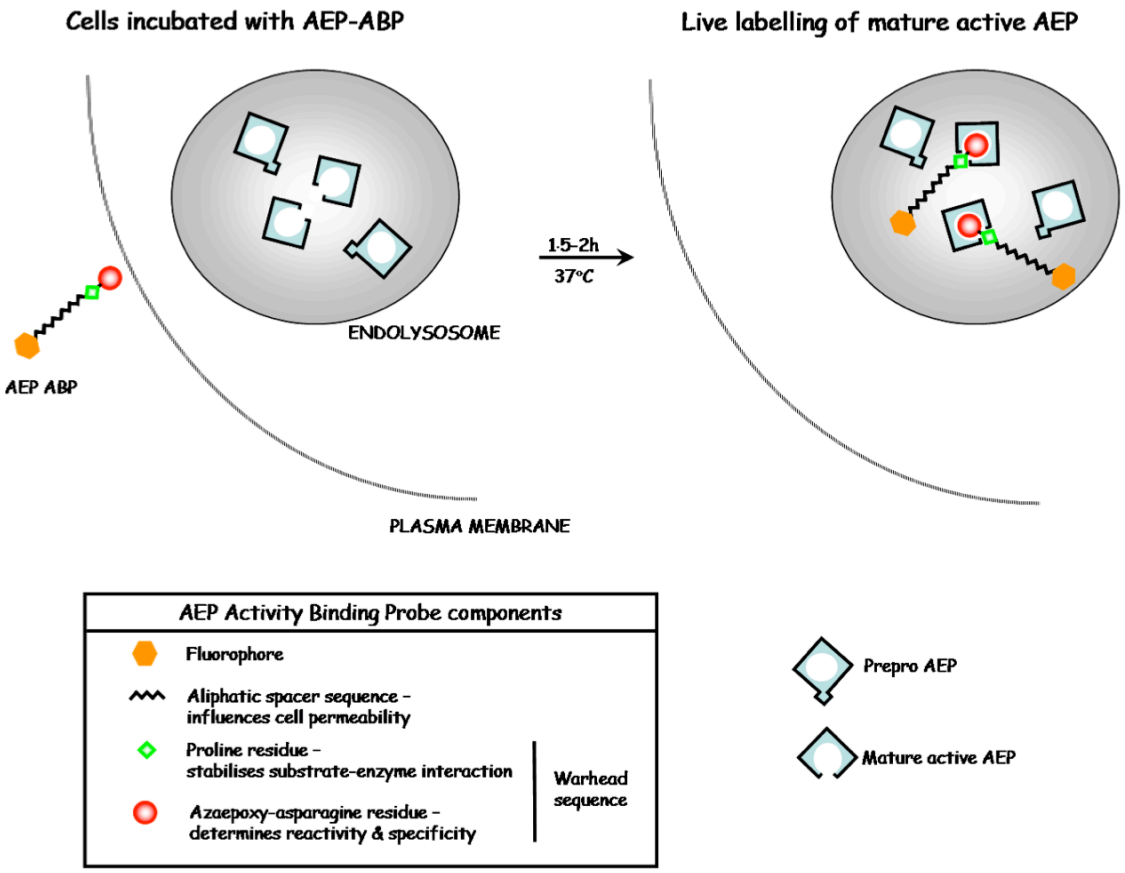

**Figure 3.5** Quantitative PCR validates microarray analysis of AEP transcript expression

Boxplot representations of AEP transcript expression in leukaemic cells as determined by microarray analysis (left) and quantitative PCR (RQPCR, right). Validation by RQPCR was performed on the microarray sample cohort. Median AEP transcript expression is higher in high-risk progenitor-B ALL than in other categories of acute leukaemia, although there is considerable overlap with standard-risk B-lineage disease.

High-risk pre-B refers to adverse-risk genetic subtypes of progenitor-B ALL (*BCR-ABL1*, *MLL* rearranged, hypodiploidy, iAMP21); standard risk pre-B refers to all other genetic progenitor-B ALL subtypes. Boxes encompass the interquartile (IQR, $25^{th}$-$75^{th}$ percentile) ranges, horizontal bars and '+' within boxes represent median and mean values respectively, whiskers denote values 1.5× IQR, outlier values are represented by open and filled circles. Microarray analysis was performed on Affymetrix HG_U133A oligonucleotide arrays and evaluated using the GeneSpring analysis package (v7.3.1). RQ-PCR was performed using on-demand Taqman assays and reported using the ΔΔCt approximation method with β2M expression as endogenous reference and HRC57 cell line expression as calibrator.

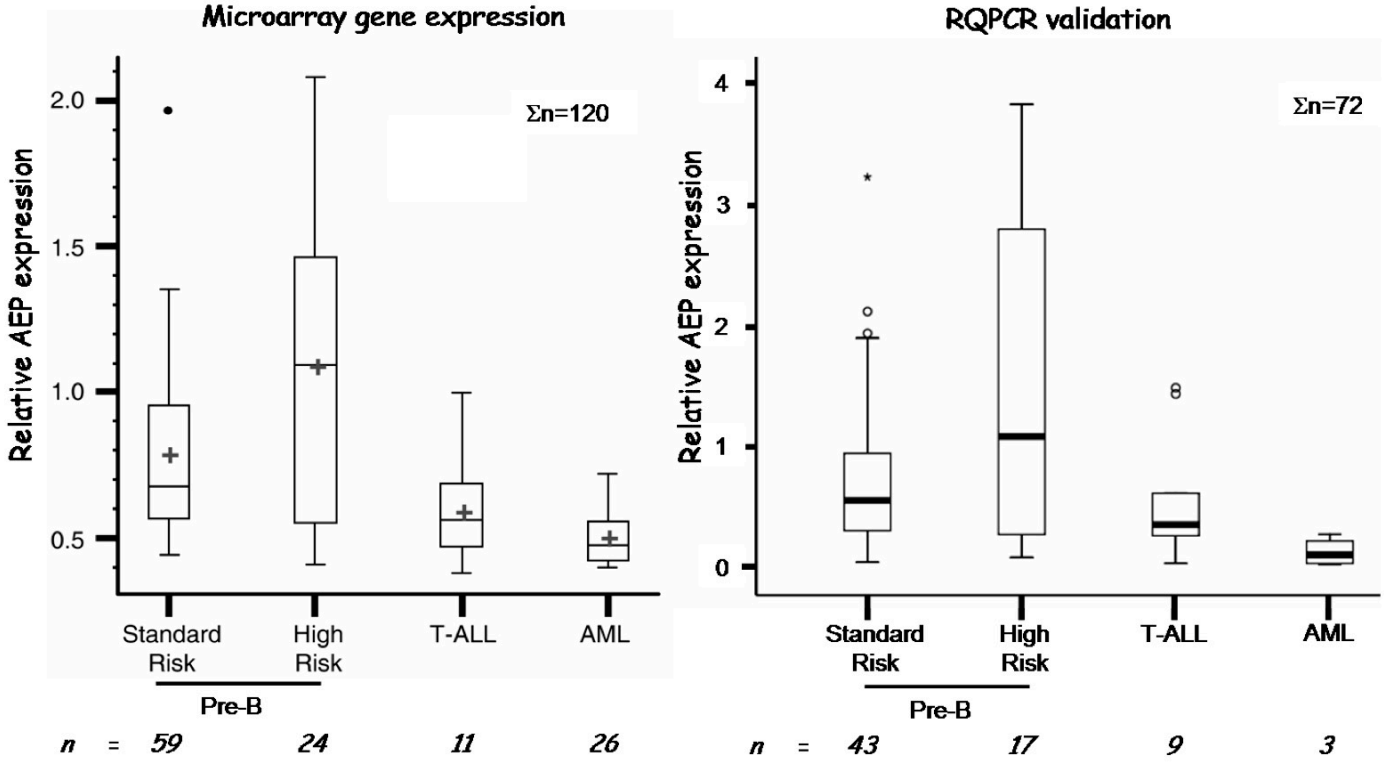

**Figure 3.6** AEP enzyme activity matches immunoblot protein expression

AEP immunoblots (A) and relative enzyme activity (B, fluorescent substrate cleavage assay) in whole cell lysates from malignant lymphoid (SD1, REH, SupB15, HRC57, 697, RPMI-8402, U266) and myeloid (MV4:11, K562, HL60) cell lines. Enzyme activity parallels immunoblot detection, suggesting expression of wild type AEP. The doublet 56kDa immunoblot detection bands in U266 probably represent different glycosylation states of the AEP zymogen. AEP enzyme activity is expressed relative to the reference HRC57 cell line.

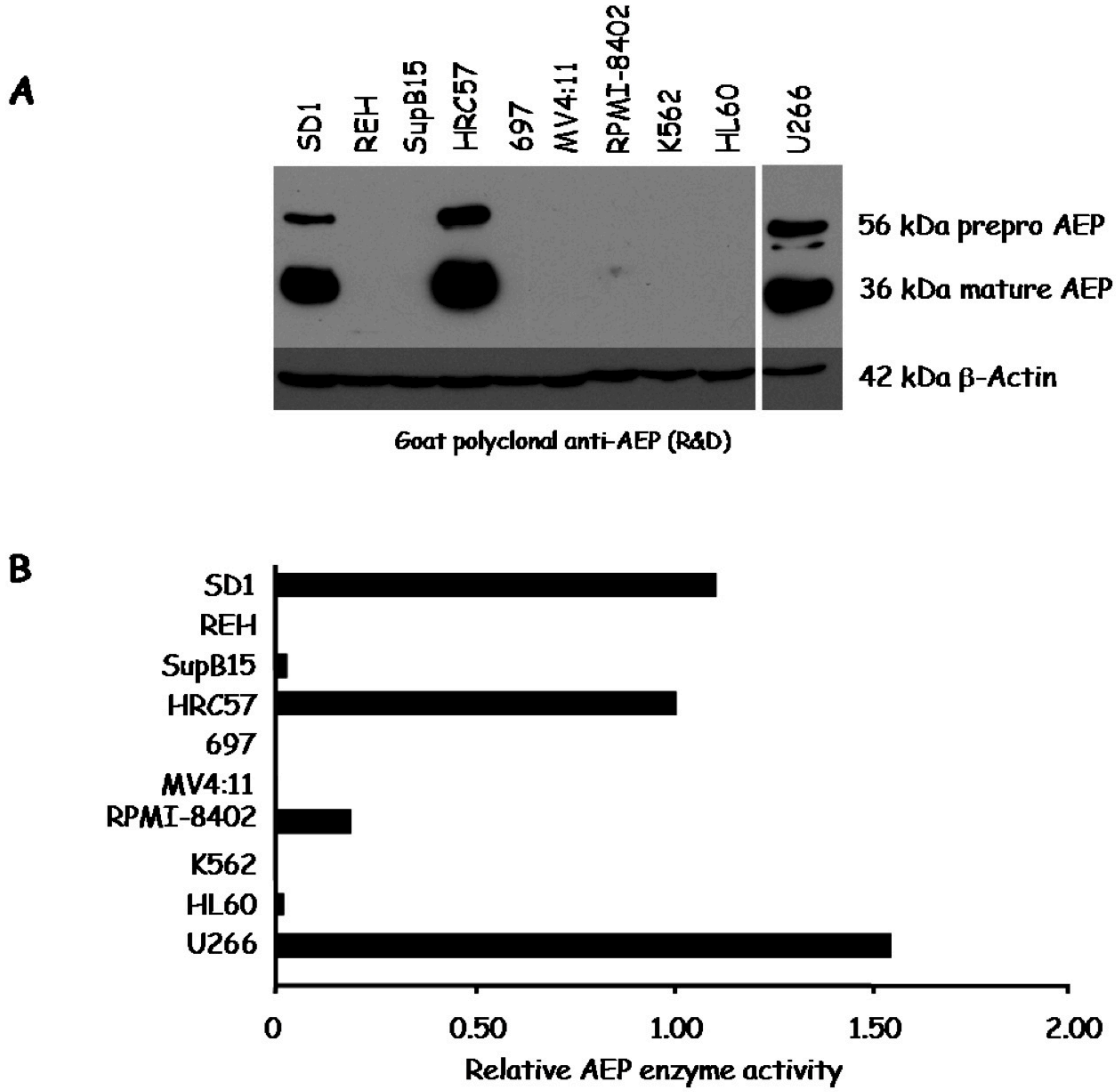

**Figure 3.7** AEP transcript and protein expressions do not necessarily correlate

*Upper panel*: AEP immunoblot on primary ALL bone marrow mononuclear whole cell lysates (polyclonal anti-AEP antibody). *Lower panel*: Paired relative AEP transcript expression and enzyme activity in primary ALL samples; expression is normalised to the HRC57 cell line (dashed horizontal). While AEP activity parallels protein expression, transcript expression is discordant (lower panel, UPN 2 and 10, highlighted by vertical arrows). High transcript-low protein expression (UPN10) may be attributed to transcript silencing or accelerated protein degradation. Low transcript-high protein expression (UPN2) could be a consequence of post-translation negative feedback [3].

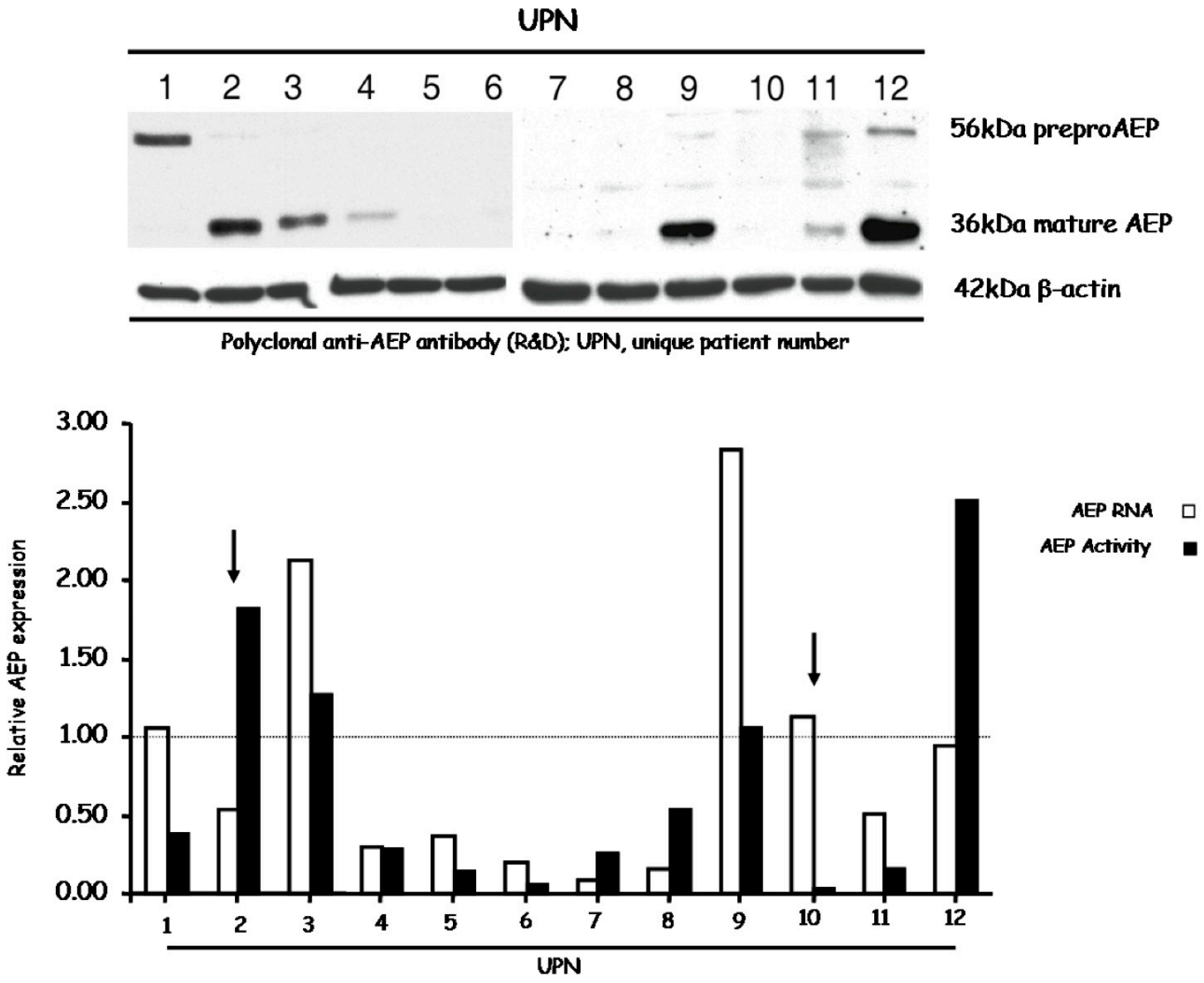

**Figure 3.8** AEP expression in SD1 cells is heterogeneous, from stippled, predominant perinuclear expression to giant peripheral macrovesicular staining

Fluorescence imaging of cytospin preparations of SD1 cells. In panels A and B, formalin-fixed and permeabilised SD1 cells were serially probed with goat polyclonal anti-human AEP (1:100) and an Alexa Fluor 488 conjugated secondary (green). In panel C, SD1 cells were live-labelled with a BODIPY 530/580-tagged aza-epoxypeptide class AEP activity-binding probe (AEP-ABP, red; 1μM, $2\times10^5$cells, 2 hour incubation, 37°C) prior to cytospin preparation and formalin-fixation. In both cases, DAPI (blue) counterstained the nucleus. Images were acquired using the Olympus BX51 microscope (equipped with the Photometrics CoolSnap HQ cooled CCD camera) and the Zeiss Axiovert 200M inverted low-light microscope system (equipped with the Photometric Cascade II:1024 EMCCD camera), both operated by the Metamorph advanced imaging software. Representative images are presented.

The pattern of AEP expression in SD1 cells is strikingly heterogeneous. Stippled predominantly perinuclear staining [Panels A (40×), B (a)] reflects typical lysosomal distribution. Coarser macrovesicular staining is also noted [Panel B, (c), (d)] and often, a mixed expression pattern is observed [Panel B, (b) and (f)]. Of note, macrovesicular AEP staining is distributed largely towards the cell periphery [Panels B, (e), (f); C (a)] and is sometimes characterised by impressive giant vesicular expression [Panel C (b)].

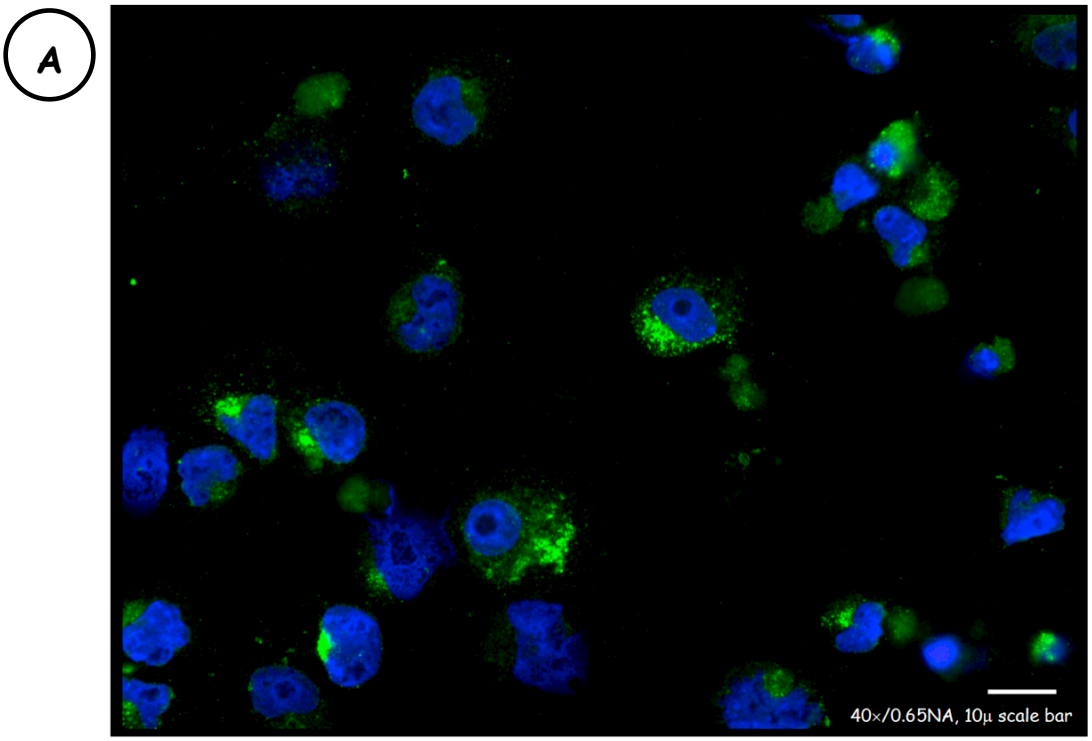

B

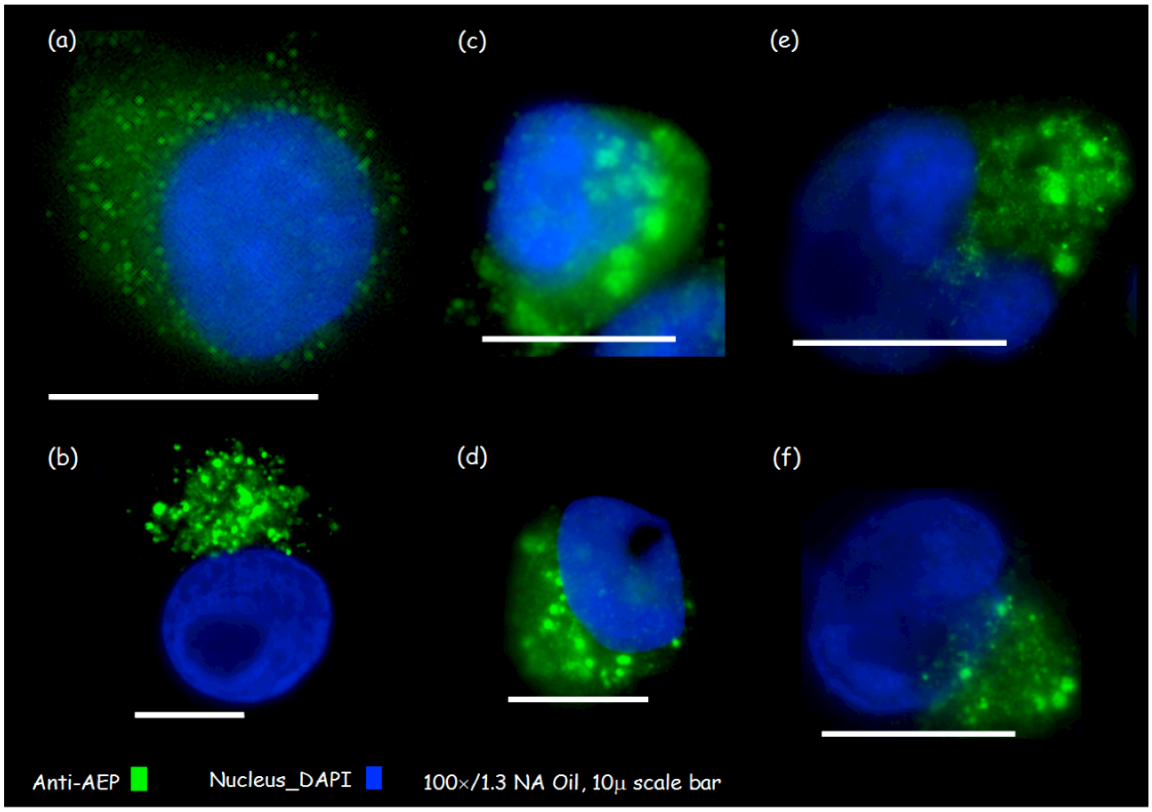
(a)
(c)
(e)
(b)
(d)
(f)
Anti-AEP
Nucleus_DAPI
100×/1.3 NA Oil, 10μ scale bar

C

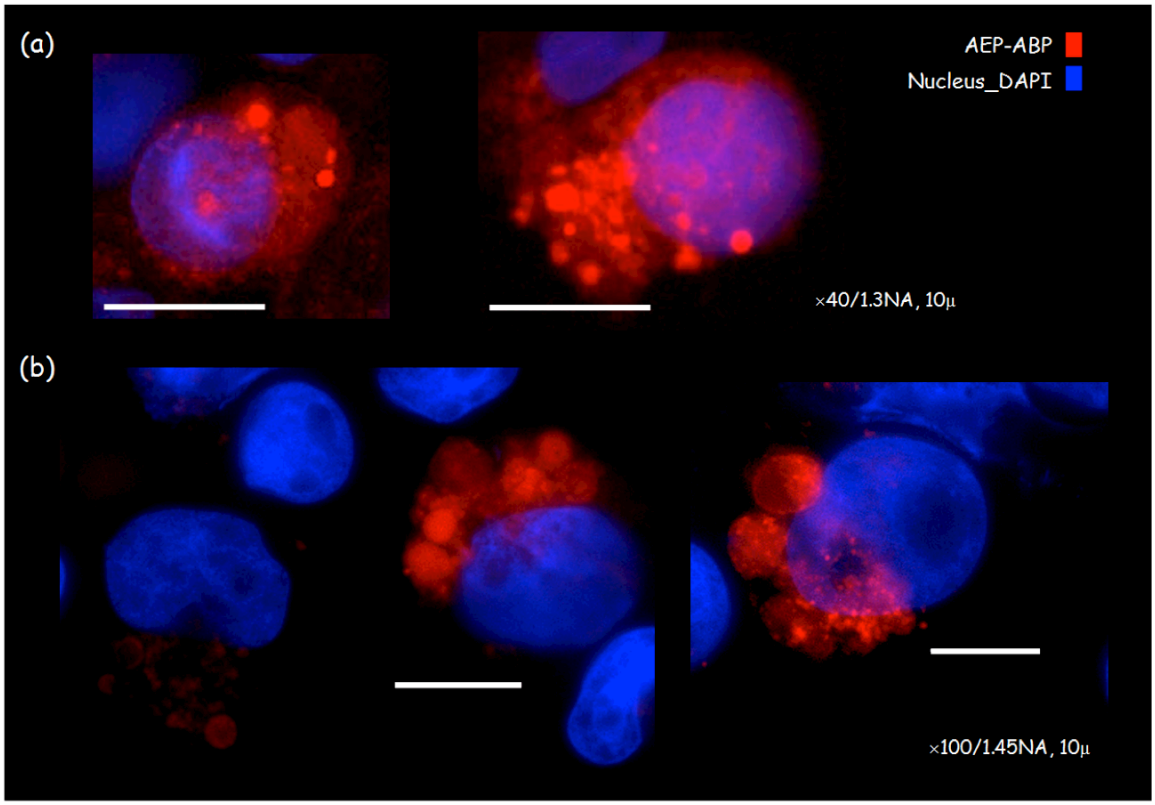
(a)
AEP-ABP
Nucleus_DAPI
×40/1.3NA, 10μ
(b)
×100/1.45NA, 10μ

**Figure 3.9** AEP in SD1 cells is distributed in peripherally localised acidified LAMP1-positive vesicles

Fluorescence imaging of cytospin preparations of SD1 cells. In Panels A, B and D, SD1 cells were live-labelled with the acidotropic LysoTracker Red DND-99 probe (LyTR; 500nM, 45 minutes, 37°C; red) followed by cytospin preparation, formalin-fixation, permeabilisation and serial probing with a polyclonal anti-AEP primary and an Alexa Fluor 488-conjugated secondary. In Panel C, SD1 cells were live-labelled with the AEP activity-based probe (AEP-ABP) and subsequently, cytocentrifuged, formalin-fixed, permeabilised and probed serially with monoclonal anti-LAMP1 primary (murine HA-43 clone, 1:100) and an Alexa Fluor 488 conjugated secondary. DAPI (blue) counterstained the nucleus. Images were acquired using a Zeiss Axiovert 200M low-light microscope system equipped with an Optovar module and an EMCCD camera operated by the Metamorph imaging system. Representative images are shown.

SD1 cells demonstrate large peripherally localised acidified (i.e. LysoTracker Red labelled) vesicles (*Panel A*). Dual staining localises AEP to these acidified vesicles (*Panel B, Panel D [cell in centre, merged image]*), which on account of the low intravesicular pH, must largely exist as the mature protease. This is supported by dual staining using the AEP-ABP and the anti-LAMP1 antibody (*Panel C*). Here, mature AEP is observed in distinct peripherally-localised LAMP1-ringed endolysosomal vesicles, possibly on the verge of exocytosis. Also observed is peripheral localisation of AEP independent of LyTR labelling (*Panel D*, *arrow highlight*), suggesting additional perimembranous localisation of immature AEP-containing vesicles.

A

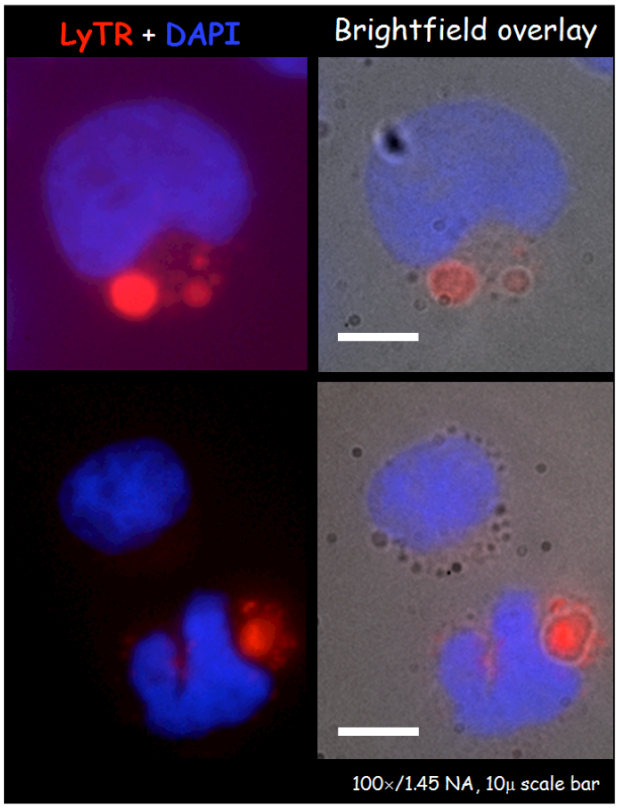
LyTR + DAPI
Brightfield overlay
100×/1.45 NA, 10μ scale bar

B

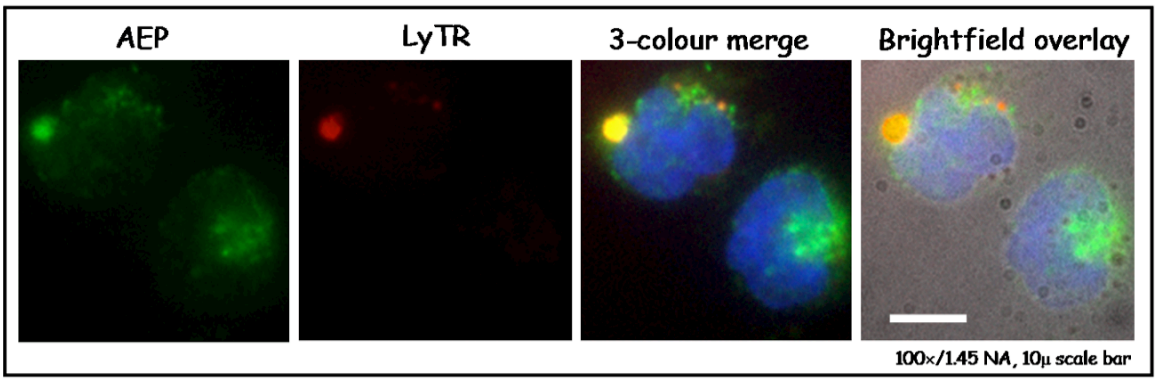
AEP
LyTR
3-colour merge
Brightfield overlay
100×/1.45 NA, 10μ scale bar

C

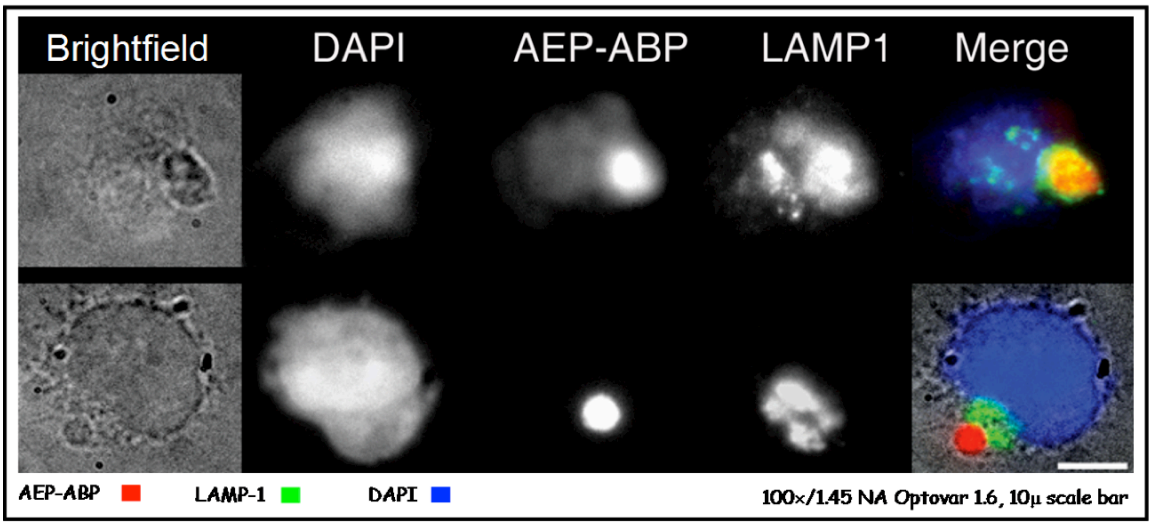
Brightfield
DAPI
AEP-ABP
LAMP1
Merge
AEP-ABP
LAMP-1
DAPI
100×/1.45 NA Optovar 1.6, 10µ scale bar

D

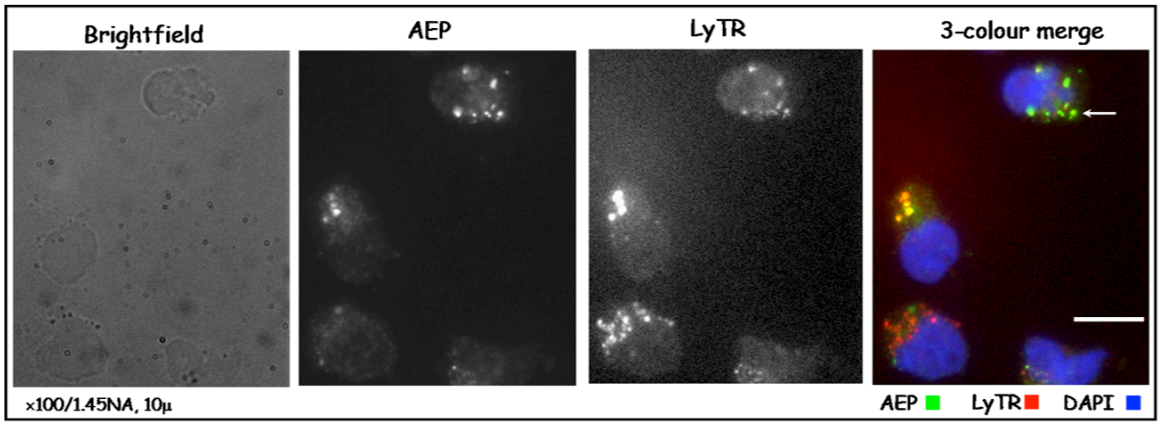
Brightfield
AEP
LyTR
3-colour merge
×100/1.45NA, 10µ
AEP
LyTR
DAPI

**Figure 3.10** AEP-expressing lymphoblasts at testicular relapse of iAMP21 ALL

H&E and AEP-immunostained sections of testicular tissue in a 10-year old boy with gonadal relapse of iAMP21 ALL. *Upper panel*: H&E section. Prepubertal seminiferous tubules are surrounded by a prominent intersititial infiltrate of uniform small round blue cells (20×, 75μ scale bar) *Lower panel*: AEP immunohistochemistry. Whorls of AEP-expressing (brown) lymphoblasts (40×/0.75NA, 50μ scale bar) demonstrate fine granular and coarse vesicular (arrow) cytoplasmic staining (100×/1.35NA, 25μ scale bar). Images were acquired using an Olympus BX51 microscope equipped with a Photometrics CoolSnap HQ CCD camera operated by the Metamorph advanced imaging software.

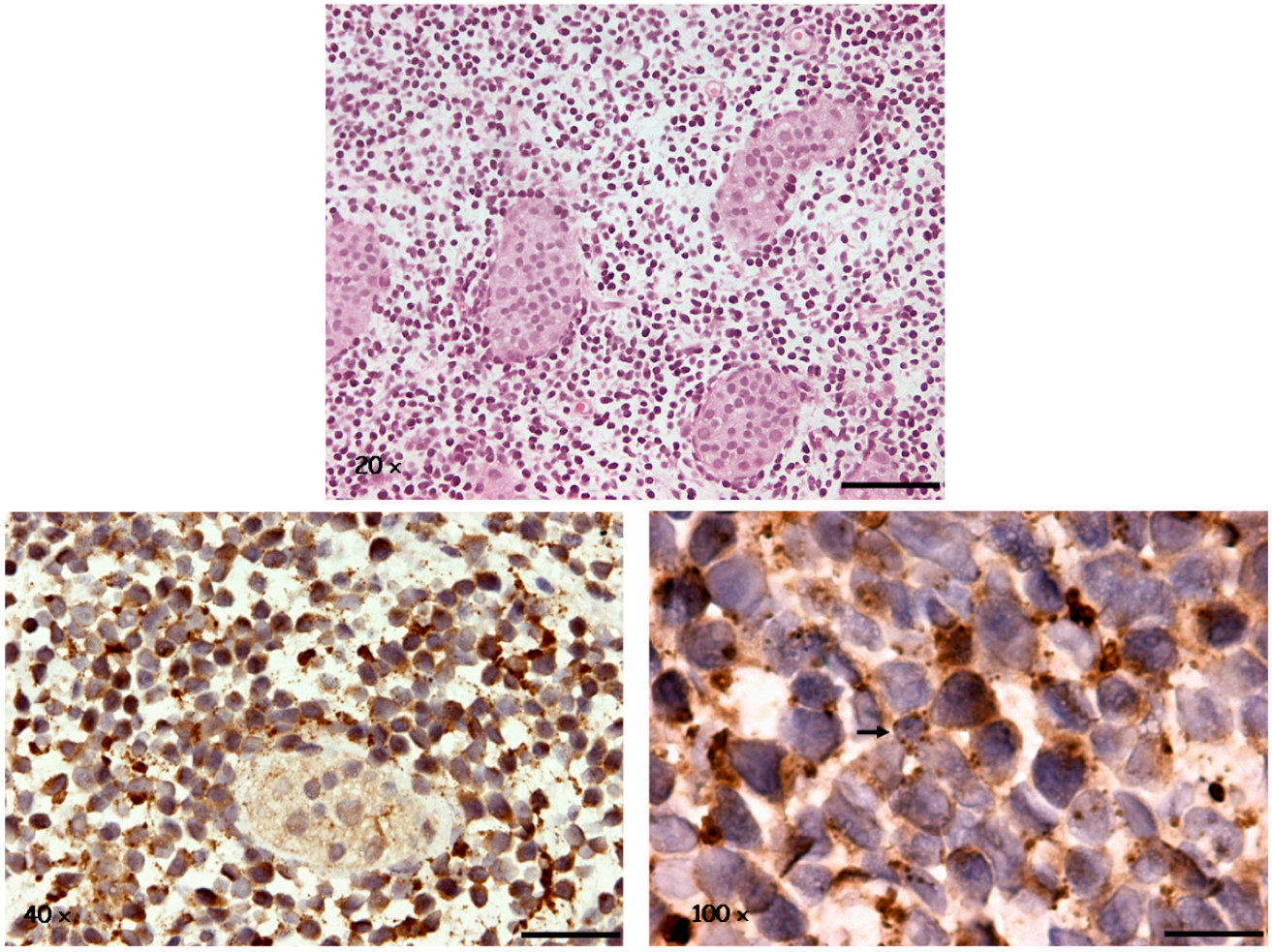


Heat retrieval Tris-EDTA, peroxidase quenching, goat polyclonal anti-AEP, avidin-streptavidin amplification, DAB chromogen, Olympus BX51, AnalySIS

**Figure 3.11** Peripherally localised acidified AEP-containing vesicles are also observed in primary ALL cells

Fluorescence imaging of primary progenitor-B lymphoblasts obtained from a cryostored mononuclear cell isolate of diagnostic bone marrow cells sampled from patient UPN9 with iAMP21 ALL.

*Upper panel*: Flow cytometry and light microscopy confirmation of a predominant (>95%) progenitor-B lymphoblast population in sample. Thawed cells were incubated with fluorophore-conjugated anti-CD19 and anti-CD10 monoclonal antibodies (singly and combined, 4°C, light-shielded, 30 minutes) together with 7-aminoactinomycin D as cell viability marker; events were acquired on the BD-LSRII flow cytometer and examined using the FlowJo analysis package (Tree Star). The majority of gated viable cells were CD10+CD19+. Light microscopy of an MGG-stained cytospin preparation reveals large cells with scanty cytoplasm, homogenous open chromatin and prominent nucleoli, all features typical of lymphoblasts.

*MGG, May-Grünwald Giemsa; PE, phycoerythrin; PE-Cy7 phycoerythrin-Cyanine 7 tandem fluorochrome.*

*Lower panel*: Cytospins of LysoTracker Red (LyTR, 500nM; red) live-labelled cells were formalin-fixed, permeabilised and serially incubated with the goat polyclonal anti-AEP antibody (1:100) and an Alexa Fluor 488-conjugated secondary (green); cell nucleus was counterstained blue with DAPI. Images were acquired using the Zeiss Axiovert 200M inverted low-light microscope system equipped with a Photometrics Cascade II EMCCD camera operated by the Metamorph advanced imaging software; a representative image is shown. The arrow highlight indicates typical colocalised fluorescence (yellow) in a distinct peripherally-sited vesicle. In this field alone, several cells demonstrate peripheral vesicular LyTR labelling, often colocalised with AEP staining.

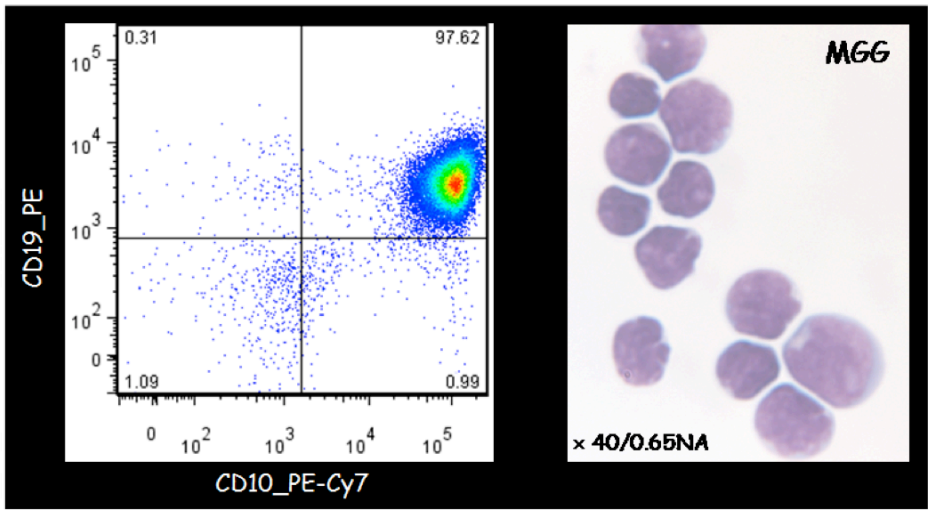
0.31
97.62
1.09
0.99
CD19_PE
CD10_PE-Cy7
MGG
× 40/0.65NA

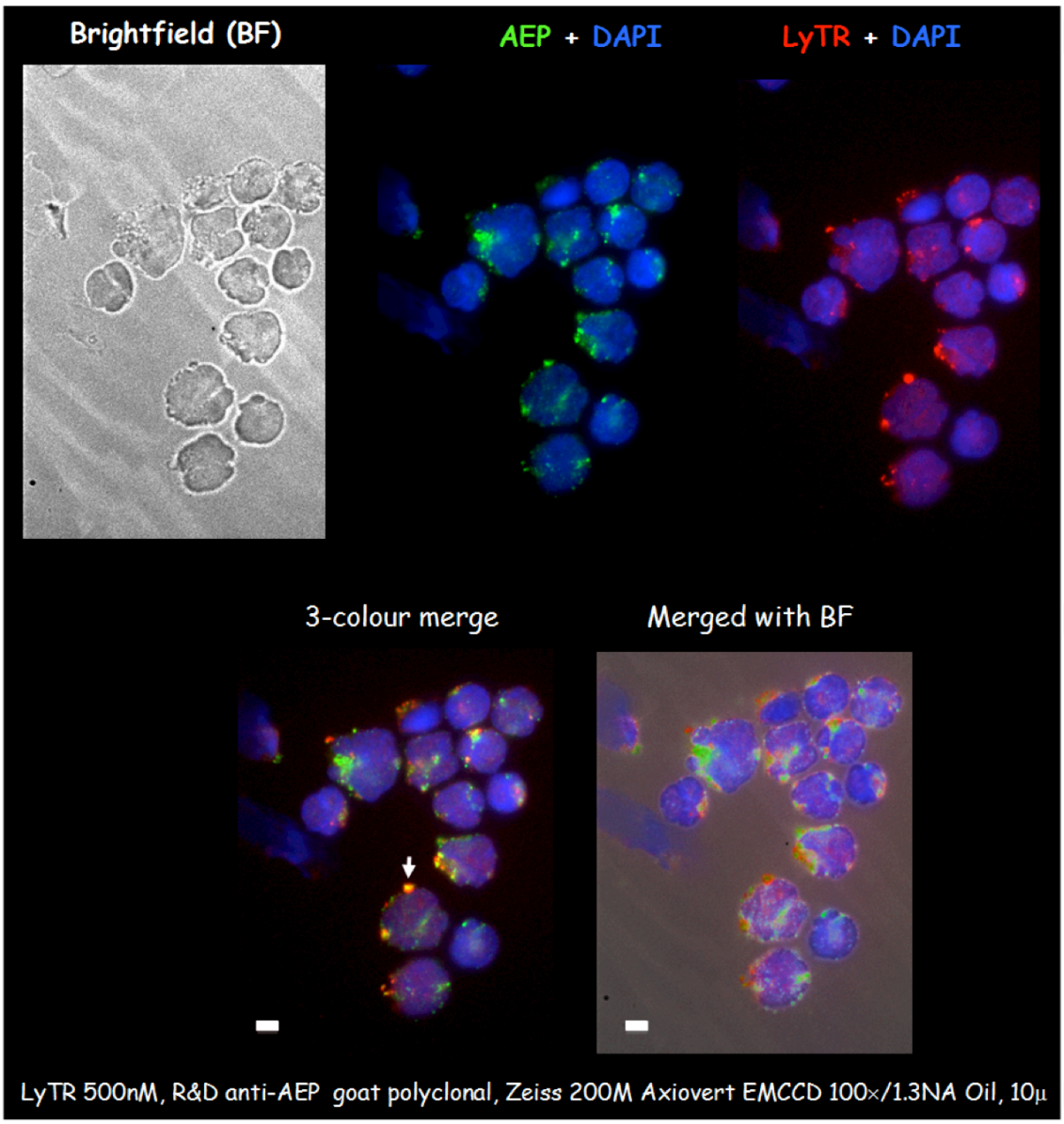
Brightfield (BF)
AEP + DAPI
LyTR + DAPI
3-colour merge
Merged with BF
LyTR 500nM, R&D anti-AEP goat polyclonal, Zeiss 200M Axiovert EMCCD 100×/1.3NA Oil, 10µ

**Figure 3.12** Fluorescence imaging of SD1 cells suggests exocytosis of mature AEP

SD1 cells labelled live with the AEP activity-based probe (AEP-ABP, green) and seeded on fibronectin-coated (10μg/mL) circular glass coverslips (10mm diameter, 4 hours, 37°C); post-labelling, cells were formalin-fixed, stained for filamentous actin (Alexa Fluor 647-labelled phalloidin, red) and DAPI-counterstained for nucleus (blue). Composite of images captured using the Zeiss Axiovert 200M inverted low-light microscope system equipped with a Photometrics Cascade II EMCCD camera operated by the Metamorph advanced imaging software.

The SD1 cell in the centre demonstrates a green blush of mature AEP extending beyond the cell boundary (as outlined by filamentous actin staining), suggesting exocytosis of the active protease.

*F-actin, filamentous actin, 100× /1.45NA objective, 10μ scale bar*

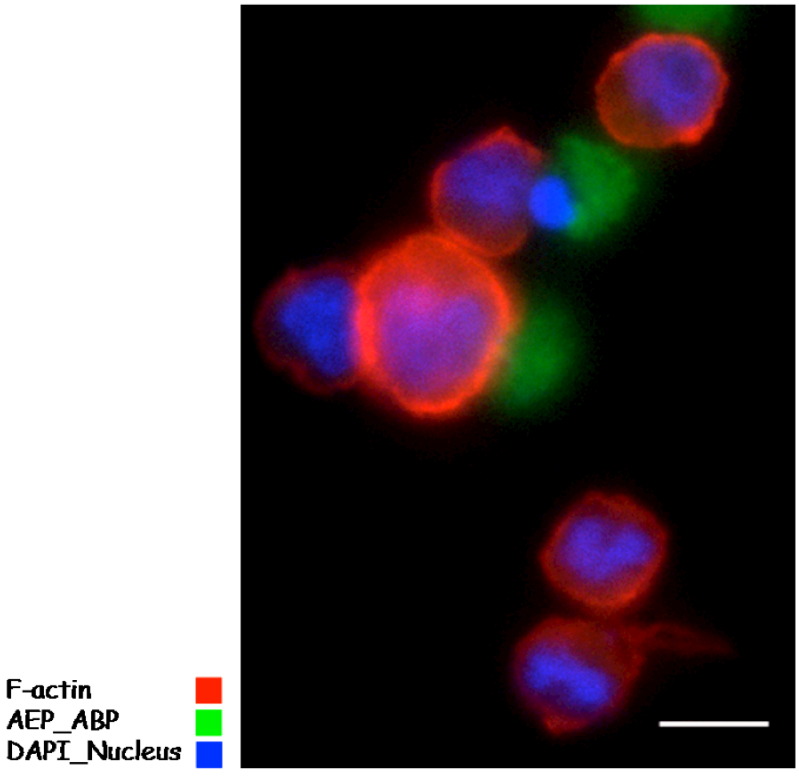

**Figure 3.13** SD1 cells shed microvesicles in cell culture

Phase-contrast microscopy images of SD1 cells in culture. On low-power magnification, fine suspended particulate matter is noted surrounding pleomorphic SD1 cells (20× ; scale bar, 10μ). On higher magnification (40×, 10μ scale bar), sub-micrometer spherical membranous particles (asterisks) are observed, characteristic of microvesicles

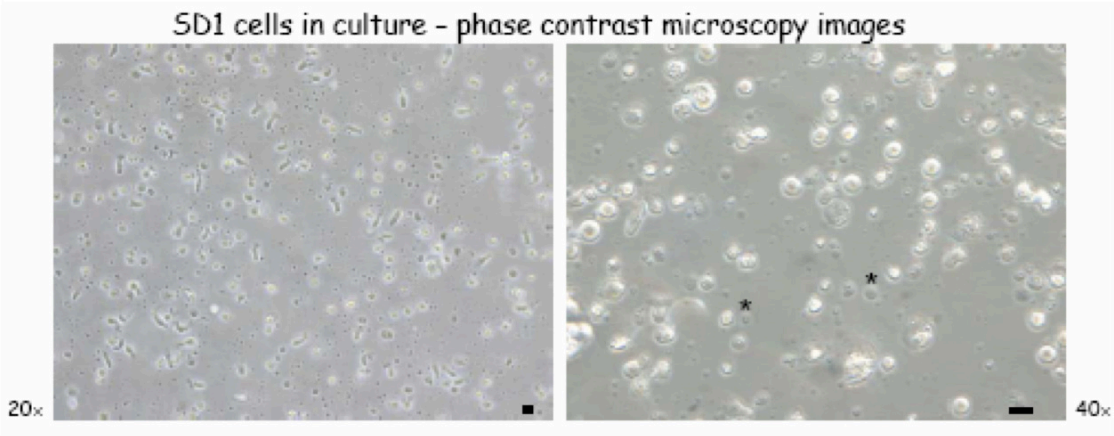


**Figure 3.14** SD1 cells shed preproAEP in microvesicles

(A) Microvesicle isolation protocol. Care was taken to ensure that cell viability was ~100% at time of microvesicle harvest to control for passive extracellular leak of cytoplasmic contents. Serum-free cell culture for 48 hours was sufficient for an adequate yield of microvesicles (MV).

(B) AEP and Cathepsin B (CTSB) immunoblots of whole cell lysates (WCL) and lysates of SD1 microvesicles (SD1-MV) created in NP40 lysis buffer. PreproAEP but not mature AEP is detected in SD1-MV isolates. β-actin served as loading control and the detection of this cytoskeletal protein in SD1-MV lysates suggests plasma membrane shedding. Unlike AEP, active heavy chain subunits of the lysosomal protease CTSB (24-27kDa) are uniformly detected in all samples. SB15, SupB15

(C) AEP immunoblot of acidified citrate-NP40 SD1-MV lysates (SD1MV-CitLB1 and SD1MV-CitLB2) and MV-free supernatant (S/N). Evidence for the presence of preproAEP in SD1-MV comes from AEP immunoblot of SD1-MV lysates prepared in acid citrate-NP40 lysis buffer (pH 5.0). The lower 47kDa band detected in acidified MV lysates represents intermediate pro-AEP generated by autoactivating cleavage of preproAEP in acid pH. Note the presence of free preproAEP in supernatant isolated from a low-viability culture of SD1 cells.

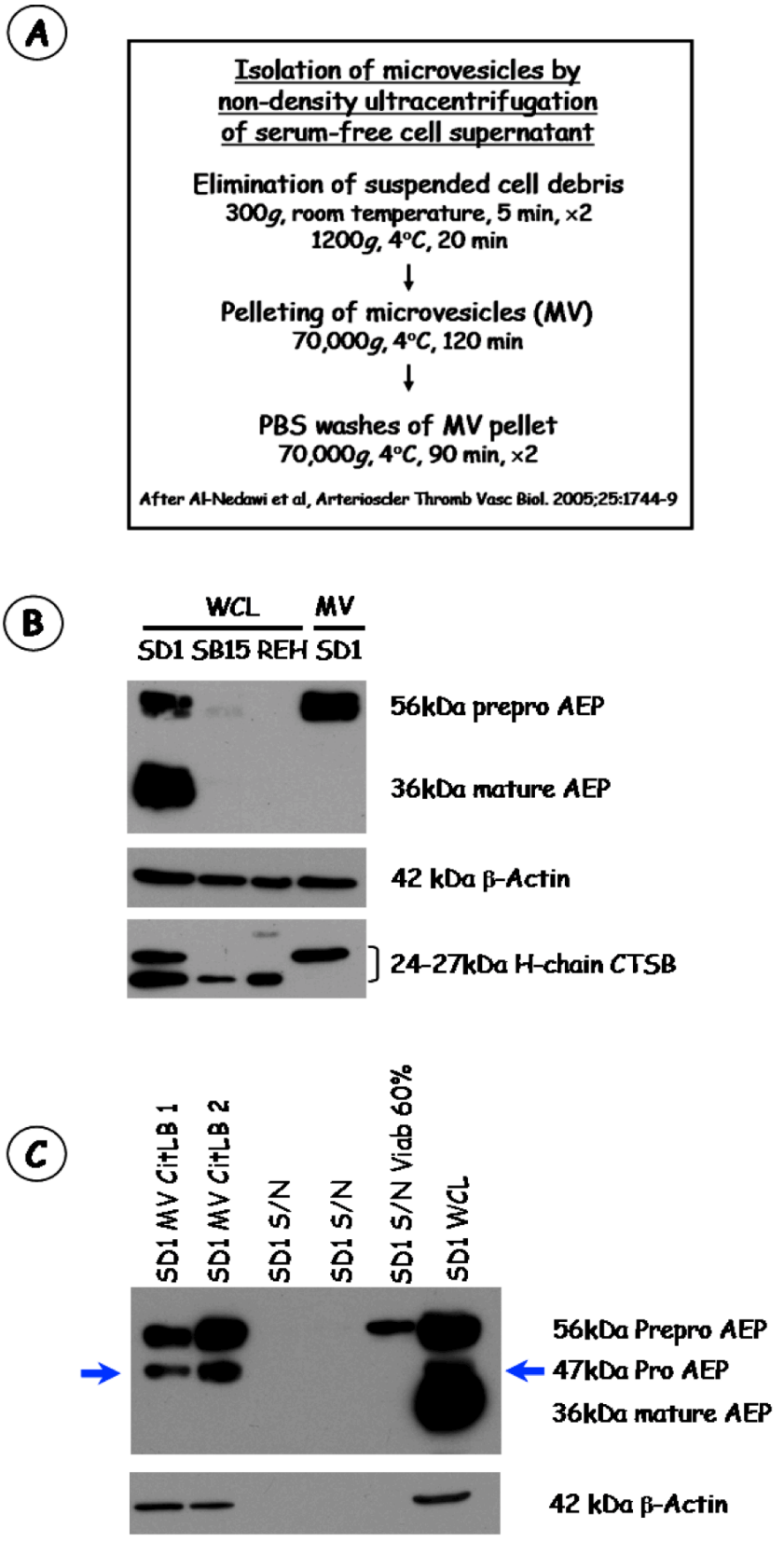
A
Isolation of microvesicles by non-density ultracentrifugation of serum-free cell supernatant
Elimination of suspended cell debris
300g, room temperature, 5 min, ×2
1200g, 4°C, 20 min
Pelleting of microvesicles (MV)
70,000g, 4°C, 120 min
PBS washes of MV pellet
70,000g, 4°C, 90 min, ×2
After Al-Nedawi et al, Arterioscler Thromb Vasc Biol. 2005;25:1744-9
B
WCL
MV
SD1 SB15 REH SD1
56kDa prepro AEP
36kDa mature AEP
42 kDa β-Actin
24-27kDa H-chain CTSB
C
SD1 MV CitLB 1
SD1 MV CitLB 2
SD1 S/N
SD1 S/N
SD1 S/N Viab 60%
SD1 WCL
56kDa Prepro AEP
47kDa Pro AEP
36kDa mature AEP
42 kDa β-Actin

**Figure 3.15** Summary cartoon representation of the postulated consequences of aberrant lysosomal dynamics in lymphoblasts

A lymphoblast is depicted interacting with extracellular components (stromal cell and matrix) through integrin-ICAM (intercellular adhesion family molecule) associations, often at sites of podosome protrusion. Acidified, aberrantly localised large peripheral endolysosomes discharge active hydrolases, include AEP, into the stroma. Active lysosomal enzymes degrade extracellular matrix molecules (e.g. AEP and fibronectin), activate counterpart enzymes (e.g. AEP and papain-family cathepsins) and liberate matrix-bound growth factors (including cytokines that potentially amplify these interactions). Peripheral localisation of lysosomes and postulated interaction of lysosomal hydrolases with integrin receptors (e.g. AEP RGD domain and β-integrin subunit) suggest a role in lymphoblast plasma membrane remodeling (*). Aberrant trafficking also probably results in extracellular release as secretory lysosomes (**).

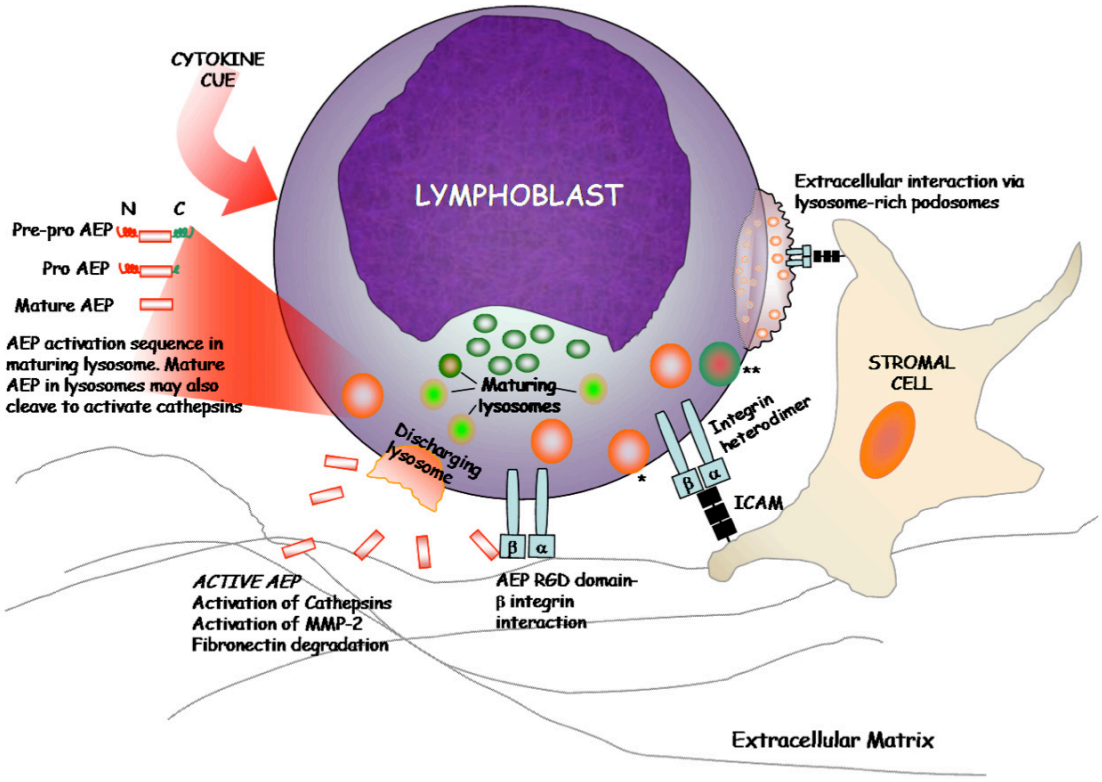

**Figure 3.16** Microarray analyses of AEP transcript expression in an independent sample cohort (St Jude Children's Research Hospital) indicates broad overlap of expression among the early progenitor-B ALL subtypes

Boxplot representations of normalised relative AEP expression across subtypes of childhood ALL. Median AEP expression is uniformly high in subtypes of early progenitor B ALL, including both adverse-risk Ph+ALL (BCR-ABL) and good-risk (TEL-AML1 and high-hyperdiploid [HD50]) subtypes, probably reflecting the physiological expression pattern in early stage B-lineage precursors. Low AEP expression in both very early and late B-lymphocyte progenitors is similarly mirrored by the neoplastic counterparts, MLL-rearranged [MLL(ALL)] and E2A-PBX1 ALL respectively.

Boxes encompass the interquartile (IQR, 25$^{th}$-75$^{th}$ percentile) ranges, horizontal bars within boxes represent median values, '+' values indicate means, whiskers denote values 1.5× IQR, outlier values are represented by asterisks, dashed lines demarcate off-scale outlier values

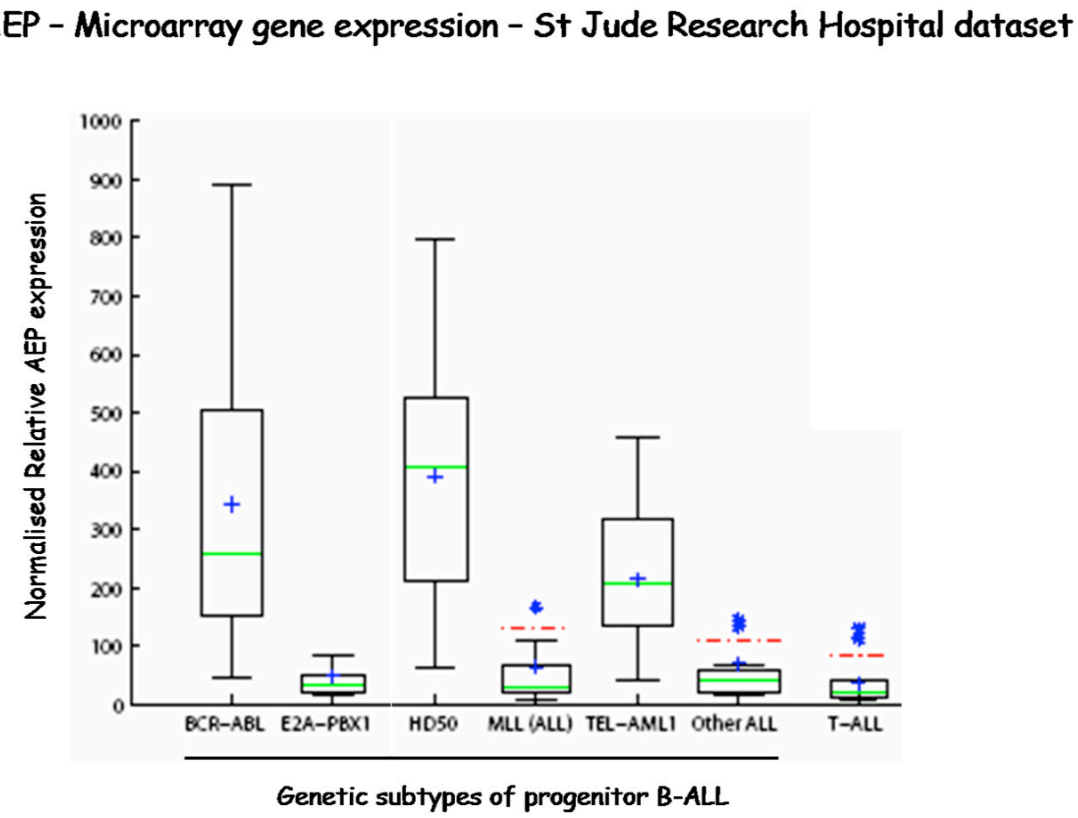

**Figure 3.17** In an independent sample cohort (University Malaya), similar relative AEP transcript overexpression in Ph+ ALL is observed

Boxplot representation of normalised relative fold AEP transcript expression as determined by quantitative PCR, in leukaemic blasts from a prospective cohort of consecutively enrolled children (n=145) with distinct genetic subtypes of progenitor-B ALL. Although there is considerable overlap, median relative AEP expression is higher in Philadephia chromosome positive ALL (BCR-ABL).

Genetic subtypes were identified by PCR identification of recurrent somatic fusion transcripts (FT): BCR-ABL, ETV6-RUNX1, TCF3-PBX1, MLL-AF4. The subset of progenitor-B ALL without identifiable fusion transcripts ('No FT') includes aneuploid (i.e., high hyperdiploid and hypodiploid) lesions. *Data courtesy of Dr. Hany Ariffin, Department of Paediatrics, University Malaya, Malaysia*

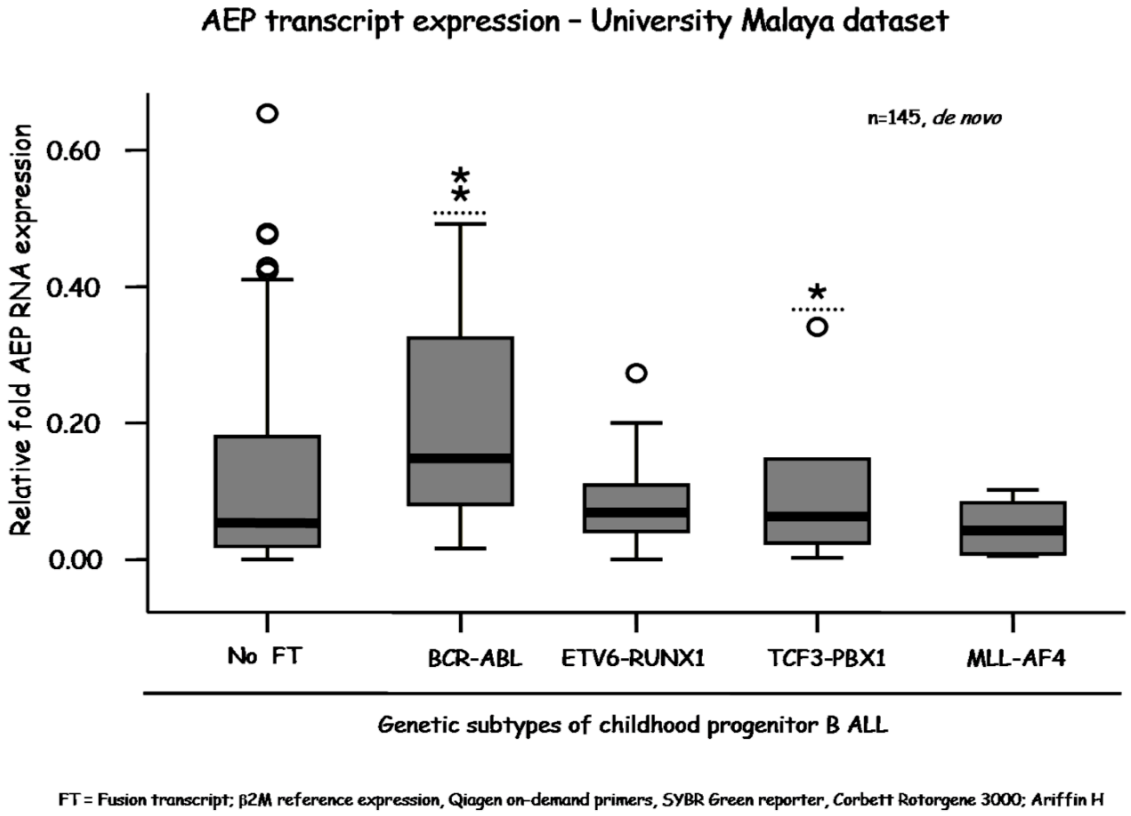


Boxes encompass the interquartile (IQR, 25$^{th}$-75$^{th}$ percentile) ranges, horizontal bars within boxes represent median values, whiskers denote values 1.5× IQR, outlier values are represented by circles (≤3× IQR) and asterisks (>3× IQR), dashed lines demarcate off-scale outlier values

**Figure 3.18** AEP upregulation in iAMP21 ALL is not associated with variant-transcript expression

Heatmap and line graph representations of microarray analysis of exon-level expression of AEP in children with iAMP21 (blue) and high hyperdiploid (HH, red) ALL. Each datapoint represents averaged normalised expression of probes for each putative exon within the coding region of the AEP transcript (reference transcript sequences NM_005606.5 and NM_001008530). Expression is uniformly high across all eight interrogated exons in iAMP21 ALL, suggesting the absence of exon-skipping and aberrant transcript expression associated with AEP overexpression in this ALL subtype. *Data courtesy of Frederick W van Delft and Olga Yiannikouris*.

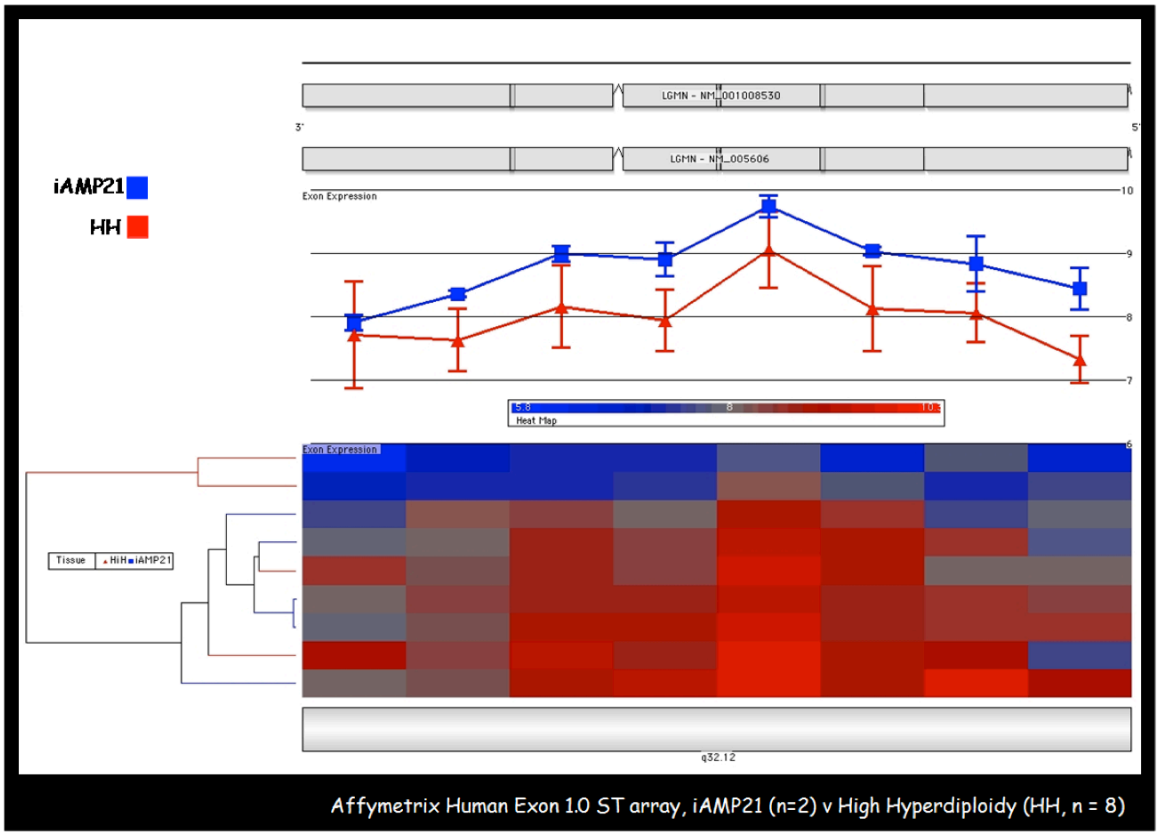

**Table 3.1 Investigation of AEP transcript expression - experimental limitations**

| | | |
|---|---|---|
| Preanalytical variables | Percentage lymphoblasts in clinical samples | Research samples are typically last in the sequence of multiple bone marrow aspirates from a single pass. The samples are therefore likely to be diluted. This lowers % blast count, even in the case of diagnostic samples where the bone marrow is ~100% infiltrated by leukaemic cells. An enrichment strategy for lymphoblasts would have addressed this concern but would also have resulted in loss of material |
| | Sample integrity | This is a lesser concern. Most samples were processed within less than 24 hours of collection. Adequate-quality RNA isolates (established by electropherogram profiles) from these samples were used for microarray studies. β2M transcript expression was used as an additional surrogate estimate of sample integrity. |
| Validation of microarray analysis | Relative quantitation of AEP transcript expression was performed on the same sample set used for microarray analysis | Although relative transcript quantitation helped validate results of microarray analysis, a more informative approach would have been to examine relative AEP expression in an independent sample cohort. This is now being investigated (see Table 3.2) |

**Table 3.2 AEP expression in ALL - some as yet unresolved questions**

| Issue | State of knowledge |
|---|---|
| Is AEP overexpression (genomic region 14q32.1) merely an epiphenomenon of somatic rearrangement events occurring at the neighbouring immunoglobulin heavy chain locus (14q32.3) in a progenitor-B cell? | This for the moment remains an open question. Microarray analysis from the St Jude group indicates broad overlap in expression among distinct genetic ALL subtypes sharing an early progenitor-B immune phenotype (**Figure 3.16**) suggesting that AEP expression is merely an ontogenic marker. Conversely, prospective examination of AEP transcript expression in an independent patient cohort indicated relative median overexpression in adverse risk Philadelphia-chromosome positive ALL (**Figure 3.17**) |
| What is the correlation between AEP transcript and protein expression? | This would be specifically addressed by an ongoing prospective biomarker study undertaken by the Children's Cancer Group. This study, a component of the current UK childhood ALL trial (ALL2003), is in part, examining potential associations between AEP transcript/protein expression and other risk variables (clinical, genetic and response) |
| Is AEP upregulation associated with aberrant transcript or protein expression? | *Limited* indirect evidence suggests that this is probably not the case.<br>• AEP transcript overexpression is not associated with exon-skipping in iAMP21 ALL (Figure 3.18)<br>• Immunoblot protein overexpression is matched by elevated AEP enzyme activity |
| | At the transcript level, use of complementary Taqman primer-probe pairs for AEP transcript quantitation or direct sequencing of transcript in an unbiased sample would be able to better address the question of variant AEP transcript expression |
| What is the mechanism of AEP overexpression in adverse-risk progenitor B childhood ALL? | This is at present not known. RUNX1 for instance is among the transcription factors predicted to bind to the putative AEP promoter [4]* and may account for the overexpression observed in iAMP21 ALL. |
| | Gene amplification may be a mechanism and may account for AEP overexpression observed in High Hyperdiploid ALL where somatic whole chromosome 14 duplications are common. Of note though, AEP overexpression is not a uniform feature in this genotype. |

**Table 3.2 AEP expression in ALL** (continued)

| Issue | State of knowledge |
|---|---|
| Mechanism of AEP overexpression in adverse-risk progenitor B childhood ALL (continued) | Rearrangements at the 14q32.1 genomic locus may also drive AEP overexpression but have not been specifically investigated. This is pertinent since rearrangement at the pseudoautosomal region of somatic sex chromosomes results in upregulated expression of CRLF2 (cytokine receptor like factor 2), a cytokine receptor subunit molecule recently reported to be strikingly overexpressed in adverse-risk progenitor B ALL. |
| | Additional mechanisms such as enhanced transcript or protein stability may also be operative but are not readily investigated. |
| Does AEP expression correlate with adverse clinical outcomes? | This question is being investigated as part of the ALL biomarker study alluded to earlier. Multivariable analysis will be performed to examine whether a pre-determined threshold of AEP transcript or protein expression independently influences minimal residual disease clearance or risk of relapse |

*Supplementary Material, Additional File 2, Reference [4]

**Table 3.3 Microscopy investigations of intracellular AEP expression – experimental limitations**

| *Issue* | *Limitation* | *Measures to address* |
|---|---|---|
| Cytospin preparations | Although the easiest technique for microscopy examination of cells in suspension, cytocentrifugation and air-drying of smears potentially introduce morphology artifacts | *In situ* examination of leukaemic cells allowed to adhere to coated/treated coverslips or glass-bottomed dishes will partially address this concern but the strategy of induced adhesion may in itself, not be representative |
| Examination of single-cell populations | Microscopy examination of single populations of leukaemic cells is informative but ignores interactions with the microenvironment | *In situ* examination of leukaemic cells co-cultured with stromal and endothelial cells would be more representative; acquiring appropriate optical sections is more challenging in this context |
| Fixed cell imaging | Formalin-fixation and permeabilisation potentially introduce morphological artefacts | Live cell imaging of intracellular AEP and lysosomal dynamics in leukaemic cells using non-toxic cell-permeable probes would be more representative but also technically more challenging |
| AEP-activity based probe (AEP-ABP) | Specificity of the AEP-ABP has not been rigorously demonstrated. Validation experiments were limited by availability of the AEP-ABP compound but a gift of additional probe has recently been obtained. | To better establish probe specificity, the following approaches would be informative: (a) Is there colocalisation of florescence following dual AEP labelling using both the AEP antibody and activity-based probe?; and (b) Is AEP-ABP labelling absent in *mutH148A*-AEP+ cells where the AEP catalytic site is inactivated? |
| Primary ALL cells | Observations on intracellular AEP distribution have been essentially based on investigations in ALL cell lines. | This is set to change. A biorepository of childhood ALL samples has been in operation for the past two years and would be a source of primary diagnostic material for microcopy analysis |

# 4

# AEP expression and cell motility

Relapses in the central nervous system (CNS) pose a major therapeutic challenge in childhood ALL. It is postulated that aberrant lymphoblast trafficking and motility results in blood-borne infiltration of the CNS through an orchestrated process of homing, endothelial adhesion-signalling, cytoskeletal reorganisation and matrix degradation (**Chapter 1**, **Figure 1.17**). In solid cancers, AEP expression is associated with local invasiveness and tumour metastasis, suggesting that in overexpressing leukaemic cells, the protease could potentially function as a mediator of aberrant motility.

Investigators at the Scripps Research Institute (Liu C and colleagues, Department of Immunology) have previously reported enhanced *in vitro* and *in vivo* motility of human embryonic kidney (HEK293) cells engineered to ectopically overexpress AEP (Chapter 2, [24]). Observations in the model AEP-overexpressing poor-risk invasive progenitor-B ALL cell line, SD1 corroborate these findings. AEP downregulation, either by transcript depletion or chemical inhibition, significantly attenuated SD1 cell motility (**Figure 4.1**). AEP accelerates cell motility through mechanisms that presumably include extracellular matrix degradation, activating cleavage of pro-motility molecules and signalling interactions with β-integrin receptors. This chapter describes *in vitro* motility studies of ectopic AEP-overexpressing HEK293 cells. Although non-representative, HEK293 cells were chosen primarily for ease of transfection. Motility assays were performed as prelude to proposed studies of AEP-interacting proteins and identification of candidate pathways associated with the motile phenotype. However as elaborated in this chapter, the observations diametrically differed from findings of the Scripps group. Reasons for this discordance are discussed.

## Experimental methods

*HEK293 cells*

Native and modified cells were routinely maintained in serum-supplemented DMEM and passaged at 75-80% confluence; modified cells were additionally maintained in selection agent-supplemented complete medium. Typical cell handling steps included trypsin EDTA mobilisation-neutralisation, PBS washes and 300*g* room temperature centrifugation. Early passage (less than 20) near-100% viable cells were used in all experiments. Native HEK293 cells were sourced from CRUK Central Cell Services.

*AEP expression plasmid constructs*

Full-length AEP cDNA insert (Appendix A) was amplified, purified, sequence-verified (**Figure 4.2**) and placed in destination mammalian expression vectors (**Table 4.1**), either by restriction-enzyme site ligation or Gateway recombination (**Figure 4.3**).

*Creation of AEP-overexpressing HEK293 cells*

HEK293 cells were lipid-transfected with AEP expression plasmid constructs. Transfected cells were maintained and propagated in the presence of selection agents to establish stable polyclonal constitutive (enforced) and inducible AEP-expressing HEK293 cells (**Figure 4.4**). The inducible expression system is designed to enable tighter regulation of baseline and activated gene expression (**Figure 4.5**).

*Boyden chamber motility assays*

Assays were performed in 24-well formats. Modified HEK293 cells, passaged to subconfluence 48 hours prior, were reconstituted in serum-free medium and seeded into porous (8μm) upper chamber cell inserts; lower chambers contained serum-supplemented growth medium (**Figure 4.6**). Inserts were coated with 1:50 dilution Matrigel in some assays. Matrigel at this dilution forms a thin non-obstructive membranous protein coat that facilitates cell adhesion and migration

[1]. Assays using dilute Matrigel-coated cell inserts essentially reflect non-barrier cell motility and do not materially differ from uncoated-insert assays. Lower chamber cell counts were estimated 24 hours later by coulter counter or by microscopy of stained cell inserts (**Figure 4.7**). All assays were performed with parallel controls, including in some cases the PC3 human prostate carcinoma cell line as reference positive control.

*Complete details on reagents, materials and optimisation-validation experiments are available in the Methods chapter*.

## Results

*Ectopic AEP overexpression does not confer a motile phenotype to HEK293 cells*

Contrary to observations of the Scripps group, inducible and enforced AEP-expressing cells did not demonstrate enhanced motility. Lower chamber cell counts of AEP-expressing HEK293 cells, estimated using both coulter counting (**Figure 4.8**, **Supplementary Table S4.1**) and stained cell insert microscopy (**Figure 4.9**), did not significantly differ from controls. Performing extended timepoint Boyden chamber assays did not alter these conclusions (**Figure 4.10**, **Supplementary Table S4.2**).

## Discussion

The objective of these experiments was to investigate the role of AEP in cell motility. In studies in leukaemic cell lines sharing the *BCR-ABL1* genotype, AEP-overexpressing SD1 cells were significantly more motile than non-expressing SupB15 cells. This motility was attenuated following AEP inhibition suggesting a pro-motility role for the lysosomal protease.

In reports from the Scripps Institute, enforced expression of AEP resulted in increased motility of HEK293 fibroblasts. As described in this Chapter, these observations were however not replicated, despite adopting a similar experimental approach. Dissimilarities in cell clonality, genotype and assay

methodology may partly account for this discrepancy (**Table 4.2**). The observations were also limited by failure to establish and investigate clonal populations of low, intermediate and high-expressing cells (**Table 4.3**).

Despite the limitations highlighted above, the observation of a lack of effect of ectopic AEP expression on cell motility is corroborated by other findings from within the group. In these studies, the SD1 cell line has served as a representative high-risk model, associated as it is with both the *BCR-ABL1* genotype as well as with CNS disease when injected into mice (**Figure 4.1**). Data from experimental studies suggest that the pro-motility role of AEP in SD1 cells is contingent upon the simultaneous co-expression of a fundamental complement of adhesion and signalling molecules that include the LFA-1 integrin ($\alpha_L\beta_2$)::ICAM-1 (intercellular adhesion molecule 1) dyad and the small-molecule G protein second messenger molecule Rac2. Thus, in SupB15 cells that lack these key adhesion-signalling molecules, sole ectopic AEP overexpression had little impact on the motility phenotype. Although enforced AEP overexpression in REH cells did result in a significant increase in motility compared to wild-type cells, the extent of increase was still far less than that observed in constitutive AEP-expressing SD1 cells (**Figure 4.11**). As noted in Chapter 7 (**Figure 7.2**), studies are underway investigating the consequence of ectopic candidate molecule co-expression (e.g. AEP and Rac2) on REH and SupB15 cell motility. These studies have now been expanded to systematically investigate the mechanistic basis for lymphoblast motility, including determination of the requisite repertoire of adhesion, signalling and lysosomal matrix-degrading molecules in leukaemic cells as well as microscopy studies of lymphoblast-stromal and lymphoblast-endothelial interactions that govern transvascular motility. Results from these studies will be validated on primary material.

**Figure 4.1** The Philadelphia chromosome-positive progenitor-B ALL cell line, SD1, overexpresses AEP, demonstrates brisk *in vitro* motility across basement membrane barriers that is in part AEP-dependent, and infiltrates the central nervous system when introduced into immunocompromised mice.

(A) AEP immunoblot of cell line whole cell lysates. Both SD1 and the B-lymphoblastoid cell line HRC57, overexpress AEP. SupB15 (SB15) is another Philadelphia chromosome-positive progenitor-B ALL cell line; REH is an *ETV6-RUNX1* progenitor-B ALL cell line. Doublet detection bands associated with the precursor protein represent different states of glycosylation. β-actin serves as loading control.

(B) Lower chamber cell counts (cells/mL) following 24-hour Boyden chamber assays using 5-micron pore Matrigel-coated (1:10 dilution, ~1mg/mL) cell inserts seeded with $1\times10^5$ cells. SD1 is at least 5-6× more invasive across Matrigel basement membrane barrier when compared to SupB15 and REH cell lines. Matrigel invasion is significantly reduced (by between 50-60%, $p$=0.0003) when SD1 cells are treated with a non-toxic dose of a cell-permeable AEP inhibitor (AEP*i*, MV026630) or when AEP transcript in SD1 cells is stably depleted by lentiviral shRNA silencing ($p$=0.006). Irrelevant lentiviral transcript silencing ('non-specific silencing') or AEP*i* vehicle treatment (DMSO, data not shown) had no impact on SD1 motility. Summary data from three experiments, error bars represent standard error of means, asterisks represent $p$ values from 2 sided unpaired $t$ tests

(C) Low-power magnification (4×) of GFP immunostain of sagittal section of brain from a SCID-Beige immunocompromised mouse, 4-6 weeks after tail vein injection of GFP-expressing SD1 cells. A dense leptomeningeal deposit of GFP-positive SD1 cells is observed overlying the cerebellum and occipital cortex.

*GFP, green fluorescent protein; shRNA, short hairpin RNA; SCID, severe combined immunodeficiency*. *Invasion data and mouse brain section histology, courtesy of Mark Holland and Fernanda Castro*

A

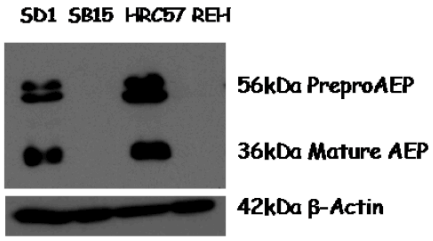


B

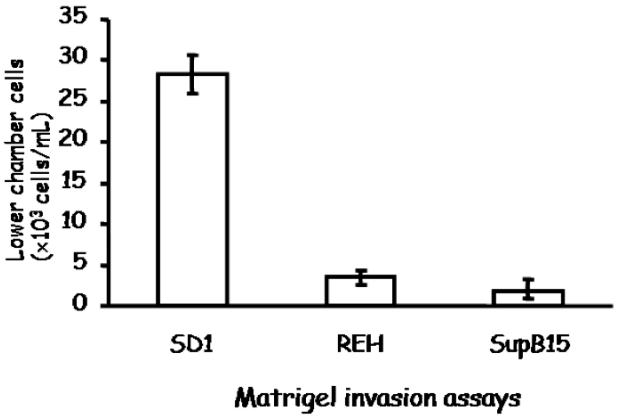


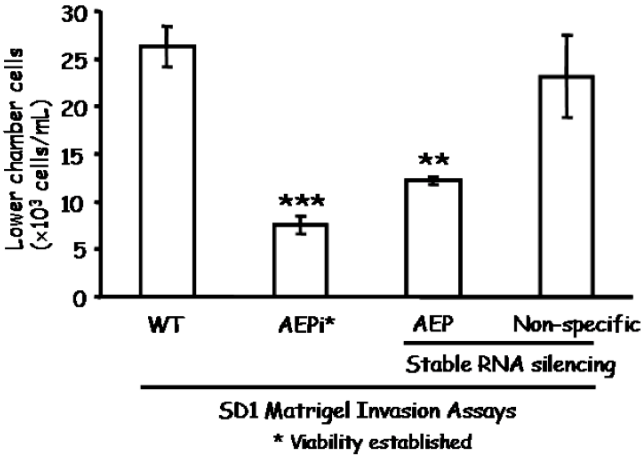


C

CNS disease in SD1-engrafted SCID/Beige mouse 4 to 6 weeks after intravenous injection

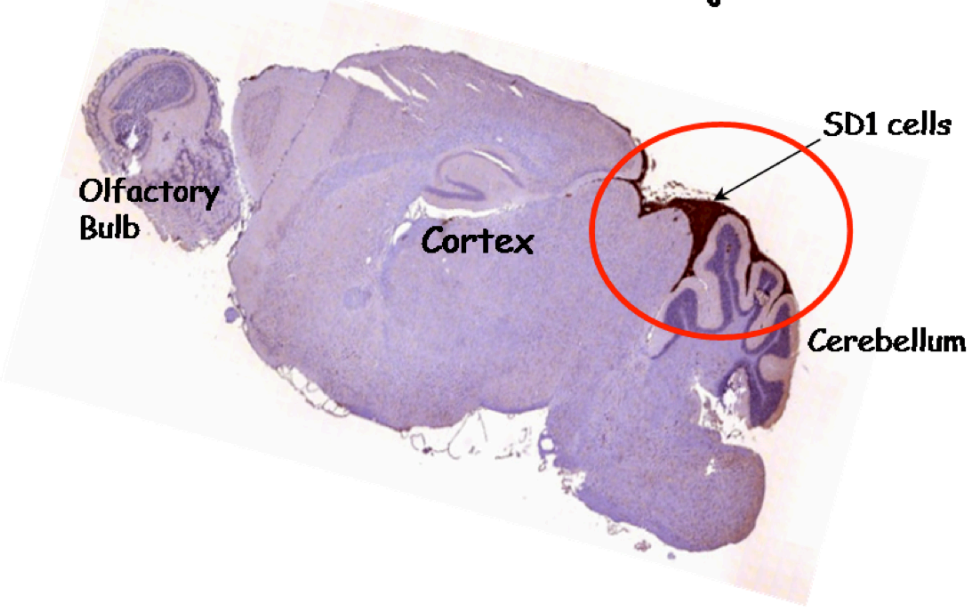

**Figure 4.2** Plasmid cloning, Step 1

Schematic outline of the initial steps in plasmid cloning, including bacterial transformation, amplification by bacterial culture, plasmid isolation (small-scale or large-scale) and sequence verification

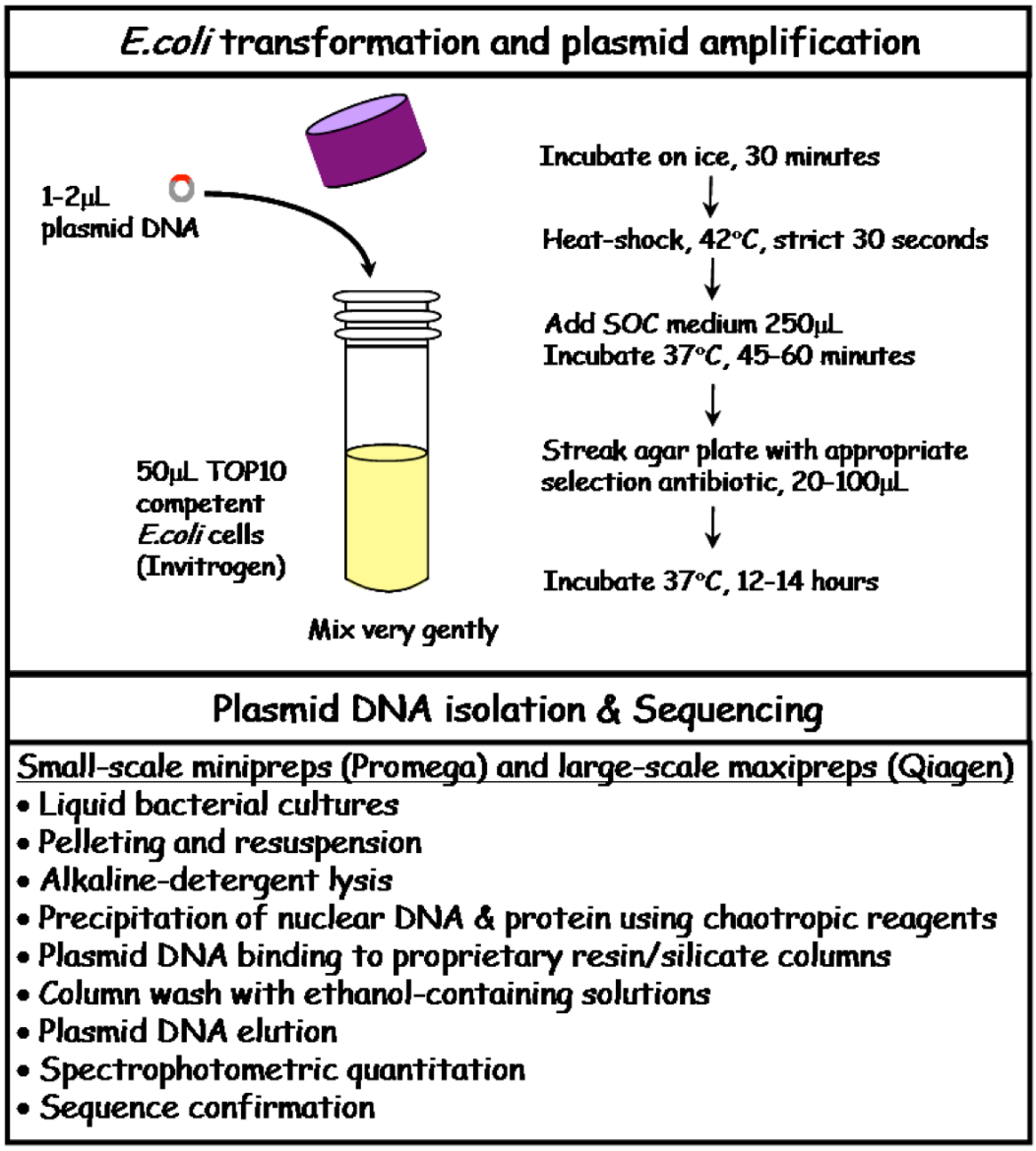

**Figure 4.3** Schematic outline of plasmid cloning, Step 2

*Upper panel*: Isolation of full length (FL) AEP cDNA insert from source plasmid by restriction enzyme digestion and purification after gel electrophoresis (left) followed by introduction into the multiple cloning site of an inducible-expression system destination vector (right)

*Lower panel*: Introduction of AEP insert into a mammalian enforced expression plasmid using Gateway cloning technology (Invitrogen)

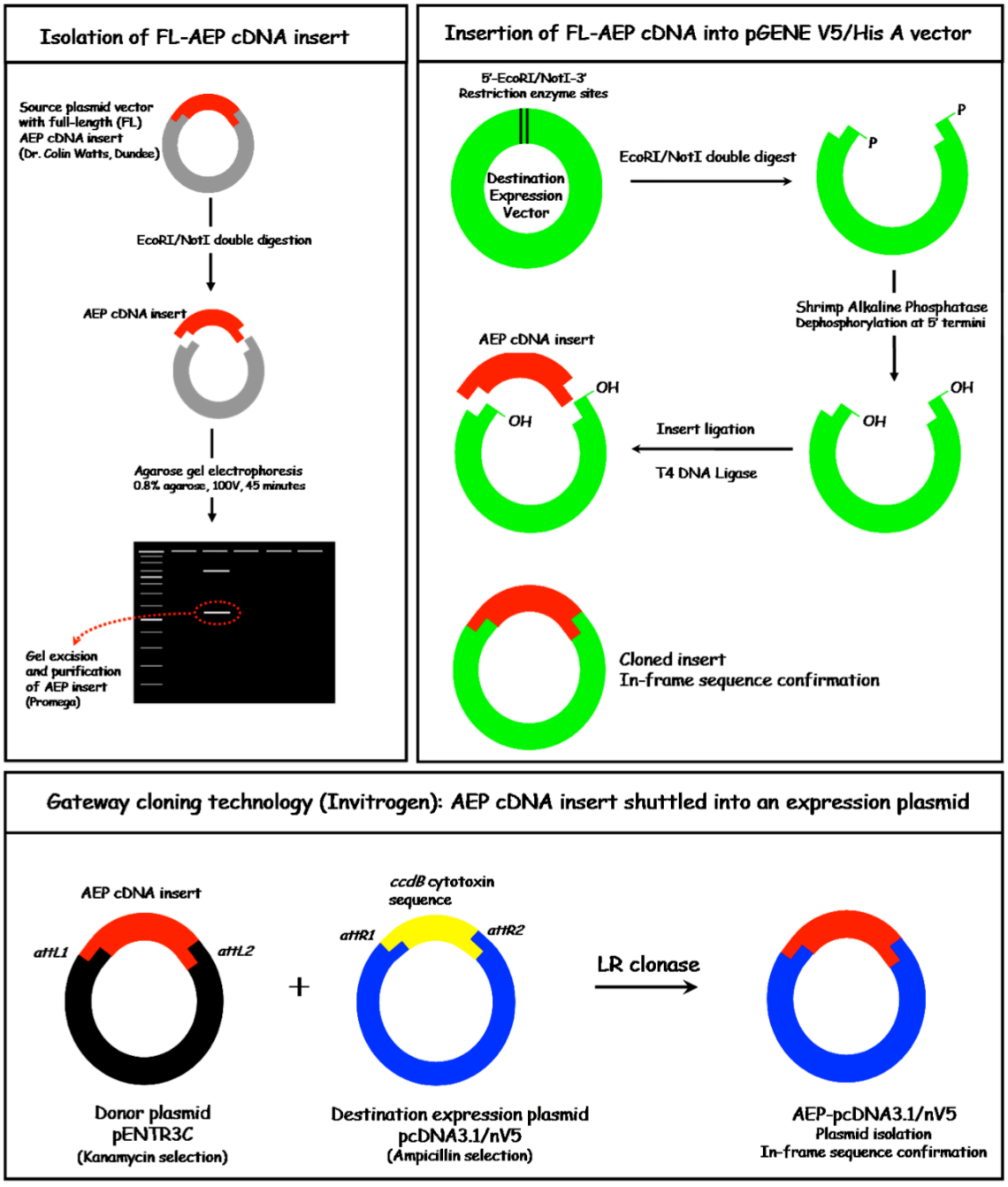

**Figure 4.4** Creation of stably-transfected enforced and inducible polyclonal AEP-overexpressing HEK293 cells

(A) Schematic outline. HEK293 human embryonic kidney fibroblasts were lipid-transfected with expression plasmid containing full-length AEP cDNA insert (NCBI RefSeq NM_005606.5, Appendix B) and were later treated with selection agents to establish a stable polyclonal population of enforced (AEP.293) and inducible (AEP.293GS) AEP-overexpressing cells.

(B) *Left*: AEP immunoblot in whole cell lysates using a goat polyclonal anti-human AEP antibody (R&D); β-actin served as loading control. *Right*: Estimation of AEP enzyme activity in citrated whole cell lysates using a fluorescent substrate cleavage assay; activity in the HRC57 cell line served as reference. Note that AEP expression (as estimated by activity) in AEP.293 cells is nearly 2× higher than in SD1 cells. The additional immunoblot band noted between precursor and mature AEP detection bands in AEP.293 probably represents an intermediate form of AEP. REH and SupB15 (SB15) are non-AEP expressing progenitor-B ALL cells. EV.293 refers to mock-transfected controls (AEP insert-free plasmid).

(C) AEP immunoblot in whole cell lysates with β-actin as loading control. Treatment of AEP.293GS cells with the inducing agent, Mifepristone (Mfp, 10nM, 24 hours) strongly activates AEP expression. There is minimal basal AEP expression in untreated AEP.293 cells. Mifepristone treatment has no effect on mock-transfected controls.

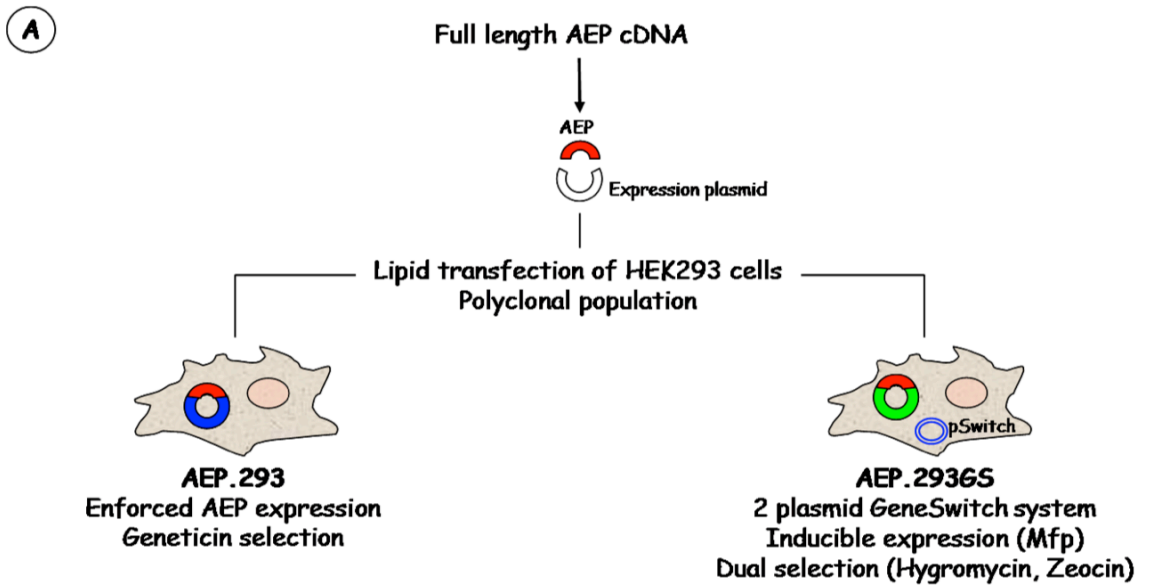
A
Full length AEP cDNA
AEP
Expression plasmid
Lipid transfection of HEK293 cells
Polyclonal population
pSwitch
AEP.293
Enforced AEP expression
Geneticin selection
AEP.293GS
2 plasmid GeneSwitch system
Inducible expression (Mfp)
Dual selection (Hygromycin, Zeocin)

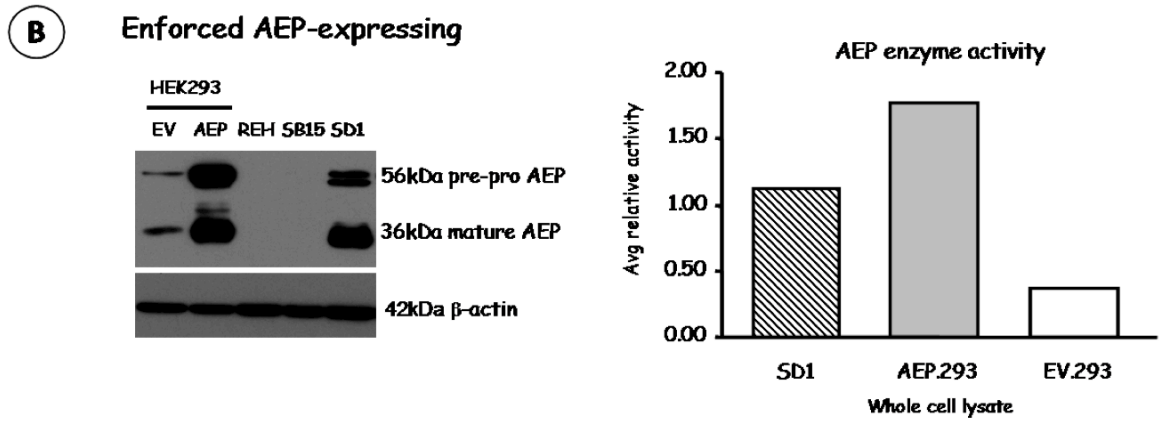
B
Enforced AEP-expressing
HEK293
EV AEP REH SB15 SD1
56kDa pre-pro AEP
36kDa mature AEP
42kDa β-actin
AEP enzyme activity
Avg relative activity
2.00
1.50
1.00
0.50
0.00
SD1
AEP.293
EV.293
Whole cell lysate

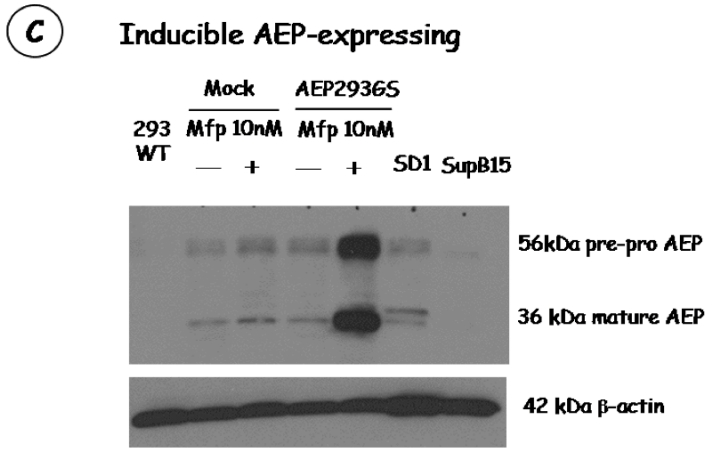
C
Inducible AEP-expressing
Mock
AEP293GS
293 WT
Mfp 10nM
Mfp 10nM
— + — +
SD1 SupB15
56kDa pre-pro AEP
36 kDa mature AEP
42 kDa β-actin

**Figure 4.5** Schematic outline of the mechanism of the dual–plasmid inducible-expression system

Mifepristone-induced conformational activation of a regulatory chimaeric protein results in transactivation of target gene expression as well as autoactivation of the regulatory protein

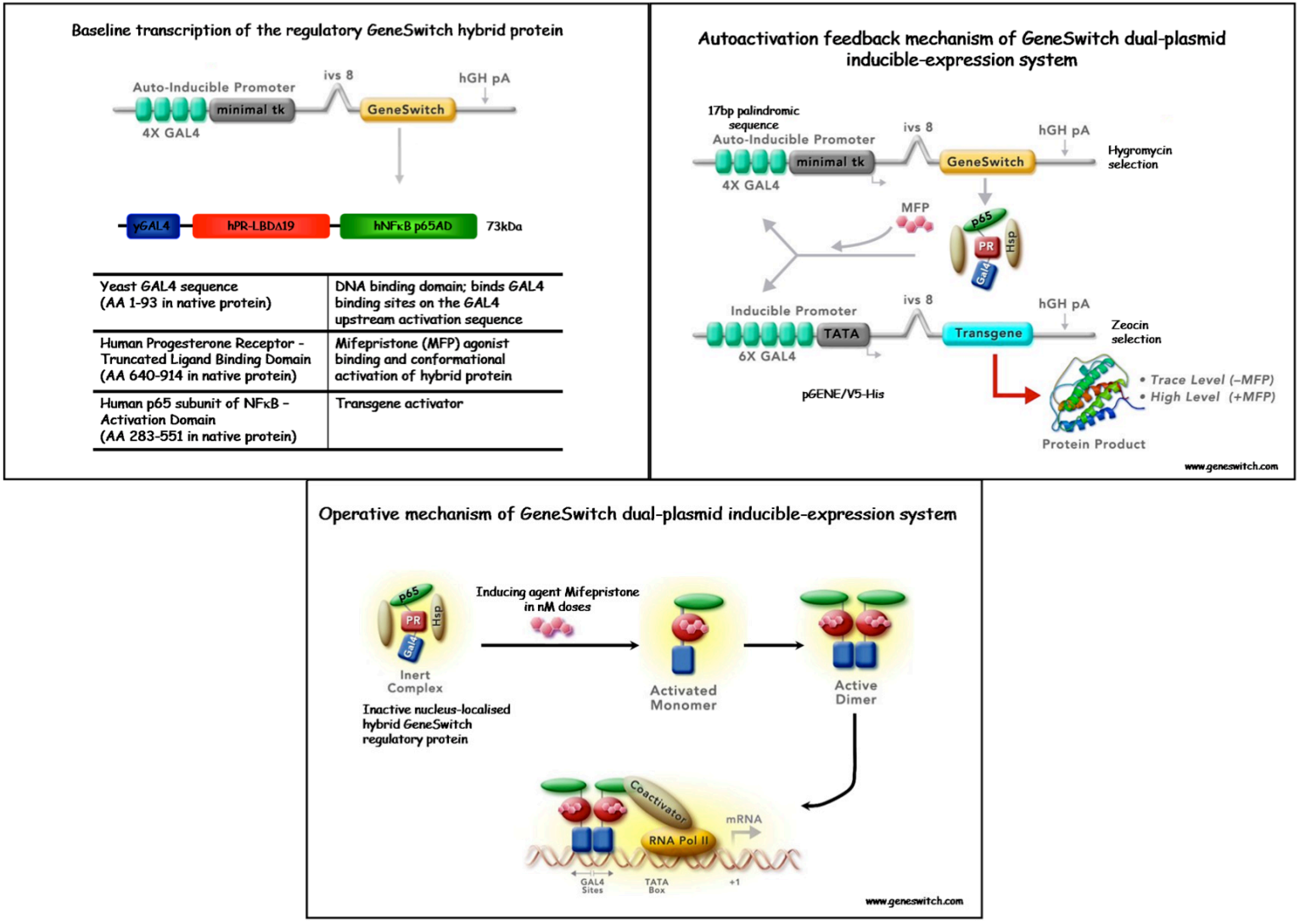

**Figure 4.6** Schematic outline of Boyden chamber motility assay work flow

For optimal confluence, ectopic AEP-overexpressing HEK293 cells were passaged 48 hours prior to assay. AEP expression was activated in inducible-expressing cells 24 hours prior to assay (Mifepristone, 10nM). Cells were trypsin-mobilised, reconstituted in serum-free DMEM and seeded at a density of $1\times10^5$ cells in 8-micron pore (Matrigel-membrane coated or -uncoated) upper chamber inserts in a 24-well format. Complete growth medium was placed in lower chamber wells to provide a chemotactic gradient. Following 24-hour incubations in humidified cell culture incubators, lower chamber cell counts were estimated by coulter counting and/or microcopy counts of crystal-violet stained cell inserts. Modified AEP non-expressing HEK293 cells served as negative controls in assays.

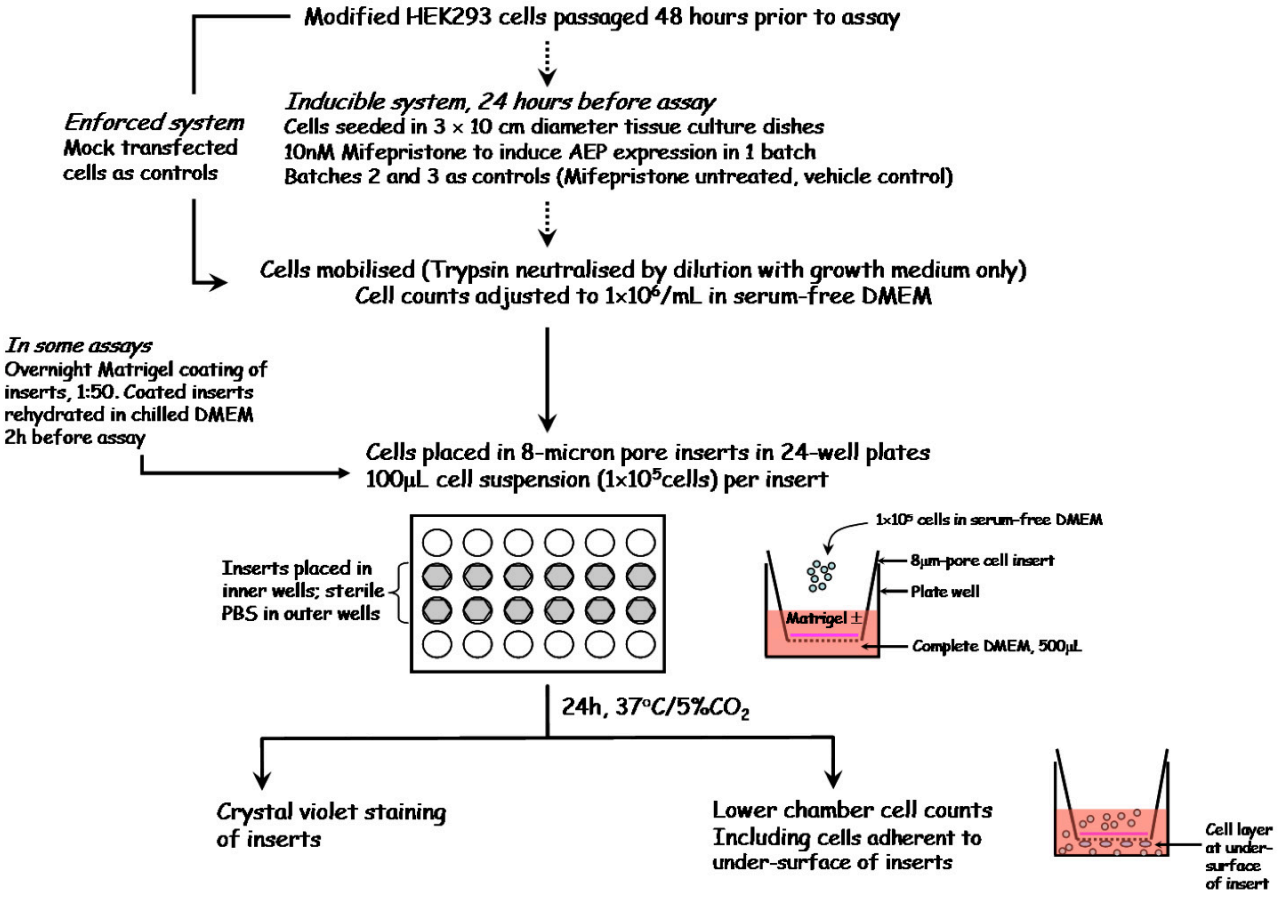

**Figure 4.7** Schematic outline of Boyden chamber assay cell counts

*Upper panel*: Lower chamber cell counts by Trypsin-EDTA mobilisation of adherent cells in cell inserts followed by coulter counting; *Lower panel*: Crystal-violet staining of adherent cells on undersurface of cell inserts

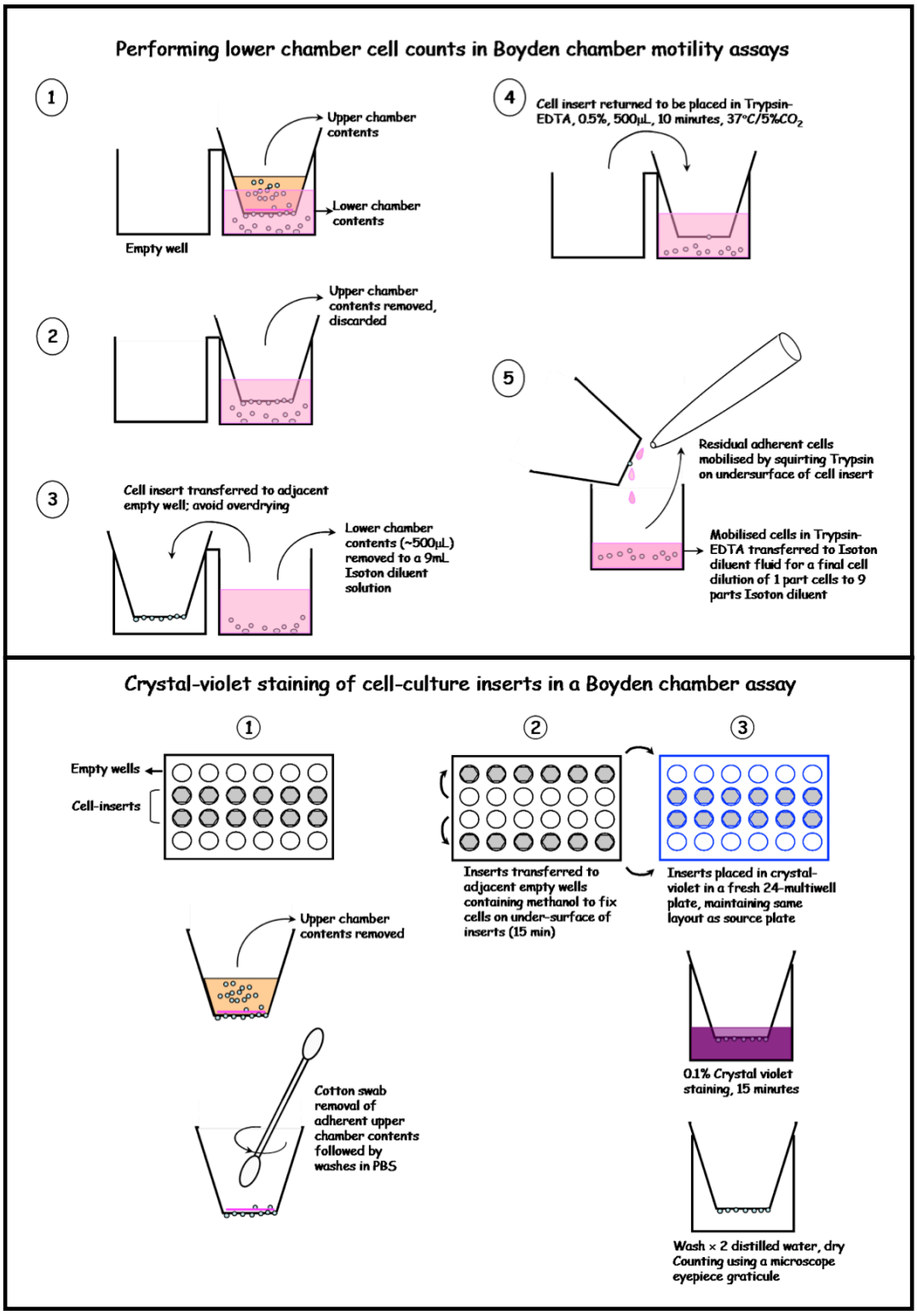

**Figure 4.8** Ectopic overexpression of AEP in HEK293 cells does not enhance cell motility

Summary boxplot representations of lower chamber cell counts (cells/mL) from 24-hour Boyden chamber assays in enforced (right) and inducible (left) AEP-overexpressing HEK293 cells.

*Left*: Summary of 6 experiments. Motility of inducible AEP-expressing HEK293 cells (AEP.293GS, mifepristone-treated [Mfp+]) across Matrigel-coated (1:50) 8-micron pore inserts did not significantly differ from non-induced and vehicle-treated controls ($p$=0.07, one-way ANOVA).

*Right*: Summary of 3 experiments. Enforced AEP-overexpressing HEK293 cells (AEP.293) did not migrate more briskly across 8-micron pore cell inserts when compared to mock-transfected controls (EV.293) ($p$=0.96, two–sided unpaired $t$-test). The PC3 human prostate carcinoma cell line served as positive control.

Boxes encompass the interquartile (IQR, 25$^{th}$-75$^{th}$ percentile) ranges, horizontal bars and asterisks within boxes represent median and mean values respectively, whiskers denote values 1.5× IQR, outlier values are represented by circles.

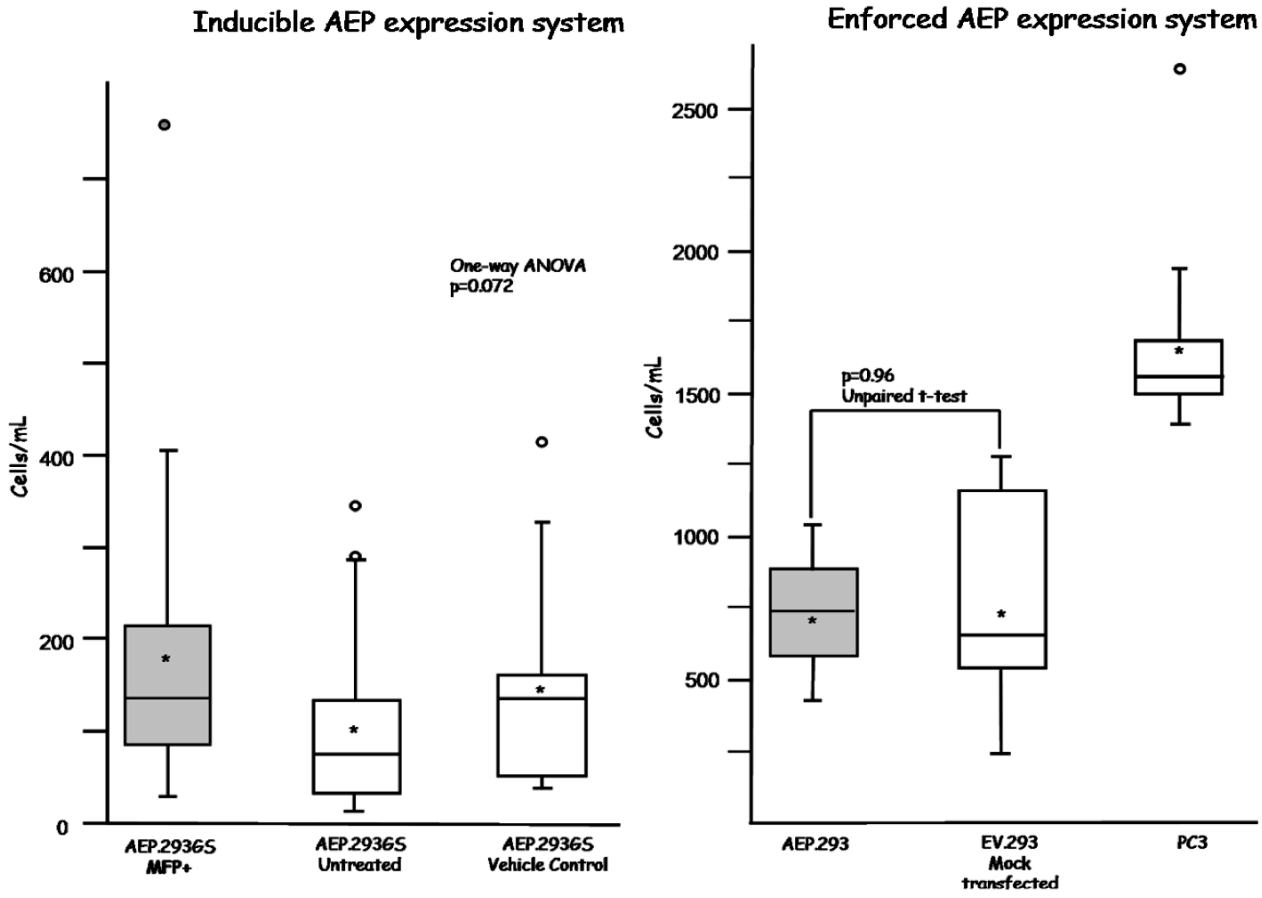

**Figure 4.9** AEP-overexpressing HEK293 cells are minimally motile

Representative images of crystal violet-methanol stained porous cell inserts from Boyden chamber motility assays. In contrast to PC3 prostate cancer cells, AEP-overexpressing HEK293 cells are not observed on the undersurface of cell inserts.

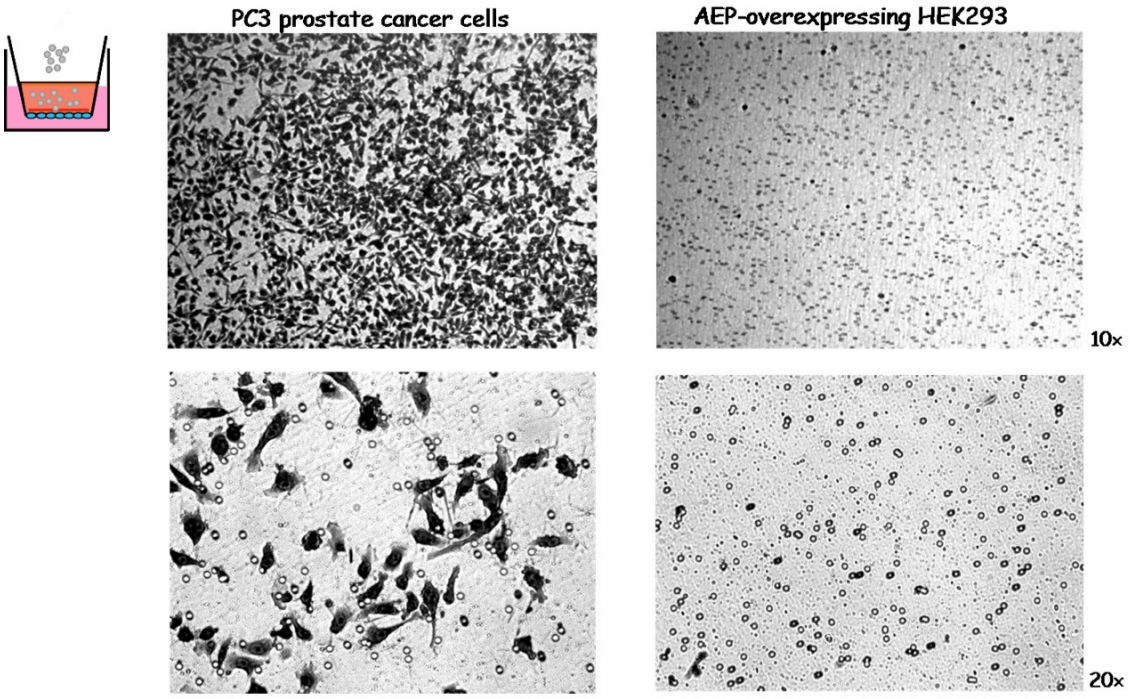

**Figure 4.10** AEP-overexpressing HEK293 cells continue to remain relatively immotile on extended timepoint Boyden chamber assays

(A) Coulter counts of enforced AEP-expressing (AEP.293) and mock-transfected (EV.293) HEK293 cells at various timepoints following seeding in 6-well plates ($1\times10^6$ cells/well, average of 3 wells/timepoint/cell-line). Counts of the two cell lines are comparable between 12 and 80 hours of observation (dashed vertical lines, Pearson coefficient of determination, $r^2$=0.87; error bars represent standard deviations) (B) Lower chamber cell counts (cells/mL) at various timepoints in Boyden chamber assays using uncoated 8-micron pore cell inserts. AEP.293 cells continue to remain relatively immotile over the 12-80 hour assay timepoints (error bars represent standard deviations).

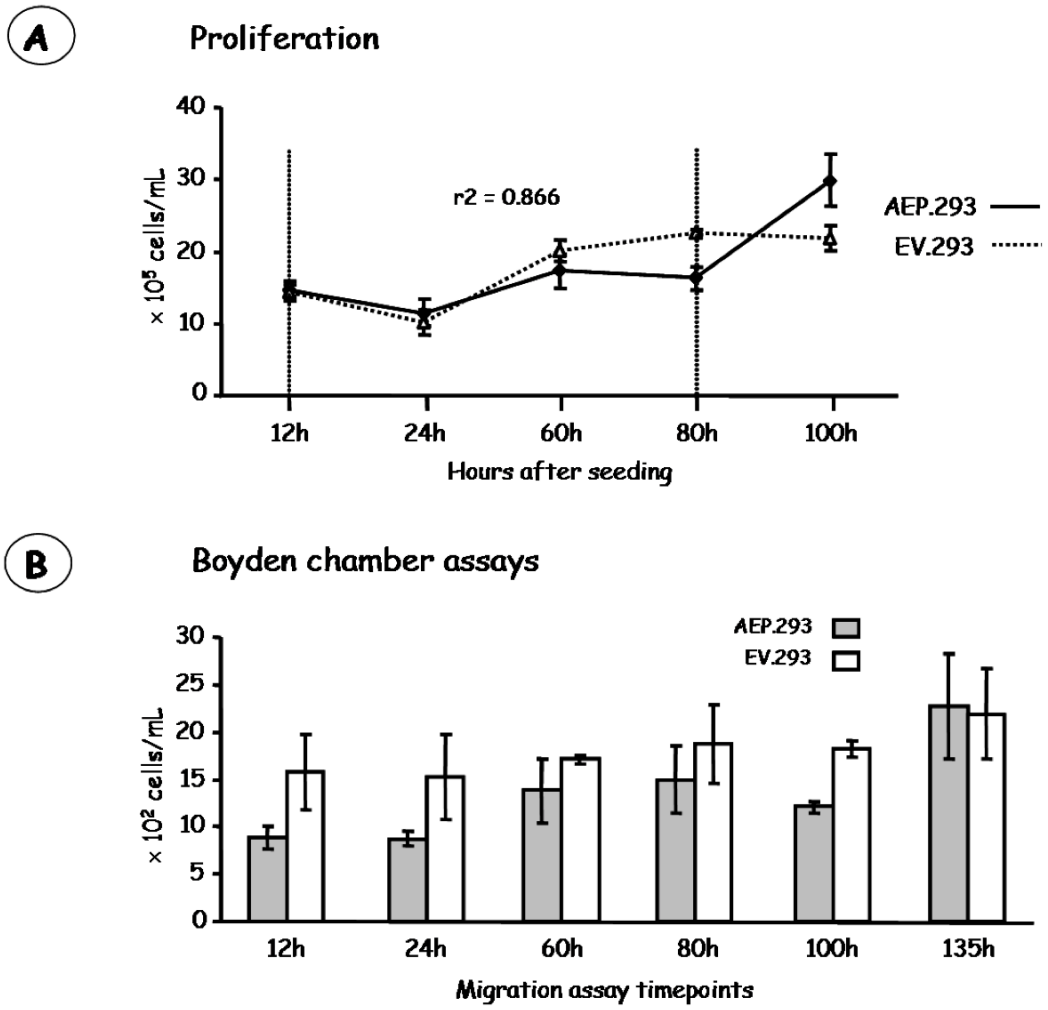

**Figure 4.11** The pro-motility role of AEP is cell-context specific and suggests requirement of additional co-operating molecules

Lower chamber cell counts (cells/mL) following 24-hour Boyden chamber motility assays of clonal lentivirally-transduced ectopic AEP-overexpressing progenitor-B ALL cell lines AEP+REH and AEP+SupB15, across Matrigel-coated (1:10 dilution, ~1mg/mL) 5-micron pore cell inserts seeded with $1\times10^5$ cells; complete growth medium was placed in the lower chamber. Ectopic AEP overexpression in REH cells resulted in ~3.5-fold increase in cell motility ($p$=0.002) that was still ~2.5-fold less than that observed with constitutive AEP-overexpressing SD1 cells. In striking contrast, ectopic AEP overexpression in SupB15 cells had no effect on motility. Taken together with observations in SD1 cells, the findings suggest that the role of AEP as a pro-motility molecule is facilitatory and cell-context specific, likely dictated by availability of additional pro-motility molecules.

*WT, wild-type REH and SupB15 cells; Mock, cells transduced with insert-free lentivirus; asterisks, estimated p-values from two-sided unpaired t-tests; error bars, standard error of means; summary of three experiments. Data courtesy of Seema Alexander*

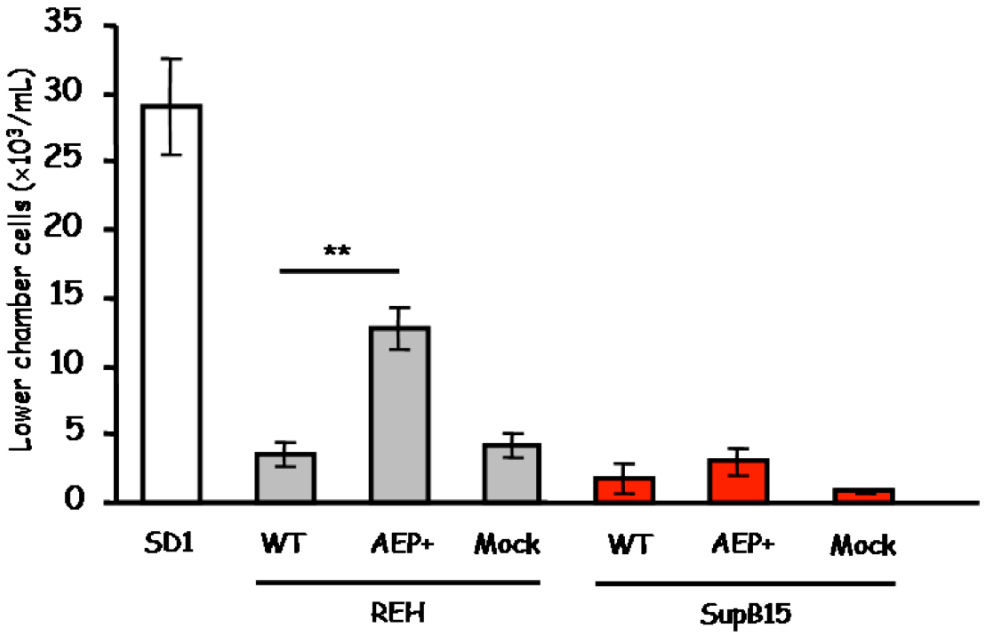

**Table 4.1 Insert and Plasmid Vectors**

| Material | Features |
|---|---|
| Insert | Full length AEP cDNA (NCBI Reference Sequence accession NM_005606.5, Appendix B)<br>Kozak sequence **A**CCATG**G**<br>C-terminal hexa-histidine tag |
| Source Vector | The pcDNA-DHFR plasmid expression vector with the full-length AEP cDNA insert cloned into EcoRV-Not1 sites (gift from Dr. Colin Watts, University of Dundee, Dundee, UK) |
| AEP.pGene A/V5-His GeneSwitch inducible mammalian expression plasmid (Invitrogen) | • AEP cDNA insert cloned in-frame into EcoRI-Not1 sites<br>• Expression regulated by a combination of six GAL4 Upstream Activating Sequences and the Adenovirus E1b TATA sequence<br>• Mifepristone-induced expression through conformational activation of a hybrid protein, GAL4/hPR-LBD/AD (GAL4 DNA binding domain/ligand binding domain of the human progesterone receptor/p65 activation domain of human NFκB) encoded by the co-transfected pSwitch plasmid<br>• Ampicillin and Zeocin resistance genes for transformation and transfection selection |
| AEP.pENTR 3C Gateway entry plasmid (Invitrogen) | • AEP cDNA insert cloned in-frame into EcoRI-Not1 sites<br>• Flanking *att*L1 and *att*L2 sites for LR recombination with a Gateway destination vector<br>• Negative selection with the *ccdb* gene located between the recombination sites<br>• Kanamycin resistance gene for selection in *E. coli* |
| AEP.pcDNA3.1/nV5-DEST Gateway destination mammalian expression plasmid (Invitrogen) | • AEP cDNA insert following LR recombination with the pENTR 3C Gateway entry vector<br>• Human cytomegalovirus (CMV) immediate-early promoter/enhancer<br>• Recombination sites *att*R1 and *att*R2 enclosing the *ccdb* gene downstream of the CMV promoter for recombinational cloning<br>• pUC origin for high copy replication and ampicillin resistance gene for selection in *E. coli*<br>• SV40 driven aminoglycoside resistance gene for selection of stably transfected cells using Geneticin (G-418) |

**Table 4.2: The influence of ectopic AEP overexpression on motility of HEK293 cells: comparison and contrast with observations of the Scripps group (Ch 2, [24])**

| |
|---|
| ***Similarities*** |
| • In both studies, lipid-based transfection was used to introduce full length AEP expression plasmid constructs.<br>• The AEP cDNA inserts (reference transcripts Y09652 and NM_005606.5) in both instances encode identical protein products<br>• Boyden chamber motility assays were performed using eight micron-pore cell inserts |
| ***Differences*** |
| • HEK293 cells used in the two studies may not necessarily be identical. Non-homogeneity is a well recognised phenomenon in widely used experimental cell lines such as HeLa and HEK293 and arises as a consequence of genetic drift from repeated and extended passages [2, 3]. Cell line authentication would have addressed this concern.<br>• The Scripps group observed increased motility of a *clonal* population of stably transfected G418-selected (0.4mg/mL) AEP-overexpressing HEK293 cells. Data on the intensity of AEP overexpression in the experimental clone is not available. By contrast, polyclonal transfected cells were used in this report.<br>• The Scripps group's data on motility of AEP-overexpressing HEK293 cells were reported relative to wild type HEK293 cells. Comparison with mock-transfected isogenic cells additionally controls for off-target effects of transfection.<br>• Lower chamber cell counts in the Scripps study were performed solely by crystal violet staining of cell inserts. Inadequate scrape-removal of upper chamber contents can potentially represent a source of false-positive error.<br>• The Scripps groups also observed increased motility in a tetracycline-regulated AEP-expressing HEK293 cell line. Full experimental details are not available. |

**Table 4.3 Experimental limitations of motility assays on ectopic AEP-expressing HEK293 cells**

| | Rationale | Limitation |
|---|---|---|
| Choice of experimental cell line | HEK293 cells were chosen for their ease of transfection. Once established, the first step was to perform motility studies in an attempt to replicate the findings of the Scripps group and as prelude to extended studies such as investigation of AEP-interacting molecules. | Clearly a non-representative cell line. AEP's role in cell motility would undoubtedly be part of a coordinated molecular machinery and is therefore likely to be cell-specific, determined by the co-expression of partner molecules. Creation of stable AEP-expressing progenitor-B ALL cell lines requires a more onerous lentiviral approach and these modified cell lines have now been established. |
| Clonality | A stable polyclonal population of overexpressing cells was created principally for experimental ease. It was anticipated that the motile phenotype in modified cells would manifest even in a polyclonal population, especially since native HEK293 cells were essentially immotile. Of interest, despite the absence of clonal selection, AEP overexpression in the Mifepristone-regulated system appeared fairly tightly clustered (as evidenced by flow cytometry), perhaps as an inadvertent consequence of use of transfection selection reagents | The role of AEP in cell motility would have been better clarified by performing motility assays on clonal populations of low, intermediate and high AEP-expressing HEK293 cells (intensity relative to SD1 AEP expression). Of note, in the progenitor-B ALL cell line SupB15, variable intensity of AEP expression in engineered clones had no influence on cell motility relative to wild-type cells (*data not shown).* |
| Experimental methodology | Pore size of upper chamber cell inserts used in Boyden chamber assays was maintained at 8 micron. This is the standard in motility experiments on adherent cell lines and was also the pore size used in the Scripps group's experiments. | Boyden chamber assays could have been performed using cell inserts with larger pore sizes (e.g. 12 micron). |

# 5

# AEP and Asparaginase

In contemporary treatment of childhood ALL, both appropriate speed [1] and depth (Chapter 1, [22]) of response powerfully influence outcome. Adverse-risk genotypes of progenitor-B childhood ALL are characterised by poor early treatment response (Chapter 1, [95]) and disease clearance (Chapter 1, [22]). Intrinsic lymphoblast chemoresistance probably accounts for this [2, 3] but conventional drug-resistance pathways (drug efflux, cell quiescence, acquired genetic mutations) have not been implicated (Chapter 1, [111]), [4]. In this chapter, a novel mechanism of lymphoblast drug resistance is postulated. Lymphoblast lysosomal proteases AEP and Cathepsin B (CTSB) degrade the drug L-asparaginase and potentially mediate resistance to this cytotoxic.

**L-asparaginase**

The protein drug L-asparaginase is a key therapeutic agent in childhood ALL (**Table 5.1**) and a critical component of the 4-drug mainstay of early treatment (**Figure 5.1**). Although still a matter of debate, the therapeutic effect of the drug is customarily attributed to extracellular depletion of asparagine (Asn) and selective apoptosis of lymphoblasts incapable of *de novo* Asn synthesis. Both therapeutic preparations, *E. coli* L-asparaginase (ASNase) and *Erwinia carotovora* L-asparaginase (Erwinase) are bacterially-derived. The longer circulating half-life of ASNase favours use of this preparation in frontline treatment protocols. A major treatment limitation is the development of hypersensitivity to these non-native proteins. Hypersensitivity occurs with repeated treatment exposures, is clinically overt in some cases but is typically characterised by silent neutralising antibodies that antagonise drug activity late in therapy.

**Poor early ASNase activity and speculative role of lymphoblast AEP**

A pilot study of serial serum ASNase activity in children with progenitor B-ALL (n=44) (**Figure 5.2**) during the initial (induction) and later (post-induction) phases of treatment indicated that nearly 10% of treated children experienced decline in drug activity during the later treatment phase. Although not specifically investigated, this observation is consistent with the development of silent drug-neutralising antibodies. Curiously, despite appropriate dosing, adequate drug activity was not obtained in up to a third of patients during the crucial early treatment phase. As this stage of treatment also coincides with the period of maximal disease burden, it is conceivable that intrinsic lymphoblast-derived mechanisms, specifically proteolytic degradation, account for the failure to establish adequate ASNase activity during early therapy. In this context, poor response to ASNase is also a feature of the AEP-overexpressing adverse-risk progenitor-B ALL genotype, Ph+ALL [41]. Together, these observations prompted the speculation that proteolytic degradation of ASNase could be mediated by AEP in overexpressing lymphoblasts, resulting in inadequate drug activity early in therapy. As a vital component of early therapy, suboptimal early ASNase activity would plausibly result in unsatisfactory early treatment response and eventual poor outcome.

**Experimental methods**

This work was supervised by and performed in partnership with Naina Patel (NP). The methodology is summarised in **Figure 5.3**. ASNase digestions, gels and immunoblots and synthesis of recombinant wild-type ASNase and variants were performed by NP. Experimental planning and analyses were jointly undertaken.

**Results**

*AEP degrades ASNase*

Purified recombinant human AEP (rhAEP) uniformly degraded all pharmacological preparations of ASNase, including a long-acting conjugated

version of the drug (PEG-ASNase) (**Figure 5.4**, **Supplementary Figure S5.1**). By contrast, the therapeutic alternative, Erwinase remained intact.

*A combination of AEP and CTSB in lymphoblast cell lysates degrades ASNase*

Whole cell lysates of progenitor-B ALL cell lines and primary samples consistently degraded ASNase (**Figure 5.5A**). In non AEP-expressing REH cells, lysate pretreatment with a broad-spectrum cocktail of protease family inhibitors (PIC) prevented ASNase degradation. To narrow in on the peptidase family responsible for ASNase degradation in REH cells, lysates were serially pretreated with individual component inhibitors of PIC (**Supplementary Figure S5.2**); pretreatment with Leupeptin alone was sufficient to prevent ASNase degradation, pointing to a papain family cathepsin as the ASNase-degrading protease in REH. Cathepsins B, L and H are the commonly implicated cathepsins in this peptidase family. Pretreatment of REH lysates with selective inhibitors to these enzymes identified Cathepsin B as the responsible protease (**Figure 5.5C**). When extended to AEP-expressing SD1 cells, ASNase degradation was prevented only when cell lysates were pretreated with a combination of the selective CTSB inhibitor CA-074Me (CTSBi) and the AEP-specific inhibitor MV026630 (AEPi) (**Figure 5.5B**).

These observations suggest that CTSB is a generic ASNase-degrading protease in ALL cells; in AEP-expressing cells, ASNase is additionally degraded by AEP. The inference is supported by ASNase digestion-inibition studies in primary samples (**Figure 5.6**, **Supplementary Figure S5.3**, **Appendix D**)

*Cathepsin B is probably a basal ASNase metabolising enzyme*

Recombinant human CTSB degraded all L-asparaginase preparations, including Erwinase (**Figure 5.7A**, **Supplementary Figure S5.1**). Microarray analysis of CTSB gene expression in a cohort of diagnostic acute childhood leukaemia samples indicated near-uniform expression in childhood ALL, suggesting constitutive housekeeping expression in this disease (**Figure 5.7B**). Limited analysis of protein expression supported this observation (**Figure 5.7C**). These

additional findings strengthen the assumption that CTSB functions as a basal ASNase metabolising enzyme.

**Discussion**

Despite acknowledged limitations (**Table 5.2**), the above *in vitro* observations provide a compelling explanation for the observation of poor early ASNase activity in a subset of patients with progenitor-B ALL. AEP in overexpressing lymphoblasts potentially accelerates ASNase cleavage resulting in suboptimal drug activity during the critical early phase of therapy (**Figure 5.8**). The fastidious cleavage specificity of AEP was exploited to both map cleavage sites (**Figure 5.9**, **upper panel**) and synthesise variant ASNase recombinants mutated at AEP-cleaved residues. Sole substitution at the N24 residue was sufficient to render ASNase resistant to AEP cleavage (**Figure 5.9**, **lower panel**), additionally suggesting that AEP cleavage of ASNase is sequential and commences at the N24 residue.

There is another facet to these observations that potentially extends the impact of lymphoblast AEP expression beyond the early phase of ASNase therapy. Cleavage fragments generated by AEP degradation of ASNase retain known B-cell epitope determinants. Conceivably, these AEP-generated antigenic fragments can trigger hypersensitivity responses, resulting in the formation of neutralising antibodies and late ASNase inactivation (**Figure 5.10**). This may explain why a proportion of patients (11% in pilot study, **Figure 5.2**) with inadequate ASNase activity during early therapy continue to demonstrate unsatisfactory drug activity during later treatment.

As part of the current UK childhood ALL trial protocol, a nationwide prospective clinical study is examining association between lymphoblast AEP expression at diagnosis and ASNase activity and hypersensitivity. AEP expression will be investigated for its significance as an independent predictive (ASNase therapy) and prognostic (clinical outcome) biomarker in childhood ALL. If borne out as a

predictive marker, AEP-expressing disease would warrant use of alternative asparaginases (Erwinase or engineered AEP-resistant ASNase) especially during early therapy. If identified as a significant prognostic risk variable, it would make a persuasive case for the development of therapeutic small-molecule AEP antagonists. In this context, restricted physiological tissue AEP expression and functional redundancy would make drug targeting a safe approach.

*This work was published [71].*

**Figure 5.1** *E. coli* L-asparaginase (ASNase) is a key component of early childhood ALL treatment and therefore, a critical determinant of early treatment response

Schematic of fundamental treatment elements in childhood ALL therapy. Although treatment duration spans ~2.5 years, the quality of response to the first 1-2 weeks of treatment powerfully influences outcome. ASNase is an integral component of early chemotherapy and therefore a key determinant of treatment outcome. The long-acting polyethylene glycol (PEG)-conjugated version of ASNase is highlighted below.

*CNS, central nervous system; D0-D8, days of treatment; IT, intrathecal therapy; MTX, methotrexate;* '×' *represents day of drug administration*

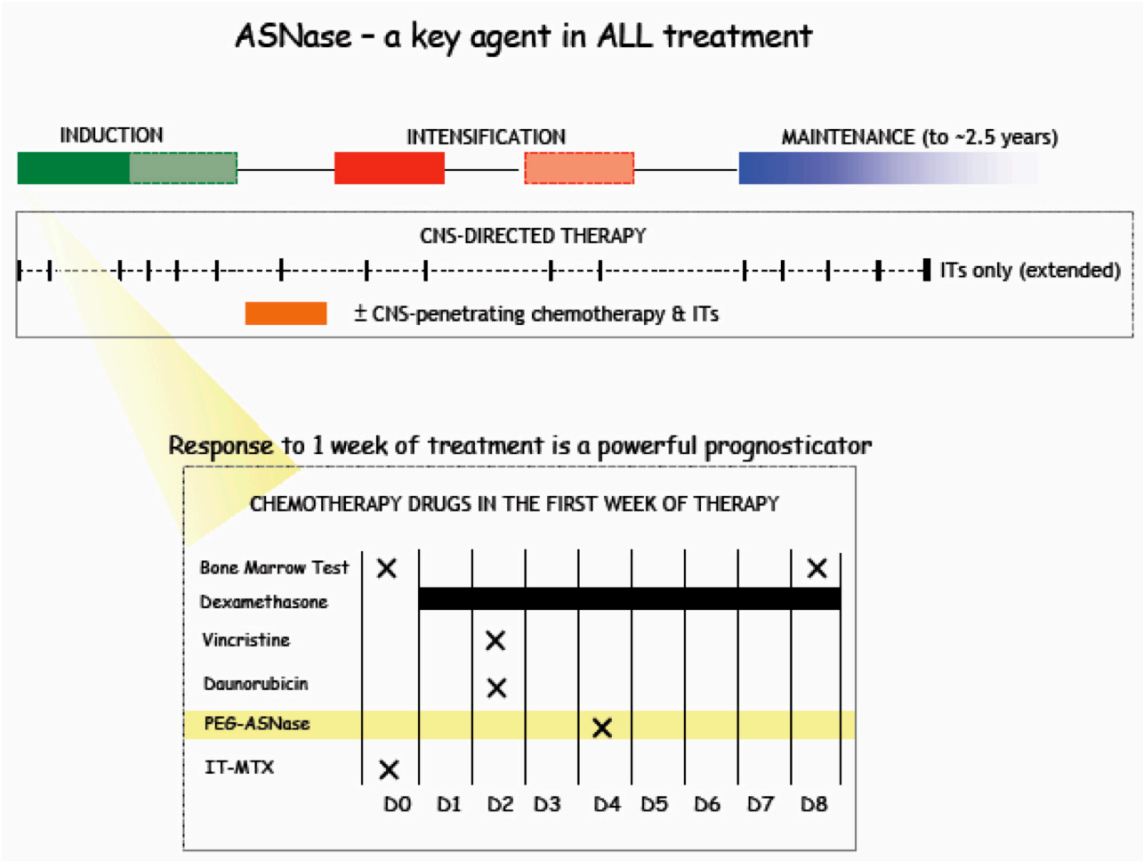

**Figure 5.2** AEP overexpression in progenitor-B lymphoblasts could possibly account for the early inadequate serum ASNase activity observed in a subset of patients

Serum ASNase activity [68] estimated during the induction and post-induction treatment phases in children with ALL (n=44). The observation of low serum ASNase activity during the early induction phase, especially in children with high-risk disease, prompted the speculation that AEP overexpressed by lymphoblasts in high-risk disease, could possibly be involved in the enzymatic cleavage and inactivation of ASNase, a bacterial protein, during early treatment. Inadequate serum activity noted in nearly 10% of patients in the post-induction phase is probably a consequence of formation of neutralising antibodies to ASNase (*Data courtesy of Nick Coe, University of Salford, Manchester*)

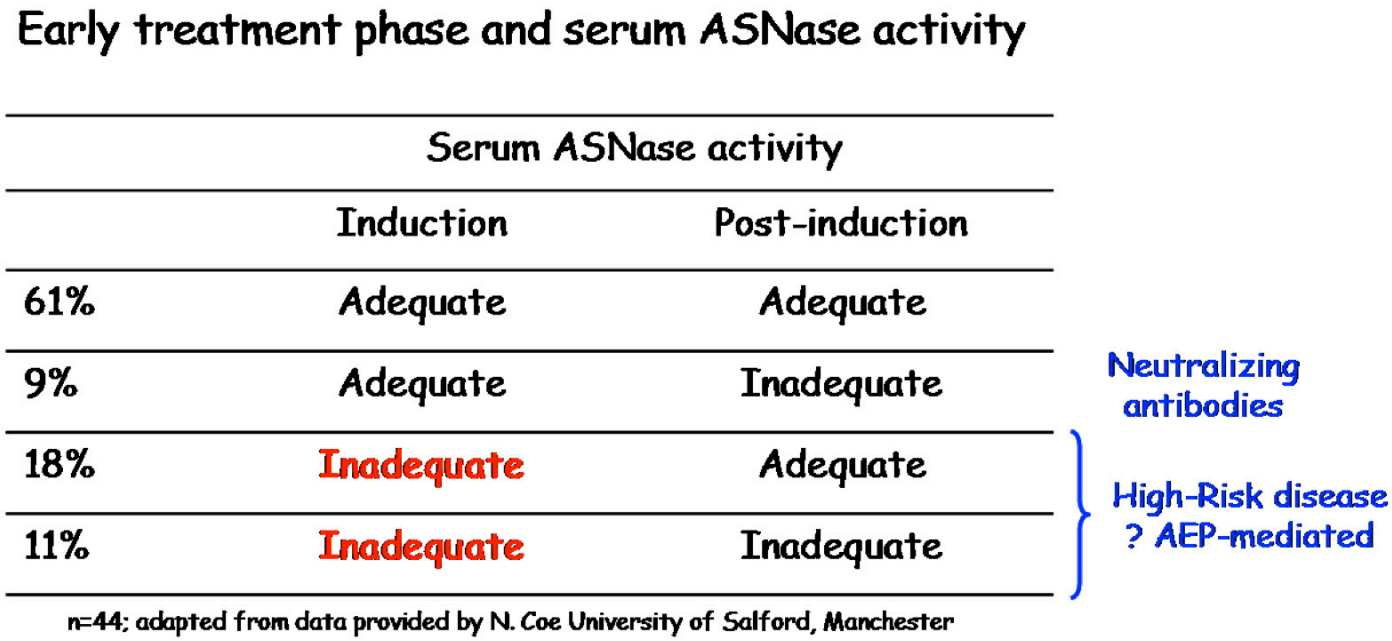

**Figure 5.3** ASNase degradation by lysosomal proteases: schematic outline of experiments

Investigations are in blue. *E. coli* L-asparaginase (ASNase) was incubated with (a) purified recombinant preparations of human AEP or CTSB and (b) whole cell lysates of ALL cell lines or primary lymphoblasts in acid citrate digests. To identify cellular proteases primarily responsible for ASNase degradation, whole cell lysates in some experiments were serially preincubated with selective inhibitors of AEP and CTSB as well as with inhibitors of different peptidase families, either singly or in combination. AEP cleavage sites were mapped to synthesise recombinant variant ASNases capable of resisting AEP degradation.

*PIC, Protease inhibitor cocktail*

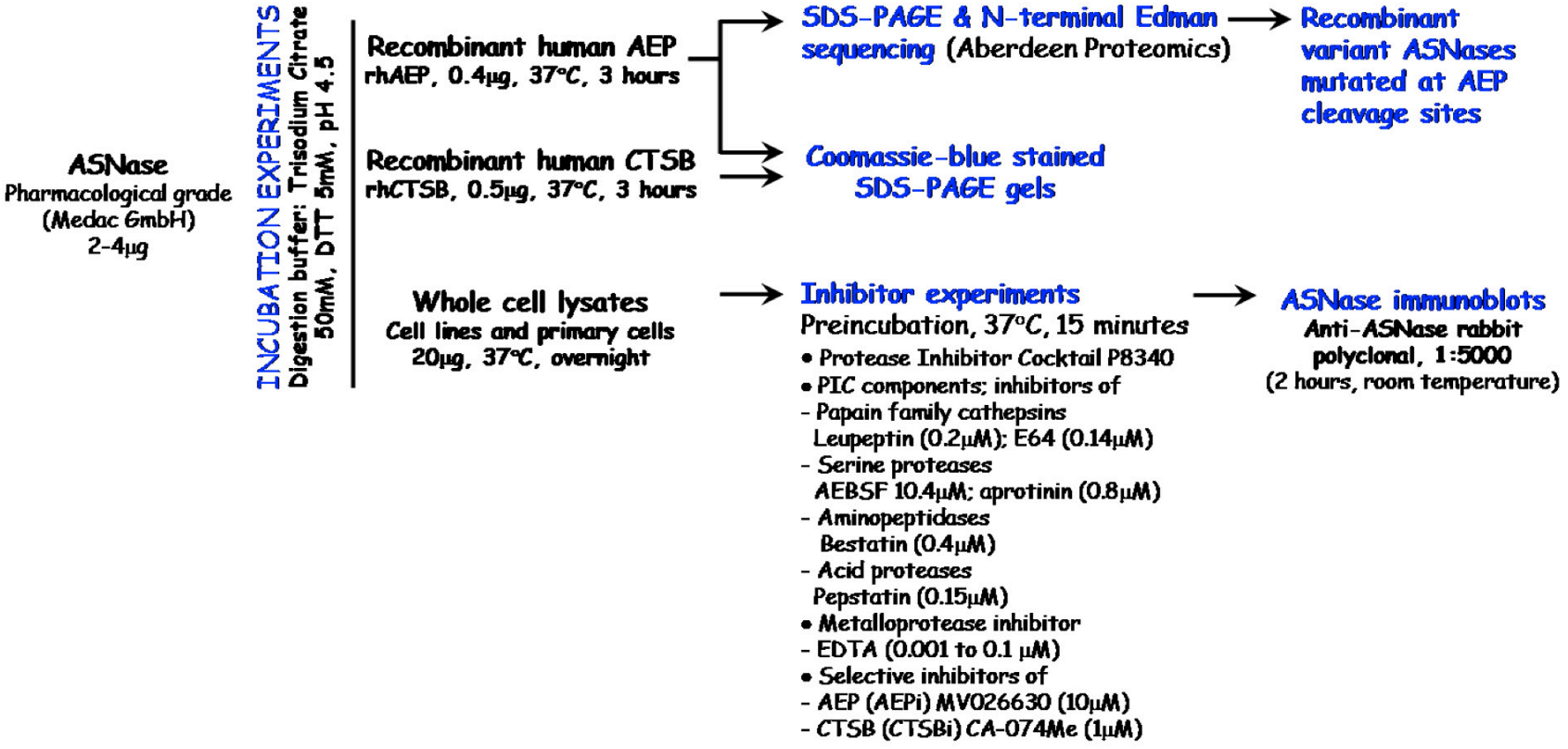

**Figure 5.4** AEP degrades ASNase but not Erwinase

Coomassie Blue stained SDS-PAGE of *E. coli* (ASNase) and *E. carotovora* (Erwinase) L-asparaginase (4μg) incubated with (+) and without (-) activated purified recombinant human AEP (rhAEP, 0.4μg) in citrate buffer digests (pH 4.5, 37°C, 3 hours). AEP degrades all pharmacological preparations of ASNase, including a high molecular weight polyethylene glycol (PEG)-conjugated form (note distinct lower molecular weight band with AEP+ digests), resulting in ~50% decline in ASNase activity (**Supplementary Figure S5.1**). No similar degradation is observed when Erwinase is incubated with AEP.

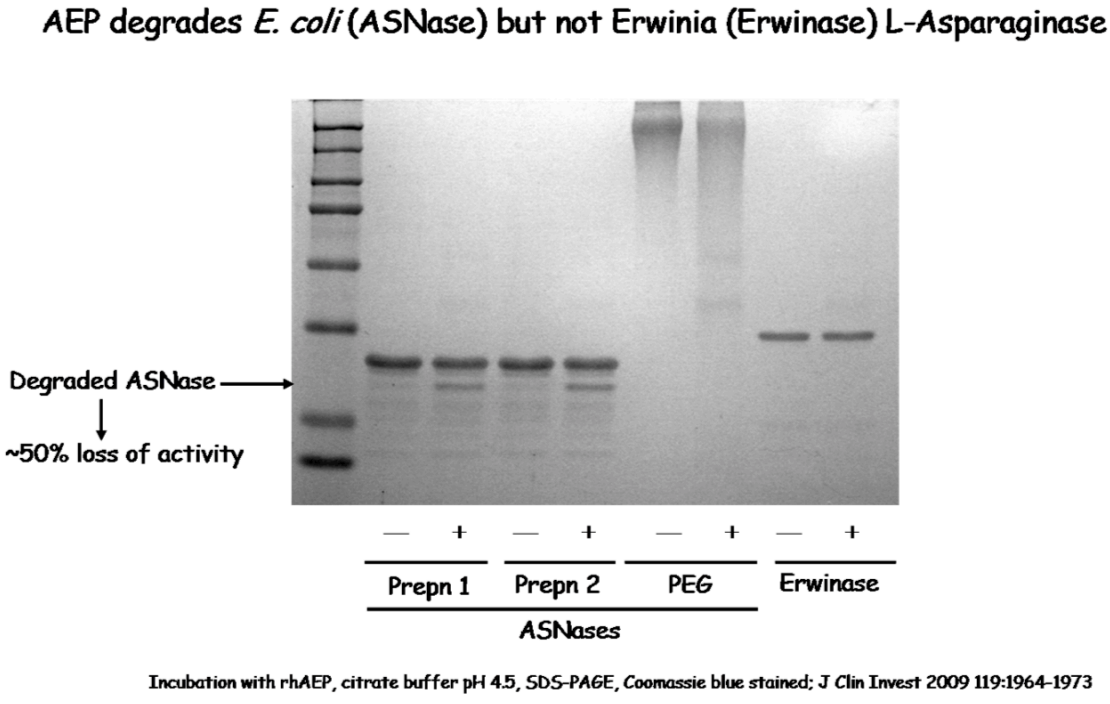

**Figure 5.5** ASNase is degraded by the lymphoblast lysosomal proteases, AEP and CTSB

(A) ASNase immunoblot of digests of purified ASNase (2μg) incubated with B-lineage lymphoblast cell line lysates (citrate buffer, pH 4.5, 37°C, 12-16 hours). ASNase degradation is observed following incubation with all cell lysates (horizontal arrow, subtle in the case of SupB15 cell lysate) but is most prominent in the AEP-expressing cell lines, SD1 and HRC57 (*inset,* AEP immunoblot)

(B) ASNase immunoblots of ASNase digests incubated with SD1 cell line lysates pre-treated with combinations of protease inhibitors, including AEPi (MV026630, selective AEP inhibitor), PIC (protease inhibitor cocktail containing broad-spectrum inhibitors of cysteine-, aspartate-, serine- and amino-peptidases), E-64 and Leupeptin (papain family cathepsin inhibitors, also components of PIC) and CTSBi (CA074-Me, selective cathepsin B [CTSB] inhibitor). Controls included untreated SD1 cell lysate and reagent vehicle (DMSO). ASNase degradation was completely prevented when SD1 cell lysates were pre-treated with a combination of [AEPi + PIC], [AEPi + Leupeptin/E-64] and [AEPi + CTSBi]. Dotted vertical lines demarcate different immunoblots

(C) ASNase immunoblots of ASNase digests incubated with the non-AEP expressing REH cell line lysate pretreated with inhibitors as above. Pre-treatment with CTSBi alone prevented ASNase degradation

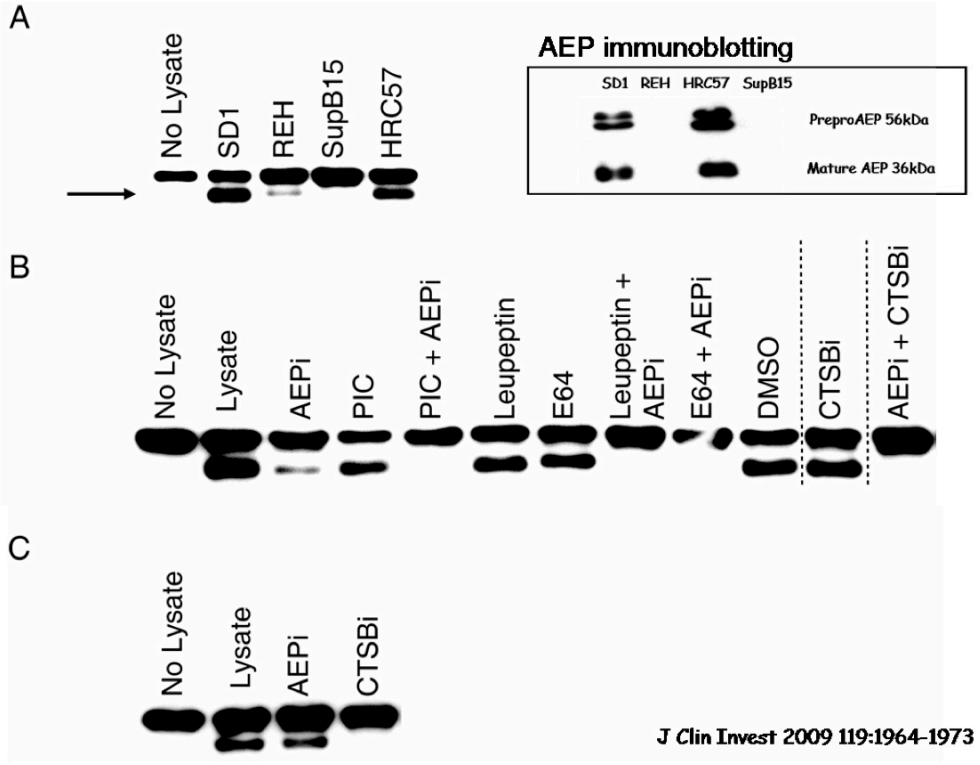

**Figure 5.6** ASNase is similarly degraded by AEP and CTSB in primary progenitor-B lymphoblasts

Composite of AEP, CTSB and β-actin loading control immunoblots (A) and AEP enzyme activity (relative to the HRC57 cell line) (B) in selected primary whole cell lysates (UPN 3, 8-10). UPN3 and UPN9 lymphoblasts overexpress AEP; CTSB expression is higher in UPN3. UPN8 and UPN10 lymphoblasts solely express CTSB. These expression patterns determine ASNase digestion profiles (C). CTSBi pre-treatment alone prevents ASNase degradation by UPN8 and UPN10 lysates, AEPi pretreatment alone is sufficient in the case of UPN3 digests and a combination of AEPi and CTSBi is required to prevent ASNase degradation in UPN8 digests.

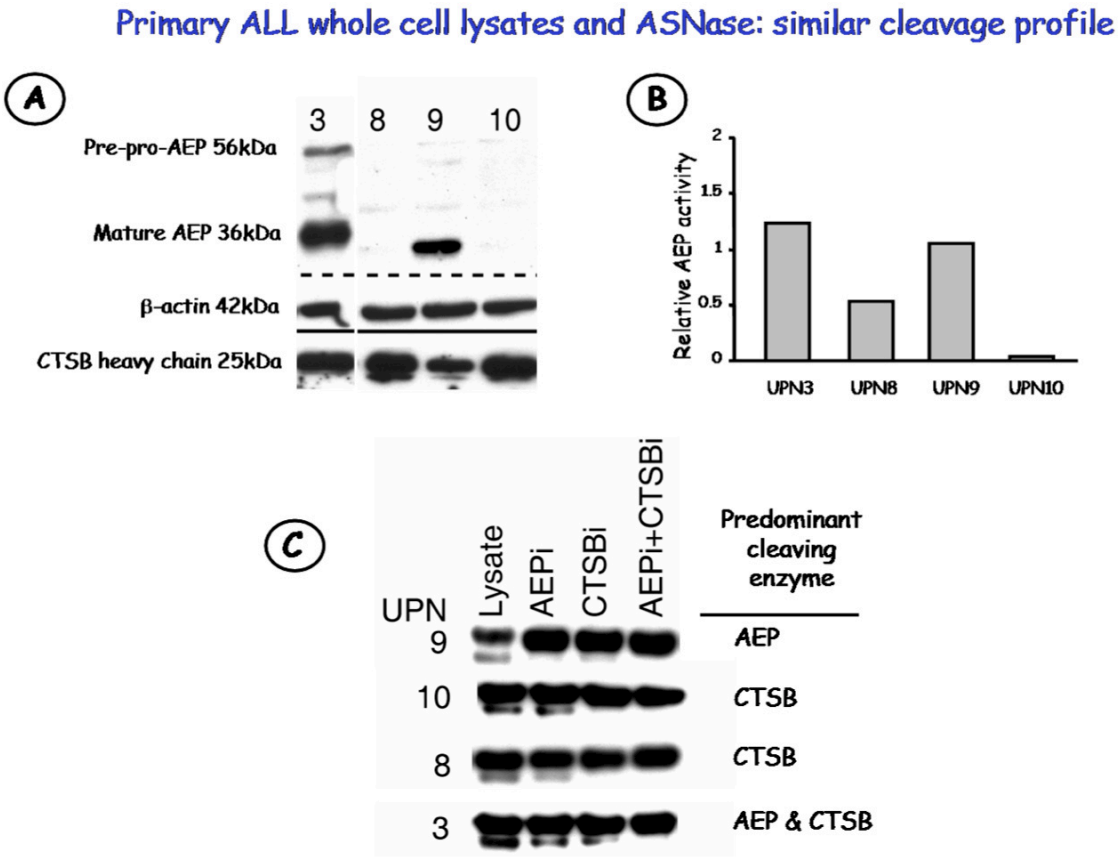

**Figure 5.7** CTSB probably basally degrades asparaginases

(A) Coomassie stained SDS-PAGE of digests of Erwinase and various preparations of ASNase incubated with (+) or without (-) recombinant purified human CTSB (0.5μg, citrate buffer pH 4.5, 37°C, 3 hours). CTSB degrades all asparaginases, including Erwinase.

(B) Boxplot representation of microarray analyses of CTSB transcript expression in acute childhood leukaemias (n=120). Near-uniform expression across all categories of acute leukaemia suggests a housekeeping role for CTSB in asparaginase metabolism. (Boxes encompass the interquartile [IQR, 25$^{th}$-75$^{th}$ percentile] ranges, horizontal bars within boxes represent median values, '+' values indicate means, whiskers denote values 1.5× IQR and outlier values are represented by circles [≤3× IQR] and asterisks [>3× IQR]). Pre-B, progenitor-B ALL; T-ALL, progenitor T-ALL

(C) CTSB immunoblot of primary progenitor-B ALL whole cell lysates UPN1-12. With the exception of UPN12, active CTSB protein is detected in all primary samples, suggesting constitutive expression in ALL. SB15, SupB15 cell line

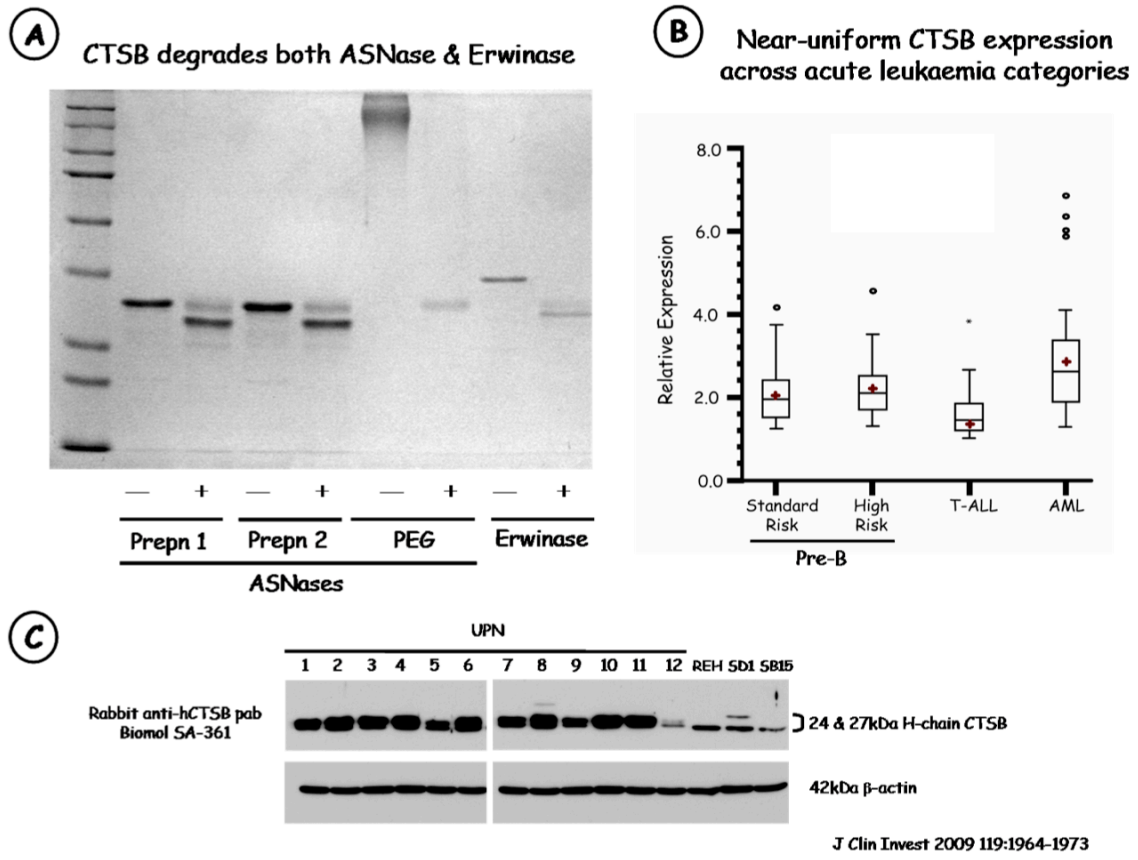

**Figure 5.8** AEP derived from overexpressing high-risk progenitor-B lymphoblasts accelerates degradation of ASNase and potentially contributes to inadequate drug activity during the early treatment phase of childhood ALL

Cartoon summary of *in vitro* observations and interpretations. CTSB basally degrades ASNase. AEP, expressed by high-risk progenitor B lymphoblasts, accelerates ASNase degradation.

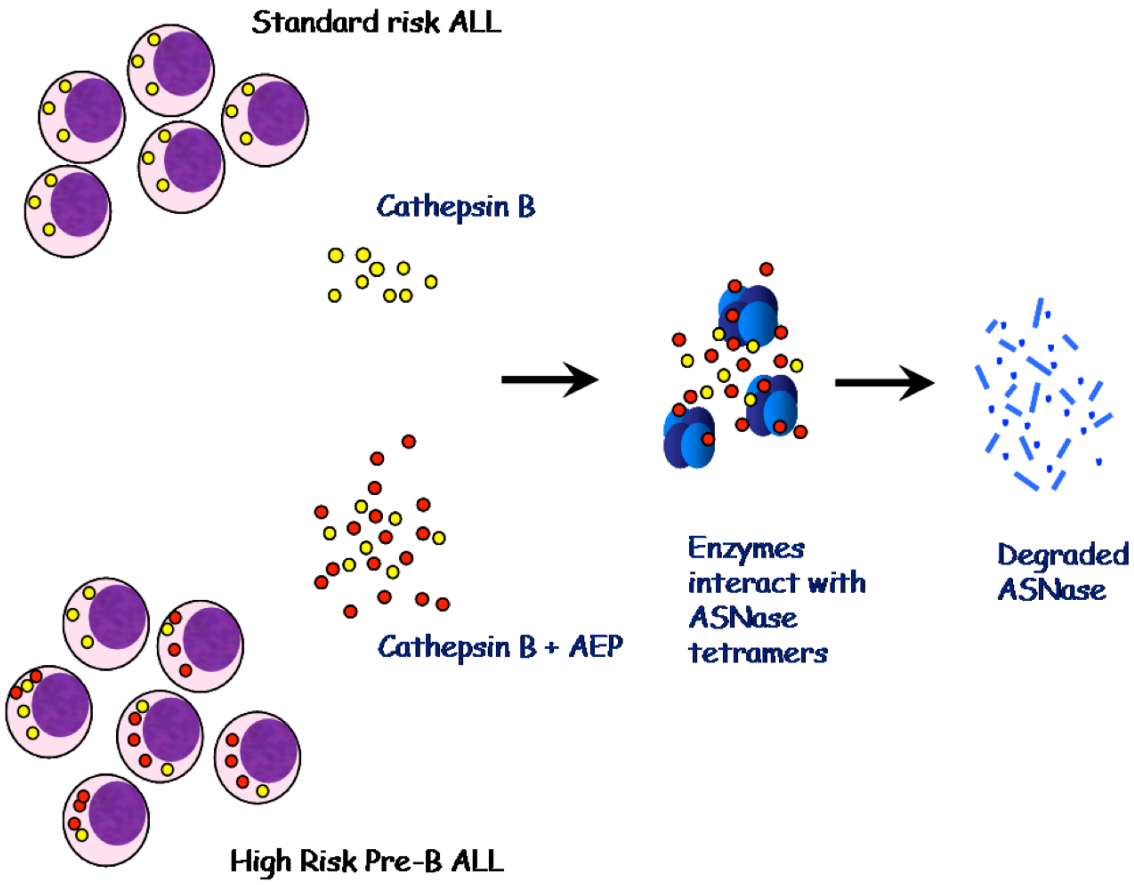

**Figure 5.9** Substitution of the N24 residue alone is sufficient to generate an ASNase variant resistant to AEP

*Upper panel*: AEP cleavage sites (red) mapped by N-terminal Edman sequencing of SDS-PAGE-resolved AEP-digested ASNase (Aberdeen Proteomics). AEP cleaves ASNase at the carboxyl-end of three amino acid residues - N24, D124 and N143. This selective cleavage specificity is characteristic of AEP. *Lower panel*: ASNase immunoblot of digests of native and variant recombinant ASNase proteins incubated with (+) and without (-) activated purified recombinant human AEP (rhAEP, 0.4μg, citrate buffer pH 4.5, 37°C, 3 hours). Amino acid substitution at the N24 cleavage site is sufficient to render ASNase resistant to AEP degradation, suggesting that AEP cleavage is initiated at this site. Modifying the conserved D124 ASNase residue abrogates protein expression. *N, asparagine residue; D, aspartate residue; G, glycine residue*

```
  1   LPNITILATGGTIAGGGDSATKSNYTVGKV   30
 31   GVENLVNAVPQLKDIANVKGEQVVNIGSQD   60
 61   MNDNVWLTLAKKINTDCDKTDGFVITHGTD   90
 91   TMEETAYFLDLTVKCDKPVVMVGAMRPSTS  120
121   MSADGPFNLYNAVVTAADKASANRGVLVVM  150
151   NDTVLDGRDVTKTNTTDVATFKSVNYGPLG  180
181   YIHNGKIDYQRTPARKHTSDTPFDVSKLNE  210
211   LPKVGIVYNYANASDLPAKALVDAGYDGIV  240
241   SAGVGNGNLYKSVFDTLATAAKTGTAVVRS  270
271   SRVPTGATTQDAEVDDAKYGFVASGTLNPQ  300
311   KARVLLQLALTQTKDPQQIQQIFNQY      327
```

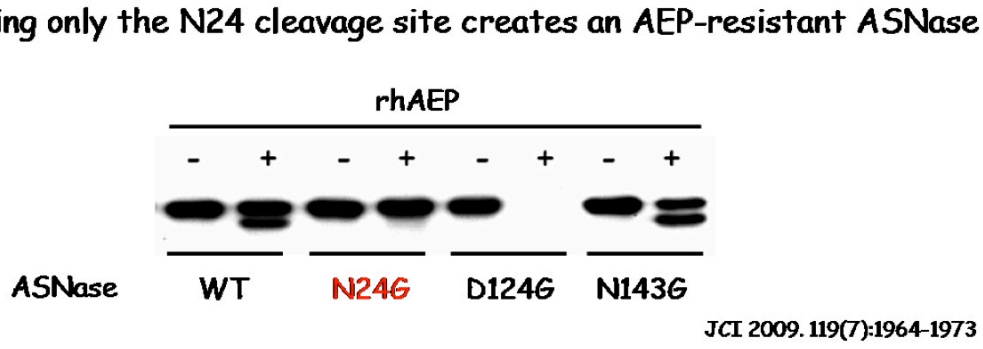

**Figure 5.10** Retention of known sensitising epitopes of ASNase in AEP-cleaved fragments can potentially trigger generation of neutralising anti-ASNase antibodies, leading to late failure of ASNase treatment.

AEP-cleaved ASNase fragments retain known sensitising epitopes (upper panel, underlined blue, [69]). These antigenic fragments potentially trigger formation of neutralising ASNase antibodies (lower panel), resulting in inadequate ASNase activity late in therapy, long after clearance of lymphoblasts ('late indirect ASNase activation')

```
  1   LPNITILATGGTIAGGGDSATKSNYTVGKV  30
 31   GVENLVNAVPQLKDIANVKGEQVVNIGSQD  60
 61   MNDNVWLTLAKKINTDCDKTDGFVITHGTD  90
 91   TMEETAYFLDLTVKCDKPVVMVGAMRPSTS 120
121   MSADGPFNLYNAVVTAADKASANRGVLVVM 150
151   NDTVLDGRDVTKTNTTDVATFKSVNYGPLG 180
181   YIHNGKIDYQRTPARKHTSDTPFDVSKLNE 210
211   LPKVGIVYNYANASDLPAKALVDAGYDGIV 240
241   SAGVGNGNLYKSVFDTLATAAKTGTAVVRS 270
271   SRVPTGATTQDAEVDDAKYGFVASGTLNPQ 300
311   KARVLLQLALTQTKDPQQIQQIFNQY     327
```

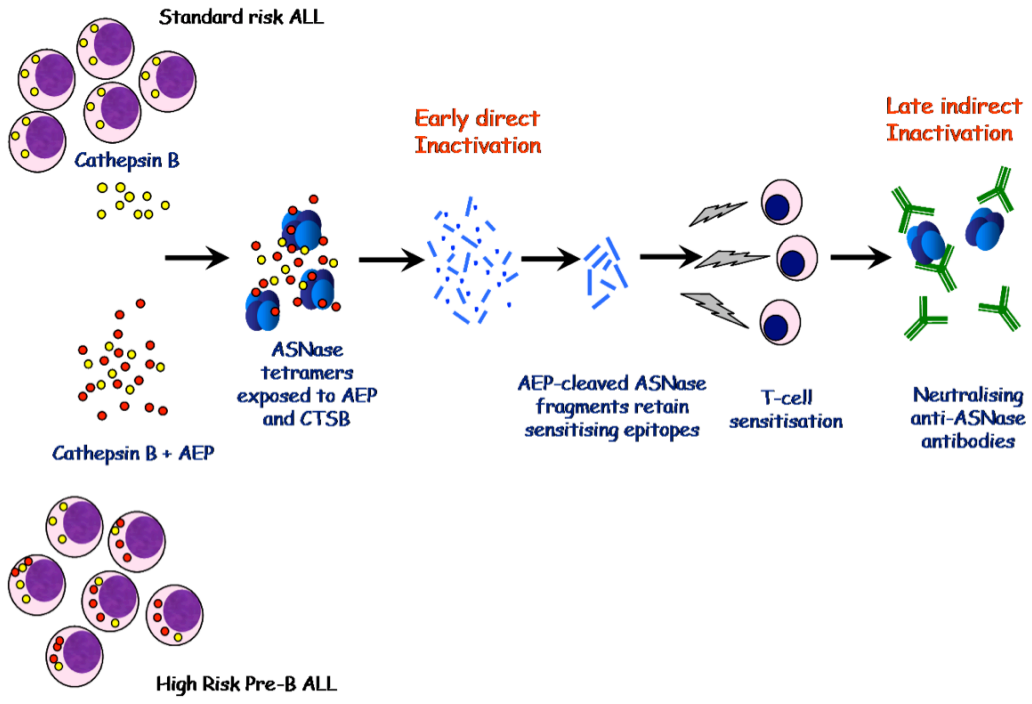

**Table 5.1 *E.coli* L-Asparaginase (ASNase): a synopsis**

| Aspects | Comments | Key references |
|---|---|---|
| Mechanism of action | Hydrolysis of amide bonds of asparagine and to a lesser extent, glutamine, resulting in extracellular depletion of these amino acids | [5], [6], [7] |
| | Lymphoblasts are considered asparagine auxotrophs, lacking the capacity to synthesise asparagine *de novo*; asparagine deprivation triggers the amino-acid deprivation response, resulting in inhibition of mTORC1 signalling and triggering of apoptosis. At higher doses, glutamine deprivation augments cytotoxicity. Normal cells retain the ability to upregulate asparagine synthetase (ASNS) and generate asparagine de novo | [8], [9], [10] |
| | Conformational change in intracellular proteins, triggering the unfolded protein response and eventual cell death | [11] |
| Structure-function relationship | Active molecule is a homotetramer or a dimer of homodimers formed of 330 amino acid 36 kDa subunits. Assembly as a tetramer creates a substrate pocket containing active catalytic sites for substrate nucleophilic attack; threonine at positions 12 (T12) and 89 (T89) are the principal active residues. A surface loop delimited by residues T12 and tyrosine 25 (Y25) functions as a substrate clamp for the active site | http://tinyurl.com/ASNase-model (last accessed, 8 Sep 2010) |
| Initial drug development | ASNase activity in guinea pig serum inhibited growth of the 6C3HED Gardner murine lymphoma cell line | [12], [13], [14], [15] |
| | Isolation and purification of Type II ASNase from E.*coli* anaerobic cultures | [16] |
| Early results of therapy | First reports of unsustained remissions (median 122 days) when used as single agent in untreated or relapsed childhood ALL | [17] |
| | Maximal efficacy in paediatric lymphoid malignancies; less impressive results in treating paediatric solid tumours; both intravenous and intramuscular routes of administration were effective; no advantage with intrathecal therapy | [18] |
| | Efficacy in combination with Vincristine and steroid for advanced or relapsed disease | [19], [20], [21] |
| | Better responses with intensification of ASNase therapy, first in relapsed disease, then *de novo* disease | [22], [23] |
| Importance in ALL therapy | Key agent in both induction and the post-induction intensification components of therapy | [24] |
| | Early response to ASNase of prognostic significance and intensification of therapy associated with better outcomes, both indicating a key role for ASNase in ALL therapy | [25], [26] |

**Table 5.1 *E. coli* L-asparaginase** (continued)

| | | |
|---|---|---|
| | Intensified ASNase therapy permitted safe dose reductions of other treatment elements associated with adverse long-term complications (e.g. anthracyclines) | Chapter 1, [56] |
| | Sustained asparagine depletion consequent to intensified ASNase dosing is key to efficacy; thus using an equipotent ASNase preparation with a shorter half-life yields an inferior outcome | [27], [28] |
| | Timed sequence of antimetabolite followed by ASNase (the Capizzi schedule) is a vital component of augmented post-induction intensification in high-risk disease | Chapter 1, [76]; [29] |
| | ASNase is particularly effective in the *ETV6-RUNX1* genotype (20-25% of childhood ALL) | [30] |
| ASNase resistance | | |
| *Intrinsic mechanism* | | |
| Lymphoblast ASNS expression | Lymphoblast upregulation of ASNS enables *de novo* synthesis of asparagine. Supporting observations from murine lymphoid and unmanipulated human leukaemic cell lines, human leukaemic cell lines manipulated to inhibit or overexpress ASNS, global gene expression studies and from ASNS transcript expression in primary non-*ETV6-RUNX1* genotype lymphoblasts | [31], [32], [33], [34], [35], [36], [37] |
| | Discordant observations from the exquisitively ASNase-sensitive but ASNS-expressing *ETV6-RUNX1* genotype lymphoblasts, suggesting alternate mechanisms of ASNase cytotoxicity | [37], [38], [39], [40] |
| Other | T-lineage and Philadelphia-chromosome positive lymphoblasts are intrinsically less sensitive to ASNase; the mechanisms are unclear | [41] |
| *Extrinsic mechanisms* | Exogenous asparagine supplied by niche stromal cells | Chapter 1, [126] |
| | Antibody-mediated accelerated clearance of bacterial protein, often clinically silent but sometimes associated with overt hypersensitivity (up to 60% incidence in high-risk patients treated with multiple ASNase doses) | [42], [43] |
| Alternative preparations | | |
| *Erwinia carotovora* ASNase | Equipotent in effecting asparagine depletion but has a considerably shorter half-life (half that of E.*coli* ASNase, 0.65 *v* 1.28 days), requiring more frequent dosing. Useful E.*coli* ASNase substitute as does not cross-react with neutralising antibodies; also less immunogenic. Established role in relapsed disease; a longer-acting PEG preparation holds promise | [44], [45], [46], [47], [48-49] |

**Table 5.1 *E. coli* L-asparaginase** (continued)

| | | |
|---|---|---|
| PEG-ASNase | E.*coli* ASNase covalently conjugated to monomethoxypolyethyleneglycol (PEG). Extended half-life (~6 days) resulting in sustained activity and asparagine depletion; lower immunogenicity but cross-reacts with antibodies to native E.*coli* ASNase. Neutralising anti-PEG antibodies may also develop. | [44], [50], [51], [52] |
| Complications | Clinical hypersensitivity (10-20%), coagulopathy with risk of cerebral venous thrombosis (5%), pancreatitis (5-15%), hepatotoxicity (glutaminase activity), non-thrombotic encephalopathy and metabolic abnormalities (glucose intolerance, hypertriglyceridaemia); by contrast, myelosuppression is not a major limiting adverse effect | [53], [54], [55], [56], [57] |
| Unresolved issues<br>Pharmacokinetic - pharmacodynamic correlations | The threshold cytotoxic dose of ASNase | [58] |
| | The importance of monitoring ASNase activity as opposed to asparagine levels and the clinical utility of using levels to prospectively inform therapy decisions | [59], [60] |
| | The importance of achieving asparagine depletion in the central nervous system as well as the need to monitor the same | [51], [61], [62] |
| | The relation between high ASNase activity and toxicity and the optimal route of administration (intravenous *v* intramuscular) | [63], [64] |
| | Mechanism of drug elimination - probably by the reticuloendothelial system (which may account for the very high liver tissue concentration, presumably localised to liver macrophages) | [65], [66], [67] |

**Table 5.2 ASNase degradation by lysosomal proteases - experimental limitations**

| *Limitation* | *Comment* |
|---|---|
| *In vivo* relevance | The postulated role of AEP in accelerating early ASNase degradation and augmenting the risk of ASNase hypersensitivity is based solely on *in vitro* observations. An ongoing study, part of the current frontline childhood ALL trial, is prospectively examining associations between lymphoblast AEP expression and serum ASNase activity, submicroscopic disease clearance and risk of serological and clinical ASNase hypersenstivity. Multivariable analysis will be performed to determine the independent predictive and prognostic significance of lymphoblast AEP expression. |
| Degradation of PEG-conjugated ASNase | All *in vitro* observations examined the degradation of unconjugated ASNase. The conjugated version, PEG-ASNase is increasingly used in contemporary therapy. Although AEP appeared to similarly degrade PEG-ASNase, additional experiments examining the extent of loss of activity or potential alteration in the cleavage profile as a result of PEG conjugation, were not performed |
| Extracellular release of active AEP | Robust direct evidence of this has yet to be adduced. Indirect evidence comes from *in vitro* observations of the Scripps group (liberation of cell-permeable doxorubicin from a cell-impermeable doxorubicin prodrug conjugated to an AEP-specific substrate). Limited direct evidence is available from AEP immunoblots of human bone marrow plasma (Chapter 2, [40]). Although not directly investigated, the size of the ASNase macromolecule probably precludes endocytic uptake and makes the alternative possibility, that of intracellular lysosomal degradation, less likely. |
| ASNase degradation and progenitor-T ALL | Relative resistance to ASNase has been observed in progenitor-T ALL blasts [41]. *In vitro* investigations did not examine the role of lysosomal proteases in mediating this resistance. |
| Erwinase | Although the primary focus of investigations was to examine ASNase degradation, similar investigations of the alternative asparaginase  Erwinase, would have been additionally informative, especially since Erwinase is used as a therapeutic substitute for ASNase |

# 6

# Additional lines of investigation

## Expression of AEP by tumour-associated macrophages (TAMs) in paediatric solid cancers

*Experiments performed with Hany Ariffin, University Malaya, Malaysia*

AEP expression in a spectrum of paediatric solid cancers was investigated using tissue immunohistochemistry (n=57). Stromal AEP expression was a feature in several tumours (~75%) and was localised to tumour-associated macrophages (TAMs) (**Figure 6.1**, **Figure 6.2**).

TAMs comprise the inflammatory component of the tumour stroma. Several i*n vitro* studies and clinical observations suggest that TAMs promote tumour progression and are associated with adverse prognosis. These macrophages are similar to the M2-polarised macrophages that participate in physiological wound repair. By establishing paracrine signalling loops with tumour cells, TAMs are believed to facilitate tumour progression through mechanisms that include matrix remodelling, angiogenesis and suppression of tumour-directed adaptive immune responses (for comprehensive reviews, [1], [2]).

AEP expressed by TAMs presumably has a role in both matrix degradation and paracrine tumour signalling. In this context, a DNA vaccine strategy targeting AEP-expressing TAMs in experimental models strikingly protected against fatal tumour challenge, tumour dissemination and angiogenesis (Chapter 2, [67]).

*Details of materials, immunohistology protocols and experimental optimisation-validation procedures are provided in the relevant sections in the Methods chapter*.

**Design of an equipotent AEP-resistant *E. coli* L-asparaginase**

*In collaboration with Marc Offman, Marcin Krol and Paul Bates, Biomolecular modeling laboratory, CRUK London Research Institute, London*

Amino acid substitution at the asparagine 24 (N24) residue was sufficient to prevent proteolytic cleavage of *E. coli* L-asparagine (ASNase) by AEP. Although replacement at this site did not disrupt the tetramer configuration of the protein necessary for function, the substituting glycine residue resulted in a variant protein (N24G) with considerably diminished enzymatic (asparagine deamidation) activity. Subsequent biomolecular modelling studies suggest a critical role for the N24 residue in determining enzyme activity. The residue forms part of a surface lid-loop sequence that functions as a substrate clamp. This sequence is delimited by the catalytic residues, T12 (threonine) and Y25 (tyrosine). The N24 residue participates in a local hydrogen bond network that stabilises the catalytic residues, maintains appropriate orientation of catalytic residue side chains towards substrate nucleophilic attack and regulates the flexibility of the lid-loop (and thus, substrate lock) (**Figure 6.3**). Substitution with an alanine residue at 24 (N24A ASNase) recapitulates these hydrogen-bond arrangements, allowing preservation of activity while resisting AEP cleavage. Additional substitution at the monomer-monomer interface of the ASNase tetramer (Arginine 195 residue) was predicted to optimally decrease undesirable glutaminase activity of the protein. Enzyme activity and cytotoxicity assays confirm these predictions (**Figure 6.4**).

**Figure 6.1** Stromal expression of AEP in paediatric solid cancers is localised to tumour-associated macrophages.
*Left panel*: AEP immunohistology, paraffin section, poorly differentiated neuroblastoma. Distinct stromal staining (brown) is noted (scale bar, 50μ). *Right panel*: Dual immunohistofluorescence staining for AEP (green) and the macrophage marker, CD68 (red) in glioblastoma multiforme (high grade anaplastic glioma). Sections were deparaffinised, rehydrated, heat-treated for epitope retrieval, and serially layered with primary and fluorophore-labelled secondary antibodies. Fluorescence colocalisation (yellow) localises AEP expression to stromal tumour-associated macrophages (scale bar, 10μ). Images were acquired using an Olympus BX51 microscope equipped with a Photometrics CoolSnap HQ CCD camera operated by the Metamorph advanced imaging software.

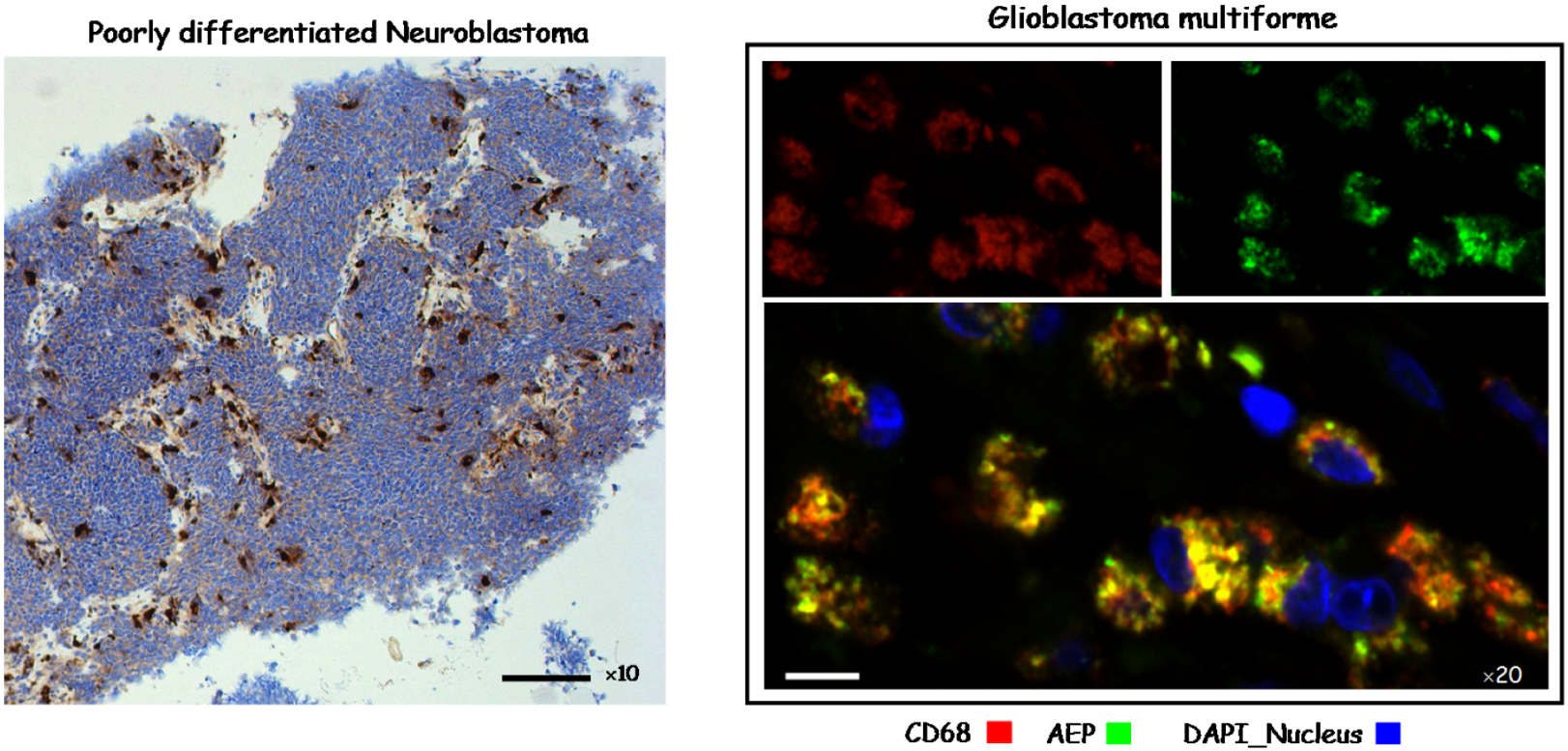

**Figure 6.2** Magnified view of AEP expression in a Tumour-associated macrophage

Photomicrographs of dual-antigen immunohistofluorescence staining of a glioblastoma multiforme (anaplastic high-grade glioma) paraffin tissue section. CD68 is a human pan-macrophage/monocyte marker. Note the characteristic coarse vesicular staining of AEP. Images were acquired using an Olympus BX51 microscope equipped with a Photometrics CoolSnap HQ CCD camera operated by the Metamorph advanced imaging software. 100×/1.35NA Oil immersion, 10μ scale bar.

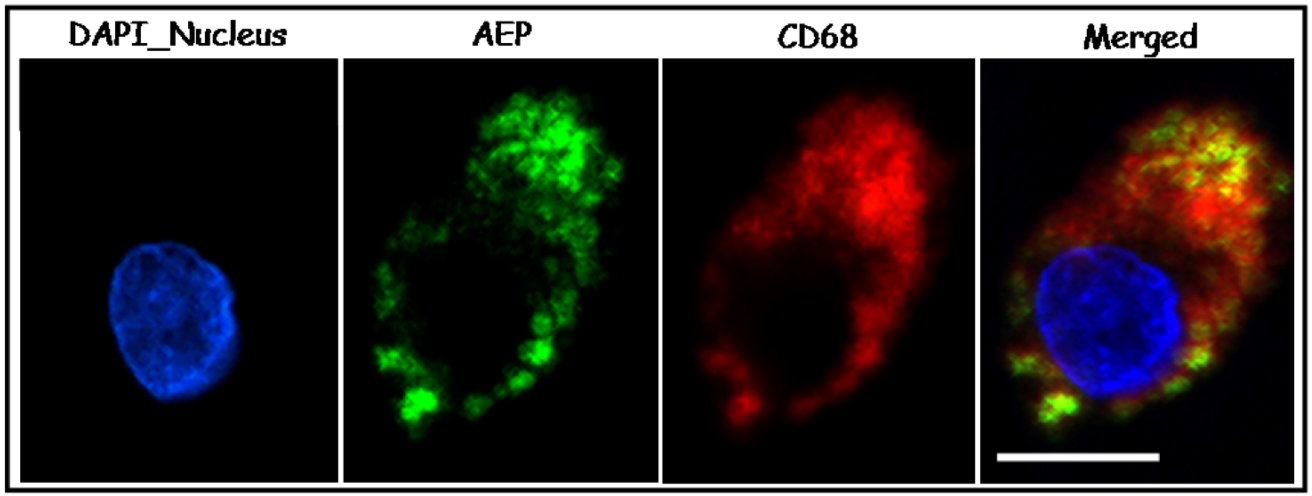

**Figure 6.3** Cartoon representation of the hydrogen bond network that surrounds the ASNase lid-loop sequence

The N24 residue is part of a lid-loop sequence that includes the catalytic residues T12 and Y25. The residue participates in a local hydrogen bond network (dotted lines) that also involves neighbouring residues D281 and E283. The hydrogen bond interaction determines flexibility of the lid-loop as substrate clamp, stabilises the catalytic residues and maintains the appropriate nucleophile attack orientation of the T12 hydroxyl side chain.

Alphabet codes for amino acid residues: D, aspartate; E, glutamate; N, asparagine; T, threonine; Y, tyrosine. AS, active substrate docking site of ASNase formed at the monomer-monomer interface of the homotetramer molecule

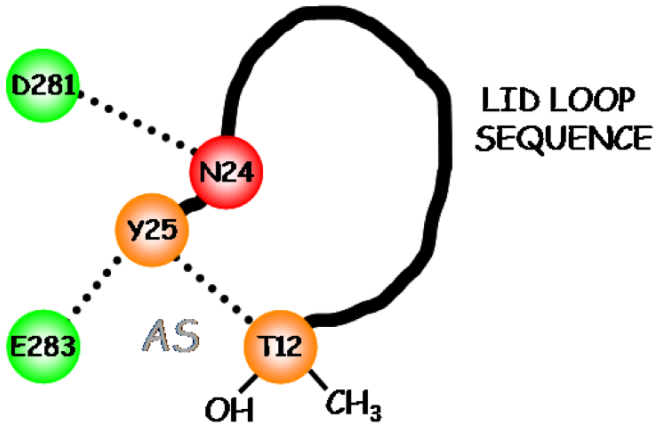

**Figure 6.4** Computational modelling enables rational design of a potential next-generation ASNase molecule with equivalent efficacy, potentially longer *in vivo* activity and potentially reduced toxicity

Purified recombinant AEP-resistant [asparagine (N) 24 substituted] ASNase variants exhibit varying asparagine and glutamine hydrolysis activities relative to wild type (WT) recombinant. Compounds were tested in cytotoxicity assays using the ASNase-sensitive ALL cell line, SupB15; half-maximal inhibitory concentrations (IC50, IU/mL) are reported relative to WT ASNase. Near-complete abolition of glutaminase activity also results in diminished cytototoxic efficacy (N24AIY250L). The N24AIR195S variant with attenuated glutaminase activity retains asparaginase activity and demonstrates cytotoxicity equivalent to WT. This variant is therefore a promising next-generation ASNase candidate, with anticipated longer half-life in AEP-expressing disease and potential for reduced toxicity (lower glutaminase activity).

WT, wild type; N24G, glycine at position 24; N24A, alanine at position 24; N24AIR195S, alanine at position 24, serine instead of arginine at position 195 adjacent to the monomer-monomer interface of the ASNase tetramer; N24AIY250L, alanine at position 24, tyrosine replaced by leucine at position 250 adjacent to the monomer-monomer interface of the tetramer. Results are reported relative to purified recombinant WT (horizontal dashed line); N24G was not tested in cytotoxicity assays. Similar results were obtained with ASNase-resistant (REH) and intermediate-sensitive (MV4:11) leukaemic cell lines.

*With thanks to Naina Patel (synthesis of ASNase recombinants and asparagine hydrolysis assay), Protein Production Laboratory, University of York (recombinant purification) and Jizhong Liu (cytotoxicity assays); for glutaminase activity assay methodology, see* ***Supplementary Table S6.1***

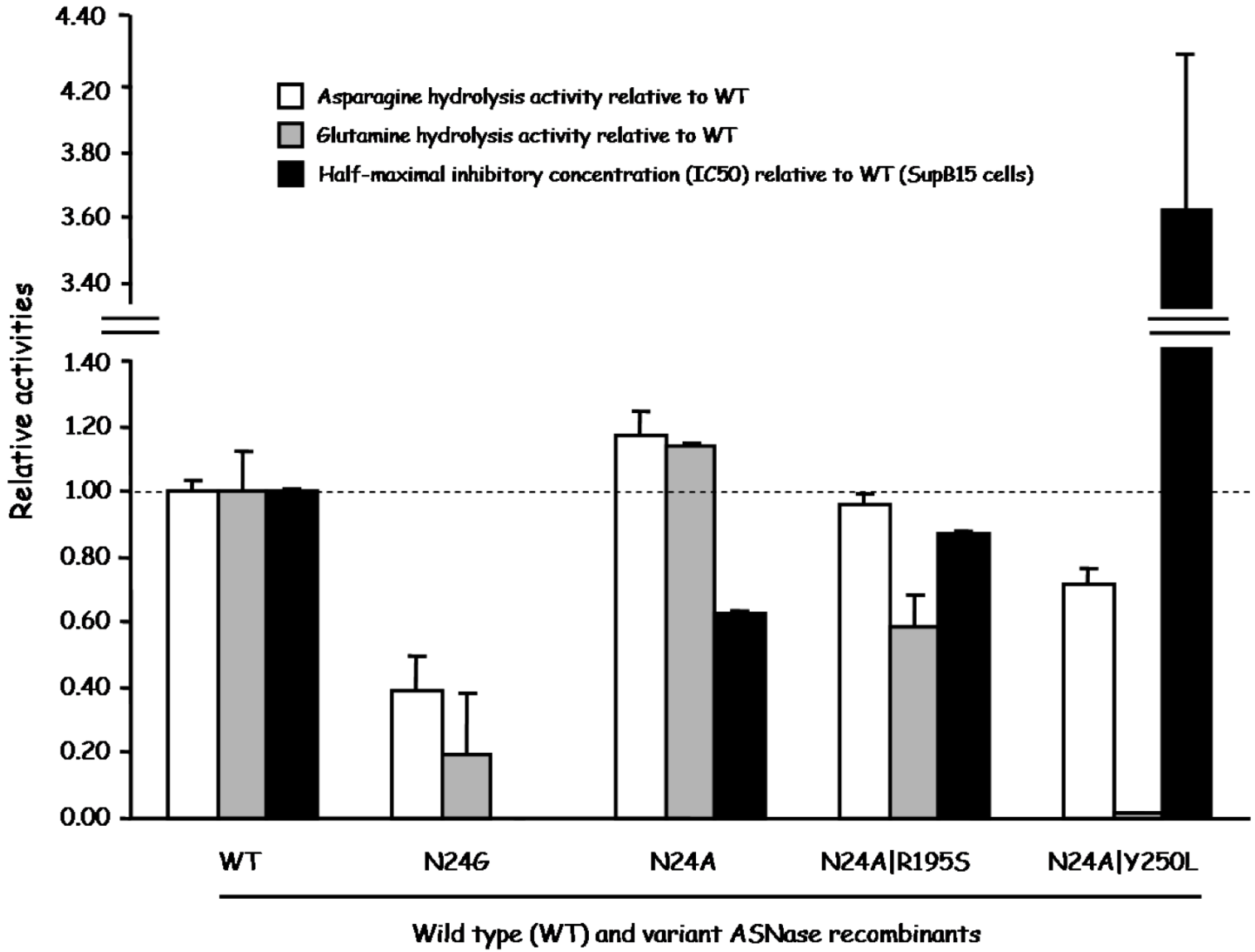
Asparagine hydrolysis activity relative to WT
Glutamine hydrolysis activity relative to WT
Half-maximal inhibitory concentration (IC50) relative to WT (SupB15 cells)
Relative activities
4.40
4.20
3.80
3.60
3.40
1.40
1.20
1.00
0.80
0.60
0.40
0.20
0.00
WT
N24G
N24A
N24A|R195S
N24A|Y250L
Wild type (WT) and variant ASNase recombinants

# 7

# Summary and Ongoing Studies

## Summary

Microarray studies identified overexpression of the lysosomal protease AEP as a candidate biomarker of the adverse-risk phenotype in progenitor-B ALL. Validation studies performed in the discovery cohort confirmed AEP transcript overexpression; limited sample availability precluded conclusive demonstration of concurrent protein overexpression. Microscopy studies, largely in cell lines, indicated a heterogeneous pattern of intracellular AEP expression and aberrant localisation in peripheral endolysosomal macrovesicles. Cell line observations additionally suggested constitutive shedding of precursor AEP protein in microparticles, which together with the microscopy findings, suggest aberrant vesicle trafficking as a feature of ALL pathobiology. Functional studies investigated the role of AEP as a pro-motility molecule and as a mediator of lymphoblast resistance to the key anti-leukaemic drug, L-asparaginase. Contrary to published reports, enforced and induced ectopic overexpression in human embryonic kidney fibroblasts was not accompanied by enhanced motility. Discordant motility phenotypes in constitutive and ectopic AEP-overexpressing progenitor-B ALL cells suggest that AEP's pro-motility role is cell context-specific, requiring concomitant expression of other pro-motility molecules. *In vitro* observations suggest that accelerated degradation of *E. coli*–derived L-asparaginase (ASNase) by AEP-overexpressing lymphoblasts provides a plausible explanation for poor early plasma ASNase activity observed in some clinical samples. Additionally, proteolytic degradation by AEP can potentially trigger ASNase hypersensitivity and formation of ASNase-neutralising antibodies, resulting in sustained treatment failure with this vital drug. AEP expression is currently being evaluated as part of a prospective UK-wide biomarker study of treatment failure (ASNase activity and hypersensitivity, submicroscopic disease clearance kinetics) in childhood ALL. A summary of the work is outlined in **Figure 7.1**.

### Additional studies

This work is best viewed within the framework of ongoing research activities in the Children's Cancer Group. The overarching research goal is to improve outcomes in children with adverse-risk childhood ALL. The group leads and participates in international clinical trials investigating new treatments in this group of patients. In the laboratory, work is progressing on several interlinked fronts to unravel mechanisms leading to treatment failure (**Figure 7.2**). To avoid reductionism, the candidate molecule AEP has been used as a lead-in to wider investigation of putative adverse-risk molecular and cellular phenotypes. Here, the AEP-expressing Ph+ ALL progenitor-B ALL cell line, SD1 has proven to be a particularly informative disease model. Candidate adverse-risk markers from discovery proteomics in SD1 cells have already been observed to be over-represented in early studies of high-risk clinical samples. Perturbed vesicle homeostasis emerges as a recurring theme in studies on SD1 cells and detailed investigations of aberrant vesicle biology are proposed (**Figure 7.3**). In undertaking these studies, the major drawback of cell line-derived information is well-recognised and is being actively addressed by attempting to corroborate all observations in clinical material. The ongoing national AEP biomarker study in childhood ALL represents one such endeavour to prospectively validate *in vitro* observations. To enable implementation of this study, a national biospecimen repository has been established (Centre for Integrated Genomic Medical Research, University of Manchester) to receive, fractionate and store plasma, lysates and cells from clinical samples. Global microarray technologies have been applied to interrogate adverse-risk determinants in clinical samples from patients treated on the European Phase III trial of Imatinib mesylate in Ph+ ALL (EsPhALL). Candidate markers shall be investigated in other high-risk ALL categories to establish their broad relevance as adverse-risk determinants. The longer term objective is to juxtapose these findings with results from *in vitro* studies to discover conserved molecular and cellular determinants of the adverse-risk phenotype suitable for therapeutic targeting.

**Figure 7.1** Summary of experimental observations

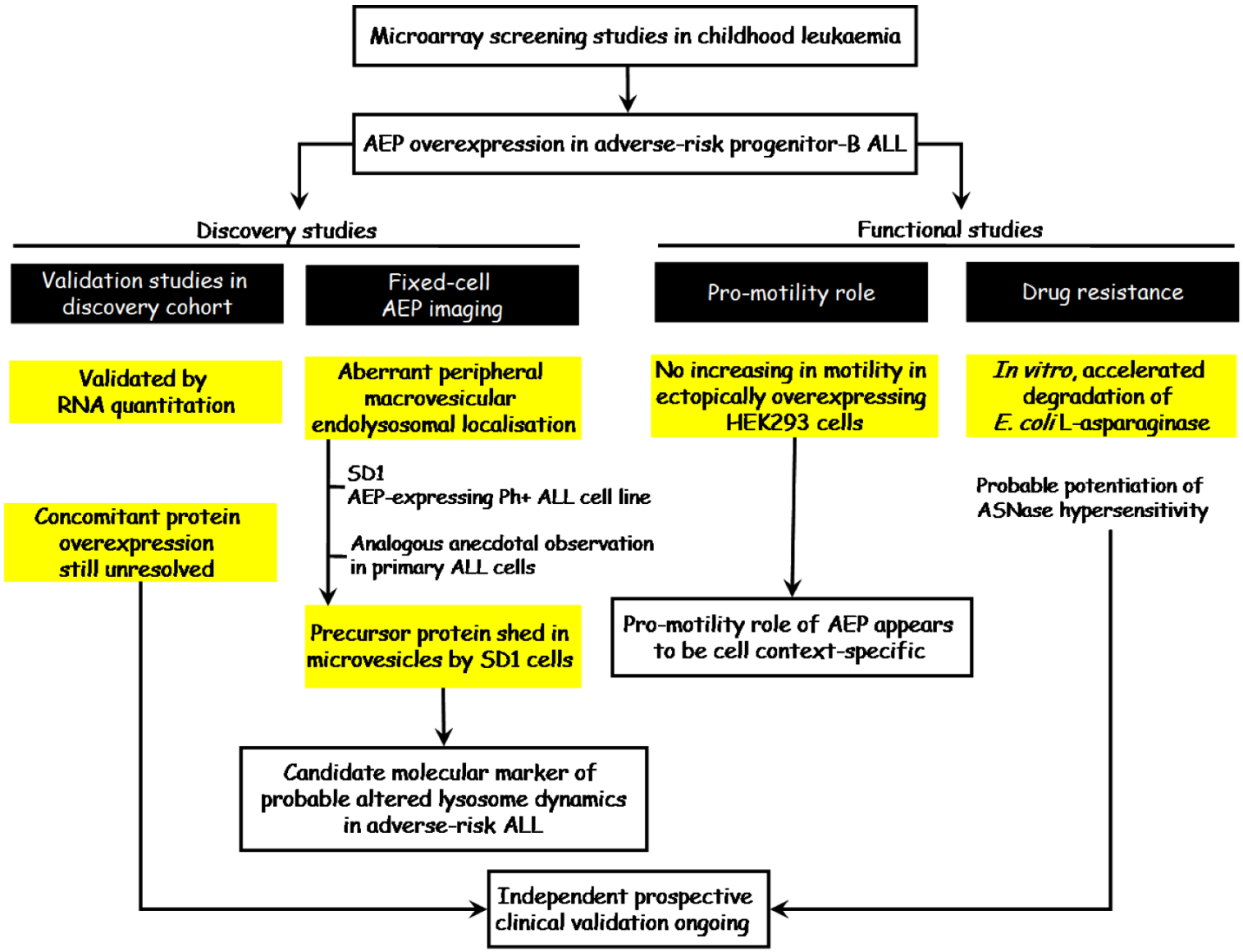

**Figure 7.2** Broad schematic outline of ongoing laboratory investigations in the Children's Cancer Group.

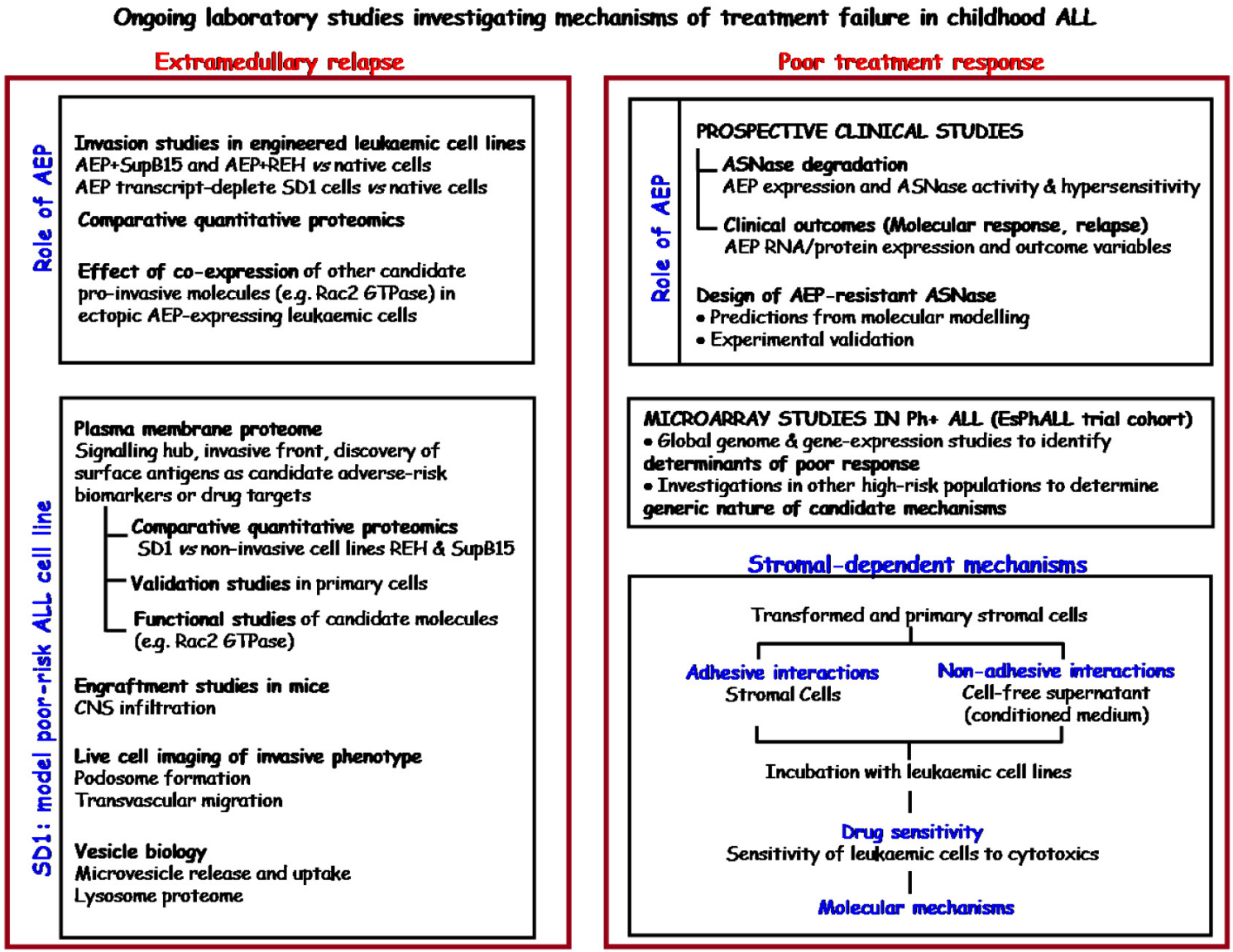

**Figure 7.3** Microvesicle biology: schematic outline of proposed experimental studies

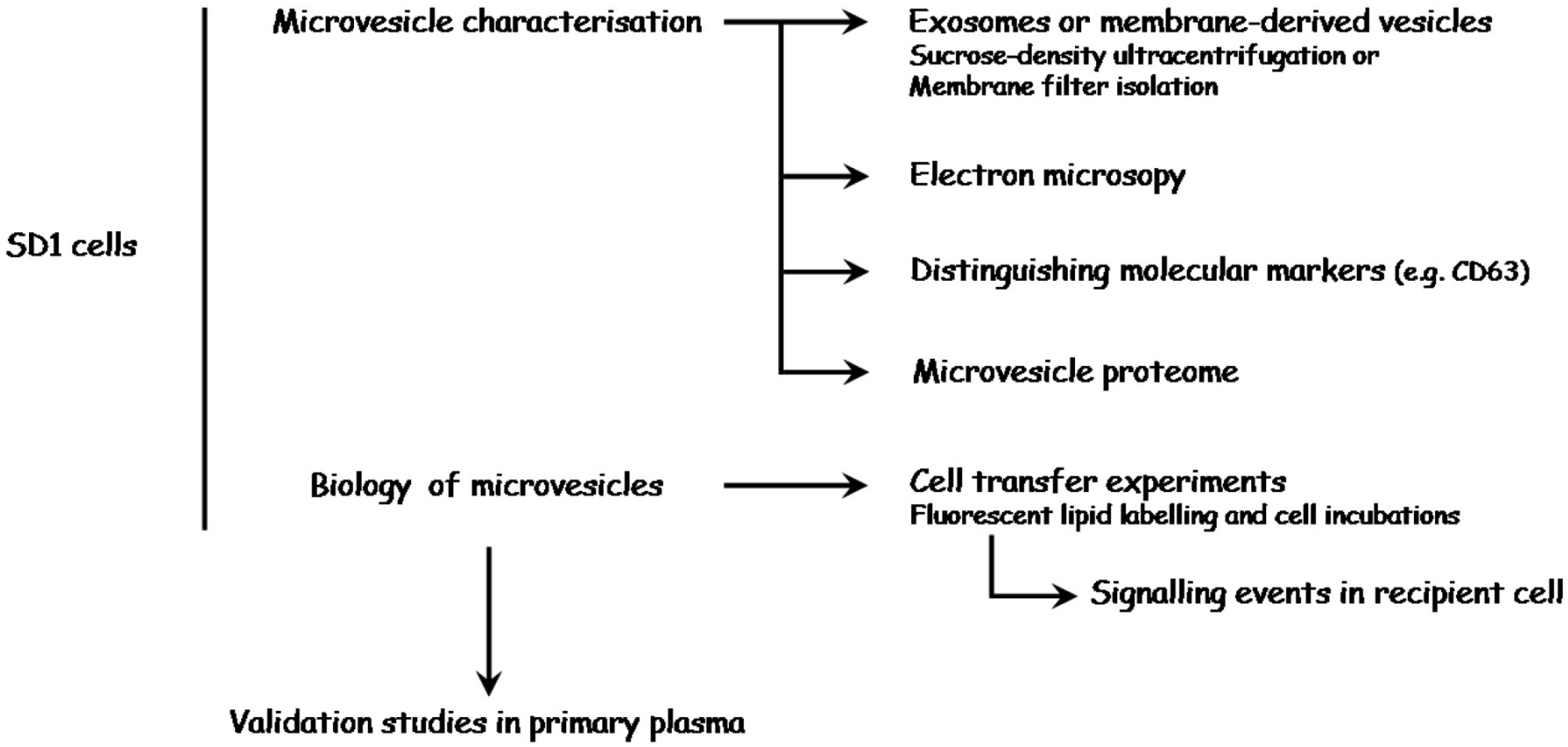

# Methods


| | | Page |
|---|---|---|
| 8.1 | Non-Reagent Material | 139 |
| 8.2 | Reagents, Buffers and Reaction Mixes | 144 |
| 8.3 | Protocol Outlines | 163 |
| 8.4 | Protocol worksheets | 172 |
| 8.5 | Optimisation and Validation procedures | 177 |
| 8.6 | Statistics | 189 |
| 8.7 | Life Science Suppliers | 190 |
| | Figures | 194 |
| | Tables | 208 |

## Section 8.1 Material - non-reagent components

GENERAL

(a) Class II laminar flow hood

(b) Refrigerated centrifuges for 15-50mL (swinging bucket) and 0.5-2.0mL volumes (Eppendorf)

(c) Tissue culture incubators (37°C, humidified 5% $CO_2$; Binder CB series)

(d) Thermal cyclers (Biorad)

(e) The Nanodrop ND-1000 UV-Vis spectrophotometer for DNA and RNA quantitation in microliter volumes

(f) Microplate reader - FLUOstar Omega (BMG Labtech, Aylesbury, UK) for UV absorbance spectrometry and fluorescence intensity readout

(g) Others

Pipettes (0.1-10μL, 2-20μL, 20-200μL, 200-100μL, Gilson)

Sterile pipette tips (filtered and non-filtered)

Serological pipettes (5mL, 10mL, 25mL volumes) and Pasteur pipettes

Electronic pipettors

Sterile polypropylene microcentrifuge tubes (0.5-2.0mL)

Sterile polypropylene conical centrifuge tubes (15-50mL) (BD, Sarstedt)

Cryotubes – 1.8mL, internal thread screw-cap tubes (Nunc)

Sterile flat-bottomed polystyrene multiwell plates (6-96 well) (BD)

Sterile vented tissue culture flasks (25, 75, 175 $cm^2$, Corning)

Refrigerators (2-8°C, Liebherr) and freezers (-20°C, 80°C; Sanyo)

Liquid nitrogen vessel

Laboratory ice machine (Scotsman), dry-ice storage vessel, ice buckets

Racks for microcentrifuge and conical centrifuge tubes

Others – vortex mixers, 700W microwave, dry heat blocks, water bath, Neubauer haemocytometer cell counting chamber

DNA CLONING

(a) Incubators (37°C) – for agar plates and liquid cultures (agitated, aerobic)

(b) The Sorvall RC 5B Superspeed centrifuge for large-scale plasmid purification
(c) Horizontal gel electrophoresis unit with power supply pack
(d) UV gel imaging unit (Syngene, Cambridge, UK)
(e) 30mL and 250mL polypropylene screw-cap plasmid fixed-angle rotor centrifuge tubes for large-scale plasmid DNA isolation

RNA ISOLATION, REVERSE TRANSCRIPTION, QUANTITATION

(a) Optical 384 well reaction plate with optical adhesive film (Applied Biosystems)
(b) The epMotion 5070 automated pipetting system (Eppendorf)
(c) ABI Prism 7900HT Fast Real Time PCR system for 96 and 384 well plates, operated by the Sequence Detection System package (Applied Biosystems)

IMMUNOBLOTTING

(a) Protein electrophoresis unit – including gel casting stand and frame, casting plates (short and 1.0mm integrated spacer glass plates), 10-well 1.0mm gel combs, electrophoresis tank and sample loading guide (MiniProtean3, Biorad)
(b) Gel loading tips (2-20μL, Anachem)
(c) Semi-dry protein blot transfer unit (Biorad)
(d) PVDF protein blotting membranes (Immobilon P, Millipore; 7cm × 10cm)
(e) High current power supply unit (400mA, Biorad)
(f) Extra-thick blot paper for protein transfer sandwich (Biorad)
(g) Rocking platform unit
(h) Atraumatic non-serrated forceps for membrane handling (Millipore)
(i) Imaging films (Kodak MXB blue-sensitive X-ray films, 30 × 40cm)
(j) X-ray film cassette
(k) Film developer station (dark room)
(l) Others – square petri dishes for immunoblotting (BD), plastic sheet envelope for PVDF membrane, membrane roller, walk-in cold-room for overnight and extended 4°C antibody incubations

MOTILITY ASSAYS

(a) 8-micron pore transparent polyethylene terephthalate cell-culture inserts for 24-well plates (BD Falcon)

(b) Particle Counters

The CASY-DT cell counter (Innovatis AG, Reutlinger, Germany)

The Z1 single-threshold Coulter counter (Beckman Coulter)

(c) Others – Fine pointed forceps with curved head to handle cell culture inserts, maintained sterile by immersion in absolute ethanol; cotton-buds to scrape-remove cells from growth surface of inserts; microscope eyepiece square-grid graticule for cell counting

IMMUNOSTAINING

(a) Staining tray

(b) Microscope slides (1mm thick, 76mm × 26mm; Menzel-Glaser)

(c) Glass coverslips (No. 1.5, rectangular 22mm × 50mm, square 22mm × 22mm)

(d) Shandon Cytospin III cytocentrifuge

(e) Cytospin funnels, filter papers and stainless-steel clips (Shandon)

(f) Hydrophobic marker pen (Vector laboratories)

(g) Others – 35mm petri-dish with water (to maintain humidity), slide tray, black cover sheet for light protection

IMMUNOHISTOCHEMISTRY

(a) Formalin-fixed paraffin-embedded tissue samples (University Malaya)

(b) Five-micron tissue sections on poly-L-lysine or silane-treated microscope slides

(c) Stainless steel slide rack

(d) Pressure cooker, maximum setting 125°C

(e) Staining troughs

(f) Staining tray with lid

(g) Hydrophobic marker pen

(h) Automated glass coverslipper (CV5030, Leica Microsystems)

(i) The automated MIRAX digital histology platform (Zeiss)

MICROSCOPES

(a) The Nikon Eclipse TS100 inverted trinocular microscope for phase contrast microscopy with 10×/0.30NA PlanFluor and 20×/0.40NA Ph1 phase objectives and the DS-Fi1 camera supported by the DS-L2 software (Nikon)

(b) The Olympus BX51 upright microscope with fluorescence filter cubes, 10×/0.3NA UPlanFL, 20×/0.5NA UPlanFL N, 40×/0.75 UPlanFL N, 40× Oil/1.30 UPlanFL N and 100× Oil/1.35NA UPlanFL N objectives (Olympus) and the Photometrics CoolSNAP HQ CCD camera (Molecular Devices) operated by the Metamorph Advanced Imaging system (Molecular Devices)

(c) The Zeiss Axiovert 200M low-light system with Sedat fluorescence filter wheels, the Optovar module, 60× Oil/1.40 NA PlanApo (Olympus) and 100× Oil/1.45 NA AlphaPlanFluar (Zeiss) objectives and the Photometrics Cascade II:1024 EMCCD (electron-multiplying charge couple device) camera (Molecular Devices) operated by the Metamorph Advanced Imaging system (Molecular Devices)

ANALYSIS PACKAGES

(a) Lasergene suite of applications for genome analysis (DNAStar, v7.2)
(b) Sequence Detection System for data analysis on the ABI Prism 7900HT quantitative real-time instrument (SDS v2.0, Applied Biosystems)
(c) Adobe Photoshop (Creative Suite 3) image processing software (San Jose, CA, USA)
(d) Statistical Package for Social Sciences (SPSS) software application for Windows (v16.0, now part of IBM) and the Microsoft Excel spreadsheet application (Microsoft Windows XP Professional, 2001)

MICROVESICLE ISOLATION FROM CELL-FREE SUPERNATANT

(a) Thin-walled 36mL polyallomer ultracentrifuge tubes (Beckman Coulter)

(b) The Sorvall Discovery M120 SE refrigerated ultracentrifuge with the AH-629 swinging rotor equipped with 36mL aluminium buckets (DuPont Instruments)

## Section 8.2 Reagents, Buffers and Reaction Mixes

Unless specified, all chemicals were sourced from Sigma-Aldrich.

### GENERAL LAB REAGENTS (CENTRAL LAB SERVICES, PATERSON INSTITUTE)

1 Sterile Phosphate buffered saline (calcium, magnesium free)

One Dulbecco 'A' tablet* dissolved in 100mL distilled water (pH 7.4)

| | |
|---|---|
| Sodium Chloride 137mM | 0.8g |
| Potassium Chloride 2.7mM | 0.2g |
| $Na_2HPO_4$** 8mM | 1.15g |
| $KH_2PO_4$*** 1.5mM | 0.2g |

* Oxoid Ltd., part of Thermo-Fisher Scientific

** Disodium hydrogen phosphate ***Potassium dihydrogen phosphate

Sterilised by autoclaving (121°C, 20 minutes)

2 Sterile deionised water

Two-step purification (ELGA Optima 15 followed by ELGA Purelab Ultra purification systems) to generate ultra-pure deionised water (18.2 mohm.cm resistivity) sterilised by either UV- or autoclave- (121°C, 20 minutes) treatment; dispensed in borosilicate bottles

3 Luria-Bertani agar plates and liquid medium

4 Virkon solution, 1%, for overnight disinfection of biohazardous waste

### DNA CLONING

1 Tris Borate EDTA (TBE) buffer for agarose gel electrophoresis

For a 1L 10× stock solution,

| | |
|---|---|
| Tris base 0.89M | 108g |
| Boric acid 0.89M | 55g |
| Tetrasodium EDTA 0.02M | 9.3g |

2 Agarose for horizontal gel electrophoresis

Dedicated preparation area, ethidium bromide alert

For a 0.8% agarose gel preparation,

| | |
|---|---|
| Agarose* | 0.8g |
| TBE buffer to | 100mL |

*Ultrapure standard melting temperature agarose (Invitrogen)

Cover with thin plastic film and dissolve by heating in a 700W microwave (medium setting, 3min 40sec)

Cool, add ethidium bromide (10mg/mL) 1μL and pour on to a gel platform with sealed-off walls. Place gel comb and allow to set.

3 Tris-EDTA buffer, pH 8.0
For a 100mL 10× solution,

| | |
|---|---|
| Tris base 0.1M | 1.21g |
| Disodium EDTA 0.01M | 0.37g |

Adjust pH to 8.0 with 5N hydrochloric acid

4 Antibiotics for selection
Ampicillin 50mg/mL in sterile water
Kanamycin 50μg/mL in sterile water,
Syringe-filtered (0.22 micron) and stored in aliquots at -20°C

5 Small-scale plasmid DNA purification kit (Wizard Plus SV, Promega)
Components include:
Resuspension solution (Tris-EDTA with RNase A)
Cell lysis solution (sodium hydroxide with SDS)
Proprietary DNA-binding silica membrane minicolumns
Neutralisation solution (guanidine hydrochloride, potassium acetate)
Column wash solution (ethanol, potassium acetate, Tris-EDTA)
Nuclease-free water for elution of bound DNA

6 Large-scale endotoxin-free plasmid DNA purification kit (Maxiprep, Qiagen)
Components include:

| | |
|---|---|
| Buffer P1 (with RNase) | Bacterial resuspension solution |
| Buffers P2 and P3 | Bacterial lysis |
| Spin columns | Proprietary plasmid DNA binding resin |
| Buffer QBT | Equilibration of spin column |
| Buffer QC | Column wash |
| Buffer QF | Elution of bound DNA |

7 Isolation of plasmid DNA insert following agarose gel electrophoresis (Wizard SV Gel and PCR clean-up kit, Promega)
Components include:

Membrane binding solution - chaotropic agents (guanidine isothiocyanate, potassium acetate) to free DNA fragment from agarose gel

Spin columns - Proprietary DNA-binding silica columns

Ethanol-based membrane-wash solution – with potassium acetate, EDTA

Nuclease-free water for elution

8 Restriction endonucleases (New England Biolabs)
EcoR1 (100,000 U/mL) and Not1 (50,000U/mL)

9 Reaction mix for restriction enzyme plasmid digestion

For a 100μL reaction mix,

| | |
|---|---|
| Plasmid DNA | 0.75-1.0μg DNA (typically 10μL) |
| 5' restriction enzyme | 1.0μL (typically 50-100U/μL) |
| 3' restriction enzyme | 1.0μL (typically 50-100U/μL) |
| Compatible diluent buffer, 10×* | 10μL |
| BSA enhancer* | 5.0μL |
| PCR-grade water to | 100μL |
| Incubation conditions | 37°C, 2 hours |

10 Reaction mix for 5' dephosphorylation of digested vector termini

For a 30μL reaction mix,

| | |
|---|---|
| Digested vector plasmid mix | 20μL (see above) |
| Shrimp Alkaline Phosphatase* | 1.0μL (typically 1U/μL) |
| 10× reaction buffer* | 3.0μL |
| PCR-grade water to | 30μL |
| Incubation conditions | 37°C, 15 minutes; followed by<br>65°C, 15 minutes, to inactivate |

*Promega

11 Reaction mix for cDNA insert ligation using the T4 DNA Ligase

A 20μL reaction volume using the T4 DNA Ligase in pre-constituted microfuge tubes (GE Healthcare)

Trial of different ratios of insert cDNA* and destination vector**

| Destination vector (μL) | Insert cDNA (μL) |
|---|---|
| 0.5 | 3.5 |
| 1.0 | 3.0 |
| 1.0 | 5.0 |
| 1.0 | 10.0 |

PCR-grade water to 20μL

Incubation conditions 16°C, 60 minutes (minimum)

* Derived from source plasmid following digestion, isolation by gel electrophoresis and purification

** 100ng/μL DNA, linearised and 5' dephosphorylated at termini

12 Reaction mix for plasmid DNA sequencing

Stock sequencing primer oligonucleotides (100μM)

Supplied lyophilised, reconstituted with PCR-grade water using manufacturer-recommended volumes, mixed well by pipetting to resuspend and stored at -20°C

For use in sequencing reactions, 1μL of 100μM primer was diluted 1-in-10 with PCR grade water for a 10μM interim working concentration; 1μL of 10μM working concentration of primer was further diluted with 6μL PCR-grade water (total volume, 7μL) for a final 1.5 picomole/μL primer concentration

A 12μL reaction mix containing

| | |
|---|---|
| Plasmid DNA | 350-500ng |
| Sequencing primer | 1.5 picomole |
| PCR-grade water | to 12μL |

Samples for sequencing were submitted to the Paterson Institute's Molecular Biology Core Facility. Automated sequencing performed using the Applied Biosystems 3130 16-capillary genetic analysis system

13 Reaction mix for LR recombination reactions using the Gateway cloning system (Invitrogen)
Appropriate Gateway Entry Vector with in-frame cDNA insert and flanking att*L* recombination sites
Suitable Gateway Destination Vector with att*R* recombination sites

A 20μL reaction mix containing, in sequence

| | |
|---|---|
| Entry Vector (300ng/μL) | 1.0μL |
| Destination Vector (300ng/μL) | 1.0μL |
| Diluent buffer, 5× | 4.0μL |
| Tris-EDTA buffer | 10μL |
| LR Clonase enzyme mix* | 4.0μL |

*Thaw for 2 minutes on ice from -80°C, pulse vortex (twice, 2 seconds each), add to above reaction mix, return to -80°C immediately after use

| | |
|---|---|
| Incubation conditions | 25°C, 60 minutes |

Terminate reaction by adding Proteinase K, 2μL (4μg, pulse vortex to mix) and incubating at 37°C for 10 minutes

Reaction mix is used directly to transform competent E. *coli* cells (Top10 chemically competent cells, Invitrogen)

14 Glycerol bacterial stocks

| | |
|---|---|
| Liquid *E coli* culture | 850μL |
| Glycerol | 150μL |

Vortex vigorously to mix, snap-freeze on dry ice, store -80°C

15 Others
Sample loading buffer and DNA size markers for electrophoresis, SOC bacterial growth medium

## BLOOD/BONE MARROW MONONUCLEAR CELL ISOLATION

1 Lymphoprep density separation solution of sodium diatrizoate and a polysaccharide (density 1.077g/mL) for isolation of mononuclear cells (Axis-Shield UK) – 1 part solution to 2 parts blood or bone marrow (diluted 1:1 with PBS)

2 Trypan blue (0.4%) reagent for dye exclusion staining of viable cells – filtered (0.22 μm) to exclude precipitates and aggregates
1 part reagent mixed with 1 part cell suspension, 10μL mix applied immediately to each chamber of the Neubauer haemocytometer

3 Glacial acetic-acid (3%) with methylene blue (Stem Cell Technologies, Grenoble, France) for selective staining of mononuclear cells in the presence of heavy red cell contamination of cell suspension

4 Cryoprotectant (DMSO 10% (v/v) FBS 20% (v/v) in growth medium)
Liquid culture media (RPMI 1640 or DMEM) with 10% DMSO and 20% FBS
Add 20mL FBS and 10mL DMSO to 70mL growth medium. Mix, filter (0.22 micron) and store in 3mL aliquots at -20°C to -80°C

## RNA ISOLATION

All steps were carried out in a dedicated level II laminar flow hood.

1 TRIzol reagent (Invitrogen), containing phenol and guanidine isothiocyanate

2 Others – chloroform, isopropanol, 75% ethanol and DEPC-treated RNase-free water

## QUANTITATIVE RNA ESTIMATION

All procedures were carried out in a dedicated level II laminar flow hood. Sterile DEPC-treated RNase-free water was the diluent in all reactions

1 RNA priming mix
For a 12μL reaction volume in a 0.2mL thin-walled PCR tube*

| | |
|---|---|
| Whole cell total RNA** | Volume equivalent to 500ng |
| Random hexamers*** | 1.5μL (150ng) |
| Water to 12μL | |

*Applied Biosystems
**Total RNA extracted using the TRIzol reagent isolation protocol (Invitrogen)
**Prepared from 20μg lyophilised stock solution (Promega)

| | |
|---|---|
| Cycling condition | 70°C for 5 minutes |
| | Returned immediately to ice |

2 Reverse transcription mix for first-strand cDNA synthesis

Reaction mastermix prepared for (n+2) samples*; for an 18μL unit reaction volume:

| | |
|---|---|
| dNTPs 2.5mM** | 10μL |
| MMLV-RT enzyme*** | 2μL (400U) |
| 5× RT reaction buffer | 6μL |

*Dispensed 18μL reaction mix to each primed sample above to bring total reaction volume in each tube to 30μL

** Nucleotide mix from10mM each of dATP, dTTP, dCTP, dGTP

***The RNase H-minus point mutant Murine Moloney Leukaemia Virus (M-MLV reverse transcriptase) 200U/μL from Promega

| | |
|---|---|
| Cycling conditions | 42°C, 60 minutes |
| | 95°C, 5 minutes to terminate reaction |

Residual RNA duplexed with cDNA removed by adding RNase H 2μL (2U, GE Healthcare) each sample

| | |
|---|---|
| Cycling condition | 37°C, 20 minutes |

3 Quantitative RNA reaction mix for 96-well plates

For each sample, target and reference genes are assayed in triplicate

For 'n' cDNA samples, estimate volume equivalent to [(n+1)×4]μL for each gene assayed

Unit reaction volume: 25μL per well

| | |
|---|---|
| Quantitative PCR mastermix*, 2× | 12.5μL |
| Taqman probe-primer mix**, 20× | 1.25μL |
| Sample DNA | 1.0μL*** |
| Water to | 25μL |

*Contains hot start AmpliTaq DNA polymerase with 5'-exonuclease activity, deoxynucleotide mix (with dUTP replacing dTTP), uracil-N-glycosylase to minimise carryover contamination and the ROX passive reference dye (Applied Biosystems)

**Human gene-specific Taqman on-demand probe-primer mix for real-time quantitation from Applied Biosystems containing exon-spanning FRET labelled 25-mer oligonucleotide probes (5'FAM reporter and 3' non-fluorescent quencher) and flanking forward and reverse exon-specific primers in a probe:primer molar ratio of 1:9

***Equivalent to 16.1ng template RNA

4 Quantitative RNA reaction mix for automated loading of 384-well plates

For each gene, target and reference genes are assayed in triplicate

Reaction mix for cDNA loading

| | |
|---|---|
| Sample cDNA | 10.0μL |
| Water | 102.5μL |
| Automated volume load/well | 4.5μL* |

*Equivalent to 6.4ng template RNA

Reaction mix for Taqman probe-primer and PCR reagent*
For 'n' cDNA samples, estimate volume equivalent to [(n+1)×4]μL for each gene assayed
Unit loading volume per well: 5.5μL
Quantitative PCR mastermix, 2× 5.0μL
Taqman probe-primer mix, 20× 0.5μL

Final reaction volume loaded/well: 10μL

5 Cycling conditions for RNA quantitative PCR

| | |
|---|---|
| Uracil N-glycosylase activation | 50°C, 2 min |
| AmpliTaq DNA polymerase activation | 95°C, 10 min |
| PCR cycles, repeated 40 times: | |
| Strand denaturation | 95°C, 15 sec |
| Primer annealing/strand extension | 60°C, 1 min |

## PROTEIN IMMUNOBLOTTING

1 Lysis Buffers

A Non-ionic non-denaturing detergent lysis buffer (Nonidet P-40 based)

- Alkaline pH (pH 8.0), 0.1% NP-40 solution
  For a 100mL solution,
  Tris base 50mM 0.606g
  Sodium Chloride 150mM 0.880g
  Adjust pH to 8.0 with concentrated hydrochloric acid
  Bring volume to 100mL with sterile deionised water
  Add 100μL Igepal CA-630 (NP-40 equivalent)

  Filter (0.22 micron) and store at 4°C
  To 50mL, add 1 Complete Protease Inhibitor Cocktail tablet (Roche), mix well to dissolve, create 500μL aliquots in microfuge tubes and store at -80°C

- Acid pH (pH 5.0), 0.8% NP-40 solution
  For a 50mL solution,
  Tri Sodium Citrate, 50mM 0.736g
  Adjust pH to 5.0 with concentrated hydrochloric acid
  Bring volume to 50mL with deionised water and filter (0.22 micron)

  Create 3mL aliquots in 7mL Bijoux tubes and store at -20°C
  To thawed 3mL aliquot, add 1.1μL 2-mercaptoethanol (effectively 5mM) before use

In some experiments, 10% CHAPS 10μL was added to 2mL (effectively, 0.05% CHAPS) NP-40 citrate lysis buffer to achieve more complete solubilisation of membrane-bound proteins

B SDS sample buffer for gel loading

For 10mL of a 5× solution,

| | |
|---|---|
| Tris buffer 1.0M, pH 6.8 | 2.5mL (see 2B below) |
| SDS | 1.0g |
| Glycerol | 5.0mL |
| Bromophenol blue | 2mg |

Create 500μL aliquots and store at -20°C

Thaw by briefly heating at 65°C. Add 50μL 2-mercaptoethanol before use

2 Protein assay

Modified Lowry assay; detergent-compatible (DC) reagents from Bio-Rad

| | |
|---|---|
| Protein assay reagent A | Alkaline copper tartrate solution |
| Protein assay reagent B | Dilute Folin reagent |
| Protein assay reagent S | Surfactant |

BSA standards

Prepared from stock solution of BSA 5mg/mL (50mg in 10mL protein lysis buffer, mix well to dissolve while avoiding excessive frothing, dispense as 100μL single-use aliquots, store at -20°C)

3 Gel constituents

A Resolving gel buffer (1.5M Tris, pH 8.8)

For a 100mL solution,

| | |
|---|---|
| Tris base 1.5M | 18.2g |

Adjust pH to 8.8 with concentrated hydrochloric acid

Bring the volume to 100mL with deionised water

Filter (0.22 micron) and store at 4°C

B Stacking gel buffer (1.0M Tris, pH 6.8)

For a 100mL solution,

| | |
|---|---|
| Tris Base 1.0M | 12.1g |

Adjust pH to 6.8 with concentrated hydrochloric acid

Bring the volume to 100mL with deionised water

Filter (0.22 micron) and store at 4°C

C Resolving gel mix

For a 20mL 10% polyacrylamide gel solution, add in sequence

| | |
|---|---|
| Deionised water | 7.9mL |
| Acrylamide 30%* | 6.7mL |
| Tris 1.5M, pH 8.8 | 5.0mL |
| SDS 10%* | 0.2mL |

| | |
|---|---|
| Ammonium Persulphate** 10% | 0.2mL |
| TEMED | 0.008mL |

*National Diagnostics (Acrylamide ratio 37.5:1 acrylamide:bisacrylamide)
**Ammonium persulphate (electrophoresis grade, GE Healthcare Life Sciences) 0.5g in 5mL deionised water; 500μL aliquots at -20°C

Mix well and allow 2 minutes for initiation of polymerization. To each vertical 1.0mm-spacer glass plate assembly, dispense 4.5–5.0mL of mix and overlay with 0.01% SDS (10μL 10% SDS added to 10mL deionised water). Polymerisation time, 45 minutes – 1 hour

D Stacking gel mix
For a 10mL solution, add in sequence

| | |
|---|---|
| Deionised water | 6.8mL |
| Acrylamide 30% | 1.7mL |
| Tris 1.0M, pH 6.8 | 1.25mL |
| SDS 10% | 0.1mL |
| Ammonium persulphate 10% | 0.1mL |
| TEMED | 0.01mL |

Immediately dispense 1mL of mix and place gel combs. Polymerisation time, 15 minutes; remove combs and wash vigorously to remove residual unpolymerised material

4 Electrophoresis (running) buffer
Freshly prepare. For a 500mL 1× solution,

| | |
|---|---|
| Tris Glycine SDS buffer 10×* | 50mL |
| Deionised water | 450mL |

*Tris 0.25M, Glycine 1.92M, SDS 1% (w/v) (pH 8.3, Bio-Rad)

5 Gel transfer buffer
Freshly prepare. For a 500mL 1× solution,

| | |
|---|---|
| Tris base 25mM | 1.52g |
| Glycine 192mM | 7.20g |
| Methanol (Fisher Scientific) | 100mL (20% v/v) |
| Deionised water to 500mL | |

Maintain chilled. Gels, membranes and blot papers are presoaked in chilled transfer buffer prior to membrane transfer

6 Blocking solution (5% non-fat dried milk solution, NFDM)
Non-fat skimmed milk powder (Marvel, Premier Foods, UK), 5% (w/v) in PBS-Tween 20 0.05%
To 50mL PBS-Tween 20 0.05%, add 2.5g milk powder

7 Methanol
For hydrophilic activation of PVDF membranes (15 second treatment)
Activated PVDF membranes are maintained rocking in transfer buffer until use

8 Antibodies

A Primary antibodies (diluent, 5% non-fat milk* in PBS-Tween 20 0.05%)

- Anti-AEP
  Goat polyclonal anti-human (AF2199, R&D Systems)
  Dilution 1:2500 (80ng/mL)
  Volume: 12-20mL / membrane in square petri dishes
  Incubation: 2 hours, room temperature; 12-16 hours, 4°C; rocking

- Anti-CTSB
  Rabbit polyclonal anti-human (Biomol SA-361, Enzo Life Sciences)
  Dilution 1:10,000
  Volume: 12-20mL / membrane in square petri dishes
  Incubation: 12-16 hours, 4°C; rocking

  Other anti-CTSB antibodies tested included:
  Mouse monoclonal anti-human IgG-2a, clone CA10, directed to an epitope in the CTSB heavy chain (IM27L, Merck Biosciences)

  Mouse monoclonal anti-human IgG1, clone 155714 (MAB2176, R&D Systems)

  Two other rabbit polyclonal anti-human antibodies from Merck biosciences (product codes 219408 and PC41)

- Anti-β-actin
  Mouse monoclonal IgG1, broad species specificity, clone AC-15, directed to an N-terminal epitope (A5441, Sigma-Aldrich); dilution 1:5000 – 1:10,000

B Peroxidase-conjugated secondary antibodies (diluent as with primary antibodies)

- Anti-goat — Donkey anti-goat IgG (sc-2020, Santa Cruz)
  Dilution 1:10,000 (40ng/mL)
- Anti-rabbit — Goat anti-rabbit IgG (P0448, Dako)
  Dilution 1:20,000
- Anti-mouse — Goat anti-mouse IgG (31430, Pierce)
  Dilution 1:5000–1:10,000

9 Others

A Precision Plus dual-colour pre-stained protein electrophoresis standards (Bio-Rad); 10-12μL unit loading volume

B Phosphate Buffered saline with Tween 20 0.05%
To a 500mL PBS solution, add 250μL Tween 20; mix well

C SuperSignal West Dura extended duration chemiluminescence substrate kit containing Luminol (with an enhancer) and peroxide buffer (Pierce) –1:1 ratio of reagents
1.5mL/membrane, 5 minute incubation, ensure uniform layering, light-protection unnecessary

D 'Restore' proprietary membrane stripping buffer from Pierce

## AEP ACTIVITY ASSAY

1 Assay buffer
For a 50mL 10× solution

| | |
|---|---|
| Citric acid 395mM | 3.79g |
| $Na_2HPO_4$* 1.21M | 8.59g (anhydrous salt) |
| $Na_2EDTA$** 10mM | 0.186g |

*Disodium Hydrogen Phosphate
** Disodium EDTA

2 Other reagents

- CHAPS 10% (w/v)
  0.25g CHAPS to 2.5mL dd$H_2O$
- DTT 0.5M stock
- 7-Amino Methyl Coumarin (7-NHMeC) 20mM in DMSO stock
- AEP substrate Z-Ala-Ala-Asn-NHMeC* 10mM in DMSO stock
- AEP inhibitor MV026630** 10mM in DMSO stock

*Bachem **Cancer Research Technology, CRUK (Jon Roffey)

## CELL CULTURE

All work related to cell culture was carried out in a Level II laminar flow hood.

1 Foetal Bovine Serum (Sera Laboratories International)
Complement inactivation by heating to 56°C for 30 min
Filtered (0.22 micron), aliquots stored at -20°C to -80°C

2 L-Glutamine 200mM stock solution (PAA Laboratories)
Stock aliquots (5mL) stored at -20°C
For a 2mM solution, 5mL stock added to 495mL liquid medium

3 Complete liquid culture reagents

A Routine culture media, without antibiotics or selection agents

- RPMI 1640 and DMEM Glutamax liquid media (Invitrogen)
  Foetal Bovine Serum (FBS) 10%
  Add 55mL FBS to 500mL medium for a 10% FBS solution

- Ham F-12, 7% FBS (for the PC-3 prostate carcinoma cell line)
  To a 40mL aliquot of medium, added 3mL FBS and 400μL 200mM L-Glutamine

B With selection agents

- Hygromycin B 50μg/mL and Zeocin 400μg/mL in complete DMEM (both, Invitrogen) for the mifepristone-inducible GeneSwitch protein-expressing HEK293 cells
  To a 40mL aliquot of complete DMEM, add Hygromycin B 40μL (50mg/mL stock solution) and Zeocin 160μL (100mg/mL stock solution) just before use

- Geneticin (G-418 sulphate, PAA) 0.6mg/mL in complete DMEM for the enforced protein-expressing HEK 293 cells

  G-418 sulphate 5mg dissolved in 50mL sterile PBS, filtered (0.22 micron) and stored in 5mL aliquots (100mg/mL) at -80°C. Thawed aliquots are maintained at 4°C

  To a 40mL aliquot of complete DMEM, add 240μL G-418 sulphate (100mg/mL stock). Refresh every 48–72 hours

4 Trypsin-EDTA (Sigma-Aldrich, Lonza)
Porcine trypsin 0.5% (w/v) with tetrasodium EDTA 0.2g/L
Aliquots stored at -20°C, prewarmed (37°C) before use

Typical volumes used (undiluted)

| | | |
|---|---|---|
| 100mm dishes | 56cm$^2$ | 3mL |
| T75 flasks | 75cm$^2$ | 5mL |
| T175 flasks | 175cm$^2$ | 10mL |

Treatment time 2-5 minutes, 37°C/5%$CO_2$

Neutralisation Equivalent volumes of growth medium with 10% FBS; in special circumstances, growth medium with 1% FBS

## LIPID-BASED TRANSFECTION OF ADHERENT HUMAN CELL LINES

All steps carried out in a level II laminar flow hood; optimal cell density 1.0 – 2.0 × $10^5$ cells/well in a 6- or 12-well plate (BD Falcon)

1 Lipofectamine 2000 lipid transfection reagent (Invitrogen)
Proprietary liposome formulation containing a synthetic polycationic lipid and a neutral phosphatidyl ethanolamine lipid

2 DNA-OptiMEM I reaction mix
Unit reaction volume (100μL)*

| | |
|---|---|
| Plasmid DNA** | 10μL (100ng/μL) |
| OptiMEM I*** | 90μL |

*Final volume estimated for 'n+2' samples to be transfected with a given plasmid, i.e. [(n+2) × 100μL]
**High-purity endotoxin-free sequence-verified vector plasmid isolated by large-scale purification (Maxiprep, Qiagen); typically 1.5-2.0μg/mL, adjusted to 100ng/μL in sterile water
*** Reduced serum liquid growth medium with Glutamax (Invitrogen)

Mixed by pulse vortex at room temperature

3 Lipofectamine-OptiMEM I reaction mix
Unit reaction volume (100μL)*

| | |
|---|---|
| Lipofectamine reagent | 4μL |
| OptiMEM I | 96μL |

*Final volume estimate: (total number of samples to be treated + 2)× 100μL

Mixed by pulse vortex and allowed to stand at room temperature for 5 minutes

4 Final transfection mix
Unit volume of 200μL for each sample, containing a 1:1 mixture of DNA-OptiMEM I and Lipofectamine-OptiMEM I

Estimated volume of final transfection mix = [(n + 2) samples to be transfected with a given plasmid × 200μL]

Mixed by pulse vortex and allowed to stand at room temperature for 20 minutes

DNA-free transfection mix prepared in parallel by adding OptiMEM I only to the Lipofectamine-OptiMEM I mix in a 1:1 ratio

## CELL STAINING

1 1% (w/v) BSA in PBS
Prepared in a level II laminar flow hood; for a 50mL solution,

| | |
|---|---|
| BSA | 0.5g |
| Sterile PBS | to 50mL |

Mix well but gently to avoid frothing. Syringe-filter (0.22 micron) and store in 10mL aliquots at -20°C

2 Neutral buffered formalin
Prepared centrally by the Institute's core Histology services
For a 1L 3.7% solution,

| | |
|---|---|
| Formaldehyde 37% | 100mL |
| PBS | 900mL |

3 Triton X-100 0.25% in PBS
For a 10mL 1% (v/v) solution of Triton X-100 in PBS, add 100μL Triton X-100 to 10mL PBS. Vortex to mix
Add 500μL 1% Triton X-100 to 1500μL PBS to obtain a 2mL 0.25% solution of Triton X-100

4 Live cell labelling reagents
Performed in a level II laminar flow hood

A The LysoTracker Red DND-99 (Molecular Probes, Invitrogen) red-fluorescent acidotropic probe for labelling low pH organelles (excitation 575nm, emission 590nm)

For a labelling concentration of 100nM, dilute 1μL of the thawed 1mM probe stock solution in 10mL liquid growth medium (cell density $1\times10^5$ cells/mL, absolute cell count $1\times10^6$ cells)
For a labelling concentration of 500nM, dilute 2μL of the thawed 1mM probe stock solution in 4mL liquid growth medium (cell density $2.5\times10^5$ cells/mL, absolute cell count $1\times10^6$ cells)
Incubation time 45–60 minutes, 37°C/5%$CO_2$
Post-incubation, pellet cells to wash off excess unbound probe

B The BODIPY-labelled (excitation 530nm, emission 580nm) aza-epoxide class peptidyl (amino acid residues: P1 asparagine, P2 proline) cell-permeable AEP activity binding probe (Matthew Bogyo, Stanford University, CA, USA) for vital staining of mature (active) intracellular AEP
For a labelling concentration of 1μM, dilute 1μL of the thawed 1mM probe stock solution (in DMSO) in 1mL of liquid growth medium (cell density $2\times10^5$ cells/mL); final DMSO concentration at non-toxic 0.1% (v/v)
Incubation time 2 hours, 37°C/5%$CO_2$
Post-incubation, pellet cells to wash off excess unbound probe

5 Pre-immune animal sera (Vector laboratories)
Goat- and rabbit-derived pre-immune serum as blocking reagents in immunostaining
Remove aggregates (level II laminar flow hood) by syringe-filtration (0.22 micron) followed by high-speed centrifugation (16,200*g*, 5 minutes, 4°C). Store in aliquots at -20°C
Use as 10% solution (v/v) in 1% BSA (for a 1mL 10% serum solution, add 100μL serum to 900μL 1% BSA)

6 Antibodies

A Unconjugated primary antibodies (diluent, 1% BSA)

- Anti-AEP
  Goat polyclonal anti-human (AF2199, R&D Systems); 1:100 (2μg/mL)
- Anti-LAMP1 (lysosomal associated membrane protein 1, CD107a)
  Mouse monoclonal anti-human IgG1κ, clone HA-43 (product code 555798, BD Biosciences); 1:100 (5μg/mL)

B Fluorophore-conjugated secondary antibodies (diluent, 1%BSA)
Short centrifuge to pellet suspended aggregates before use

Alexa Fluor 488 (Excitation 495nm, Emission 519nm) conjugated secondary antibodies (Molecular Probes, Invitrogen), 1:1000 dilution (2μg/mL)

- Rabbit anti-goat IgG $F(ab')_2$ (A21222) cross-adsorbed against human and mouse serum proteins to minimise cross-reactivity

- Goat anti-mouse IgG (A11029), highly cross-adsorbed against bovine, goat, rabbit and human IgG as well as human serum

7 May-Grünwald Giemsa staining

A Sørenson buffer
Buffer of monobasic and dibasic phosphate salts

For a 100mL, 20×, 0.67M solution of monobasic phosphate solution
Potassium dihydrogen phosphate 9.1g
Deionised water to 100mL

For a 100ml, 20×, 0.67M solution of dibasic phosphate solution
Disodium hydrogen phosphate 9.5g (anhydrous)
Deionised water to 100mL

For a 200mL, 1×, 0.033M solution of Sørenson buffer
Monobasic phosphate solution, 20× 10.2mL
Dibasic phosphate solution, 20× 9.8mL
Deionised water to 200mL

Adjust pH to 6.8 with 5N hydrochloric acid

B May-Grünwald staining solution
Diluted 1 in 2; for a 40mL staining solution in a Coplin jar,

| | |
|---|---|
| May-Grünwald reagent | 20mL |
| Sørenson buffer, 1× | 20mL |
| Staining time | 20 minutes |

C Giemsa staining solution
Diluted 1 in 10; for a 40mL staining solution in a Coplin jar,

| | |
|---|---|
| Giemsa reagent | 4 mL |
| Sørenson buffer, 1× | 36mL |
| Staining time | 30 minutes |

8 Mounting medium with DAPI
DAPI 1mg/mL stock solution prepared in a level II laminar flow hood by diluting dried powder (10mg, Roche) in 10mL sterile deionised water

For a 1μg/mL solution of DAPI in fluorescent mounting medium

| | |
|---|---|
| Fluorescent mounting medium* | 1mL |
| DAPI 1mg/mL | 1μL |

* Product code S3023, Dako

Vortex briefly to mix; stored light-protected at 4°C

9 Filamentous actin (F-actin) staining
Stock solution of far red fluorescent Alexa Fluor 647-conjugated phalloidin in methanol (200 units/mL; -20°C storage; Invitrogen). Pulse-centrifuge to sediment protein aggregates before use.

Use 250μL of diluted conjugated phalloidin (1:50 dilution, 5μL stock solution to 200μL 1%BSA) for each coverslip sample staining. Incubate light-protected for 20 minutes at room temperature followed by two 5-minute PBS washes

10 Fibronectin coating of cover slips
Stock solution (1 mg/mL) diluted 1 in 10 with sterile PBS for a 10μg/mL solution. Aliquots stored at -20°C.
Acid-alcohol (absolute ethanol: concentrated hydrochloric acid 9:1) sterilised glass coverslips were placed in a petri dish and coated with 10μg/mL fibronectin. Following incubation for 30-45 minutes at 37°C, excess fibronectin was removed with PBS washes. Coated coverslips were used immediately in experiments.

## MOTILITY ASSAYS

1 Matrigel (BD Biosciences), 8-10mg/mL (batch-dependent), 10mL
Extracellular matrix secreted by the murine Engelbroth-Holm-Swarm sarcoma cell line
Chief components
- Laminin, collagen IV and entactin (nidogen)
- Heparan sulphate proteoglycan
- Growth factors – transforming growth factor beta, insulin-like growth factor, epidermal growth factor, fibroblast growth factor, tissue plasminogen activator

Does not contain fibronectin

Stored frozen (-20°C), thawed strictly on ice, 1mL aliquots created in level II laminar flow hood using pre-chilled pipettes, aliquots stored at -80°C
For 1:50 working dilution, ice-thawed 1mL aliquot diluted in chilled 49mL serum-free DMEM (0.15-0.2mg/mL, Matrigel membrane coating); 3mL aliquots stored at -80°C (in level II laminar flow hood)

For invasion assays, 100μL 1:50 diluted ice-thawed Matrigel allowed to uniformly coat bottom of 8-micron pore inserts overnight in a level II laminar flow hood. When coating, ensure level dispensing and avoid air bubbles (by setting dispensing volumes to 102μL and avoiding purge-dispensing). Before use, rehydrate Matrigel coating by adding chilled serum-free DMEM (250μL per insert) to inserts; incubate at 4°C for 2 hours

2 Mifepristone (Invitrogen)
For induction of AEP expression in the GeneSwitch dual plasmid inducible expression system in stably transfected HEK293 cells

<u>Reconstitution (in a level II laminar flow hood)</u>
For a 1mM stock solution, 100μg of mifepristone (429.6g/mol) in 233μL absolute ethanol; 110μL aliquots stored at -20°C, caps parafilm-wrapped to minimise evaporation losses

For a 10μM working solution, 100μL 1mM mifepristone in 10mL absolute ethanol; 1mL aliquots, paraffin-wrapped caps, -20°C

<u>For induction of AEP expression</u>
To 10mL of cells in growth medium, add 10μL 10μM mifepristone solution to obtain a final mifepristone concentration of 10nM
Incubate for 24 hours for maximal induction of expression

3 Crystal violet solution (0.1%) for staining of cell inserts

Stock solution (2.3% crystal violet in 20% ethanol) diluted 1 in 20 (1mL to 19mL deionised water)
Inner contents of inserts removed by pipette aspiration and cotton bud swabbing and inserts fixed by placing in methanol (15 minutes) followed by staining in 0.1% crystal violet for 15 minutes
Excess stain removed by washing twice in distilled water followed by drying
As inserts are unlabelled, care is necessary when staining; adhere to a standard multi-well plate template when handling inserts during staining

4 Isotonic diluent fluid (Isoton, Beckman Coulter) for suspending cells towards counts on the particle counter

## IMMUNOHISTOCHEMISTRY

1 Tris-EDTA heat antigen retrieval buffer

| | |
|---|---|
| Tris-Base, 10mM | 1.21g |
| Disodium EDTA, 1mM | 0.37g |
| Water | to 1L |
| Tween-20 | 0.5mL to 1L (0.05% v/v) |

2 Citrate heat antigen retrieval buffer
100mM 10× Citrate stock buffer, 500mL

| | |
|---|---|
| Trisodium citrate | 10.51g |
| Deionised water | to 500mL |

pH adjusted to 6.0

Working solution: 1 in 10 dilution of 10× stock in deionised water

3 Methanol-peroxide solution
Methanol 9 parts; 3% Hydrogen Peroxide 1 part

4 Avidin-biotin blocking solution (Vector laboratories)

| | |
|---|---|
| Avidin blocking solution | 4 drops to 1mL PBS |
| Biotin blocking solution | 4 drops to 1mL PBS |
| PBS-Tween 0.05% | 250μL Tween 20 to 500mL PBS |

5 1% BSA-Azide solution

| | |
|---|---|
| Bovine serum albumin | 2.0g |
| Sodium azide | 0.2g |
| PBS | to 200mL |

6 Antibody solutions in 1% BSA-azide (PBS in the case of dual staining)

| | |
|---|---|
| Primary antibody | Anti-AEP, 1:300<br>Goat polyclonal anti-human, R&D (AF2199) |
| | Anti-human CD68; undiluted<br>Mouse monoclonal PG-M1, Dako |

| | |
|---|---|
| Secondary antibody | Biotinylated rabbit anti-goat, 1:250<br>(Vector laboratories, BA-5000) |
| Fluorescent secondary antibodies | TRITC-conjugated rabbit anti-mouse IgG<br>(Excitation 550nm/emission 570nm)<br>1:15, Dako R 0270 |
| | Alexa Fluor 488 conjugated rabbit anti-goat IgG<br>(Invitrogen) |

7 Avidin-biotin enzyme amplification solution (Vector laboratories)
Avidin DH 20μL and Biotinylated HRP 20μL to 1mL PBS
Freshly prepared, allow to stand (not > 30 minutes), then apply

8 Diaminobenzidine (DAB) reagent (Kem-En-Tec Diagnostics A/S, Denmark)

| | |
|---|---|
| DAB | 1 tablet |
| Deionised water | 10mL |

3% hydrogen peroxide 100μL to 10mL DAB solution
Freshly prepared, incubate 15 minutes at room temperature before use

9 DPX (Distyrene Plasticiser Xylene) mounting medium

## Section 8.3 Selected Methods Outline

- Mononuclear cell isolation from bone marrow/peripheral blood
- Plasmid DNA isolation
- RNA isolation (TRIzol isolation protocol)
- Ethanol-ammonium acetate double precipitation for ultra-pure RNA yields
- Preparation of whole-cell protein lysates
- Stripping of protein immunoblot membranes
- Cryopreservation and thawing of cells
- Trypsin mobilisation of adherent cells
- AEP immunohistochemistry work flow

BONE MARROW / PERIPHERAL BLOOD MONONUCLEAR CELL ISOLATION

| | |
|---|---|
| Note | • Immediate processing<br>• Interim hold at room temperature<br>• Class II laminar flow hood<br>• Sterile filter pipette tips<br>• Phenol waste disposal<br>• Biohazardous waste disposal |
| Density separation medium (Lymphoprep, Axis Shield) | • Sample diluted 1:1 with PBS, layered on density-separation medium (volume ratios of sample and separation medium, 1:2)<br>• Centrifuge, 400*g*, room temperature, 25 minutes, slow acceleration, no deceleration brake |
| Mononuclear cells | Mononuclear cell layer interphase identified and isolated; PBS wash (300*g*, room temperature, 10 minutes) to remove residual separation medium |
| Cell count | Resulting cell pellet resuspended in PBS; aliquot removed for haemocytometer cell count (by Trypan blue exclusion, to additionally assess viability). Subsequent second wash step (300*g*, room temperature, 10 minutes) |
| Cell lysis and storage | Based on mononuclear cell counts<br>• If $\leq 10\times10^6$, cells lysed directly in TRIzol (complete lysis ensured by pulse vortex )<br>• If $>10\times10^6$, TRIzol lysis of $10\times10^6$ cells; remainder cells in cryoprotectant for liquid nitrogen storage |

## PLASMID DNA ISOLATION (HIGH COPY NUMBER PLASMID)

Small-scale isolation (Wizard Plus SV Miniprep kit, Promega)

| | |
|---|---|
| Precaution | • Dedicated cloning work station<br>• Biohazardous waste disposal |
| Bacterial cell pellet | 2mL overnight liquid culture (12-14h), 10 000*g*, 5 minutes, room temperature; decant supernatant |
| Bacterial cell resuspension | Cell resuspension solution, 250μL, mix well |
| Cell lysis | Cell lysis solution, 250μL, mix well (no vortex); incubate 1-5 minutes, room temperature for solution clearance |
| Endogenous endonuclease inactivation | Alkaline protease solution, 10μL, mix well (no vortex), incubate room temperature, 1-5 minutes (avoid exceeding 5 minutes) |
| Precipitation of bacterial nuclear DNA and proteins | • Neutralisation solution, 350μL, mix well by inversion (no vortex)<br>• Centrifuge, 14 000*g*, 10 minutes, room temperature |
| Column plasmid DNA binding | Lysate (~850μL) to spin column in 2mL collecting tubes; centrifuge 15 000*g* 1 minute, room temperature |
| Column wash | • Column wash solution, 750μL; centrifuge at room temperature 15 000*g*, 1 minute<br>• Discard flow-through; repeat column wash with 250μL wash solution and repeat centrifuge at 15 000*g*, 1 minute |
| Plasmid DNA elution | • Discard flow through, centrifuge spin column at 15 000*g*, 1 minute to collect residual wash solution<br>• Spin column to fresh 1.5mL microcentrifuge tube, 75-100μL nuclease-free water, centrifuge 15 000*g*, room temperature, 1 minute |
| Quantitation | Spectrophotometry; $A_{260/280}$ should exceed 1.8 |

Large-scale isolation (Maxiprep, endonuclease-free, Qiagen)

| | |
|---|---|
| Precaution | • Dedicated cloning work station<br>• Biohazardous waste disposal<br>• Check buffer P2 for SDS precipitation<br>• Retain supernatant from isopropanol precipitation and ethanol wash until |

| | |
|---|---|
| | plasmid DNA isolation confirmed |
| Liquid bacterial culture | Agitated culture (12-16 hours), 37°C, 5mL overnight starter inoculate in 100mL volume with appropriate selection antibiotic, 1L sterile Erlenmeyer flask |
| Bacterial stocks | Glycerol storage vials of transformed cells |
| Bacterial cell harvest and lysis | • Balanced volumes (weights) in 250mL plasmid centrifuge tubes<br>• Pellet bacterial cells - centrifuge 6 000*g*, 15 minutes, 4°C<br>• Decant supernatant, resuspend cells in 10mL buffer resuspension buffer P1 (with RNase A)<br>• Add lysis buffer P2, mix well by inversion, incubate at room temperature (do not exceed 5 minutes)<br>• Add neutralization buffer P3, mix well by inversion, incubate on ice, 20 minutes (LyseBlue to indicate adequacy of mixing) |
| Bacterial lysate clarification | • Centrifuge, ≥ 20 000*g* (15 000 rpm, Sorvall), 4°C, 30 minutes<br>• Carefully isolate supernatant |
| Plasmid DNA binding and wash | • Equilibrate resin column (Qiagen-tip 500) by applying buffer QBT, 10mL; allow to flow through by gravity into Erlenmeyer flask<br>• Apply supernatant to column (place a sterile gauze pad over mouth of column) and allow to flow through by gravity<br>• Wash column twice with buffer QC, 30mL; allow flow-through by gravity |
| Plasmid DNA elution | • Resin column to 30mL plasmid centrifuge tubes<br>• Buffer QF, 15mL, to elute bound DNA |
| DNA precipitation | • Isopropanol, 10.5mL (0.7 volume) to eluate, mix immediately, centrifuge (mark tube to indicate pellet deposit) ≥ 15 000*g*, 4°C, 30 minutes<br>• Identify precipitate, carefully aspirate supernatant; retain supernatant until satisfactory DNA isolation confirmed |
| DNA pellet wash | • Ethanol 70%, 1mL; transfer to 1.5mL microcentrifuge tube; centrifuge maximum speed, 4°C, 10 minutes<br>• Carefully pipette-remove supernatant |

| | |
|---|---|
| Reconstitution | Air-dry pellet (avoid over-drying) and resuspend in 100μL sterile Tris-EDTA buffer or deionised water (pipette-mix) |
| Quantitation | Spectrophotometry; $A_{260/280}$ should exceed 1.8 |

RNA ISOLATION (TRIZOL RNA ISOLATION PROTOCOL)

| | |
|---|---|
| Precaution | • Class II laminar flow hood<br>• Sterile filter pipette tips<br>• Phenol waste disposal<br>• Retain supernatant in all steps until satisfactory RNA isolation confirmed |
| Phase separation | • Chloroform 200μL to 1mL TRIzol lysate<br>• Mix vigorously, 15 seconds; incubate at room temperature for 5 minutes<br>• Centrifuge, 12 000*g*, 4°C, 15 minutes |
| Aqueous phase isolation | Carefully transfer upper aqueous phase to a fresh 1.5mL microcentrifuge, taking care not to disturb the interphase (volume 380-400μL) |
| RNA precipitation | • To the aqueous phase, add 500μL Isopropanol<br>• Mix well and incubate, either at room temperature for 10 minutes or overnight (12-16 hours) at 4°C<br>• Centrifuge, 10 000*g*, 4°C, 10 minutes<br>• Identify streaky white RNA pellet (base and sides of tube) |
| RNA wash | • To pellet, add 1mL 75% ethanol<br>• Centrifuge, 10 000*g*, 4°C, 10 minutes |
| RNA pellet reconstitution | • Air-dry RNA pellet until translucent; avoid overdrying<br>• Dissolve pellet in DEPC-treated water (volume estimated based on pellet size, between 10-30μL); mix by pipetting<br>• Set aside 2-5μL aliquot for spectrophotometric quantitation |
| Quantitation | $A_{260/280}$ ratio should exceed 1.8 |

## ETHANOL-AMMONIUM ACETATE DOUBLE PRECIPITATION OF RNA

| | |
|---|---|
| Objective | Isolation of high-purity RNA post-TRIzol RNA extraction |
| Precaution | • Class II laminar flow hood, filter pipette tips<br>• Retain supernatant in all steps until satisfactory RNA isolation confirmed |
| RNA precipitation | • To RNA isolate, add 0.5 volume 7.5M ammonium acetate and 2.5 volume absolute ethanol<br>• Incubate, -20°C, overnight (12-16 hours)<br>• Centrifuge, 16 000*g*, 4°C, 30 minutes |
| RNA wash | • Wash × 2, 80% chilled ethanol, 500μL<br>• Centrifuge, 16 000*g*, 4°C, 10 minutes |
| RNA reconstitution | • Air-dry RNA pellet and dissolve pellet in appropriate volume of DEPC-treated water; mix by pipetting<br>• Set aside 2-5μL aliquot for spectrophotometric quantitation |
| Quantitation | $A_{260/280}$ ratio should exceed 1.8 |

## PREPARATION OF WHOLE-CELL PROTEIN LYSATES

| | |
|---|---|
| Precaution | In Class II laminar flow hood; biohazardous waste disposal |
| Cell pellet | • Cell line or primary cell pellets in 1.5mL microcentrifuge tubes, washed twice with sterile PBS<br>• Centrifuge setting/wash cycle: 300*g*, room temperature, 5 minutes |
| Cell lysis | • In NP-40 or citrate lysis buffer; 150-200μL for every 10 million cells<br>• Incubate on ice, 15 minutes |
| Clarification | High-speed centrifugation (16 200g), 4°C, 15 minutes; isolate supernatant |
| Quantitation | Five microliter aliquots set aside for quantitation of total protein content using a modified Lowry assay; the remainder stored as 25-100μL aliquots (-80°C) |
| Immunoblotting | Volume equivalent to 25-30μg/10-15μL sample loading buffer (1×) / well. Boiled (95°C, 5 minutes) before gel loading |

## STRIPPING AND RE-PROBING OF PROTEIN IMMUNOBLOT MEMBRANES

| | |
|---|---|
| Note | Membranes awaiting stripping may be placed in PBS for up to 3 weeks at 4°C |
| Membrane stripping | Place membrane in proprietary Restore stripping buffer (20mL/membrane), 30 minutes, room temperature |
| Wash | PBS, 2 washes, 5 minute / wash |
| Blocking | 5% (w/v) non-fat milk solution, 1 hour, room temperature |
| Antibody probing | As with standard immunoblotting |

## CRYOPRESERVATION AND THAWING OF CELLS

Cryopreservation of cells

| | |
|---|---|
| Note | • In Class II laminar flow hood; biohazardous waste disposal<br>• Cryofreezing container at room temperature, with fresh (< 5 freeze-thaw cycles) isopropanol<br>• Thawed cryoprotectant solution, maintained chilled on ice |
| Cell suspension | Viable cells > 90%, early passage for cell lines (<10), known cell count, pelleted by centrifugation at 300*g*, room temperature, 5 minutes; discard supernatant and disperse pellet in residual |
| Cryoprotectant volume | Estimate 1.0mL cryoprotectant for 10-30 million cells / cryovial |
| Adding cryoprotectant | • Add along sides of tube, initially 1 drop every 10 seconds with continuous mixing; steadily accelerate drop rate after every 10 drops until required volume dispensed<br>• Dispense 1.0mL/cryovial |
| Storage | • In cryofreezing container, -80°C for 12-16 hours<br>• Subsequently, to liquid phase of liquid nitrogen vessel; record storage details |

Thawing of cryopreserved cells

| | |
|---|---|
| Note | • In Class II laminar flow hood; biohazardous waste disposal<br>• Cryovial maintained on dry ice until time of rapid thaw<br>• Risk of contamination during rapid thaw of cryovial in circulating water bath; ensure cryovial placed in water bath above level of O-ring and ethanol-spray (70%) outer walls of vial before opening |
| Rapid thaw | Water bath, 37°C, until tiny frozen residual |
| Slow resuscitation | • Transfer vial contents to a 15mL conical centrifuge tube<br>• Add pre-warmed sterile complete growth medium in drops along sides of tube, while gently mixing. Add a drop every 10 seconds and accelerate drop-rate after every 10 drops until 2.5mL; bring volume to 10mL by dripping complete growth medium along sides of tube |
| Washes | • Pellet cells by centrifugation (300*g*, room temperature, 5 minutes)<br>• Pipette-aspirate supernatant and discard<br>• Disperse pellet and resuspend in fresh complete growth medium, 10mL; re-pellet by centrifugation (300*g*, room temperature, 5 minutes) |
| Cell suspension | Resuspend cell pellet in complete growth medium (10mL) following 2$^{nd}$ wash. Cells are now suitable for downstream applications (estimate cell counts and viability before use) or may be maintained in cell culture (10mL volume in a 25cm$^2$ cell culture flask) |

TRYPSIN MOBILISATION OF ADHERENT CELLS

| | |
|---|---|
| Note | Adherent cells mobilised at a cell confluence of ~75% |
| Removal of spent medium | • Pipette-aspirate and discard spent medium without disturbing adherent cell monolayer<br>• Gently layer with warmed PBS (10mL/75cm$^2$ flask); aspirate-discard to remove residual growth medium |

| | |
|---|---|
| Trypsin-EDTA treatment | • Add 0.5% Trypsin-EDTA<br>• 2-5 minutes, 37°C/5% $CO_2$ |
| Neutralise Trypsin | Add equivalent volume of complete growth medium to neutralise Trypsin activity (for motility assays, use DMEM with 1% FBS) |
| Wash cells | Pellet cells by centrifugation, 300g, room temperature, 5 minutes; pipette-discard supernatant and disperse cell pellet |
| Resuspend cells | Reconstitute cells in fresh growth medium (with or without FBS, as the case may be) |

IMMUNOHISTOCHEMISTRY WORK FLOW

| | |
|---|---|
| Deparaffinise and rehydrate sections | • Melt wax (60°C, 20 minutes)<br>• Xylene immersions (5 minutes × 2)<br>• Immersion in serially decreasing dilutions of ethanol (100%, 80%, 50%, 5 minutes, × 2 immersions / dilution) |
| Heat-induced epitope retrieval | Tissue sections pressure-heated to 125°C in Tris-EDTA buffer for 10 minutes, then rapidly cooled in tap water (2 minutes) |
| Endogenous peroxidase and biotin quenching | • Methanol-peroxidase, 10 minutes<br>• Tap water wash<br>• Avidin blocking solution, 20 minutes<br>• PBS wash<br>• Biotin blocking solution, 20 minutes<br>• Tap water wash |
| Primary antibody layer | • 40 minutes, room temperature<br>• 1-minute PBS-Tween washes × 2<br>• Negative controls, PBS only |
| Secondary antibody layer | • 30 minutes, room temperature<br>• 1-minute PBS-Tween washes × 2 |
| Detection amplification | • Avidin-biotin complex, 20 minutes<br>• 1-minute PBS-Tween washes × 2 |
| Substrate chromogen | • DAB solution, 10 minutes, monitor browning<br>• Tap water rinse |
| Haematoxylin counterstain | • Haematoxylin 5 minutes<br>• 0.3% acid-alcohol differentiation<br>• Running water, 5 minutes, for blueing |
| Dehydration and mounting | • Dehydration in increasing concentrations of ethanol, then Xylene<br>• DPX mounting and automated coverslipping |

Dual Immunohistofluorescence staining (AEP and CD68)

| | |
|---|---|
| Deparaffinise and rehydrate sections | Tissue sections deparaffinised in CitroClear (a limolene-based xylene substitute) and serially rehydrated in decreasing strength alcohols (100%, 50%, 30%); 2 immersions each, 3 minutes per immersion |
| Heat-induced antigen retrieval | Slide sections in Tris-EDTA buffer, pressure-heated to 125°C, 2 minutes, slow cool to 85°C, then rapid cool in running tap water |
| Dual primary antibody staining | Goat polyclonal anti-AEP (1:300) and mouse monoclonal anti-CD68 (PG-M1, undiluted) in PBS; 125μL/slide section, room temperature, 45 minutes (covered) |
| Washes | PBS, 1 minute/wash × 2 |
| Secondary antibody staining | Rabbit-derived secondaries; TRITC anti-mouse and Alexa Fluor 488 anti-goat immunoglobulins; 45 minutes, covered, light-protected, room temperature |
| Washes | PBS, 1 minute/wash × 2 |
| DAPI nuclear counterstain and mounting | DAPI in fluorescent mounting medium (1:1000), 100μL/tissue section, coverslipped, in slide tray with aluminium foil wrap; 4°C storage until imaging |

## Section 8.4 Selected protocol worksheets

### FIRST STRAND CDNA SYNTHESIS

*Step 1*: Prepare RNA solution at 500ng/μL in 0.2mL PCR tubes

| Sample ID | Sample details | RNA ng/μL | Dilution factor | Volume for 500ng (μL) | Water to 10.5μL |
|---|---|---|---|---|---|
| | | | | | |

Add random primer 1.5μL (150ng) to each tube

*Step 2*: 42°C, 5 minutes; samples immediately to ice

*Step 3*: Prepare reverse transcriptase (RTase) master mix

| | 1× | (No. of samples+2)× |
|---|---|---|
| dNTP 2.5mM | 10μL | |
| RTase Buffer, 5× | 6μL | |
| M-MLV RTase 400U | 2μL | |
| Total | 18μL | |

Pulse-vortex to mix, spin to collect; dispense 18μL mastermix to each tube

*Step 4*: 42°C for 60 minutes, 95°C for 5 minutes

*Step 5*: Add RNase H 2μL (2U) to each tube; 42°C for 20 minutes

*Step 6*: Prepare cDNA samples for 384-well plate loading
Dilute 10.5μL sample cDNA in 102.5μL sterile water; vortex to mix
Include 1 tube as 'No Template' control (NTC, 112.5μL water)

### RQ-PCR REACTION MIX

Reaction mix for each transcript, estimated for 'n' samples on a 384-well plate

| | 1× | [(n+2)*4]× |
|---|---|---|
| RQ-PCR mastermix, 2× | 5.0μL | |
| Taqman probe-primer mix, 20× | 0.5μL | |
| Total | 5.5μL | |

Pulse-vortex, spin to collect, maintain at 4°C until loaded to plate

### PLATE LAYOUT FOR AUTOMATED PIPETTING OF RQ-PCR REACTION MIX

For 2 transcripts and 'n' samples ($n_1$…, including NTC) on a 384-well plate

For each sample, 4.1μL cDNA loaded/well across rows

For each transcript, 5.5μL RQ-PCR reaction mixes loaded/well along columns

| Sample | AEP | | | β2M | | |
|---|---|---|---|---|---|---|
| | Column 1 | Column 2 | Column 3 | Column 4 | Column 5 | Column 6 |
| | | | | | | |

## LIPID TRANSFECTION OF ADHERENT CELLS

Check cell confluence (~80% confluence, 0.5-2×$10^5$ cells in 1mL complete growth medium [12-well plate format])

For a 12-well plate

*Step 1*: Plasmid solution at 100ng/μL

| Plasmid | ng/μL | Volume for 5μg | Water to 50μL |
|---|---|---|---|
| | | | |
| | | | |

*Step 2*: Prepare DNA-OptiMEM I mix

For each plasmid DNA

| | 1× | (No. of wells+2)× |
|---|---|---|
| DNA 100ng/μL | 10μL | |
| OptiMEM I | 90μL | |
| Total | 100μL | |

Pulse-vortex to mix, short spin to collect and stand at room temperature

*Step 3*: Prepare Lipofectamine-OptiMEM I mix

| | 1× | (No. of wells+2)× |
|---|---|---|
| Lipofectamine 2000 | 4μL | |
| OptiMEM 1 | 96μL | |
| Total | 100μL | |

Pulse-vortex to mix, short spin to collect; stand at room temperature for 5 min

*Step 4*: Prepare DNA-OptiMEM I/Lipofectamine-OptiMEM I mix

For each plasmid DNA

| | 1× | (No. of wells+1)× |
|---|---|---|
| DNA-OptiMEM I | 100μL | |
| Lipid-OptiMEM I | 100μL | |
| Volume/well | 200μL | |

For untransfected control cells

| | 1× | (No. of wells+1)× |
|---|---|---|
| OptiMEM I only | 100μL | |
| Lipid-OptiMEM I | 100μL | |
| Volume/well | 200μL | |

Pulse-vortex to mix, short spin to collect; stand at room temperature, 20 min
Dispense 200μL of Step 4 mix to respective wells

Confirm successful transfection after 48 hours. If required, replace growth medium after 24 hours.

## PROTEIN QUANTITATION ASSAY

*Step 1*: Prepare BSA standards using the BSA stock solution (5mg/mL)

Prepare a 50μL volume of each standard (except a 100μL volume for the 100μg/mL standard to account for small-volume pipetting errors)

*Step 2:*

| Standards ID | BSA (μg/mL) | Volume of BSA stock (μL) | Volume of lysis buffer (μL) |
|---|---|---|---|
| S1 | 0 | 0 | 50 |
| S2 | 100 | 2 | 98 |
| S3 | 200 | 2 | 48 |
| S4 | 400 | 4 | 46 |
| S5 | 800 | 8 | 42 |
| S6 | 1200 | 12 | 38 |
| S7 | 1600 | 16 | 34 |
| S8 | 2000 | 20 | 30 |
| | | 64μL total | 386μL total |

Prepare appropriate dilutions (1 in 5 or 1 in 10) of test samples in lysis buffer

*Step 3*: Dispense 5μL BSA standard in duplicate in a 96-well flat-bottomed plate (BD Falcon) followed by 2-5μL of test samples (X1…, duplicates if available) (plate layout below)

| | | | | | | | | | | | |
|---|---|---|---|---|---|---|---|---|---|---|---|
| S1 | S1 | X1 | X1 | | | | | | | | |
| S2 | S2 | X2 | X2 | | | | | | | | |
| S3 | S3 | | | | | | | | | | |
| S4 | S4 | | | | | | | | | | |
| S5 | S5 | | | | | | | | | | |
| S6 | S6 | | | | | | | | | | |
| S7 | S7 | | | | | | | | | | |
| S8 | S8 | | | | | | | | | | |

*Step 4*: Reagent A'
Prepare Reagent A' (To 1mL Biorad DC assay reagent A, add 20μL Reagent S; mix). Add 25μL to each well and mix (avoid frothing)

*Step 5*: Biorad DC assay reagent B
Add 200μL to each well

Step *6*: Incubate for 15 minutes, covered, at room temperature

Step *7*: Read end-point absorbance at 690nm (650-750nm reading range); ensure nil air bubbles before reading

Step 8: Estimate volume of whole-cell lysate required for immunoblotting experiments

E.g.: For a whole cell lysate X required to load a well each in two gels,

(a) First, calculate total protein content of whole cell lysate by reading off from the BSA standard curve after appropriate corrections for sample dilution.

(b) Then for a 3mg/mL (as an example) total protein content, volume required for a well each in 2 gels at 25μg total protein/ 15μL/ well/gel

| Sample lysate | Volume for 75μg total protein (μL) | Volume of 5 × loading buffer (μL) | Volume of lysis buffer to 45μL |
|---|---|---|---|
| X (3mg/mL) | 25 | 9 | 11 |

## AEP ACTIVITY ASSAY

*Step 1*: Prepare working dilutions of reagents

1. Assay Reagent

   Prepare 10mL 1× assay reagent using deionised water

   Add 20μL 0.5M DTT (effectively, 1mM DTT)
   Add 10μL 10% CHAPS (effectively, 0.01% CHAPS)

2. Prepare 7-NHMeC standards (S1 to S8)

   Dilute 5μL stock solution in 45μL DMSO for a 2mM 7-NHMec solution
   25μL 2mM 7-NHMec + 175μL assay buffer = 250μM 7-NHMeC, 200μL
   S1 5μL 250μM 7-NHMeC + 495μL assay buffer = 2.5μM 7-NHMeC
   S2 5μL 250μM 7-AMC + 620μL assay buffer = 2.0μM 7-NHMeC
   S3 250μL S1 + 250μL assay buffer = 1.25μM 7-NHMeC
   S4 250μL S3 + 250μL assay buffer = 0.625μM 7-NHMeC
   S5 250μL S4 + 250μL assay buffer = 0.3125μM 7-NHMeC
   S6 250μL S5 + 250μL assay buffer = 0.15625μM 7-NHMeC
   S7 250μL S6 + 250μL assay buffer = 0.078125μM 7-NHMeC
   S8 250μL assay buffer only

3. Prepare working dilution of AEP synthetic fluorogenic peptide substrate
   Add 10μL Z-Ala-Ala-Asn-NHMeC to 5mL deionised water (effectively, 20μM)

4. Prepare whole cell lysates (citrate lysis buffer) in assay reagent
   For each lysate, estimate for 5 wells at 20μg total protein/50μL assay reagent/well

| ID | Sample | Protein μg/μL | Volume for 100μg (μL) | Assay buffer to 250μL |
|---|---|---|---|---|
| | | | | |
| | | | | |

5. The AEP inhibitor MV026630 (AEPi)
   Prepare a 1mM AEPi solution in assay reagent (1 in 10 dilution of stock)
   Prepare a 50μM AEPi solution in assay reagent from the 1mM working solution; volume estimated as [(no. of samples + 2) × 2] × 25μL

*Step 2*: Add reagents to 96-well plate
Order of adding reagents (plate layout below)

- Add 25μL 50μM AEPi solution to wells (in e.g., A5-F5; A6-F6)
- Add 25μL assay buffer to all other wells
- Add 50μL lysates to wells in duplicates for each condition [in e.g., X1-X6 without AEPi and X1i-X6i with AEPi]
- Add 50μL standards S1-S6 in duplicates to wells as below
- To all wells, add 25μL substrate solution

| | 1 | 2 | 3 | 4 | 5 | 6 | 7 | 8 | 9 | 10 | 11 | 12 |
|---|---|---|---|---|---|---|---|---|---|---|---|---|
| A | S1 | S1 | X1 | X1 | X1i | X1i | | | | | | |
| B | S2 | S2 | X2 | X2 | X2i | X2i | | | | | | |
| C | S3 | S3 | X3 | X3 | X3i | X3i | | | | | | |
| D | S4 | S4 | X4 | X4 | X4i | X4i | | | | | | |
| E | S5 | S5 | X5 | X5 | X5i | X5i | | | | | | |
| F | S6 | S6 | X6 | X6 | X6i | X6i | | | | | | |
| G | S7 | S7 | | | | | | | | | | |
| H | S8 | S8 | | | | | | | | | | |

*Step 3*: Incubate (covered) at 37°C for 30 minutes.

*Step 4*: Ensure nil air bubbles; ensure constant gain setting and read end-point fluorescence (excitation 360nm, emission 460nm)

*Step 5*: Subtract averaged X*n*i well fluorescence readouts from readouts in X*n* wells to derive activity-specific fluorescence

Express activity as ‘fluorescent units/μg total protein/30 minutes’

## Section 8.5 Optimisation-validation exercises in experimental protocols

- Estimation of AEP transcript expression (qRT-PCR)
- Cathepsin B immunoblotting
- Immunostaining controls
- Immunohistochemistry controls
- Enforced and inducible AEP-expressing HEK293 cells
- Boyden chamber motility assays
- Cell culture supernatants and AEP immunoblotting

---

### Estimation of AEP transcript expression (qRT-PCR)

1. This was a two-step approach, i.e. reverse transcription, followed by real-time quantitation using on-demand TaqMan probe-primer reagents
2. Relative normalized AEP transcript expression was determined using the comparative cycle threshold (Ct) method ($2^{-\Delta\Delta Ct}$).
3. Suitability of choice of β2-microglobulin (β2M) as reference transcript was established from global gene-expression microarray analyses of primary leukaemic cells (**Table 8.1**, **Figure 8.1**). Other candidate transcripts examined included β-glucuronidase (GUS), β-actin (ACTB), Glyceraldehyde-3-phosphate dehydrogenase (GAPDH) and Abelson murine leukaemia viral oncogene homolog-1 (ABL1). Of the candidates examined, expression of β2M was both physiological (i.e. near-normal distribution) and minimally variable (as determined by the coefficient of variation), making it an appropriate reference transcript.
4. Validation of suitability of applying the $2^{-\Delta\Delta Ct}$ method for relative normalised AEP transcript estimation was established by step-wise determination of the following parameters [1]
    - Dynamic linear amplification characteristics of AEP and β2M transcripts
    - Equivalence and acceptability of amplification efficiencies for both transcripts

- Appropriate working range of input RNA

5. Amplification efficiencies of AEP and β2M transcripts were appropriately equivalent (AEP 1.03, β2M, 0.98; 384-well format) and dynamically linear over a wide range of input RNA (spanning a 64-fold dilution from 31.25ng to 2.0μg), with a working range of 0.125-2.0μg input RNA as most suitable (difference in AEP and β2M transcript Ct values were best maintained over these dilutions) (**Figure 8.2**)
6. As assay protocols were previously established on 96-well reaction plates, assessment of the equivalence of 96-well and 384-well assay formats was also performed; results were comparable (**Tables 8.2 and 8.3**)
7. Assay precision was satisfactory; this was based on inter-assay estimation of normalised AEP transcript expression of the calibrator (HRC57 cell line) using RNA as starting material (**Table 8.4**)

---

Cathepsin B immunoblotting

1. Autoactivation of the inactive zymogen (44-46kDa, depending on glycosylation) to the mature 31-33kDa single-chain enzyme is triggered by increasing acidification of the maturing endosome; further transition to the 2-chain form (24-27kDa heavy chain, 5kDa light chain,) is mediated by other lysosomal proteases (e.g. AEP) [2, 3] (**Figure 8.3**).

2. The following antibodies to human Cathepsin B (CTSB) were investigated:
   a) three rabbit polyclonal antibody preparations, including two from Merck Biosciences (product codes 219408 and PC41) and one from Enzo Life Sciences (Biomol SA-361)
   b) two mouse monoclonal antibodies, including an IgG2a isotype preparation from Merck Biosciences (clone CA-10) and an IgG1 isotype preparation (clone 155714) from R&D Systems.
3. All antibodies were tested for ability to detect CTSB in whole cell lysate immunoblots from known positive human cell line controls (K562 and HeLa cell lines). Selected antibodies were also examined for ability to detect

inactive and single-chain mature forms of purified recombinant protein (recombinant human CTSB activated in 2-(-N-morpholino)ethanesulphonic acid buffer, pH 5.0).

4. Among the polyclonal preparations, Biomol SA-361 was the most satisfactory (**Figure 8.4C**). Detection bands were crisp and distinct. The antibody consistently detected the heavy-chain (H-chain) component of the 2-chain active protease in whole cell lysates. Sensitivity was retained over dilutions (1:5000 to 1:20 000) (**Figure 8.4B**) and was enhanced with use of an HRP-conjugated secondary antibody from Dako. Antibody incubation times were empirical. The antibody detected both precursor and single-chain mature forms of CTSB in an activated purified preparation but demonstrated greater affinity for the H-chain form in complex mixtures. (**Figure 8.4A**)
5. Although the CA-10 clone was generated from an epitope in the H-chain sequence, the antibody preferentially detected single-chain active CTSB in whole cell lysates (**Figure 8.4A**). Initial assessment was hampered by an unsatisfactory HRP-conjugated secondary antibody; detection was greatly enhanced with use of a secondary preparation from Dako but opportunity to further evaluate was not available. The 155714 clone failed in tests on known positive cell line controls (data not shown) and was not assessed further.
6. Results of CTSB immunoblotting in a panel of leukaemia cell line lysates indicated good agreement between the CA-10 monoclonal and Biomol SA-361 polyclonal antibodies (**Figure 8.5**).
7. Additional optimisation steps including evaluation of detection specificity (in transcript-depleted or gene-deleted samples) and correlation with enzyme activity were not performed.

---

Cell immunostaining

1. The following cell fixation protocols for AEP immunostaining were investigated on SD1 cytospin preparations (data not shown):
   a) 3.7% formalin, 15 minutes incubation at room temperature, followed by permeabilisation with 0.25% Triton X-100 in PBS

b) 100% chilled methanol, 10 minutes incubation at -20°C; no permeabilisation

c) 1:1 methanol:ethanol, equal volumes of chilled methanol and acetone with interval chilled PBS washes, serial 10-minute incubations at -20°C; no permeabilisation

Cellular features and subcellular architecture were best preserved with formalin-fixation.

2. Negative staining controls were included in all cell AEP immunostaining experiments (**Figure 8.6**). This initially included controls for both primary and secondary antibodies at equivalent dilutions in 1% BSA. As primary antibody control, non-immune goat serum (pre-cleared of aggregates by syringe filtration and centrifugation) substituted the goat polyclonal anti-human AEP antibody. As secondary antibody control, 1% BSA substituted the fluorophore-conjugated anti-goat secondary. Images of controls were captured using microscope camera settings identical to those of test samples. Both negative controls were satisfactory and subsequent experiments only included the secondary antibody control.
3. Live cell labelling of acidic organelles was initially performed using a 100nM concentration of the LysoTracker Red DND-99 (LyTR) probe. Incubation time and cell density were as advised by manufacturer. Although labelling was successful, signal intensities were weak and required extended exposures for image capture despite use of a sensitive low-light imaging system. Probe labelling concentration was increased to 500nM with resulting improvement in signal intensity and no apparent non-specific labelling.
4. Live cell labelling of mature AEP using the fluorophore-tagged activity binding probe was performed as advised by Dr. Matthew Bogyo's lab (Stanford University, CA, USA). DMSO vehicle concentrations in live culture did not exceed the recommended 0.1% (v/v). Probe specificity was established by examining labelling in SD1 cells pre-incubated with the cell-permeable AEP inhibitor (AEPi), MV026630 (using an established non-lethal dose of 100μM, 12 hours, 37°C; **Figure 8.7**). Further evaluation of probe specificity, including

intracellular labelling in stable AEP transcript-depleted SD1 cells and in cells transduced with catalytically-inactive AEP, was precluded by limited probe availability. The Bogyo lab has recently reported on the labelling performance of the probe (Chapter 3, [2]).

5. Labelling specificity of AEP antibody and activity-binding probe was additionally confirmed by fixed cytospin staining of the AEP non-expressing ALL cell lines REH and SupB15 (**Figures 8.8 and 8.9**)
6. Only a secondary antibody negative control was assessed when staining for LAMP1 with the mouse HA-43 monoclonal antibody.

---

AEP Immunohistochemistry

The following components of the experimental protocol were evaluated and optimised:

1. Identification of positive staining controls

   These included formalin-fixed paraffin sections of colorectal adenocarcinoma and the HRC57 cell line. Agarose moulds of HRC57 were created by resuspending cell pellets ($2 \times 10^6$ cells) in 1-2 drops of cooled ultra-pure low melting point agarose (fluid at 37°C, setting temperature <25°C; Invitrogen) in 1.5mL microfuge tubes; post-set, cell moulds were loosened by tapping the base of microfuge tubes and submitted for formalin fixation and paraffin embedding (Experimental Pathology division, CRUK London Research Institute). Positive controls were included in each staining run.
2. Optimal antigen retrieval technique
   a) Heat-induced antigen retrieval of de-paraffinised tissue sections in Tris-EDTA was the optimal epitope unmasking technique for AEP tissue immunostaining.
   b) Also examined were heat-induced antigen retrieval in Citrate buffer and proteolytic enzyme antigen retrieval using Pronase (pre-warmed [37°C] de-paraffinised tissue sections were incubated in a Coplin jar with Pronase [1mg/mL in PBS; Sigma-Aldrich] for 15 minutes at 37°C)

3. Minimisation of endogenous tissue peroxidase and biotin activity

   Attempts to minimise irrelevant background tissue staining were performed immediately following antigen retrieval and included

   a) Quenching of endogenous peroxidase activity by immersion of tissue sections in hydrogen peroxide-methanol (0.3% hydrogen peroxide, 10 minutes) and use of sodium azide in diluent solutions of primary and secondary antibodies
   b) Quenching of endogenous biotin activity using a proprietary avidin-biotin blocking solution

4. Negative staining controls (**Figure 8.10**)

   Created for each sample in parallel with primary antibody layer; AEP antibody substituted by 1% BSA in primary layer (secondary antibody control)

5. AEP antibody dilution

   A dilution of between 1:300 and 1:400 was established to be optimal

6. Controls for AEP-CD68 dual tissue immunofluorescence labelling

   Single-fluorescence labelling controls and controls for antibody cross-reactivity (primary-secondary antibody combinations for AEP with isotype-secondary antibody combinations for CD68 and vice-versa) were not examined as sufficient tissue sections were not available

---

Stable enforced and inducible AEP-expressing HEK 293 cells

The following procedures were evaluated and optimised as part of this line of work:

1. Optimal selection dose of G-418 sulphate for isolation and maintenance of enforced AEP-expressing HEK293 cells

   HEK293 cells were placed in 6-well plates ($0.5\times10^6$ cells in 2mL complete DMEM / well) and incubated with a range of G-418 doses (0, 0.2, 0.4, 0.8, 1.0, 1.2 mg/mL). G-418 selection was refreshed every 48-72 hours. Viability was serially assessed by phase-contrast microscopy. Complete cell kill was observed at a G-418 dose of 0.8mg/mL (day 8-10) while viable cells were still observed at lower doses. An initial G-418 dose of 0.8mg/mL was therefore

used for positive selection of transfected cells. Once growth of transfected cells was established and enforced expression confirmed, selection was switched to a lower G-418 maintenance dose of 0.6mg/mL.

2. Mifepristone (Mfp) dosing for optimal expression in inducible AEP-expressing HEK293 cells
   a) Stably transfected inducible-expressing cells ($0.5\times10^6$ cells in 1mL complete DMEM, 12-well plate) were treated for 24 hours with different concentrations of Mifepristone (0.01-100nM). Cells were subsequently mobilised, pelleted, washed and lysed in NP-40 protein lysis buffer. AEP expression was examined by immunoblotting. Induction of expression was best observed with a 10nM dose of Mifepristone (**Figure 8.11**, *upper panel*). This was also the induction dose recommended by the manufacturer.
   b) Duration of induced AEP expression was determined by serially tracking expression in transfected cells treated with a 24-hour pulse of 10nM Mifepristone. Cells were placed in 12-well plates ($0.5\times10^6$ cells in 1mL complete DMEM). Post-treatment, growth medium was refreshed and cells were harvested at different time points (12, 24, 48, 72 and 96 hours). AEP expression was examined by immunoblotting. Expression was observed 24 hours following pulse treatment and was maintained for at least 72 hours (**Figure 8.11**, *lower panel*).
   c) Optimal duration of Mifepristone treatment for induction of AEP expression was not investigated. A 24-hour treatment was advised by the manufacturer.
   d) Some baseline AEP expression was observed in non-treated controls. This could potentially be a consequence of endogenous steroid hormones in foetal bovine serum (FBS) mimicking the inducing effect of Mifepristone. Assessment of impact of elimination of endogenous steroid hormones on baseline AEP expression, for instance by charcoal treatment of FBS, was not performed.
3. Evaluation of variability of AEP expression in inducible-expressing cells

Flow cytometry was used in a single experiment to assess the variation in AEP expression in the stably transfected polyclonal population of inducible-expressing HEK293 cells. Mifepristone-treated cells ($2\times10^5$, passage 15) were fixed-permeabilised (Cytofix/Cytoperm reagent, BD) and incubated with anti-AEP primary (1:100 dilution, 2μg/mL) and Alexa Fluor 488-conjugated secondary (1:1000 dilution) antibodies with appropriate intervening wash steps (Perm/Wash buffer, BD). Negative controls included Mifepristone-untreated cells and treated cells incubated with either non-immune goat serum or 1% BSA in PBS as primary antibody substitute. Fluorescence was acquired on the BD FACScan instrument (488nm laser, FL1 530/30 bandpass filter) and examined using the WinMidi analysis package.

Despite polyclonality, intracellular AEP expression was closely clustered and was 1-2 logs higher than non-induced control (**Figure 8.12**). Negative controls were appropriate (not shown).

4. Evaluation of variability and intracellular localisation of AEP expression in enforced AEP-overexpressing cells

   In a single experiment, AEP immunostaining was used to examine expression characteristics in enforced expressing and mock-transfected controls. Cells ($1\times10^5$, pass 9) were cultured to sub-confluence in 35mm glass bottom dishes (ibidi GmbH) and stained in-situ. Negative primary and secondary antibody controls were included. As expected, expression was heterogenous in the over-expressing polyclonal population and included a mix of strong-, intermediate- and weak/non-expressing cells. Intracellular localisation was similarly variable, occurring as either peripheral or perinuclear aggregates, or in some cases, a combination of the two (**Figure 8.13**).

5. Interval confirmation of overexpressing phenotype, including after cryostorage retrieval

   Interval assessment of AEP overexpression by immunoblotting and enzyme activity was performed through the course of experiments to monitor phenotype stability and detect cross-contamination between experimental and control cells.

6. Concentration of selection agents (Hygromycin and Zeocin) in the isolation and maintenance of inducible-expressing HEK293 cells were as recommended by manufacturer.
7. Clonal isolation (e.g. by limiting dilution) of transfected HEK293 cells to establish low-, intermediate- and high-expressing clones, was not performed.

---

Boyden chamber motility assays

Experimental procedures were largely based on local expert advice. The following components of the experimental protocol were evaluated;

1. Matrigel coating of inserts

   Boyden chamber assays of inducible-expressing HEK293 cells were performed using 8-micron pore inserts coated with Matrigel at varying dilutions (in serum-free DMEM). At dilutions of up to 1 in 10 (1mg/mL), Matrigel polymerises to form a surrogate basement membrane matrix while at higher dilutions, it merely forms a non-barrier protein membrane coat that perhaps facilitates cell adhesion and motility. At higher Matrigel dilutions (1 in 20 upwards), lower chamber counts of Mifepristone-untreated cells assessed 24 hours after insert loading, were fairly constant while results were variable for Mifepristone-treated cells (10nM, 24 hours) (**Figure 8.14**). Based on published work (Chapter 2, [24]), subsequent assays were performed using a Matrigel coating dilution of 1 in 50.
2. Cell culture conditions pre-assay

   The following variables were assessed

   a) Cell passage

      Enforced- and inducible-expressing cells were passaged 48 hours prior to Boyden chamber assays. This ensured that cells were optimally sub-confluent and could be mobilised without forming aggregates. Assays were only performed when cell viabilities (Trypan Blue exclusion staining) were near 100%. In inducible-expressing cells, Mifepristone (10nM) or vehicle control (ethanol, equivalent volume) was added to growth medium 24 hours pre-assay.

b) Serum starvation to minimise background adhesion-motility signals

Cells were serum-starved for 24 hours by replacement of complete growth medium with serum-free DMEM. Serum starvation altered cell phenotype, with aberrant morphology (cytoplasmic swelling on phase-contrast microscopy) and enhanced adhesion (i.e. difficult Trypsin-EDTA mobilisation of cell monolayers in culture flasks and dishes). Cells were therefore *not* serum-starved pre-assay. Shorter serum withdrawal times were not assessed.

3. Loading cell counts in inserts were as recommended by manufacturer ($1\times10^5$ cells in $0.3m^2$ 8-micron pore inserts). Inserts with greater pore diameters (e.g. 12-micron) were not assessed.
4. All Boyden chamber assays using matrigel-coated inserts were evaluated after 24 hours incubation. Extended incubation times were not investigated,

---

AEP activity assay

The fluorometric substrate cleavage assay was adapted from a published report [4] and from a protocol established in Dr. Colin Watts' lab (Cell Biology and Immunology, University of Dundee). The following parameters were evaluated and optimised:

1. Fluorescence standard

   In serial experiments, reference range of the 7-amino 4-methyl coumarin fluorescence standard was calibrated such that mean fluorescence generated by the positive control, SD1 whole cell lysate, fell within the middle of the linear standards dilution curve.
2. Inhibition of substrate cleavage

   To enable detection of AEP-specific substrate cleavage in whole cell lysates, reactions were performed with and without the addition of a selective AEP inhibitor (AEPi, MV026630; [5]). Optimal AEPi concentration was initially assessed in SD1 control lysates and was established at 50μM.
3. Assay performance was monitored by including SD1 as control lysate in experiment runs.

---

## AEP in cell supernatants

Appropriate RPMI growth medium requirements for investigation of AEP in cell-free supernatants were evaluated. AEP immunoblotting of complete growth medium alone consistently revealed a 56kDa protein band, similar to that seen with pre proAEP (**Figure 8.15**). The confounding protein band was detected across all dilutions of foetal bovine serum (FBS) and was observed even after microvesicle depletion of FBS by ultracentrifugation (data not shown) but was not detected in serum-free RPMI. Thus, experiments investigating AEP expression in cell supernatants were performed by culturing cells in serum-free RPMI. To control for passive extracellular protein leak as a result of cell death, cell viability was assessed (Trypan blue exclusion) and ascertained to be near 100% in experiments.

---

## Experimental protocols adopted en bloc

The following experimental procedures were adopted largely unmodified based on either well-established local practice or robust manufacturer protocols; additional comments are appended

1. Protein quantitation and immunoblotting

   The goat polyclonal anti-human AEP antibody (R&D) has been evaluated against non-commercial mouse monoclonal antibodies (clones 6E3 and 11B7, Dr. Colin Watts) in whole cell lysates and in purified recombinant protein preparations (not shown). When combined with an HRP-conjugated donkey secondary from Santa Cruz, the optimal working dilution of the polyclonal antibody was 1:2500 (80ng/mL) with incubation times of 2 hours (room temperature) or 12-16 hours (4°C). Antibody specificity has subsequently been demonstrated in immunoblotting experiments of lysates from transcript-deplete and enforced-expressing cells as well as in monoclonal antibody immunoprecipitates of cell lysates. A protein-expressing positive control was included in all immunoblotting experiments.

2. Mononuclear cell isolation in clinical samples

   Bone marrow samples typically had in excess of 90% lymphoblasts at diagnosis and additional blast enrichment was not performed. Lymphoblast proportion in mononuclear cell isolates was not assessed post-processing. Almost all primary samples used in experiments were processed within less than 24 hours of collection. Sample integrity was indirectly estimated by examining relative transcript expression of the housekeeping β2M gene.

3. RNA isolation

   RNA was isolated from banked samples, aliquots of which were previously used for RNA extraction towards microarray experiments. The satisfactory quality of RNA in microarray experiments serves as a surrogate estimate of sample integrity.

4. Plasmid cloning

   Most procedures were based on robust manufacturer protocols.

5. Lipid-based transfection

   Procedure was essentially based on manufacturer protocol.

## 8.6 Statistics

Groups were compared using two-sided paired or unpaired *t* tests (2 groups) or by analysis of variance (more than 2 groups). Box-plot displays were used to better represent data dispersion. Linear association between continuous variables was investigated using the Pearson's product moment correlation. The statistical significance threshold for single comparisons was 0.05. Analyses were performed using the SPSS analysis package and the MS-Excel software.

## Section 8.7 Catalogue of Product Suppliers

| | |
|---|---|
| Abcam Plc<br>(www.abcam.com) | Cambridge Science Park<br>Cambridge, UK |
| Applied Biosystems<br>(www3.appliedbiosystems.com) | Applied Biosystems<br>Lingley House, Birchwood Boulevard<br>Warrington, UK |
| Anachem Ltd<br>(www.anachem.co.uk) | Anachem Ltd.,<br>Anachem House, Charles Street, Luton,<br>Bedfordshire, UK |
| Appleton Woods<br>(www.appletonwoods.co.uk) | Appleton Woods Ltd.<br>Lindon House, Heeley Road, Selly Oak<br>Birmingham, UK |
| Affymetrix<br>(www.affymetrix.com) | Affymetrix UK Ltd.<br>Voyager, Mercury Park,<br>Wycombe Lane, Wooburn Green<br>High Wycombe, UK |
| Axis-Shield UK<br>(www.axis-shielduk.com) | Axis-Shield UK<br>Ouse Road, Bicton Industrial Park<br>Cambridgeshire |
| Bachem<br>(www.bachem.com) | Bachem Distribution Services GmbH<br>Hegenheimer Strasse, Weil am Rhein, Germany |
| Beckman Coulter (UK)<br>(www.beckmancoulter.co.uk) | Beckman Coulter (UK) Ltd<br>Oakley Court, Kingsmead Business Park<br>London Road, High Wycombe |
| BD Biosciences<br>(www.bdeurope.com) | BD Becton Dickinson UK Ltd.<br>The Danby Building, Edmund Halley Road<br>Oxford Science Park, Oxford, UK |
| Bio-Rad Laboratories<br>(www3.bio-rad.com) | Bio-Rad Laboratories Ltd.<br>Bio-Rad House, Maxted Road<br>Hemel Hempstead, Hertfordshire, UK |

| | |
|---|---|
| Carl Zeiss UK<br>(www.zeiss.co.uk) | Carl Zeiss Ltd.<br>Woodfield Road, Welwyn Garden City<br>Hertfordshire, UK |
| Corning<br>(www.corning.com/lifesciences) | Corning B.V. Life Sciences<br>Fogostraat , Amsterdam, The Netherlands |
| Dako UK<br>(www.dako.co.uk) | Dako UK Ltd.<br>Cambridge House, St. Thomas Place,<br>Ely, Cambridgeshire, UK |
| DNAStar<br>(www.dnastar.com) | DNASTAR, Inc.<br>Regent Street, Madison, WI 53705, USA |
| Enzo Life Sciences<br>(www.enzolifesciences.com) | Enzo Life Sciences (UK) Ltd.<br>Palatine House, Matford Court<br>Exeter, UK |
| Eppendorf<br>(www.eppendorf.co.uk) | Eppendorf UK Ltd.<br>Endurance House, Chivers Way<br>Histon, Cambridge, UK |
| Fisher Scientific<br>(www.fisher.co.uk) | Fisher Scientific UK Ltd<br>Bishop Meadow Road, Loughborough,<br>Leicestershire, UK |
| GE Healthcare Life Sciences<br>(www6.gelifesciences.com) | GE Healthcare Life Sciences<br>Amersham Place, Little Chalfont<br>Buckinghamshire, UK |
| Integrated Biodiagnostics<br>(www.ibidi.de) | ibidi GmbH<br>Am Klopferspitz<br>Martinsried (München), Germany |
| Invitrogen<br>(www.invitrogen.com) | Invitrogen Ltd<br>Fountain Drive, Inchinnan Business Park<br>Paisley, UK |
| Laboratory Sales UK<br>(www.ls-uk.com) | Laboratory Sales (UK) Ltd.<br>Transpennine Trading Estate<br>Rochdale , UK |

| | |
|---|---|
| Merck4Biosciences<br>(www.merck-chemicals.co.uk) | Merck Chemicals Ltd.<br>Boulevard Industrial Park, Padge Road,<br>Beeston, Nottingham, UK |
| Millipore<br>(www.millipore.com) | Millipore (U.K.) Ltd.<br>Croxley Green Business Park<br>Watford, UK |
| Molecular Devices<br>(www.moleculardevices.com) | Molecular Devices<br>Sunnyvale, CA, USA |
| National Diagnostics<br>(www.nationaldiagnostics.com) | Distributed by Fisher Scientific UK |
| New England Biolabs<br>(www.neb.com) | New England Biolabs (UK) Ltd.<br>Knowl Piece, Wilbury Way<br>Hitchin, Herts. UK |
| Nikon Instruments Europe<br>(www.nikoninstruments.eu) | Nikon UK Ltd.<br>Richmond Road, Kingston Upon Thames<br>Surrey, UK |
| Nunc-Nalgene products<br>(www.nuncbrand.com) | Part of ThermoFisher Scientific |
| Olympus UK<br>(www.olympus.co.uk) | Olympus UK Ltd<br>KeyMed House, Stock Road<br>Southend-on-Sea, Essex, UK |
| PAA Laboratories<br>(www.paa.com) | PAA Laboratories Ltd.<br>Termare Close, Houndstone Business Park<br>Yeovil, Somerset, UK |
| Pierce Biotechnology<br>(www.piercenet.com) | Part of Thermo Fisher Scientific UK |
| Promega<br>(www.promega.com) | Promega UK<br>Delta House, Southampton Science Park<br>Southampton, UK |
| Qiagen<br>(www1.qiagen.com) | Qiagen House<br>Fleming Way, Crawley<br>West Sussex, UK |

| | |
|---|---|
| R&D Systems<br>(www.rndsystems.com) | R&D Systems Europe Ltd.<br>Barton Lane, Abingdon Science Park<br>Abingdon, UK |
| Roche Applied Science<br>(www.roche-applied-science.com) | Roche Diagnostics Ltd.<br>Charles Avenue,<br>Burgess Hill, UK |
| Santa Cruz Biotechnology<br>(www.scbt.com) | Santa Cruz Biotechnology Inc.<br>Heidelberg, Germany |
| Sera Laboratories International<br>(www.seralab.co.uk) | Sera Laboratories International Ltd<br>Bolney Grange Business Park<br>Haywards Heath, West Sussex, UK |
| Sigma-Aldrich<br>(www.sigmaaldrich.com) | Sigma-Aldrich Company Ltd.<br>Dorset, UK |
| Scientific Laboratory Supplies<br>(www.scientificlabs.co.uk) | SLS Ltd.<br>Wilford Industrial Estate<br>Ruddington Lane, Wilford, Nottingham, UK |
| Starlab<br>(www.starlab.co.uk) | Starlab UK Ltd<br>Tanners Drive, Blakelands<br>Milton Keynes, UK |
| VWR<br>(uk.vwr.com) | VWR International Ltd.<br>The Birches, Willard Way,<br>Imberhorne Industrial Estate<br>East Grinstead, West Sussex, UK |
| Vector Labs<br>(www.vectorlabs.com) | Vector Laboratories (UK) Ltd.<br>Accent Park, Bakewell Road<br>Orton Southgate, Peterborough, UK |
| Wolf Laboratories<br>(www.wolflabs.co.uk) | Wolf Laboratories Ltd.<br>Colenso House, Deans Lane,<br>Pocklington, York, UK |

**Figure 8.1** β2M expression is near-normally distributed in childhood acute leukaemia

Histograms with overlaid distribution curves of microarray expression of candidate reference genes in primary childhood leukaemia samples

ACTB, β actin; GUS, β glucuronidase; ABL1, Abelson murine leukaemia viral oncogene homolog 1, GAPDH, Glyceraldehyde-3-phosphate dehydrogenase; values represent relative normalised mean fluorescent intensities on the Affymetrix HG-U133A gene expression array platform, analysed using the Genespring 7.3.1 software package (**Table 8.1**)

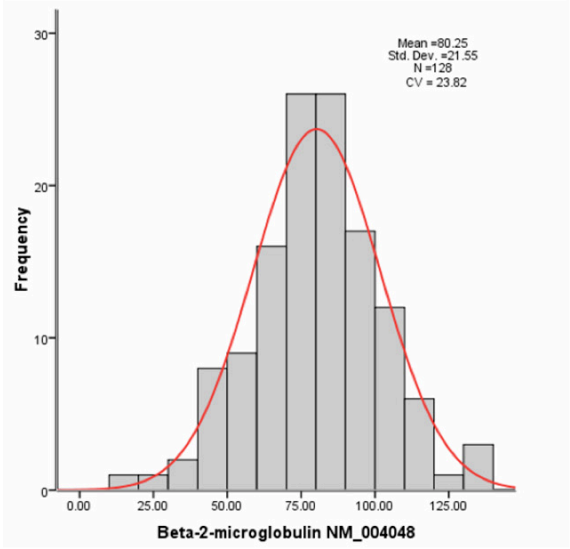


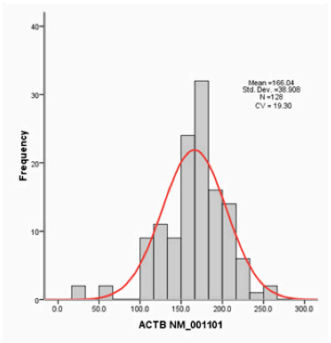


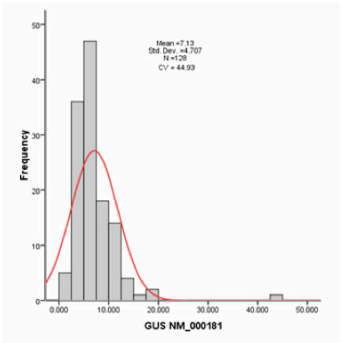


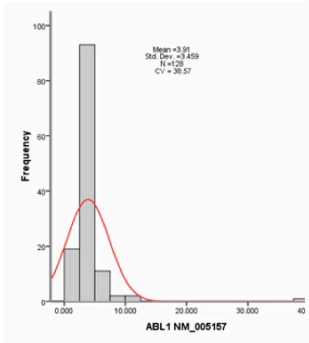


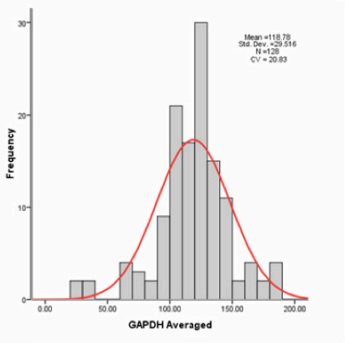

**Figure 8.2** Amplification characteristics of AEP and β2M transcripts are similar.

(A) Estimation of amplification efficiencies and dynamic linear range of AEP and β2M transcripts in the HRC57 cell line, using both 96- and 384-well Taqman reaction formats (B) Normalised AEP transcript expression (the difference between AEP and β2M Ct values or Delta Ct) was best maintained over a 16-fold input RNA dilution of 0.125 μg to 2.0μg (**Tables 8.2**, **8.3**)

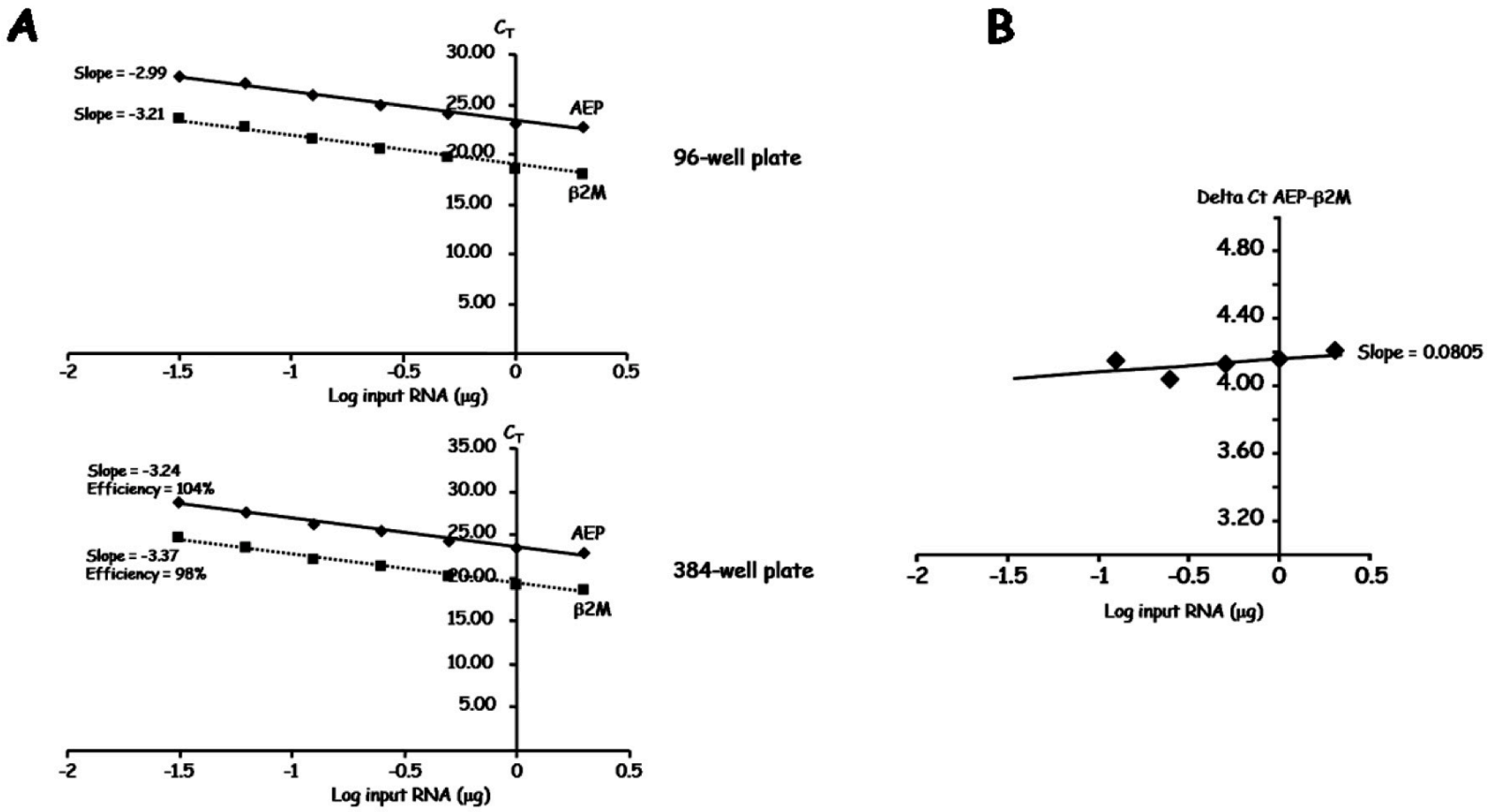

**Figure 8.3** Schematic representation of maturation sequence of human CTSB

Progressive acidification in the maturing endosome generates a single-chain mature form through autoactivation. Additional cleavage by extrinsic proteases yields a two-chain form. Variability in molecular weights reflects glycosylation status.

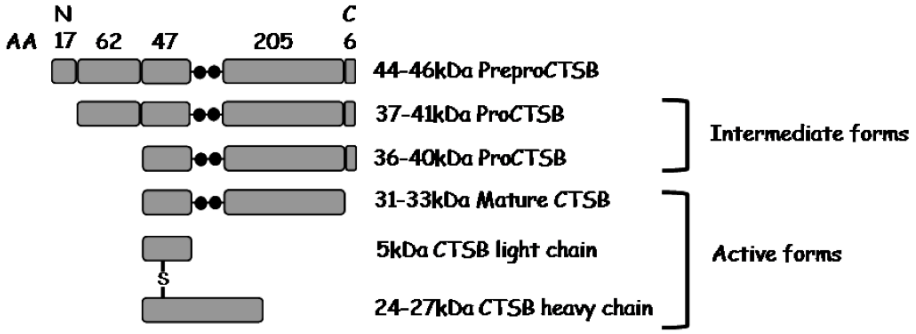


**Figure 8.4** Evaluation of candidate anti-human CTSB antibodies for immunoblotting

Both the Biomol SA-361 rabbit (Rb) polyclonal and CA-10 mouse monoclonal antibodies (ab) detect precursor and single-chain mature forms in activated purified recombinant (rh) preparations (A). Biomol SA-361 has preferential affinity for the heavy chain (H-chain) form in whole cell lysates (A), is sensitive over a range of dilutions (B) and unlike other candidate polyclonal antibodies (C), is associated with crisp detection bands.

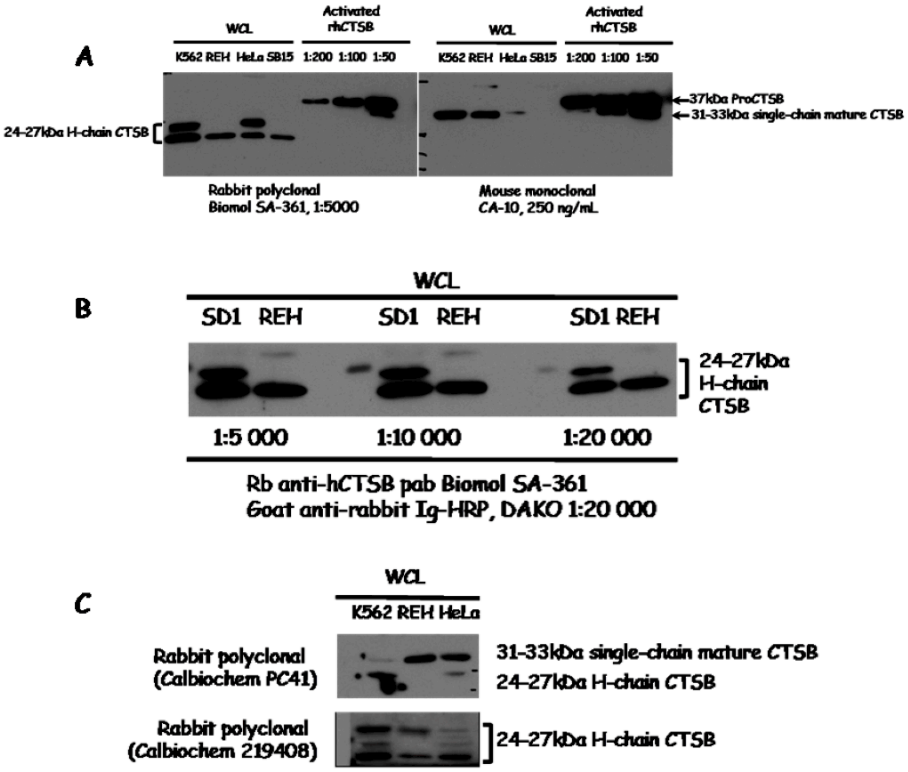

**Figure 8.5** Concordance in polyclonal and monoclonal CTSB immunoblots

Good agreement in results of CTSB immunoblotting in a panel of human leukaemia cell line whole cell lysates using the monoclonal CA-10 and polyclonal Biomol SA-361 antibodies; sole discordance was observed in the RPMI-8402 T-lineage leukaemia cell line (detection of inactive protein only with CA-10; detection of active H-chain form with Biomol SA-361)

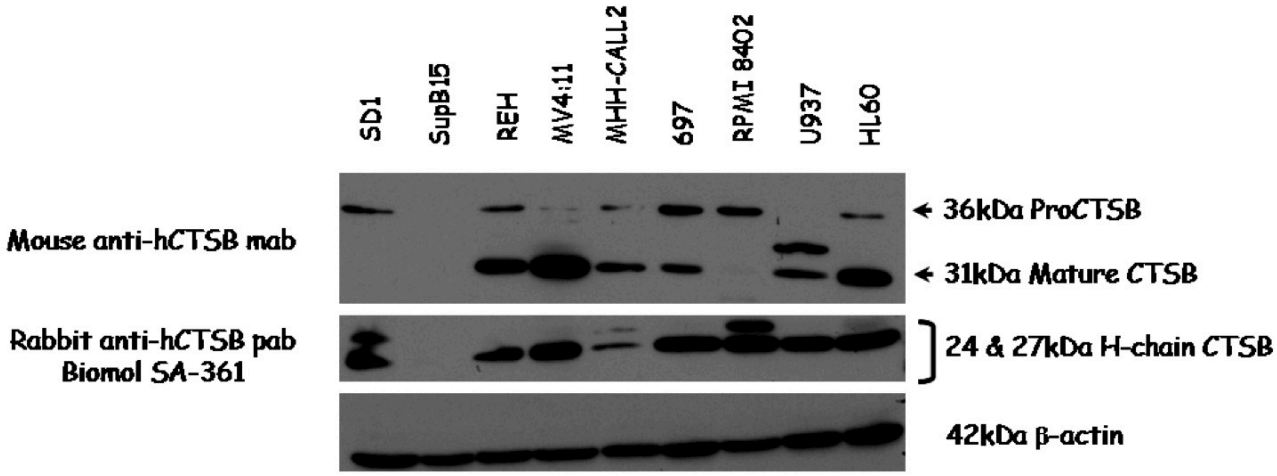

**Figure 8.6** Satisfactory negative AEP immunostaining antibody controls Representative microscopic images of SD1 cytospins. Upper panel: LysoTracker Red (LyTR)-labelled SD1 cells counterstained with DAPI (nucleus); non-immune goat serum replaced polyclonal goat-derived anti-human AEP as primary antibody control; Lower panel: SD1 cells labelled with DAPI; 1% BSA in PBS replaced anti-AEP as control for secondary antibody

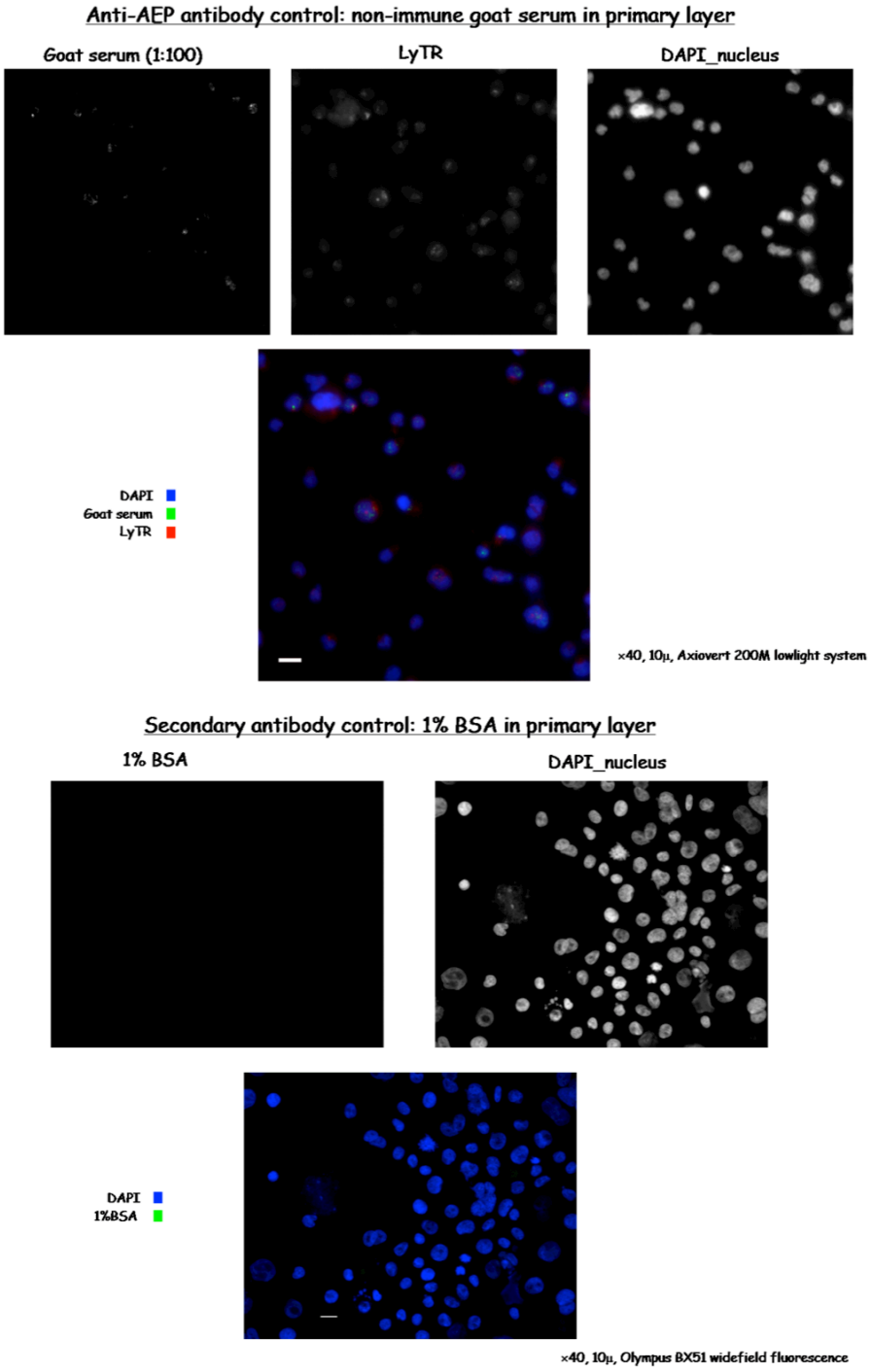

**Figure 8.7** The AEP activity-binding probe is relatively specific

Live-cell labelling of AEP with activity-binding probe (ABP) in SD1 cells pre-incubated with a cell-permeable AEP inhibitor (MV026630, 100μM, 12 hours, 37°C). SD1 cytospin preparations were counterstained with the DAPI nuclear stain before imaging. Scale bars 50μ, 10×; 10μ, 40×; Axiovert 200M Lowlight system, Metamorph imaging software

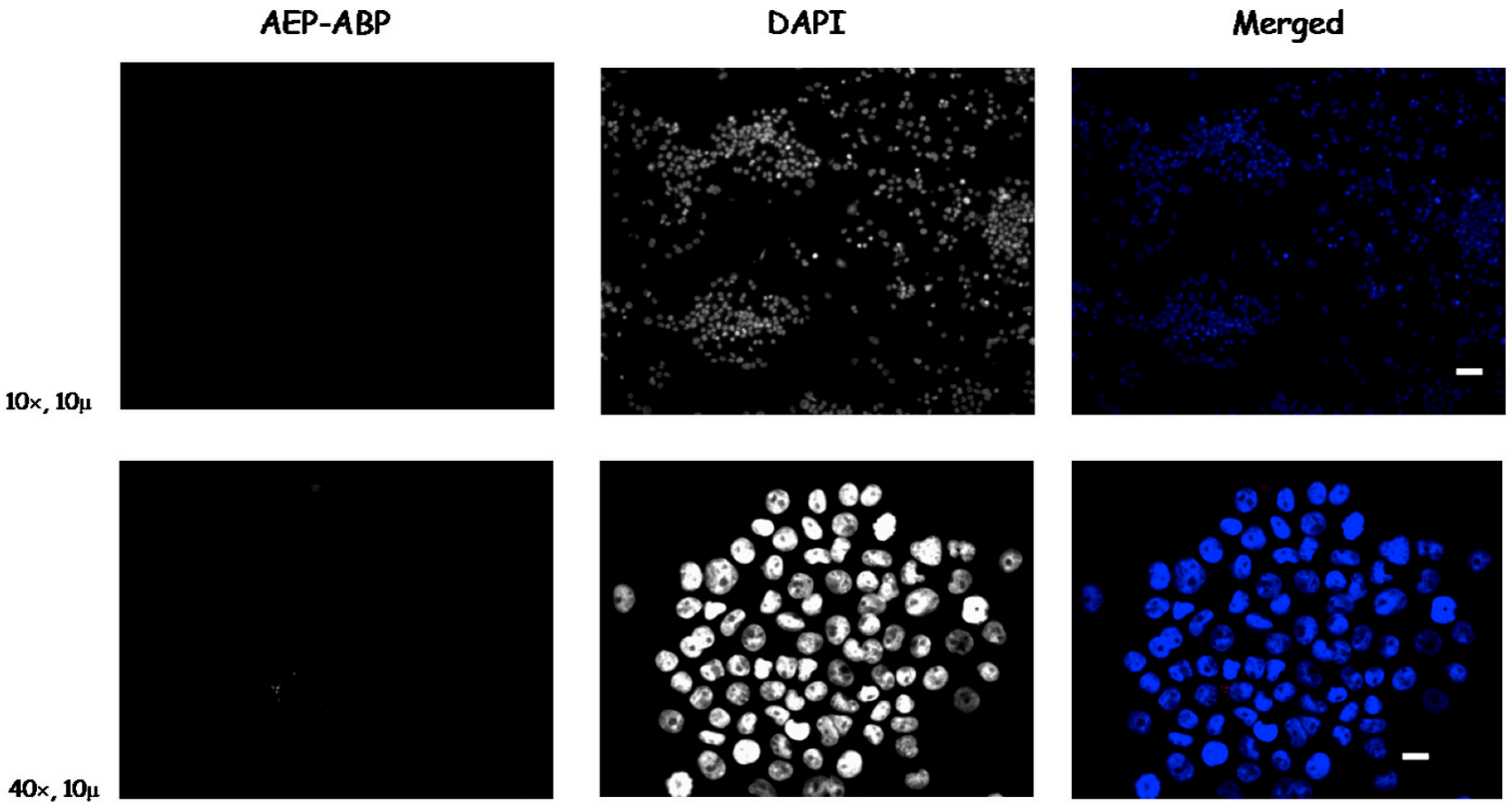

**Figure 8.8** Fluorescent antibody labelling is not observed in the non AEP-expressing cell lines, REH and SupB15

Immunofluorescence staining of formalin-fixed cytospins. The non AEP-expressing progenitor-B ALL cell lines, SupB15 and REH, were labelled with anti-AEP primary (goat polyclonal, R&D) and Alexa Fluor 488-tagged rabbit anti-goat IgG secondary antibodies. In SD1-negative control samples, 1% BSA replaced the primary antibody layer and served as secondary antibody control. As expected, green fluorescent labelling was absent in all three samples. Images were acquired using an Olympus BX51 microscope equipped with a Photometrics CoolSnap HQ CCD camera operated by the Metamorph advanced imaging software. Scale bar, 10μ; DAPI nuclear counterstain.

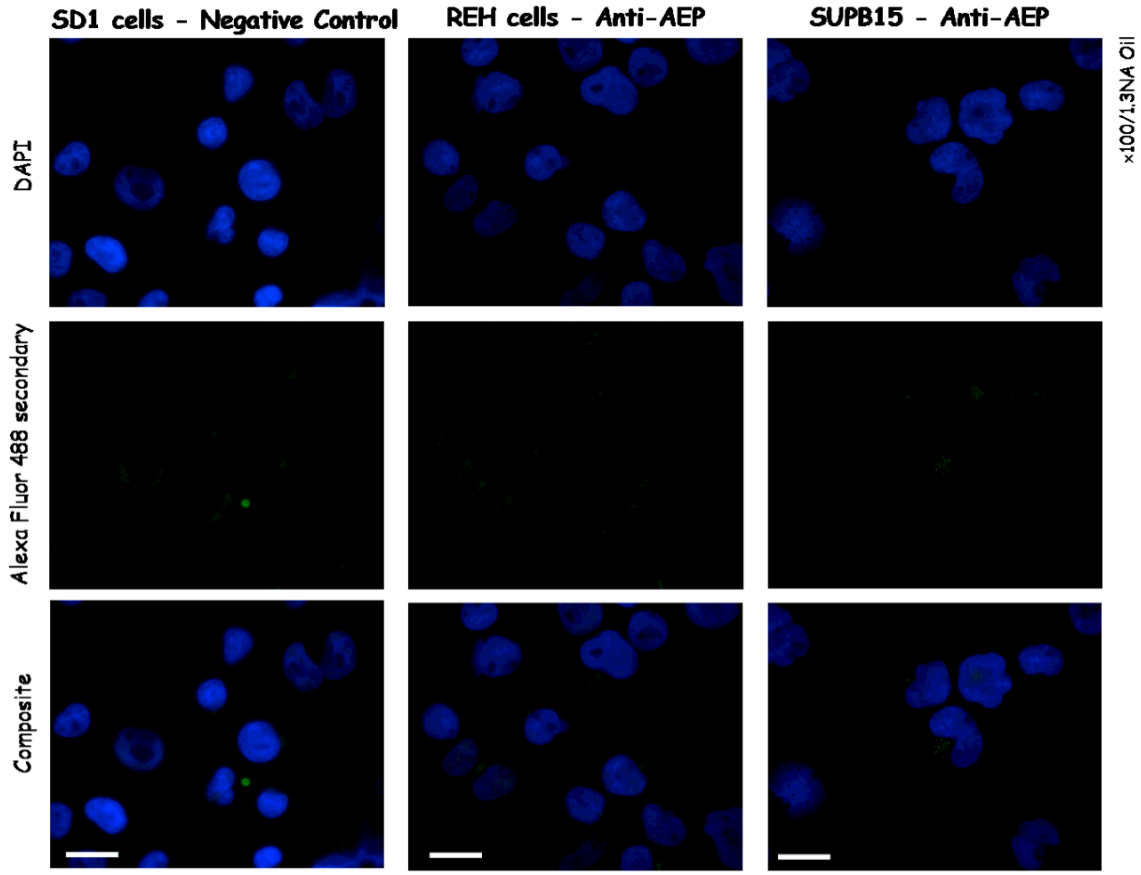

**Figure 8.9** The AEP non-expressing leukaemic cell lines, REH and SupB15, are not labelled by an AEP activity-based probe

DAPI-counterstained, formalin-fixed cytospins of REH (upper panel) and SupB15 (lower panel) cells ($2\times10^5$) labelled live with a BODIPY (λex/em 530/580)-tagged AEP activity-based probe (1μM, 2 hours, 37°C; orange-red fluorescence); merged images are shown. Acquired using an Olympus BX51 microscope equipped with a Photometrics CoolSnap HQ CCD camera operated by the Metamorph advanced imaging software.

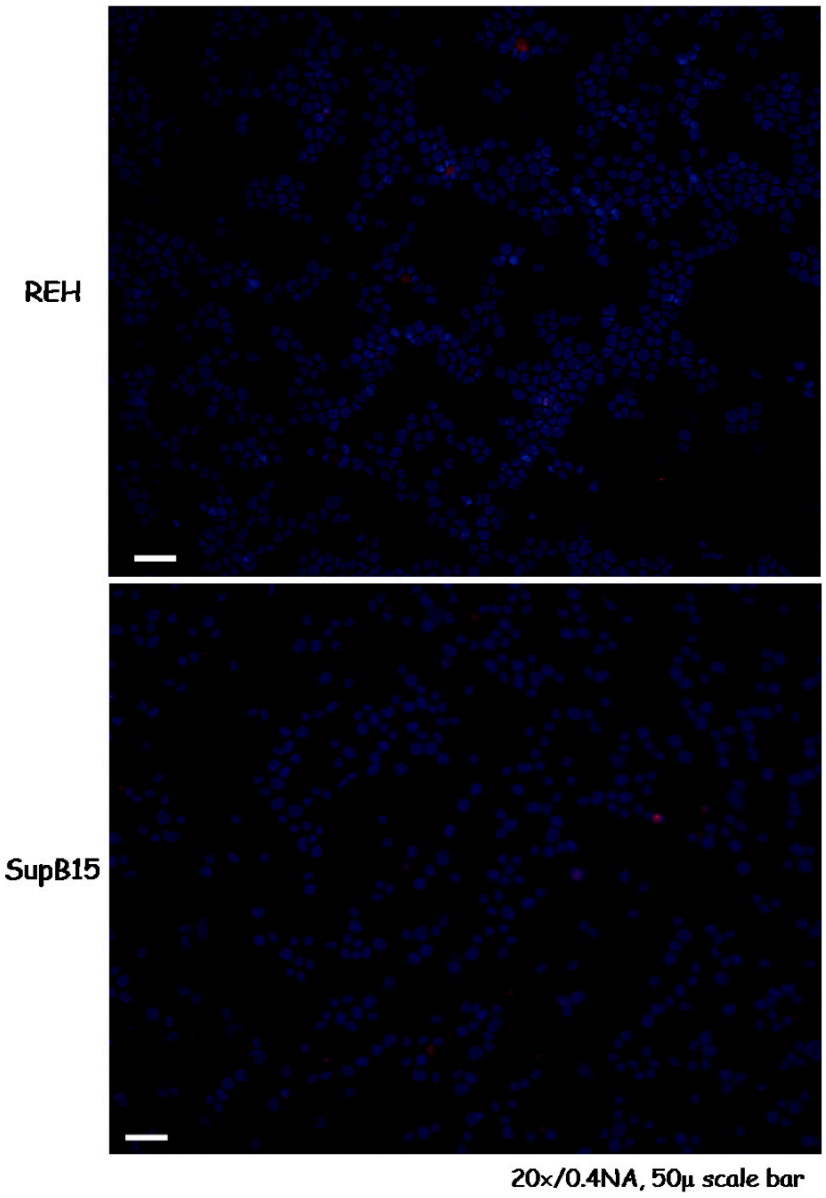

**Figure 8.10** AEP Immunohistochemistry staining controls

Representative images of parallel positive (A) and negative (B) staining controls of colon adenocarcinoma tissue sections; higher magnification images of colon carcinoma (C) and HRC57 (D) positive staining controls

Images were acquired using the Olympus BX51 microscope equipped with a cooled CCD camera operated by the Olympus Soft Imaging System package (analySIS)

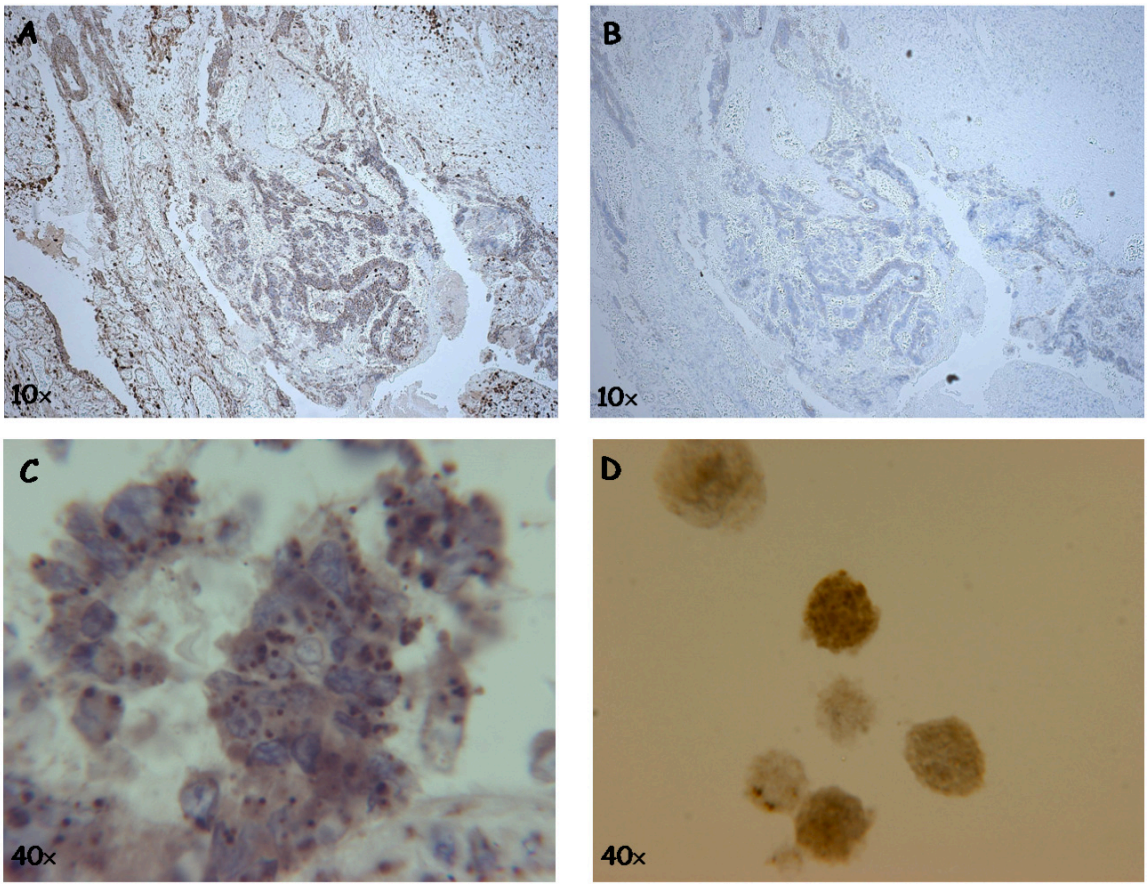

**Figure 8.11** Mifepristone dose-finding and AEP expression kinetics in inducible-expressing HEK293 cells

*Upper panel* Immunoblot of AEP expression in AEP293GS treated for 24 hours with an ascending range of Mifepristone (Mfp) concentrations; an induction dose of 10nM was optimal. *Lower panel* Immunoblot of AEP expression in AEP293GS cells at different timepoints following a 24-hour induction pulse of 10nM Mfp; AEP expression was established 24 hours following induction and was maintained for at least another 48 hours. Untr, untreated

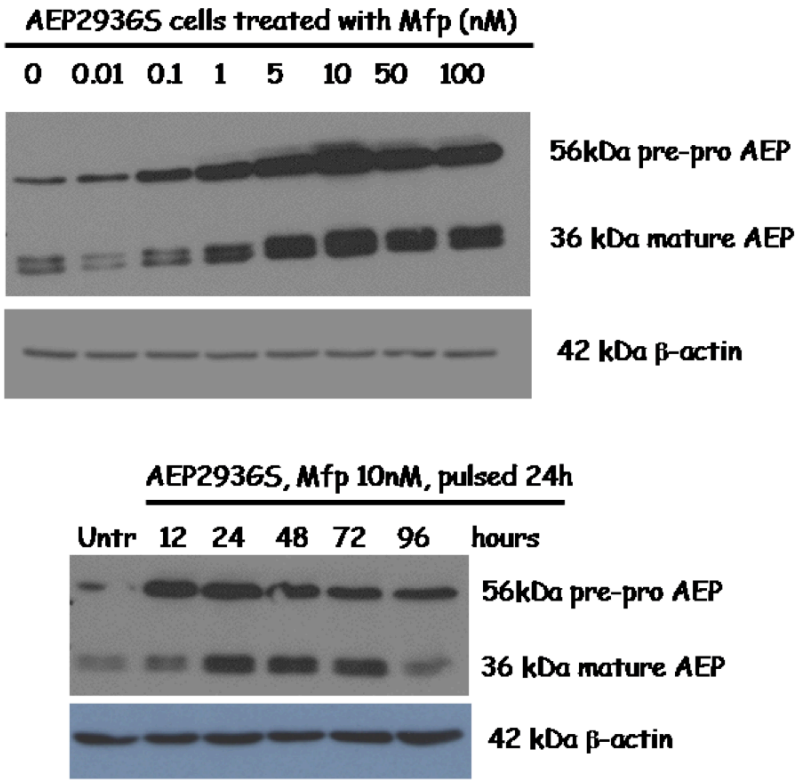

**Figure 8.12** Relative homogenous AEP expression in inducible-expressing HEK293 cells

Flow cytometry dot-plot (forward scatter *v* fluorescence) and histogram (fluorescence v cell count) representations of intracellular AEP expression in Mifepristone-treated and untreated inducible-expressing HEK293 cells (AEP.293GS). Following Mifepristone induction (24-hour, 10nM), intracellular AEP expression in AEP.293GS cells was relatively uniformly clustered at 1-2 logs higher than baseline.

*FSC-H, forward scatter parameter; FL1-H, λ530/30 fluorescent emission filter*

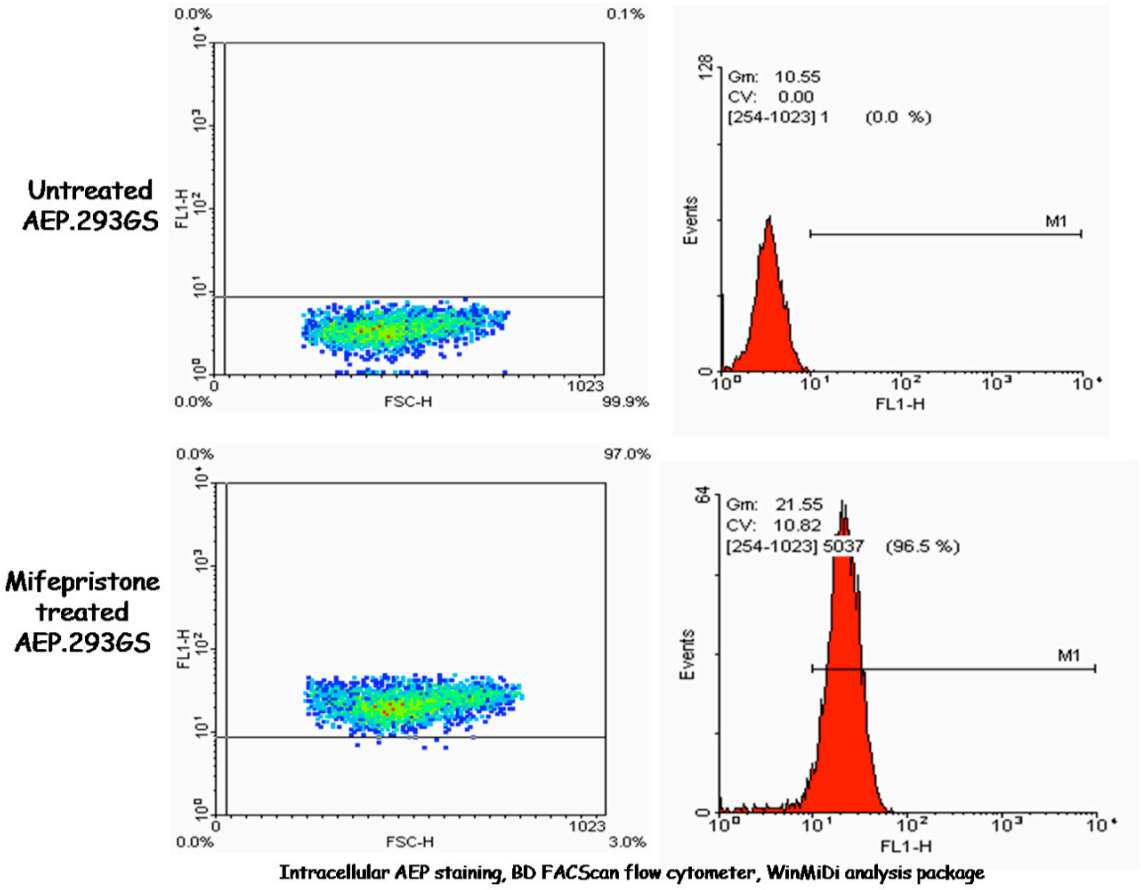

**Figure 8.13** Heterogeneous AEP expression in polyclonal enforced-expressing HEK293 cells

AEP immunostaining in enforced-expressing (AEP.293) and mock-transfected (EV.293) HEK293 cells. As expected, AEP expression in polyclonal AEP.293 cells is heterogeneous with a mix of strongly-expressing and non-expressing cells. Intracellular expression is either peripherally localised (100×, middle panel) or perinuclearly clustered (100×, lower) and in other cases, a combination of the two (100×/Optovar 1.5, lower). Images were acquired using an Axiovert 200M Lowlight microscope equipped with a Photometrics CoolSnap HQ CCD camera operated by the Metamorph advanced imaging software.

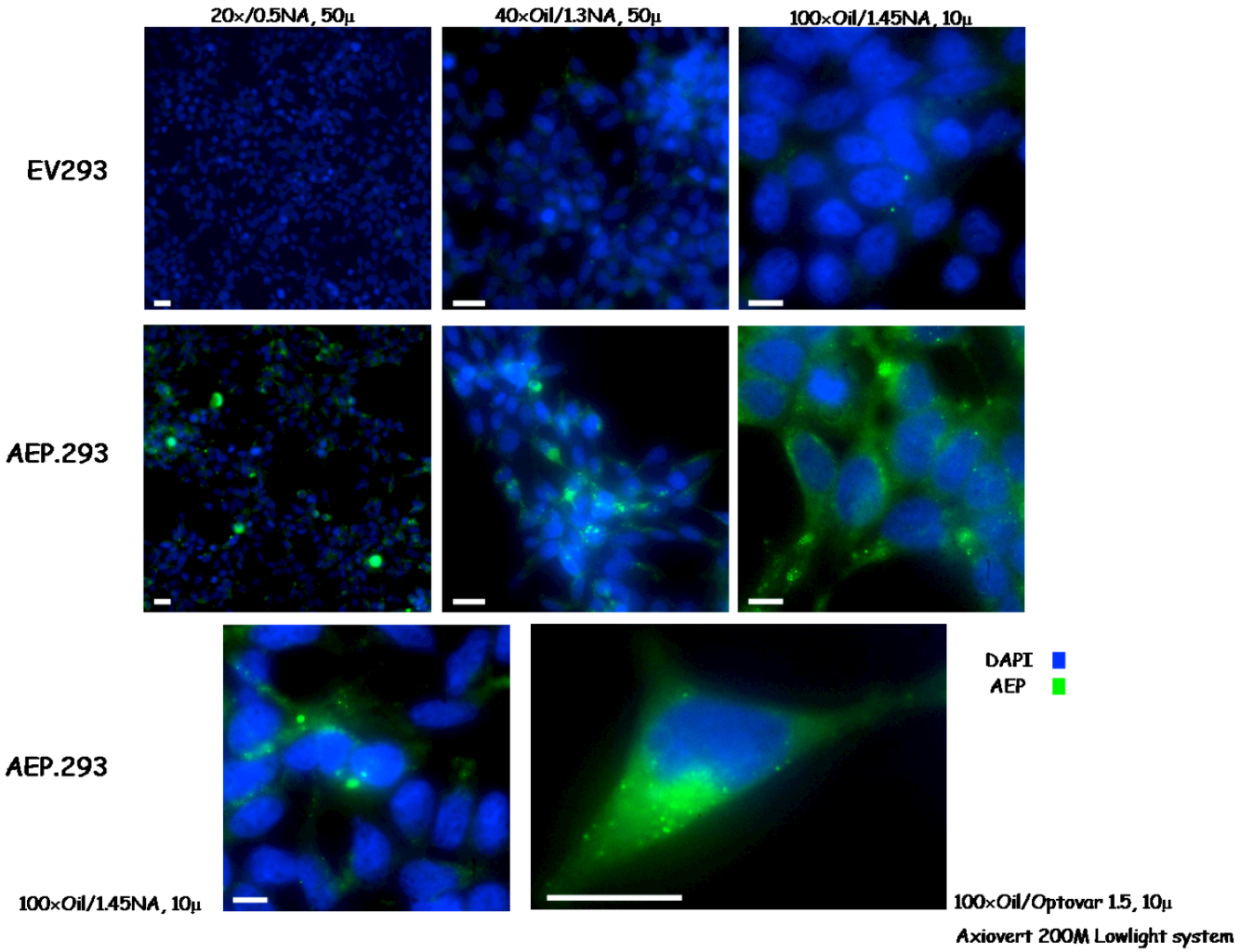

**Figure 8.14** Motility of inducible-expressing HEK293 cells in Boyden chamber assays was better observed at higher Matrigel dilutions

Lower chamber cell counts (cells/mL, 24-hour assays) across a range of Matrigel coating dilutions. Motility of Mifepristone (Mfp) untreated inducible-expressing cells was relatively constant at higher Matrigel dilutions (1 in 20 upwards) while results were variable with Mfp-treated cells. Plus error bars, standard deviation of replicate counts; summary of 2 experiments

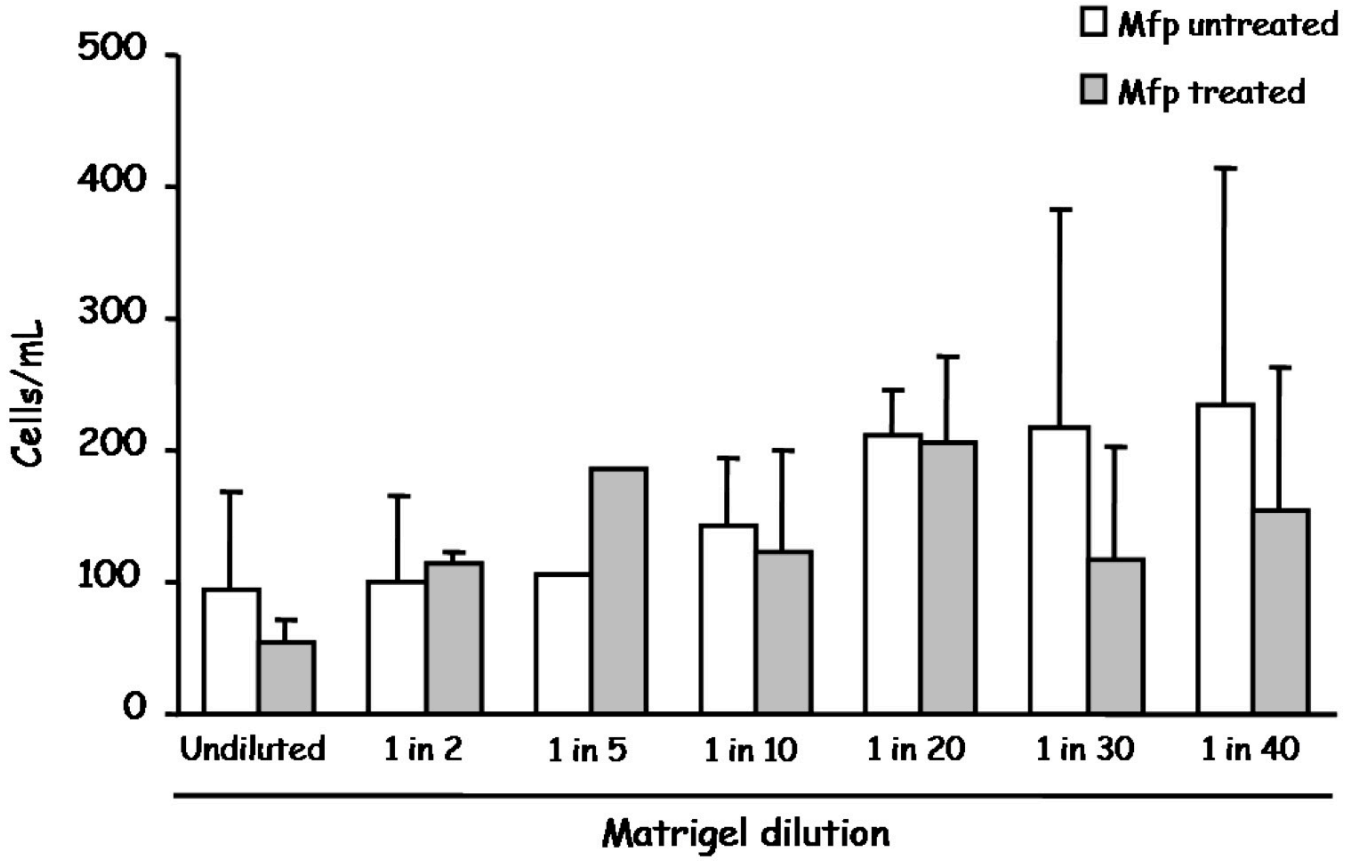

**Figure 8.15** A confounding 56kDa protein band is consistently observed in serum-supplemented growth medium

Immunoblotting for AEP in whole cell lysates and cell-free supernatants of leukaemic cell lines (SD1, REH, SupB15). A 56kDa protein band is consistently detected in cell-free supernatants. Note that this band is also observed in cell-free complete growth medium (lane labeled 'ONLY', RPMI with 2% FBS in this experiment) but not in cell-free serum-unsupplemented RPMI. Also note the trace detection of β-actin in SD1 supernatant; this was a consistent finding in SD1 supernatant isolates despite rigorous measures to ensure cell viability (~100% at time of centrifugation) and harvest of cell-free solution.

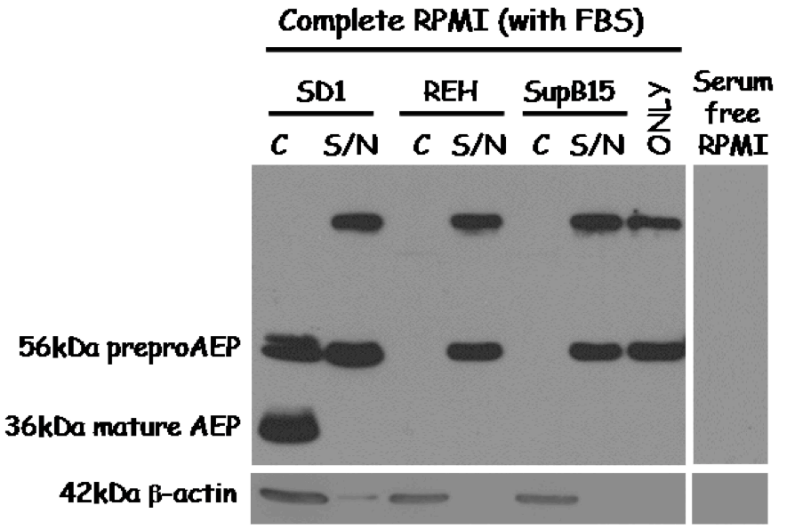


C, whole cell lysate; S/N, cell-free supernatant

**Table 8.1 Microarray expression (normalised intensity values) of candidate reference transcripts (n=120).**

β2M, Beta-2 microglobulin; GUS, β glucuronidase; ABL1, Abelson murine leukaemia viral oncogene homolog 1; GAPDH, glyceraldehydes-3-phosphate dehydrogenase ACTB, β actin

| *Cytogenetic subtype* | *β2M NM_004048* | *GUS NM_000181* | *ABL1 NM_005157* | *GAPDH Averaged* | *ACTB NM_001101* |
|---|---|---|---|---|---|
| **Progenitor B-ALL** | | | | | |
| *TCF3-PBX1* | | | | | |
| ID_1 | 77.42 | 4.738 | 3.905 | 122.05 | 178.9 |
| ID_94 | 79.02 | 4.51 | 3.251 | 111.35 | 187.3 |
| *ETV6-RUNX1* | | | | | |
| ID_4 | 88.65 | 3.364 | 2.074 | 100.66 | 153.4 |
| ID_5 | 88.94 | 3.398 | 2.352 | 66.625 | 171.6 |
| ID_15 | 117.5 | 3.785 | 2.955 | 75.305 | 165.3 |
| ID_16 | 108.6 | 2.419 | 2.314 | 68.91 | 169.4 |
| ID_18 | 81.16 | 6.152 | 2.643 | 77.48 | 162.9 |
| ID_28 | 100.2 | 6.023 | 4.729 | 129.8 | 176.7 |
| ID_40 | 69.73 | 6.454 | 4.387 | 128.3 | 134.1 |
| ID_45 | 114.7 | 7.677 | 4.225 | 130.25 | 220 |
| ID_ 48 | 94.76 | 7.682 | 2.796 | 139.1 | 191.8 |
| ID_55 | 92.51 | 4.875 | 3.715 | 142.85 | 178.6 |
| ID_62 | 78.83 | 4.113 | 3.969 | 102.88 | 157.4 |
| ID_64 | 99.55 | 5.499 | 2.641 | 112.97 | 166.9 |
| ID_65 | 82.97 | 6.519 | 4.586 | 126.6 | 162 |
| ID_69 | 48.86 | 8.665 | 4.392 | 103.115 | 173.9 |
| ID_75 | 60.37 | 8.815 | 3.393 | 122.41 | 167.8 |
| ID_89 | 99.27 | 4.759 | 2.322 | 104.845 | 177.9 |
| ID_103 | 79.9 | 6.889 | 2.992 | 121.6 | 158.5 |
| *High Hyperdiploidy* | | | | | |
| ID_0 | 107.1 | 4.868 | 4.09 | 114.03 | 161.7 |
| ID_19 | 81.27 | 4.799 | 4.073 | 85.29 | 207.1 |
| ID_23 | 71.71 | 5.945 | 4.558 | 123 | 152.7 |
| ID_24 | 102.7 | 5.781 | 3.523 | 127.6 | 238.1 |
| ID_27 | 111.5 | 4.263 | 2.547 | 130.7 | 152 |
| ID_30 | 94.27 | 4.117 | 3.38 | 109.785 | 153 |
| ID_35 | 66.68 | 3.773 | 4.171 | 116.575 | 171.5 |
| ID_38 | 71.05 | 5.447 | 2.586 | 121.45 | 141.7 |
| ID_52 | 104.9 | 6.796 | 2.145 | 115.335 | 190.1 |
| ID_53 | 99.91 | 5.307 | 3.695 | 123.95 | 130.6 |
| ID_54 | 100.2 | 4.32 | 4.073 | 127.45 | 113.1 |
| ID_63 | 71.7 | 3.552 | 3.26 | 107.405 | 152.3 |
| ID_66 | 94.86 | 6.465 | 2.665 | 112.605 | 143.8 |
| ID_76 | 75.61 | 7.024 | 3.011 | 103.595 | 176.3 |
| ID_78 | 71.82 | 5.072 | 3.01 | 122.3 | 109.3 |
| ID_80 | 86.04 | 5.553 | 3.219 | 125.75 | 147.8 |
| ID_82 | 73.61 | 6.374 | 4.82 | 124.4 | 147.2 |
| ID_83 | 73.03 | 6.799 | 5.048 | 120.5 | 123.9 |

| *Subtype* | *β2m* | *GUS* | *ABL1* | *GAPDH* | *ACTB* |
|---|---|---|---|---|---|
| ID_84 | 75.32 | 3.932 | 4.279 | 99.865 | 201 |
| ID_85 | 91.13 | 4.171 | 2.523 | 123.9 | 155.6 |
| ID_90 | 87.7 | 4.132 | 3.864 | 144 | 132.2 |
| ID_95 | 85.14 | 6.493 | 3.813 | 134.15 | 175.9 |
| ID_96 | 100.5 | 3.95 | 2.098 | 124.85 | 149.9 |
| *Normal Karyotype* | | | | | |
| ID_10 | 77.1 | 6.675 | 6.742 | 126.9 | 166.1 |
| ID_34 | 101.9 | 3.912 | 5.316 | 33.77 | 159.7 |
| ID_39 | 87.01 | 11.18 | 3.065 | 104.675 | 177.1 |
| ID_57 | 74.56 | 6.681 | 4.812 | 147.45 | 181.9 |
| ID_59 | 85.39 | 3.966 | 3.739 | 93.27 | 129.6 |
| ID_79 | 95.76 | 9.808 | 3.121 | 93.555 | 188.9 |
| ID_113 | 77.73 | 8.683 | 2.138 | 119.05 | 184.1 |
| *MLL rearranged* | | | | | |
| ID_87 | 69.34 | 6.733 | 4.604 | 114.85 | 151.4 |
| ID_106 | 63.07 | 6.611 | 2.84 | 106.855 | 144 |
| ID_114 | 54.1 | 5.569 | 2.077 | 132.7 | 124.7 |
| ID_116 | 71.9 | 9.137 | 3.834 | 128.65 | 191.2 |
| *BCR-ABL1* | | | | | |
| ID_70 | 101.8 | 6.572 | 8.105 | 115.485 | 205 |
| ID_88 | 58.39 | 7.586 | 7.16 | 109.95 | 171.2 |
| ID_91 | 81.9 | 7.579 | 10.75 | 64.325 | 152.6 |
| ID_98 | 99.05 | 7.016 | 7.265 | 121.35 | 187.4 |
| ID_109 | 118.6 | 5.379 | 3.379 | 139.7 | 116 |
| *iAMP21* | | | | | |
| ID_56 | 110.3 | 5.845 | 3.996 | 116.35 | 115.4 |
| ID_81 | 98.17 | 14.3 | 4.725 | 108.165 | 156.8 |
| ID_99 | 38.89 | 5.963 | 2.328 | 143.35 | 61.69 |
| ID_100 | 42.06 | 6.484 | 2.575 | 159.85 | 128 |
| ID_101 | 75.55 | 5.754 | 1.874 | 100.295 | 116.8 |
| ID_107 | 60.67 | 9.056 | 3.07 | 111.245 | 103.3 |
| ID_108 | 68.41 | 5.975 | 2.836 | 117.7 | 110.7 |
| *RUNX1 multiple copies* | | | | | |
| ID_9 | 72.11 | 5.089 | 2.814 | 128.225 | 150.2 |
| ID_13 | 91.27 | 4.172 | 2.643 | 109.215 | 161.2 |
| ID_61 | 120.2 | 10.13 | 2.599 | 130.4 | 225.6 |
| ID_72 | 100.5 | 6.029 | 5.048 | 109.285 | 190.4 |
| ID_104 | 82.2 | 11.1 | 1.706 | 113.62 | 125.2 |
| *Hypodiploidy* | | | | | |
| ID_68 | 108.9 | 9.921 | 4.978 | 114.26 | 152 |
| ID_111 | 69.92 | 6.035 | 2.887 | 130.5 | 132.4 |
| ID_115 | 99.89 | 8.735 | 2.642 | 180.4 | 175.6 |
| *Miscellaneous* | | | | | |
| ID_2 | 90.81 | 3.35 | 4.305 | 134.1 | 198.8 |
| ID_17 | 94.61 | 5.363 | 7.519 | 108.325 | 210.3 |
| ID_20 | 85.97 | 6.336 | 3.142 | 119.715 | 177.8 |
| ID_22 | 80.68 | 5.816 | 3.232 | 126.85 | 167.4 |
| ID_42 | 72.84 | 2.106 | 3.457 | 90.385 | 158.2 |
| ID_50 | 85.34 | 6.255 | 4.792 | 97.415 | 183.1 |
| ID_60 | 67.49 | 6.321 | 3.155 | 104.085 | 127.5 |

| *Subtype* | *β2m* | *GUS* | *ABL1* | *GAPDH* | *ACTB* |
|---|---|---|---|---|---|
| ID_93 | 59.59 | 4.887 | 3.842 | 92.805 | 215.9 |
| ID_97 | 135.1 | 3.965 | 2.763 | 62.87 | 199.2 |
| ID_119 | 71.93 | 10.31 | 5.73 | 124.75 | 179.4 |
| **Progenitor T-ALL** | | | | | |
| ID_8 | 53.9 | 2.45 | 1.815 | 135.5 | 172.2 |
| ID_25 | 89.09 | 4.435 | 2.608 | 91.815 | 205 |
| ID_37 | 87.42 | 4.463 | 2.767 | 113.555 | 176.8 |
| ID_44 | 84.84 | 3.025 | 3.232 | 141.25 | 200.7 |
| ID_46 | 65.12 | 10.81 | 3.048 | 189.2 | 199.7 |
| ID_51 | 82.09 | 3.74 | 4.163 | 131.6 | 164.6 |
| ID_71 | 56.73 | 4.075 | 6.04 | 132.85 | 172.9 |
| ID_73 | 130.1 | 3.89 | 3.365 | 101.015 | 233.3 |
| ID_74 | 71.7 | 5.709 | 3.174 | 105.59 | 169.4 |
| ID_105 | 75.99 | 4.188 | 3.392 | 144.95 | 204.6 |
| ID_118 | 58.44 | 5.629 | 3.676 | 163.8 | 176.7 |
| **Acute Myeloid Leukaemia** | | | | | |
| ID_3 | 95 | 11.58 | 3.208 | 142.4 | 252.2 |
| ID_6 | 59.64 | 10.37 | 2.609 | 158.65 | 167.4 |
| ID_7 | 66.34 | 19.18 | 3.625 | 99.435 | 138.3 |
| ID_11 | 83.97 | 10.42 | 5.713 | 123.7 | 159.5 |
| ID_12 | 89.37 | 4.254 | 2.688 | 102.295 | 191.9 |
| ID_14 | 77.09 | 8.887 | 2.937 | 123.5 | 167.3 |
| ID_21 | 64.44 | 10.77 | 2.544 | 106.035 | 181.8 |
| ID_26 | 86.85 | 9.119 | 3.446 | 120.85 | 202.6 |
| ID_29 | 75.47 | 10.65 | 2.765 | 171.25 | 201.3 |
| ID_31 | 62.57 | 2.984 | 1.108 | 107.745 | 147.8 |
| ID_32 | 63 | 6.322 | 4.416 | 84.41 | 171 |
| ID_33 | 108.4 | 9.412 | 3.45 | 136.6 | 180 |
| ID_36 | 72.87 | 5.888 | 3.429 | 129.8 | 201 |
| ID_41 | 72.89 | 13.78 | 3.048 | 174.55 | 193.1 |
| ID_43 | 60.78 | 9.584 | 5.391 | 149.05 | 200.4 |
| ID_47 | 97.84 | 4.455 | 4.768 | 141.7 | 231.9 |
| ID_49 | 43.06 | 14.55 | 3.133 | 187.7 | 199.9 |
| ID_58 | 47.43 | 12.34 | 2.457 | 134.15 | 207.5 |
| ID_67 | 56.39 | 11.01 | 2.366 | 140.65 | 188.3 |
| ID_77 | 62.32 | 6.297 | 3.556 | 98.12 | 124.9 |
| ID_86 | 47.95 | 12.48 | 3.946 | 110.275 | 187.2 |
| ID_92 | 53.79 | 9.559 | 3.49 | 148.5 | 203.9 |
| ID_102 | 84.02 | 10.32 | 2.592 | 165.15 | 223.5 |
| ID_110 | 48.69 | 8.26 | 2.059 | 126.9 | 107 |
| ID_112 | 85.85 | 17.05 | 2.512 | 169.3 | 166.6 |
| ID_117 | 47.09 | 6.932 | 3.832 | 136.6 | 105.3 |
| Mean | 81.09 | 6.80 | 3.62 | 120.44 | 168.44 |
| SD | 19.32 | 3.06 | 1.40 | 25.09 | 32.51 |
| Median | 80.92 | 6.09 | 3.31 | 121.53 | 170.2 |
| CV | 23.82% | 44.93% | 38.58% | 20.83% | 19.30% |
| Lower 95% CI | 43.22 | 0.81 | 0.88 | 71.26 | 104.73 |
| Upper 95% CI | 118.95 | 12.80 | 6.35 | 169.61 | 232.15 |
| Minimum | 38.89 | 2.106 | 1.108 | 33.77 | 61.69 |
| Maximum | 135.1 | 19.18 | 10.75 | 189.2 | 252.2 |

**Table 8.2 Raw Ct values of AEP and β2m transcripts across a 64-fold dilution (0.03125-2μg) of input HRC57 cell line RNA**

| HRC57 RNA quantity (μg) | AEP Ct | | | | β2M Ct | | | | AEP- β2M ΔCt | |
|---|---|---|---|---|---|---|---|---|---|---|
| | 96-well replicates | Average (CV%) | 384-well replicates | Average (CV%) | 96-well replicates | Average (CV%) | 384-well replicates | Average (CV%) | 96-well assay | 384-well assay |
| Nil Template | — | | — | — | — | | — | | — | — |
| | — | | — | — | — | | — | | | |
| | — | | — | | — | | — | | | |
| HRC57 | 22.766 | 22.720 | 22.810 | 22.94 | 18.045 | 17.92 | 18.654 | 18.64 | 4.80 | 4.29 |
| 2μg | 22.696 | 0.17% | 23.139 | 0.77% | 17.892 | 0.65% | 18.605 | 0.19% | | |
| | 22.700 | | 22.865 | | 17.816 | | 18.673 | | | |
| HRC57 | 23.155 | 23.096 | 23.487 | 23.55 | 18.521 | 18.44 | 19.010 | 19.24 | 4.66 | 4.31 |
| 1μg | 22.981 | 0.43% | 23.648 | 0.37% | 18.442 | 0.48% | 19.357 | 1.02% | | |
| | 23.150 | | 23.515 | | 18.346 | | 19.345 | | | |
| HRC57 | 24.239 | 24.136 | 24.347 | 24.28 | 19.601 | 19.58 | 20.277 | 20.07 | 4.55 | 4.21 |
| 0.5μg | 23.916 | 0.79% | 24.231 | 0.24% | 19.575 | 0.09% | 20.014 | 0.92% | | |
| | 24.255 | | 24.270 | | 19.570 | | 19.923 | | | |
| HRC57 | 24.979 | 24.959 | 25.439 | 25.48 | 20.571 | 20.53 | 21.257 | 21.32 | 4.43 | 4.16 |
| 0.250μg | 25.037 | 0.36% | 25.503 | 0.13% | 20.424 | 0.44% | 21.522 | 0.84% | | |
| | 24.861 | | 25.483 | | 20.588 | | 21.178 | | | |
| HRC57 | 25.838 | 25.977 | 26.236 | 26.29 | 21.479 | 21.47 | 22.149 | 22.16 | 4.51 | 4.13 |
| 0.125μg | 26.143 | 0.59% | 26.485 | 0.67% | 21.670 | 0.97% | 22.254 | 0.40% | | |
| | 25.952 | | 26.142 | | 21.256 | | 22.079 | | | |
| HRC57 | 27.195 | 27.094 | 27.645 | 27.51 | 22.608 | 22.64 | 23.565 | 23.47 | 4.46 | 4.04 |
| 0.0625μg | 26.910 | 0.59% | 27.659 | 0.90% | 22.751 | 0.46% | 23.332 | 0.52% | | |
| | 27.177 | | 27.224 | | 22.548 | | 23.519 | | | |
| HRC57 | 27.608 | 27.867 | 28.554 | 28.76 | 23.564 | 23.49 | 24.614 | 24.61 | 4.38 | 4.15 |
| 0.03125μg | 28.036 | 0.82% | 28.937 | 0.67% | 23.548 | 0.53% | 24.703 | 0.41% | | |
| | 27.957 | | 28.776 | | 23.342 | | 24.500 | | | |

**Table 8.3 TaqMan assay estimation of dynamic linear range of AEP, β2m and GAPDH transcript expression (Ct) in the HRC57 cell line (calibrator) using both 96-well and 384-well reaction formats.**

| *Input RNA (μg)* | *Log input RNA* | *AEP Ct* | | *β2M Ct* | | *GAPDH Ct* | |
|---|---|---|---|---|---|---|---|
| | | 96-well | 384-well | 96-well | 384-well | 96-well | 384-well |
| 2 | 0.30103 | 22.72 | 22.94 | 17.92 | 18.64 | 18.97 | 19.08 |
| 1 | 0 | 23.10 | 23.55 | 18.44 | 19.24 | 19.83 | 19.79 |
| 0.5 | -0.30103 | 24.14 | 24.28 | 19.58 | 20.07 | 20.65 | 20.57 |
| 0.25 | -0.60206 | 24.96 | 25.47 | 20.53 | 21.32 | 22.04 | 22.27 |
| 0.125 | -0.90309 | 25.98 | 26.29 | 21.47 | 22.16 | 23.35 | 23.11 |
| 0.0625 | -1.20412 | 27.09 | 27.51 | 22.64 | 23.47 | — | — |
| 0.03125 | -1.50515 | 27.87 | 28.76 | 23.48 | 24.61 | 26.78 | 26.85 |

**Table 8.4 Estimation of TaqMan inter-assay precision (HRC57 RNA, 384-well format); CV = coefficient of variation**

| HRC57 RNA | AEP Ct | Mean (CV) | β2M Ct | Mean (CV) | AEP-β2M ΔCt |
|---|---|---|---|---|---|
| Assay 1 | 22.77 | 22.78 | 17.78 | 17.86 | 4.91 |
| | 22.76 | (0.06%) | 17.96 | (0.49%) | |
| | 22.79 | | 17.85 | | |
| Assay 2 | 22.73 | 22.69 | 17.91 | 17.94 | 4.76 |
| | 22.47 | (0.92%) | 17.97 | (0.16%) | |
| | 22.88 | | 17.94 | | |
| Assay 3 | 23.58 | 23.61 | 18.96 | 19.00 | 4.61 |
| | 23.54 | (0.34%) | 18.91 | (0.58%) | |
| | 23.70 | | 19.12 | | |
| Assay 4 | 23.19 | 23.3 | 18.75 | 18.6 | 4.7 |
| | 23.36 | (0.4%) | 18.40 | (1.0%) | |
| | 23.27 | | 18.53 | | |

## References


| | Page |
|---|---|
| Chapter 1 | 214 |
| Chapter 2 | 233 |
| Chapter 3-4 | 248 |
| Chapter 5 | 249 |
| Chapter 6 | 257 |
| Chapter 8 | 258 |

## REFERENCES

### Chapter 1


1. Bennett JM, Catovsky D, Daniel MT, Flandrin G, Galton DA, Gralnick HR, et al. The morphological classification of acute lymphoblastic leukaemia: concordance among observers and clinical correlations. *Br J Haematol.* 1981;47:553-561.

2. Miller DR, Steinherz PG, Feuer D, Sather H, Hammond D. Unfavorable prognostic significance of hand mirror cells in childhood acute lymphoblastic leukemia. A report from the Childrens Cancer Study Group. *Am J Dis Child*. 1983;137:346-350.

3. Cerezo L, Shuster JJ, Pullen DJ, Brock B, Borowitz MJ, Falletta JM, et al. Laboratory correlates and prognostic significance of granular acute lymphoblastic leukemia in children. A Pediatric Oncology Group study. *Am J Clin Patho*l. 1991;95:526-531.

4. Crist WM, Grossi CE, Pullen DJ, Cooper MD. Immunologic markers in childhood acute lymphocytic leukemia. *Semin Oncol.* 1985;12:105-121.

5. Pui CH, Gaynon PS, Boyett JM, Chessells JM, Baruchel A, Kamps W, et al. Outcome of treatment in childhood acute lymphoblastic leukaemia with rearrangements of the 11q23 chromosomal region. *Lancet*. 2002;359:1909-1915.

6. Coustan-Smith E, Mullighan CG, Onciu M, Behm FG, Raimondi SC, Pei D, et al. Early T-cell precursor leukaemia: a subtype of very high-risk acute lymphoblastic leukaemia. *Lancet Oncol.* 2009;10:147-156.

7. Pui CH, Behm FG, Crist WM.Clinical and biologic relevance of immunologic marker studies in childhood acute lymphoblastic leukemia. *Blood*. 1993;82:343-362.

8. Williams DL, Harber J, Murphy SB, Look AT, Kalwinsky DK, Rivera G, et al. Chromosomal translocations play a unique role in influencing prognosis in childhood acute lymphoblastic leukemia. *Blood.* 1986;68:205-212.

9. Harrison CJ. Cytogenetics of paediatric and adolescent acute lymphoblastic leukaemia. *Br J Haematol.* 2009;144:147-156.

10. Mullighan CG, Downing JR. Genome-wide profiling of genetic alterations in acute lymphoblastic leukemia: recent insights and future directions. *Leukemia.* 2009;23:1209-1218.

11. Mastrangelo R, Poplack D, Bleyer A, Riccardi R, Sather H, D'Angio G. Report and recommendations of the Rome workshop concerning poor-prognosis acute lymphoblastic leukemia in children: biologic bases for staging, stratification, and treatment. *Med Pediatr Oncol.* 1986;14:191-194.

12. Smith M, Arthur D, Camitta B, Carroll AJ, Crist W, Gaynon P, et al. Uniform approach to risk classification and treatment assignment for children with acute lymphoblastic leukemia. *J Clin Oncol.* 1996;14:18-24.

13. Bloomfield CD, Secker-Walker LM, Goldman AI, Van Den Berghe H, de la Chapelle A, Ruutu T, et al. Six-year follow-up of the clinical significance of karyotype in acute lymphoblastic leukemia. *Cancer Genet Cytogenet.* 1989;40:171-185.

14. Nachman JB. Treatment: the most important prognostic variable. *J Pediatr Hematol Oncol.* 2002;24:704-705.

15. Pui CH, Campana D, Evans WE. Childhood acute lymphoblastic leukaemia--current status and future perspectives. *Lancet Oncol.* 2001;2:597-607.

16. Riehm H, Reiter A, Schrappe M, Berthold F, Dopfer R, Gerein V, et al. Corticosteroid-dependent reduction of leukocyte count in blood as a prognostic factor in acute lymphoblastic leukemia in childhood (therapy study ALL-BFM 83). *Klin Padiatr.* 1987;199:151-160. German.

17. Frei E 3rd, Sallan SE. Acute lymphoblastic leukemia: treatment. *Cancer.* 1978;42:828-838.

18. Steinherz PG, Gaynon PS, Breneman JC, Cherlow JM, Grossman NJ, Kersey JH, et al. Cytoreduction and prognosis in acute lymphoblastic

leukemia--the importance of early marrow response: report from the Childrens Cancer Group. *J Clin Oncol.* 1996;14:389-398.

19. Basso G, Veltroni M, Valsecchi MG, Dworzak MN, Ratei R, Silvestri D, et al. Risk of relapse of childhood acute lymphoblastic leukemia is predicted by flow cytometric measurement of residual disease on day 15 bone marrow. *J Clin Oncol.* 2009;27:5168-5174.

20. Coustan-Smith E, Behm FG, Sanchez J, Boyett JM, Hancock ML, Raimondi SC, et al. Immunological detection of minimal residual disease in children with acute lymphoblastic leukaemia. *Lancet*. 1998;351:550-554.

21. van Dongen JJ, Seriu T, Panzer-Grümayer ER, Biondi A, Pongers-Willemse MJ, Corral L, et al. Prognostic value of minimal residual disease in acute lymphoblastic leukaemia in childhood. *Lancet.* 1998;352:1731-1738.

22. Conter V, Bartram CR, Valsecchi MG, Schrauder A, Panzer-Grümayer R, Möricke A, et al. Molecular response to treatment redefines all prognostic factors in children and adolescents with B-cell precursor acute lymphoblastic leukemia: results in 3184 patients of the AIEOP-BFM ALL 2000 study. *Blood.* 2010;115:3206-3214.

23. Stow P, Key L, Chen X, Pan Q, Neale GA, Coustan-Smith E, et al. Clinical significance of low levels of minimal residual disease at the end of remission induction therapy in childhood acute lymphoblastic leukemia. *Blood.* 2010;115:4657-4663.

24. Simone JV. History of the treatment of childhood ALL: a paradigm for cancer cure. *Best Pract Res Clin Haematol.* 2006;19:353-359.

25. Goldie JH, Coldman AJ. A model for tumor response to chemotherapy: an integration of the stem cell and somatic mutation hypotheses. *Cancer Invest.* 1985;3:553-564.

26. Johnson RE. An experimental therapeutic approach to L1210 leukemia in mice: combined chemotherapy and central nervous system irradiation. *J Natl Cancer Inst.* 1964;32:1333-1341.

27. Simon R, Norton L. The Norton-Simon hypothesis: designing more effective and less toxic chemotherapeutic regimens. *Nat Clin Pract Oncol.* 2006;3:406-407.

28. Skipper HE, Schabel FM Jr, Wilcox WS. Experimental evaluation of potential anticancer agents. XIII. On the criteria and kinetics associated with "curability" of experimental leukemia. *Cancer Chemother Rep*. 1964;35:1-111.

29. Farber S, Diamond LK. Temporary remissions in acute leukemia in children produced by folic acid antagonist, 4-aminopteroyl-glutamic acid. *N Engl J Med.* 1948;238:787-793.

30. Skipper HE, Thomson JR, Elion GB, Hitchings GH. Observations on the anticancer activity of 6-mercaptopurine. *Cancer Res.* 1954;14:294-298.

31. Djerassi I, Farber S, Abir E, Neikirk W.Continuous infusion of methotrexate in children with acute leukemia. *Cancer*. 1967;20:233-242.

32. Krivit W, Brubaker C, Hartmann J, Murphy ML, Pierce M, Thatcher G. Induction of remission in acute leukemia of childhood by combination of prednisone and either 6-mercaptopurine or methotrexate. *J Pediatr.* 1966;68:965-968.

33. Frei E 3rd, Freireich EJ, Gehan E, Pinkel D, Holland JF, Selawry O, et al. Studies of sequential and combination antimetabolite therapy in acute leukemia: 6-mercaptopurine and methotrexate. *Blood* 1961;18:431-454.

34. Mathé G, Hayat M, Schwarzenberg L, Amiel JL, Schneider M, Cattan A, et al. Acute lymphoblastic leukaemia treated with a combination of prednisone, vincristine, and rubidomycin. Value of pathogen-free rooms. *Lancet.* 1967;2:380-382.

35. Oettgen HF, Old LJ, Boyse EA, Campbell HA, Philips FS, Clarkson BD. Inhibition of leukemias in man by L-asparaginase. *Cancer Res.* 1967;27:2619-2631.

36. Jacquillat C, Boiron M, Weil M, Tanzer J, Najean Y, Bernard J. Rubidomycin. A new agent active in the treatment of acute lymphoblastic leukaemia. *Lancet.* 1966;2:27-28.

37. Ellison RR, Holland JF, Weil M, Jacquillat C, Boiron M, Bernard J, et al. Arabinosyl cytosine: a useful agent in the treatment of acute leukemia in adults. *Blood.* 1968;32:507-523.

38. Fernbach DJ, Griffith KM, Haggard ME, Holcomb TM, Sutow WW, Vietti TJ, et al. Chemotherapy of acute leukemia in childhood. Comparison of cyclophosphamide and mercaptopurine. *N Engl J Med.* 1966;275:451-456.

39. Han T, Stutzman L, Cohen E, Kim U. Effect of platelet transfusion on hemorrhage in patients with acute leukemia. An autopsy study. *Cancer.* 1966;19:1937-1942.

40. Pinkel D, Simone J, Hustu HO, Aur RJ. Nine years' experience with "total therapy" of childhood acute lymphocytic leukemia. *Pediatrics.* 1972;50:246-251.

41. Bodey GP, Buckley M, Sathe YS, Freireich EJ. Quantitative relationships between circulating leukocytes and infection in patients with acute leukemia. *Ann Intern Med.* 1966;64:328-340.

42. Advances and challenges in infectious diseases supportive care of patients with hematologic malignancies, hematopoietic stem cell transplantation, and severe aplastic anemia. *Semin Hematol.* 2009;46:191-197.

43. Nowak-Göttl U, Kenet G, Mitchell LG. Thrombosis in childhood acute lymphoblastic leukaemia: epidemiology, aetiology, diagnosis, prevention and treatment. *Best Pract Res Clin Haematol.* 2009;22:103-114.

44. Rivera GK, Raimondi SC, Hancock ML, Behm FG, Pui CH, Abromowitch M, et al. Improved outcome in childhood acute lymphoblastic leukaemia with reinforced early treatment and rotational combination chemotherapy. *Lancet.* 1991;337:61-66.

45. Pui CH, Pei D, Sandlund JT, Ribeiro RC, Rubnitz JE, Raimondi SC, et al. Long-term results of St Jude Total Therapy Studies 11, 12, 13A, 13B, and 14 for childhood acute lymphoblastic leukemia. *Leukemia.* 2010;24:371-382.

46. Educational symposium on long-term results of large prospective clinical trials for childhood acute lymphoblastic leukemia (1985–2000). *Leukemia.* 2010; 24:253-428.

47. Woods WG, Ramsay NK, Kersey JH. Long-term follow-up of individuals undergoing allogeneic bone marrow transplantation for acute lymphocytic leukemia. *J Clin Oncol.* 1986;4:1015-1016.

48. Hahn T, Wall D, Camitta B, Davies S, Dillon H, Gaynon P, et al. The role of cytotoxic therapy with hematopoietic stem cell transplantation in the therapy of acute lymphoblastic leukemia in children: an evidence-based review. *Biol Blood Marrow Transplant.* 2005;11:823-861.

49. Pinkel D. 'Allogeneic marrow transplantation in children with acute leukemia: a practice whose time has gone': twenty years later. *Leukemia.* 2009;23:2189-2196.

50. Jeha S, Gaynon PS, Razzouk BI, Franklin J, Kadota R, Shen V, et al. Phase II study of clofarabine in pediatric patients with refractory or relapsed acute lymphoblastic leukemia. *J Clin Oncol.* 2006;24:1917-1923.

51. Berg SL, Blaney SM, Devidas M, Lampkin TA, Murgo A, Bernstein M, et al. Phase II study of nelarabine (compound 506U78) in children and young adults with refractory T-cell malignancies: a report from the Children's Oncology Group. *J Clin Oncol.* 2005;23:3376-3382.

52. Towatari M, Yanada M, Usui N, Takeuchi J, Sugiura I, Takeuchi M, et al; Japan Adult Leukemia Study Group. Combination of intensive chemotherapy and imatinib can rapidly induce high-quality complete remission for a majority of patients with newly diagnosed BCR-ABL-positive acute lymphoblastic leukemia. *Blood.* 2004;104:3507-3512.

53. Aricò M, Valsecchi MG, Camitta B, Schrappe M, Chessells J, Baruchel A, et al. Outcome of treatment in children with Philadelphia chromosome-positive acute lymphoblastic leukemia. *N Engl J Med.* 2000;342:998-1006.

54. Pui CH, Gaynon PS, Boyett JM, Chessells JM, Baruchel A, Kamps W, et al. Outcome of treatment in childhood acute lymphoblastic leukaemia with rearrangements of the 11q23 chromosomal region. *Lancet.* 2002;359:1909-1915.

55. Heerema NA, Nachman JB, Sather HN, Sensel MG, Lee MK, Hutchinson R, et al. Hypodiploidy with less than 45 chromosomes confers adverse risk in childhood acute lymphoblastic leukemia: a report from the children's cancer group. *Blood.* 1999;94:4036-4045.

56. Schrappe M, Reiter A, Ludwig WD, Harbott J, Zimmermann M, Hiddemann W, et al. Improved outcome in childhood acute lymphoblastic leukemia despite reduced use of anthracyclines and cranial radiotherapy: results of trial ALL-BFM 90. German-Austrian-Swiss ALL-BFM Study Group. *Blood.* 2000;95:3310-3322.

57. Mattano LA Jr, Sather HN, Trigg ME, Nachman JB. Osteonecrosis as a complication of treating acute lymphoblastic leukemia in children: a report from the Children's Cancer Group. *J Clin Oncol.* 2000;18:3262-3272.

58. Nachman J. Clinical characteristics, biologic features and outcome for young adult patients with acute lymphoblastic leukaemia. *Br J Haematol.* 2005;130:166-173.

59. Nathan PC, Wasilewski-Masker K, Janzen LA. Long-term outcomes in survivors of childhood acute lymphoblastic leukemia. *Hematol Oncol Clin North Am.* 2009;23:1065-1082.

60. George P, Hernandez K, Hustu O, Borella L, Holton C, Pinkel D. A study of "total therapy" of acute lymphocytic leukemia in children. *J Pediatr.* 1968;72:399-408.

61. Aur RJ, Simone J, Hustu HO, Walters T, Borella L, Pratt C, et al. Central nervous system therapy and combination chemotherapy of childhood lymphocytic leukemia. *Blood.* 1971;37:272-281.

62. D'Angio GJ, Littman P, Nesbit M, Sather H, Hittle R, Ortega J, et al. Evaluation of radiation therapy factors in prophylactic central nervous system irradiation for childhood leukemia: a report from the Children's Cancer Study Group. *Int J Radiat Oncol Biol Phys.* 1981;7:1031-1038.

63. Nesbit ME, Sather H, Robison LL, Donaldson M, Littman P, Ortega JA, et al. Sanctuary therapy: a randomized trial of 724 children with previously untreated acute lymphoblastic leukemia: A Report from Children's Cancer Study Group. *Cancer Res.* 1982;42:674-680.

64. Littman P, Coccia P, Bleyer WA, Lukens J, Siegel S, Miller D, Sather H, Hammond D. Central nervous system (CNS) prophylaxis in children with low risk acute lymphoblastic leukemia (ALL). *Int J Radiat Oncol Biol Phys.* 1987;13:1443-1449.

65. Sullivan MP, Chen T, Dyment PG, Hvizdala E, Steuber CP. Equivalence of intrathecal chemotherapy and radiotherapy as central nervous system prophylaxis in children with acute lymphatic leukemia: a pediatric oncology group study. *Blood.* 1982;60:948-958.

66. Nesbit ME Jr, Sather HN, Robison LL, Ortega J, Littman PS, D'Angio GJ, et al. Presymptomatic central nervous system therapy in previously untreated childhood acute lymphoblastic leukaemia: comparison of 1800 rad and 2400 rad. A report for Children's Cancer Study Group. *Lancet.* 1981;1:461-466.

67. Tubergen DG, Gilchrist GS, O'Brien RT, Coccia PF, Sather HN, Waskerwitz MJ, et al. Prevention of CNS disease in intermediate-risk acute lymphoblastic leukemia: comparison of cranial radiation and intrathecal methotrexate and the importance of systemic therapy: a Childrens Cancer Group report. *J Clin Oncol.* 1993;11:520-526.

68. Pui CH, Campana D, Pei D, Bowman WP, Sandlund JT, Kaste SC, et al. Treating childhood acute lymphoblastic leukemia without cranial irradiation. *N Engl J Med.* 2009;360:2730-2741.

69. Mitchell CD, Richards SM, Kinsey SE, Lilleyman J, Vora A, Eden TO. Benefit of dexamethasone compared with prednisolone for childhood acute lymphoblastic leukaemia: results of the UK Medical Research Council ALL97 randomized trial. *Br J Haematol.* 2005;129:734-745.

70. Ochs JJ. Neurotoxicity due to central nervous system therapy for childhood leukemia. *Am J Pediatr Hematol Oncol.* 1989;11:93-105.

71. Bleyer WA, Fallavollita J, Robison L, Balsom W, Meadows A, Heyn R, et al. Influence of age, sex, and concurrent intrathecal methotrexate therapy on intellectual function after cranial irradiation during childhood: a report from the Children's Cancer Study Group. *Pediatr Hematol Oncol.* 1990;7:329-338.

72. Laningham FH, Kun LE, Reddick WE, Ogg RJ, Morris EB, Pui CH. Childhood central nervous system leukemia: historical perspectives, current therapy, and acute neurological sequelae. *Neuroradiology.* 2007;49:873-888.

73. Riehm H. Leukemia Research: Advances in Cell Biology and Treatment (Murphy SB, Gilbery JR, eds). *NY Elsevier Biomed.* 1983:251-260.

74. Aricò M, Valsecchi MG, Conter V, Rizzari C, Pession A, Messina C, et a. Improved outcome in high-risk childhood acute lymphoblastic leukemia defined by prednisone-poor response treated with double Berlin-Frankfurt-Muenster protocol II. *Blood.* 2002;100:420-426.

75. Lange BJ, Bostrom BC, Cherlow JM, Sensel MG, La MK, Rackoff W, et al. Double-delayed intensification improves event-free survival for children with intermediate-risk acute lymphoblastic leukemia: a report from the Children's Cancer Group. *Blood.* 2002;99:825-833.

76. Nachman JB, Sather HN, Sensel MG, Trigg ME, Cherlow JM, Lukens JN, et al. Augmented post-induction therapy for children with high-risk acute

lymphoblastic leukemia and a slow response to initial therapy. *N Engl J Med.* 1998;338:1663-1671.

77. Capizzi RL. Asparaginase revisited. *Leuk Lymphoma.* 1993;10Suppl:147-150.

78. Clavell LA, Gelber RD, Cohen HJ, Hitchcock-Bryan S, Cassady JR, Tarbell NJ, et al. Four-agent induction and intensive asparaginase therapy for treatment of childhood acute lymphoblastic leukemia. *N Engl J Med.* 1986;315:657-663.

79. Chessells JM. Acute lymphoblastic leukemia. *Semin Hematol.* 1982;19:155-171.

80. Miller DR, Leikin SL, Albo VC, Sather H, Hammond GD. Three versus five years of maintenance therapy are equivalent in childhood acute lymphoblastic leukemia: a report from the Childrens Cancer Study Group. *J Clin Oncol.* 1989;7:316-325.

81. Duration and intensity of maintenance chemotherapy in acute lymphoblastic leukaemia: overview of 42 trials involving 12 000 randomised children. Childhood ALL Collaborative Group. *Lancet.* 1996;347:1783-1788.

82. Conter V, Valsecchi MG, Silvestri D, Campbell M, Dibar E, Magyarosy E, et al. Pulses of vincristine and dexamethasone in addition to intensive chemotherapy for children with intermediate-risk acute lymphoblastic leukaemia: a multicentre randomised trial. *Lancet.* 2007;369:123-131.

83. Kamen BA. Serendipity-methotrexate and 6-mercaptopurine for continuation therapy for patients with acute lymphoblastic leukemia: the leukemic stem cell and beyond? *J Pediatr Hematol Oncol.* 2009;31:383-384.

84. Pui CH, Crist WM. Biology and treatment of acute lymphoblastic leukemia. *J Pediatr.* 1994;124:491-503.

85. Lin TL, Vala MS, Barber JP, Karp JE, Smith BD, Matsui W, et al. Induction of acute lymphocytic leukemia differentiation by maintenance therapy. *Leukemia.* 2007;21:1915-1920.

86. Schmiegelow K, Al-Modhwahi I, Andersen MK, Behrendtz M, Forestier E, Hasle H, et al. Methotrexate/6-mercaptopurine maintenance therapy influences the risk of a second malignant neoplasm after childhood acute lymphoblastic leukemia: results from the NOPHO ALL-92 study. *Blood.* 2009;113:6077-6084.

87. Schultz KR, Bowman WP, Aledo A, Slayton WB, Sather H, Devidas M, et al. Improved early event-free survival with imatinib in Philadelphia chromosome-positive acute lymphoblastic leukemia: a children's oncology group study. *J Clin Oncol.* 2009;27:5175-5181.

88. Harvey RC, Mullighan CG, Chen IM, Wharton W, Mikhail FM, Carroll AJ, et al. Rearrangement of CRLF2 is associated with mutation of JAK kinases, alteration of IKZF1, Hispanic/Latino ethnicity, and a poor outcome in pediatric B-progenitor acute lymphoblastic leukemia. *Blood.* 2010;115:5312-5321.

89. Zipursky A, Poon A, Doyle J. Leukemia in Down syndrome: a review. *Pediatr Hematol Oncol*. 1992;9:139-149.

90. Xavier AC, Taub JW. Acute leukemia in children with Down syndrome. *Haematologica*. 2010;95:1043-1045.

91. Gale KB, Ford AM, Repp R, Borkhardt A, Keller C, Eden OB, et al. Backtracking leukemia to birth: identification of clonotypic gene fusion sequences in neonatal blood spots. *Proc Natl Acad Sci U S A*. 1997;94:13950-13954.

92. McNally RJ, Eden TO. An infectious aetiology for childhood acute leukaemia: a review of the evidence. *Br J Haematol*. 2004;127:243-263.

93. Stiller CA, Kroll ME, Boyle PJ, Feng Z. Population mixing, socioeconomic status and incidence of childhood acute lymphoblastic leukaemia in England and Wales: analysis by census ward. *Br J Cancer*. 2008;98:1006-1011.

94. Kinlen LJ, Clarke K, Hudson C. Evidence from population mixing in British New Towns 1946-85 of an infective basis for childhood leukaemia. *Lancet*. 1990;336:577-582.

95. Moorman AV, Ensor HM, Richards SM, Chilton L, Schwab C, Kinsey SE, et al. Prognostic effect of chromosomal abnormalities in childhood B-cell precursor acute lymphoblastic leukaemia: results from the UK Medical Research Council ALL97/99 randomised trial. *Lancet Oncol.* 2010;11:429-438.

96. Heerema NA, Sather HN, Sensel MG, Zhang T, Hutchinson RJ, Nachman JB, et al. Prognostic impact of trisomies of chromosomes 10, 17, and 5 among children with acute lymphoblastic leukemia and high hyperdiploidy (> 50 chromosomes). *J Clin Oncol.* 2000;18:1876-1887.

97. Armstrong SA, Mabon ME, Silverman LB, Li A, Gribben JG, Fox EA, et al. FLT3 mutations in childhood acute lymphoblastic leukemia. *Blood.* 2004;103:3544-3546.

98. Whitehead VM, Vuchich MJ, Lauer SJ, Mahoney D, Carroll AJ, Shuster JJ, et al. Accumulation of high levels of methotrexate polyglutamates in lymphoblasts from children with hyperdiploid (greater than 50 chromosomes) B-lineage acute lymphoblastic leukemia: a Pediatric Oncology Group study. *Blood.* 1992;80:1316-1323.

99. Nachman JB, Heerema NA, Sather H, Camitta B, Forestier E, Harrison CJ, et al. Outcome of treatment in children with hypodiploid acute lymphoblastic leukemia. *Blood.* 2007;110:1112-1115.

100. Greaves M. Darwin and evolutionary tales in leukemia. The Ham-Wasserman Lecture. *Hematology Am Soc Hematol Educ Program.* 2009:3-12.

101. Romana SP, Poirel H, Leconiat M, Flexor MA, Mauchauffé M, Jonveaux P, et al. High frequency of t(12;21) in childhood B-lineage acute lymphoblastic leukemia. *Blood.* 1995;86:4263-4269.

102. Raynaud S, Cave H, Baens M, Bastard C, Cacheux V, Grosgeorge J, et al. The 12;21 translocation involving TEL and deletion of the other TEL allele: two frequently associated alterations found in childhood acute lymphoblastic leukemia. *Blood.* 1996;87:2891-2899.

103. Loh ML, Goldwasser MA, Silverman LB, Poon WM, Vattikuti S, Cardoso A, et al. Prospective analysis of TEL/AML1-positive patients treated on Dana-Farber Cancer Institute Consortium Protocol 95-01. *Blood.* 2006;107:4508-4513.

104. Raimondi SC, Behm FG, Roberson PK, Williams DL, Pui CH, Crist WM, et al. Cytogenetics of pre-B-cell acute lymphoblastic leukemia with emphasis on prognostic implications of the t(1;19). *J Clin Oncol.* 1990;8:1380-1388.

105. Jeha S, Pei D, Raimondi SC, Onciu M, Campana D, Cheng C, et al. Increased risk for CNS relapse in pre-B cell leukemia with the t(1;19)/TCF3-PBX1. *Leukemia.* 2009;23:1406-1409.

106. Uckun FM, Sensel MG, Sather HN, Gaynon PS, Arthur DC, Lange BJ, et al. Clinical significance of translocation t(1;19) in childhood acute lymphoblastic leukemia in the context of contemporary therapies: a report from the Children's Cancer Group. *J Clin Oncol.* 1998;16:527-535.

107. Jones LK, Saha V. Philadelphia positive acute lymphoblastic leukaemia of childhood. *Br J Haematol.* 2005;130:489-500.

108. Chen CS, Sorensen PH, Domer PH, Reaman GH, Korsmeyer SJ, Heerema NA, et al. Molecular rearrangements on chromosome 11q23 predominate in infant acute lymphoblastic leukemia and are associated with specific biologic variables and poor outcome. *Blood.* 1993;81:2386-2393.

109. Armstrong SA, Staunton JE, Silverman LB, Pieters R, den Boer ML, Minden MD, et al. MLL translocations specify a distinct gene expression profile that distinguishes a unique leukemia. *Nat Genet.* 2002;30:41-47.

110. Inaba T, Roberts WM, Shapiro LH, Jolly KW, Raimondi SC, Smith SD, et al. Fusion of the leucine zipper gene HLF to the E2A gene in human acute B-lineage leukemia. *Science.* 1992;257:531-534.

111. Aifantis I, Raetz E, Buonamici S. Molecular pathogenesis of T-cell leukaemia and lymphoma. *Nat Rev Immunol.* 2008;8:380-390.

112. Bergeron J, Clappier E, Radford I, Buzyn A, Millien C, Soler G, et al. Prognostic and oncogenic relevance of TLX1/HOX11 expression level in T-ALLs. *Blood.* 2007;110:2324-2330.

113. Van Vlierberghe P, Pieters R, Beverloo HB, Meijerink JP. Molecular-genetic insights in paediatric T-cell acute lymphoblastic leukaemia. *Br J Haematol.* 2008;143:153-168.

114. Mullighan CG. Mutations of NOTCH1, FBXW7, and prognosis in T-lineage acute lymphoblastic leukemia. *Haematologica.* 2009;94:1338-1340.

115. Nguyen K, Devidas M, Cheng SC, La M, Raetz EA, Carroll WL, et al. Factors influencing survival after relapse from acute lymphoblastic leukemia: a Children's Oncology Group study. *Leukemia.* 2008;22:2142-2150.

116. Gatta G, Zigon G, Capocaccia R, Coebergh JW, Desandes E, Kaatsch P, et al; EUROCARE Working Group. Survival of European children and young adults with cancer diagnosed 1995-2002. *Eur J Cancer.* 2009;45:992-1005.

117. Mullighan CG, Phillips LA, Su X, Ma J, Miller CB, Shurtleff SA, et al. Genomic analysis of the clonal origins of relapsed acute lymphoblastic leukemia. *Science.* 2008;322:1377-1380.

118. Kang H, Chen IM, Wilson CS, Bedrick EJ, Harvey RC, Atlas SR, et al. Gene expression classifiers for relapse-free survival and minimal residual disease improve risk classification and outcome prediction in pediatric B-precursor acute lymphoblastic leukemia. *Blood.* 2010;115:1394-1405.

119. Mullighan CG, Zhang J, Harvey RC, Collins-Underwood JR, Schulman BA, Phillips LA, et al. JAK mutations in high-risk childhood acute lymphoblastic leukemia. *Proc Natl Acad Sci U S A.* 2009;106:9414-9418.

120. Den Boer ML, van Slegtenhorst M, De Menezes RX, Cheok MH, Buijs-Gladdines JG, Peters ST, et al. A subtype of childhood acute lymphoblastic leukaemia with poor treatment outcome: a genome-wide classification study. *Lancet Oncol.* 2009;10:125-134.

121. Mullighan CG, Su X, Zhang J, Radtke I, Phillips LA, Miller CB, et al; Children's Oncology Group. Deletion of IKZF1 and prognosis in acute lymphoblastic leukemia. *N Engl J Med.* 2009;360:470-480.

122. Kirschner-Schwabe R, Lottaz C, Tödling J, Rhein P, Karawajew L, Eckert C, et al. Expression of late cell cycle genes and an increased proliferative capacity characterize very early relapse of childhood acute lymphoblastic leukemia. *Clin Cancer Res.* 2006;12:4553-4561.

123. Colmone A, Amorim M, Pontier AL, Wang S, Jablonski E, Sipkins DA. Leukemic cells create bone marrow niches that disrupt the behavior of normal hematopoietic progenitor cells. *Science.* 2008;322:1861-1865.

124. Yang JJ, Cheng C, Yang W, Pei D, Cao X, Fan Y, et al. Genome-wide interrogation of germline genetic variation associated with treatment response in childhood acute lymphoblastic leukemia. *JAMA.* 2009;301:393-403.

125. Stanulla M, Schaeffeler E, Flohr T, Cario G, Schrauder A, Zimmermann M, et al. Thiopurine methyltransferase (TPMT) genotype and early treatment response to mercaptopurine in childhood acute lymphoblastic leukemia. *JAMA.* 2005;293:1485-1489.

126. Iwamoto S, Mihara K, Downing JR, Pui CH, Campana D. Mesenchymal cells regulate the response of acute lymphoblastic leukemia cells to asparaginase. *J Clin Invest.* 2007;117:1049-1057.

127. Meads MB, Hazlehurst LA, Dalton WS. The bone marrow microenvironment as a tumor sanctuary and contributor to drug resistance. *Clin Cancer Res.* 2008;14:2519-2526.

128. Krishnan S, Wade R, Moorman AV, Mitchell C, Kinsey SE, Eden TO, et al. Temporal changes in the incidence and pattern of central nervous system relapses in children with acute lymphoblastic leukaemia treated on four consecutive Medical Research Council trials, 1985-2001. *Leukemia.* 2010;24:450-459.

129. Papayannopoulou T, Scadden DT. Stem-cell ecology and stem cells in motion. *Blood.* 2008;111:3923-3930.

130. Massberg S, von Andrian UH. Novel trafficking routes for hematopoietic stem and progenitor cells. *Ann N Y Acad Sci.* 2009;1176:87-93.

131. Fragoso R, Pereira T, Wu Y, Zhu Z, Cabeçadas J, Dias S. VEGFR-1 (FLT-1) activation modulates acute lymphoblastic leukemia localization and survival within the bone marrow, determining the onset of extramedullary disease. *Blood.* 2006;107:1608-1616.

132. Hansson F, Toporski J, Månsson R, Johansson B, Norén-Nyström U, Jacobsen SE, et al. Exit of pediatric pre-B acute lymphoblastic leukaemia cells from the bone marrow to the peripheral blood is not associated with cell maturation or alterations in gene expression. *Mol Cancer.* 2008;7:67.

133. Juarez JG, Thien M, Dela Pena A, Baraz R, Bradstock KF, Bendall LJ. CXCR4 mediates the homing of B cell progenitor acute lymphoblastic leukaemia cells to the bone marrow via activation of p38MAPK. *Br J Haematol.* 2009;145:491-499.

134. Crazzolara R, Bernhard D. CXCR4 chemokine receptors, histone deacetylase inhibitors and acute lymphoblastic leukemia. *Leuk Lymphoma.* 2005;46:1545-1551.

135. Crazzolara R, Kreczy A, Mann G, Heitger A, Eibl G, Fink FM, et al. High expression of the chemokine receptor CXCR4 predicts extramedullary organ infiltration in childhood acute lymphoblastic leukaemia. *Br J Haematol.* 2001;115:545-553.

136. Bendall LJ, Nilsson SK, Khan NI, James A, Bonnet C, Lock RB, et al. Role of CD44 variant exon 6 in acute lymphoblastic leukaemia: association with altered bone marrow localisation and increased tumour burden. *Leukemia.* 2004;18:1308-1311.

137. Khan NI, Cisterne A, Devidas M, Shuster J, Hunger SP, Shaw PJ, et al. Expression of CD44, but not CD44v6, predicts relapse in children with B cell progenitor acute lymphoblastic leukemia lacking adverse or favorable genetics. *Leuk Lymphoma.* 2008;49:710-718.

138. Taçyildiz N, Cavdar AO, Yavuz G, Gözdaşoglu S, Unal E, Ertem U, et al. Serum levels and differential expression of CD44 in childhood leukemia and malignant lymphoma: correlation with prognostic criteria and survival. *Pediatr Int.* 2001;43:354-360.

139. Buonamici S, Trimarchi T, Ruocco MG, Reavie L, Cathelin S, Mar BG, at al. CCR7 signalling as an essential regulator of CNS infiltration in T-cell leukaemia. *Nature.* 2009;459:1000-1004.

140. Cario G, Izraeli S, Teichert A, Rhein P, Skokowa J, Möricke A, et al. High interleukin-15 expression characterizes childhood acute lymphoblastic leukemia with involvement of the CNS. *J Clin Oncol.* 2007;25:4813-4820.

141. Juric D, Lacayo NJ, Ramsey MC, Racevskis J, Wiernik PH, Rowe JM, et al. Differential gene expression patterns and interaction networks in BCR-ABL-positive and -negative adult acute lymphoblastic leukemias. *J Clin Oncol.* 2007;25:1341-1349.

142. Rhein P, Mitlohner R, Basso G, Gaipa G, Dworzak MN, Kirschner-Schwabe R, et al. CD11b is a therapy resistance- and minimal residual disease-specific marker in precursor B-cell acute lymphoblastic leukemia. *Blood.* 2010;115:3763-3771.

143. Polman CH, O'Connor PW, Havrdova E, Hutchinson M, Kappos L, Miller DH, et al; AFFIRM Investigators. A randomized, placebo-controlled trial of

natalizumab for relapsing multiple sclerosis. *N Engl J Med.* 2006;354:899-910.

144. Lobb RR, Hemler ME. The pathophysiologic role of alpha 4 integrins in vivo. *J Clin Invest.* 1994;94:1722-1728.

145. Friedl P, Bröcker EB. T cell migration in three-dimensional extracellular matrix: guidance by polarity and sensations. *Dev Immunol.* 2000;7:249-266.

146. Bradstock KF, Gottlieb DJ. Interaction of acute leukemia cells with the bone marrow microenvironment: implications for control of minimal residual disease. *Leuk Lymphoma.* 1995;18:1-16.

147. Engelhardt B, Wolburg H. Mini-review: Transendothelial migration of leukocytes: through the front door or around the side of the house? *Eur J Immunol.* 2004;34:2955-2963.

148. Bartholomäus I, Kawakami N, Odoardi F, Schläger C, Miljkovic D, Ellwart JW, et al. Effector T cell interactions with meningeal vascular structures in nascent autoimmune CNS lesions. *Nature.* 2009;462:94-98.

149. Carman CV. Mechanisms for transcellular diapedesis: probing and pathfinding by 'invadosome-like protrusions'. *J Cell Sci.* 2009;122:3025-3035.

150. Stefanidakis M, Karjalainen K, Jaalouk DE, Gahmberg CG, O'Brien S, Pasqualini R, et al. Role of leukemia cell invadosome in extramedullary infiltration. *Blood.* 2009;114:3008-3017.

151. Kuittinen O, Savolainen ER, Koistinen P, Möttönen M, Turpeenniemi-Hujanen T. MMP-2 and MMP-9 expression in adult and childhood acute lymphatic leukemia (ALL). *Leuk Res.* 2001;25:125-131.

152. Suminoe A, Matsuzaki A, Hattori H, Koga Y, Ishii E, Hara T. Expression of matrix metalloproteinase (MMP) and tissue inhibitor of MMP (TIMP) genes in blasts of infant acute lymphoblastic leukemia with organ involvement. *Leuk Res.* 2007;31:1437-1440.

153. Klein G, Vellenga E, Fraaije MW, Kamps WA, de Bont ES. The possible role of matrix metalloproteinase (MMP)-2 and MMP-9 in cancer, e.g. acute leukemia. *Crit Rev Oncol Hematol.* 2004;50:87-100.

154. Jevnikar Z, Obermajer N, Bogyo M, Kos J. The role of cathepsin X in the migration and invasiveness of T lymphocytes. *J Cell Sci.* 2008;121:2652-2661.

155. Gocheva V, Joyce JA. Cysteine cathepsins and the cutting edge of cancer invasion. *Cell Cycle.* 2007;6:60-64.

156. Ghinassi B, Martelli F, Verrucci M, D'Amore E, Migliaccio G, Vannucchi AM, et al. Evidence for organ-specific stem cell microenvironments. *J Cell Physiol.* 2010;223:460-470.

157. Han J, Koh YJ, Moon HR, Ryoo HG, Cho CH, Kim I, et al. Adipose tissue is an extramedullary reservoir for functional hematopoietic stem and progenitor cells. *Blood.* 2010;115:957-964.

158. Kaplan RN, Riba RD, Zacharoulis S, Bramley AH, Vincent L, Costa C, et al. VEGFR1-positive haematopoietic bone marrow progenitors initiate the pre-metastatic niche. *Nature.* 2005;438:820-827.

159. Gerber HP, Malik AK, Solar GP, Sherman D, Liang XH, Meng G, et al. VEGF regulates haematopoietic stem cell survival by an internal autocrine loop mechanism. *Nature.* 2002;417:954-958.

160. Gaundar SS, Bradstock KF, Bendall LJ. p38MAPK inhibitors attenuate cytokine production by bone marrow stromal cells and reduce stroma-mediated proliferation of acute lymphoblastic leukemia cells. *Cell Cycle.* 2009;8:2975-2983.

161. Mullighan CG, Collins-Underwood JR, Phillips LA, Loudin MG, Liu W, Zhang J, et al. Rearrangement of CRLF2 in B-progenitor- and Down syndrome-associated acute lymphoblastic leukemia. *Nat Genet.* 2009;41:1243-1246.

162. Ayala F, Dewar R, Kieran M, Kalluri R. Contribution of bone microenvironment to leukemogenesis and leukemia progression. *Leukemia.* 2009;23:2233-2241.

163. Madan S, Kumar S. Review: extramedullary disease in multiple myeloma. *Clin Adv Hematol Oncol.* 2009;7:802-804.

164. Astier AL, Svoboda M, Hinds E, De Beaumont R, Munoz O, Freedman AS. Integrins regulate survival of pre-B-ALL cells through differential IAP and caspase-7 ubiquitination and degradation. *Leukemia.* 2004;18:873-875.

165. Nervi B, Ramirez P, Rettig MP, Uy GL, Holt MS, Ritchey JK, et al. Chemosensitization of acute myeloid leukemia (AML) following mobilization by the CXCR4 antagonist AMD3100. *Blood.* 2009;113:6206-6214.

166. Heyn C, Ronald JA, Ramadan SS, Snir JA, Barry AM, MacKenzie LT, et al. In vivo MRI of cancer cell fate at the single-cell level in a mouse model of breast cancer metastasis to the brain. *Magn Reson Med.* 2006;56:1001-1010.

167. Rameshwar P. Breast cancer cell dormancy in bone marrow: potential therapeutic targets within the marrow microenvironment. *Expert Rev Anticancer Ther.* 2010;10:129-132.

## Chapter 2

1. Strefford JC, van Delft FW, Robinson HM, Worley H, Yiannikouris O, Selzer R, et al. Complex genomic alterations and gene expression in acute lymphoblastic leukemia with intrachromosomal amplification of chromosome 21. *Proc Natl Acad Sci U S A.* 2006;103:8167-8172.

2. Moorman AV, Richards SM, Robinson HM, Strefford JC, Gibson BE, Kinsey SE, et al; UK Medical Research Council (MRC)/National Cancer Research Institute (NCRI) Childhood Leukaemia Working Party (CLWP).Prognosis of children with acute lymphoblastic leukemia (ALL) and intrachromosomal amplification of chromosome 21 (iAMP21). *Blood.* 2007;109:2327-2330.

3. Li DN, Matthews SP, Antoniou AN, Mazzeo D, Watts C. Multistep autoactivation of asparaginyl endopeptidase in vitro and in vivo. *J Biol Chem.* 2003;278:38980-38990.

4. Dalton JP, Brindley PJ, Donnelly S, Robinson MW. The enigmatic asparaginyl endopeptidase of helminth parasites. *Trends Parasitol.* 2009;25:59-61.

5. León-Félix J, Ortega-López J, Orozco-Solís R, Arroyo R. Two novel asparaginyl endopeptidase-like cysteine proteinases from the protist Trichomonas vaginalis: their evolutionary relationship within the clan CD cysteine proteinases. *Gene.* 2004;335:25-35.

6. Ramón-Luing LA, Rendón-Gandarilla FJ, Cárdenas-Guerra RE, Rodríguez-Cabrera NA, Ortega-López J, Avila-González L, et al. Immunoproteomics of the active degradome to identify biomarkers for Trichomonas vaginalis. *Proteomics.* 2010;10:435-444.

7. Wu B, Yin J, Texier C, Roussel M, Tan KS. Blastocystis legumain is localized on the cell surface, and specific inhibition of its activity implicates a pro-survival role for the enzyme. *J Biol Chem.* 2010;285:1790-1798.

8. Tort J, Brindley PJ, Knox D, Wolfe KH, Dalton JP. Proteinases and associated genes of parasitic helminths. *Adv Parasitol.* 1999;43:161-266.

9. Skelly PJ, Shoemaker CB. Schistosoma mansoni proteases Sm31 (cathepsin B) and Sm32 (legumain) are expressed in the cecum and protonephridia of cercariae. *J Parasitol.* 2001;87:1218-1221.

10. Mathieu MA, Bogyo M, Caffrey CR, Choe Y, Lee J, Chapman H, et al. Substrate specificity of schistosome versus human legumain determined by P1-P3 peptide libraries. *Mol Biochem Parasitol.* 2002;121:99-105.

11. Sajid M, McKerrow JH, Hansell E, Mathieu MA, Lucas KD, Hsieh I, et al. Functional expression and characterization of Schistosoma mansoni cathepsin B and its trans-activation by an endogenous asparaginyl endopeptidase. *Mol Biochem Parasitol.* 2003;131:65-75.

12. Li C, Shi Y. Observation on the effect of Sj32DNA vaccine of Schistosoma japonicum. *Zhongguo Ji Sheng Chong Xue Yu Ji Sheng Chong Bing Za Zhi*. 1999;17:70-73. Chinese

13. Laha T, Sripa J, Sripa B, Pearson M, Tribolet L, Kaewkes S, et al. Asparaginyl endopeptidase from the carcinogenic liver fluke, Opisthorchis viverrini, and its potential for serodiagnosis. *Int J Infect Dis.* 2008;12:e49-59.

14. Tkalcevic J, Ashman K, Meeusen E. Fasciola hepatica: rapid identification of newly excysted juvenile proteins. *Biochem Biophys Res Commun.* 1995;213:169-174.

15. Ju JW, Joo HN, Lee MR, Cho SH, Cheun HI, Kim JY, et al. Identification of a serodiagnostic antigen, legumain, by immunoproteomic analysis of excretory-secretory products of Clonorchis sinensis adult worms. *Proteomics.* 2009;9:3066-3078.

16. Murray J, Manoury B, Balic A, Watts C, Maizels RM. Bm-CPI-2, a cystatin from Brugia malayi nematode parasites, differs from Caenorhabditis elegans cystatins in a specific site mediating inhibition of the antigen-processing enzyme AEP. *Mol Biochem Parasitol.* 2005;139:197-203.

17. Sojka D, Hajdusek O, Dvorák J, Sajid M, Franta Z, Schneider EL, et al. IrAE: an asparaginyl endopeptidase (legumain) in the gut of the hard tick Ixodes ricinus. *Int J Parasitol.* 2007;37:713-724.

18. Sojka D, Franta Z, Horn M, Hajdusek O, Caffrey CR, Mares M, et al.. Profiling of proteolytic enzymes in the gut of the tick Ixodes ricinus reveals an evolutionarily conserved network of aspartic and cysteine peptidases. *Parasit Vectors.* 2008;1:7.

19. Horn M, Nussbaumerová M, Sanda M, Kovárová Z, Srba J, Franta Z, et al. Hemoglobin digestion in blood-feeding ticks: mapping a multipeptidase pathway by functional proteomics. *Chem Biol.* 2009;16:1053-1063.

20. Abdul Alim M, Tsuji N, Miyoshi T, Khyrul Islam M, Huang X, Motobu M, et al. Characterization of asparaginyl endopeptidase, legumain induced by blood

feeding in the ixodid tick Haemaphysalis longicornis. *Insect Biochem Mol Biol.* 2007;37:911-922.

21. Alim MA, Tsuji N, Miyoshi T, Islam MK, Huang X, Hatta T, et al. HlLgm2, a member of asparaginyl endopeptidases/legumains in the midgut of the ixodid tick Haemaphysalis longicornis, is involved in blood-meal digestion. J Insect Physiol. 2008;54:573-585.

22. Alim MA, Tsuji N, Miyoshi T, Islam MK, Hatta T, Fujisaki K. Legumains from the hard tick Haemaphysalis longicornis play modulatory roles in blood feeding and gut cellular remodelling and impact on embryogenesis. *Int J Parasitol.* 2009;39:97-107.

23. Chen JM, Dando PM, Rawlings ND, Brown MA, Young NE, Stevens RA, et al. Cloning, isolation, and characterization of mammalian legumain, an asparaginyl endopeptidase. *J Biol Chem.* 1997;272:8090-8098.

24. Liu C, Sun C, Huang H, Janda K, Edgington T. Overexpression of legumain in tumors is significant for invasion/metastasis and a candidate enzymatic target for prodrug therapy. *Cancer Res.* 2003;63:2957-2964.

25. Tarte K, Zhan F, De Vos J, Klein B, Shaughnessy J Jr. Gene expression profiling of plasma cells and plasmablasts: toward a better understanding of the late stages of B-cell differentiation. *Blood.* 2003;102:592-600.

26. Manoury B, Mazzeo D, Li DN, Billson J, Loak K, Benaroch P, et al. Asparagine endopeptidase can initiate the removal of the MHC class II invariant chain chaperone. *Immunity.* 2003;18:489-498.

27. Manoury B, Hewitt EW, Morrice N, Dando PM, Barrett AJ, Watts C. An asparaginyl endopeptidase processes a microbial antigen for class II MHC presentation. *Nature.* 1998;396:695-699.

28. Antoniou AN, Blackwood SL, Mazzeo D, Watts C. Control of antigen presentation by a single protease cleavage site. *Immunity.* 2000;12:391-398.

29. Matthews SP, Werber I, Deussing J, Peters C, Reinheckel T, Watts C. Distinct protease requirements for antigen presentation in vitro and in vivo. *J Immunol.* 2010;184:2423-2431.

30. Manoury B, Mazzeo D, Fugger L, Viner N, Ponsford M, Streeter H, et al. Destructive processing by asparagine endopeptidase limits presentation of a dominant T cell epitope in MBP. *Nat Immunol.* 2002;3:169-174.

31. Maehr R, Hang HC, Mintern JD, Kim YM, Cuvillier A, Nishimura M, et al. Asparagine endopeptidase is not essential for class II MHC antigen presentation but is required for processing of cathepsin L in mice. *J Immunol.* 2005;174:7066-7074.

32. Sepulveda FE, Maschalidi S, Colisson R, Heslop L, Ghirelli C, Sakka E, et al. Critical role for asparagine endopeptidase in endocytic Toll-like receptor signaling in dendritic cells. *Immunity.* 2009;31:737-748.

33. Wolk K, Grütz G, Witte K, Volk HD, Sabat R. The expression of legumain, an asparaginyl endopeptidase that controls antigen processing, is reduced in endotoxin-tolerant monocytes. *Genes Immun.* 2005;6:452-456.

34. Probst-Kepper M, Geffers R, Kröger A, Viegas N, Erck C, Hecht HJ, et al. GARP: a key receptor controlling FOXP3 in human regulatory T cells. *J Cell Mol Med.* 2009;13:3343-3357.

35. Zeeuwen PL, van Vlijmen-Willems IM, Hendriks W, Merkx GF, Schalkwijk J. A null mutation in the cystatin M/E gene of ichq mice causes juvenile lethality and defects in epidermal cornification. *Hum Mol Genet.* 2002;11:2867-2875.

36. Zeeuwen PL, van Vlijmen-Willems IM, Olthuis D, Johansen HT, Hitomi K, Hara-Nishimura I, et al. Evidence that unrestricted legumain activity is involved in disturbed epidermal cornification in cystatin M/E deficient mice. *Hum Mol Genet.* 2004;13:1069-1079.

37. Zeeuwen PL. Epidermal differentiation: the role of proteases and their inhibitors. *Eur J Cell Biol.* 2004;83:761-773.

38. Kubota K, Wakabayashi K, Matsuoka T. Proteome analysis of secreted proteins during osteoclast differentiation using two different methods: two-dimensional electrophoresis and isotope-coded affinity tags analysis with two-dimensional chromatography. *Proteomics.* 2003;3:616-626.

39. Choi SJ, Kurihara N, Oba Y, Roodman GD. Osteoclast inhibitory peptide 2 inhibits osteoclast formation via its C-terminal fragment. *J Bone Miner Res.* 2001;16:1804-1811.

40. Choi SJ, Reddy SV, Devlin RD, Menaa C, Chung H, Boyce BF, et al. Identification of human asparaginyl endopeptidase (legumain) as an inhibitor of osteoclast formation and bone resorption. *J Biol Chem.* 1999;274:27747-27753.

41. Ledgard AM, Lee RS, Peterson AJ. Bovine endometrial legumain and TIMP-2 regulation in response to presence of a conceptus. *Mol Reprod Dev.* 2009;76:65-74.

42. Usami M, Mitsunaga K, Nakazawa K. Comparative proteome analysis of the embryo proper and yolk sac membrane of day 11.5 cultured rat embryos. *Birth Defects Res B Dev Reprod Toxicol.* 2007;80:383-395.

43. Mattock KL, Gough PJ, Humphries J, Burnand K, Patel L, Suckling KE, et al. Legumain and cathepsin-L expression in human unstable carotid plaque. *Atherosclerosis.* 2010;208:83-89.

44. Clerin V, Shih HH, Deng N, Hebert G, Resmini C, Shields KM, et al. Expression of the cysteine protease legumain in vascular lesions and functional implications in atherogenesis. *Atherosclerosis.* 2008;201:53-66.

45. Papaspyridonos M, Smith A, Burnand KG, Taylor P, Padayachee S, Suckling KE, et al. Novel candidate genes in unstable areas of human atherosclerotic plaques. *Arterioscler Thromb Vasc Biol.* 2006;26:1837-1844.

46. Ishizaki T, Erickson A, Kuric E, Shamloo M, Hara-Nishimura I, Inácio AR, et al. The asparaginyl endopeptidase legumain after experimental stroke. *J Cereb Blood Flow Metab.* 2010 Mar 17. [Epub ahead of print]

47. Liu Z, Jang SW, Liu X, Cheng D, Peng J, Yepes M, et al. Neuroprotective actions of PIKE-L by inhibition of SET proteolytic degradation by asparagine endopeptidase. *Mol Cell.* 2008;29:665-678.

48. Nagata N, Oshida T, Yoshida NL, Yuyama N, Sugita Y, Tsujimoto G, et al. Analysis of highly expressed genes in monocytes from atopic dermatitis patients. *Int Arch Allergy Immunol.* 2003;132:156-167.

49. Shirahama-Noda K, Yamamoto A, Sugihara K, Hashimoto N, Asano M, Nishimura M, et al. Biosynthetic processing of cathepsins and lysosomal degradation are abolished in asparaginyl endopeptidase-deficient mice. *J Biol Chem.* 2003;278:33194-33139.

50. Chan CB, Abe M, Hashimoto N, Hao C, Williams IR, Liu X, et al. Mice lacking asparaginyl endopeptidase develop disorders resembling hemophagocytic syndrome. *Proc Natl Acad Sci U S A.* 2009;106:468-473.

51. Nagasawa T. Microenvironmental niches in the bone marrow required for B-cell development. *Nat Rev Immunol.* 2006;6:107-116.

52. van Zelm MC, van der Burg M, de Ridder D, Barendregt BH, de Haas EF, Reinders MJ, et al. Ig gene rearrangement steps are initiated in early human precursor B cell subsets and correlate with specific transcription factor expression. *J Immunol.* 2005;175:5912-5922. Supplemental data.

53. Yeoh EJ, Ross ME, Shurtleff SA, Williams WK, Patel D, Mahfouz R, et al. Classification, subtype discovery, and prediction of outcome in pediatric acute lymphoblastic leukemia by gene expression profiling. *Cancer Cell.* 2002;1:133-143. (Table 11, Supplementary data).

54. Kohlmann A, Schoch C, Schnittger S, Dugas M, Hiddemann W, Kern W, et al. Pediatric acute lymphoblastic leukemia (ALL) gene expression signatures classify an independent cohort of adult ALL patients. *Leukemia.* 2004;18:63-71.

55. De Vos J, Thykjaer T, Tarte K, Ensslen M, Raynaud P, Requirand G, et al. Comparison of gene expression profiling between malignant and normal plasma cells with oligonucleotide arrays. *Oncogene.* 2002;21:6848-6857.

56. Dave SS, Wright G, Tan B, Rosenwald A, Gascoyne RD, Chan WC, et al. Prediction of survival in follicular lymphoma based on molecular features of tumor-infiltrating immune cells. *N Engl J Med.* 2004;351:2159-2169.

57. Murthy RV, Arbman G, Gao J, Roodman GD, Sun XF. Legumain expression in relation to clinicopathologic and biological variables in colorectal cancer. *Clin Cancer Res.* 2005;11:2293-2299.

58. Gawenda J, Traub F, Lück HJ, Kreipe H, von Wasielewski R. Legumain expression as a prognostic factor in breast cancer patients.*Breast Cancer Res Treat.* 2007;102:1-6.

59. Moparthi SB, Arbman G, Wallin A, Kayed H, Kleeff J, Zentgraf H, et al. Expression of MAC30 protein is related to survival and biological variables in primary and metastatic colorectal cancers. *Int J Oncol.* 2007;30:91-95.

60. Widegren E, Onnesjö S, Arbman G, Kayed H, Zentgraf H, Kleeff J, et al. Expression of FXYD3 protein in relation to biological and clinicopathological variables in colorectal cancers. *Chemotherapy.* 2009;55:407-413.

61. Wu W, Luo Y, Sun C, Liu Y, Kuo P, Varga J, et al. Targeting cell-impermeable prodrug activation to tumor microenvironment eradicates multiple drug-resistant neoplasms. *Cancer Res.* 2006;66:970-980.

62. Morita Y, Araki H, Sugimoto T, Takeuchi K, Yamane T, Maeda T, et al. Legumain/asparaginyl endopeptidase controls extracellular matrix remodeling through the degradation of fibronectin in mouse renal proximal tubular cells. *FEBS Lett.* 2007;581:1417-1424.

63. Chen JM, Fortunato M, Stevens RA, Barrett AJ. Activation of progelatinase A by mammalian legumain, a recently discovered cysteine proteinase. *Biol Chem.* 2001;382:777-783.

64. Liu C. Annual Scientific Report 2006, Dept of Immunology, The Scripps Research Institute. (http://tinyurl.com/ScrippsLGMN, last accessed 15 July 2010).

65. Sarandeses CS, Covelo G, Díaz-Jullien C, Freire M. Prothymosin alpha is processed to thymosin alpha 1 and thymosin alpha 11 by a lysosomal asparaginyl endopeptidase. *J Biol Chem.* 2003;278:13286-13293.

66. Ueda H, Fujita R, Yoshida A, Matsunaga H, Ueda M. Identification of prothymosin-alpha1, the necrosis-apoptosis switch molecule in cortical neuronal cultures. *J Cell Biol.* 2007;176:853-862.

67. Qin Y, Chen FD, Zhou L, Gong XG, Han QF. Proliferative and anti-proliferative effects of thymosin alpha1 on cells are associated with manipulation of cellular ROS levels. *Chem Biol Interact.* 2009;180:383-388.

68. Luo Y, Zhou H, Krueger J, Kaplan C, Lee SH, Dolman C, et al. Targeting tumor-associated macrophages as a novel strategy against breast cancer. *J Clin Invest.* 2006;116:2132-2141.

69. Xiang R, Luo Y, Niethammer AG, Reisfeld RA. Oral DNA vaccines target the tumor vasculature and microenvironment and suppress tumor growth and metastasis. *Immunol Rev.* 2008;222:117-128.

70. Lewēn S, Zhou H, Hu HD, Cheng T, Markowitz D, Reisfeld RA, et al. A Legumain-based minigene vaccine targets the tumor stroma and suppresses breast cancer growth and angiogenesis. *Cancer Immunol Immunother.* 2008;57:507-515.

71. Vigneswaran N, Wu J, Nagaraj N, James R, Zeeuwen P, Zacharias W. Silencing of cystatin M in metastatic oral cancer cell line MDA-686Ln by siRNA increases cysteine proteinases and legumain activities, cell proliferation and in vitro invasion. *Life Sci.* 2006;78:898-907.

72. Briggs JJ, Haugen MH, Johansen HT, Riker AI, Abrahamson M, Fodstad Ø, et al. Cystatin E/M suppresses legumain activity and invasion of human melanoma. *BMC Cancer.* 2010;10:17.

73. Hughes SJ, Glover TW, Zhu XX, Kuick R, Thoraval D, Orringer MB, et al. A novel amplicon at 8p22-23 results in overexpression of cathepsin B in esophageal adenocarcinoma. *Proc Natl Acad Sci U S A*. 1998;95:12410-12415.

74. Lin L, Aggarwal S, Glover TW, Orringer MB, Hanash S, Beer DG. A minimal critical region of the 8p22-23 amplicon in esophageal adenocarcinomas defined using sequence tagged site-amplification mapping and quantitative polymerase chain reaction includes the GATA-4 gene. *Cancer Res.* 2000;60:1341-1347.

75. Berquin IM, Cao L, Fong D, Sloane BF. Identification of two new exons and multiple transcription start points in the 5'-untranslated region of the human cathepsin-B-encoding gene. *Gene.* 1995;159:143-149.

76. Seth P, Mahajan VS, Chauhan SS. Transcription of human cathepsin L mRNA species hCATL B from a novel alternative promoter in the first intron of its gene. *Gene.* 2003 Dec 4;321:83-91.

77. Arora S, Chauhan SS. Identification and characterization of a novel human cathepsin L splice variant. *Gene.* 2002;293:123-131.

78. Yan S, Sloane BF. Molecular regulation of human cathepsin B: implication in pathologies. *Biol Chem.* 2003;384:845-854.

79. Gong Q, Chan SJ, Bajkowski AS, Steiner DF, Frankfater A. Characterization of the cathepsin B gene and multiple mRNAs in human tissues: evidence for alternative splicing of cathepsin B pre-mRNA. *DNA Cell Biol.* 1993;12:299-309.

80. Berquin IM, Yan S, Katiyar K, Huang L, Sloane BF, Troen BR. Differentiating agents regulate cathepsin B gene expression in HL-60 cells. *J Leukoc Biol.* 1999;66:609-616.

81. Reddy VY, Zhang QY, Weiss SJ. Pericellular mobilization of the tissue-destructive cysteine proteinases, cathepsins B, L, and S, by human

monocyte-derived macrophages. *Proc Natl Acad Sci U S A.* 1995;92:3849-3853.

82. Punturieri A, Filippov S, Allen E, Caras I, Murray R, Reddy V, et al. Regulation of elastinolytic cysteine proteinase activity in normal and cathepsin K-deficient human macrophages. *J Exp Med.* 2000;192:789-799.

83. Allinen M, Beroukhim R, Cai L, Brennan C, Lahti-Domenici J, Huang H, et al. Molecular characterization of the tumor microenvironment in breast cancer. *Cancer Cell.* 2004;6:17-32.

84. Flannery T, Gibson D, Mirakhur M, McQuaid S, Greenan C, Trimble A, et al. The clinical significance of cathepsin S expression in human astrocytomas. *Am J Pathol.* 2003;163:175-182.

85. Mikkelsen T, Yan PS, Ho KL, Sameni M, Sloane BF, Rosenblum ML. Immunolocalization of cathepsin B in human glioma: implications for tumor invasion and angiogenesis. *J Neurosurg.* 1995;83:285-290.

86. Campo E, Muñoz J, Miquel R, Palacín A, Cardesa A, Sloane BF, et al. Cathepsin B expression in colorectal carcinomas correlates with tumor progression and shortened patient survival. *Am J Pathol.* 1994;145:301-309.

87. Podgorski I, Linebaugh BE, Sameni M, Jedeszko C, Bhagat S, Cher ML, et al. Bone microenvironment modulates expression and activity of cathepsin B in prostate cancer. *Neoplasia.* 2005;7(3):207-223.

88. Schraufstatter IU, Trieu K, Zhao M, Rose DM, Terkeltaub RA, Burger M. IL-8-mediated cell migration in endothelial cells depends on cathepsin B activity and transactivation of the epidermal growth factor receptor. *J Immunol.* 2003;171:6714-6722.

89. Nishimura Y, Itoh K, Yoshioka K, Uehata M, Himeno M. Small guanosine triphosphatase Rho/Rho-associated kinase as a novel regulator of intracellular redistribution of lysosomes in invasive tumor cells. *Cell Tissue Res.* 2000;301:341-351.

90. Nishimura Y, Itoh K, Yoshioka K, Tokuda K, Himeno M. Overexpression of ROCK in human breast cancer cells: evidence that ROCK activity mediates intracellular membrane traffic of lysosomes. *Pathol Oncol Res.* 2003;9:83-95.

91. Nishimura Y, Yoshioka K, Bernard O, Himeno M, Itoh K. LIM kinase 1: evidence for a role in the regulation of intracellular vesicle trafficking of lysosomes and endosomes in human breast cancer cells. *Eur J Cell Biol.* 2004;83:369-380.

92. Steffan JJ, Williams BC, Welbourne T, Cardelli JA. HGF-induced invasion by prostate tumor cells requires anterograde lysosome trafficking and activity of Na+-H+ exchangers. *J Cell Sci.* 2010;123:1151-1159.

93. Fukuda M. Lysosomal membrane glycoproteins. Structure, biosynthesis, and intracellular trafficking. *J Biol Chem.* 1991;266:21327-21330.

94. Krueger S, Haeckel C, Buehling F, Roessner A. Inhibitory effects of antisense cathepsin B cDNA transfection on invasion and motility in a human osteosarcoma cell line. *Cancer Res.* 1999;59:6010-6014.

95. Mohanam S, Jasti SL, Kondraganti SR, Chandrasekar N, Lakka SS, Kin Y, t al. Down-regulation of cathepsin B expression impairs the invasive and tumorigenic potential of human glioblastoma cells. *Oncogene.* 2001;20:3665-3673.

96. Krueger S, Kellner U, Buehling F, Roessner A. Cathepsin L antisense oligonucleotides in a human osteosarcoma cell line: effects on the invasive phenotype. *Cancer Gene Ther.* 2001;8:522-528.

97. Cavallo-Medved D, Mai J, Dosescu J, Sameni M, Sloane BF. Caveolin-1 mediates the expression and localization of cathepsin B, pro-urokinase plasminogen activator and their cell-surface receptors in human colorectal carcinoma cells. *J Cell Sci.* 2005;118:1493-1503.

98. Mai J, Finley RL Jr, Waisman DM, Sloane BF. Human procathepsin B interacts with the annexin II tetramer on the surface of tumor cells. *J Biol Chem.* 2000;275:12806-12812.

99. Cavallo-Medved D, Dosescu J, Linebaugh BE, Sameni M, Rudy D, Sloane BF. Mutant K-ras regulates cathepsin B localization on the surface of human colorectal carcinoma cells. *Neoplasia.* 2003;5:507-519.

100. Roshy S, Sloane BF, Moin K. Pericellular cathepsin B and malignant progression. *Cancer Metastasis Rev.* 2003;22:271-286.

101. Cougoule C, Le Cabec V, Poincloux R, Al Saati T, Mège JL, Tabouret G, et al. Three-dimensional migration of macrophages requires Hck for podosome organization and extracellular matrix proteolysis. *Blood.* 2010;115:1444-1452.

102. Collette J, Bocock JP, Ahn K, Chapman RL, Godbold G, Yeyeodu S, et al. Biosynthesis and alternate targeting of the lysosomal cysteine protease cathepsin L. *Int Rev Cytol.* 2004;241:1-51.

103. Idone V, Tam C, Andrews NW. Two-way traffic on the road to plasma membrane repair. *Trends Cell Biol.* 2008;18:552-559.

104. Gronowicz G, Swift H, Steck TL. Maturation of the reticulocyte in vitro. *J Cell Sci.* 1984 ;71:177-197.

105. Obermajer N, Jevnikar Z, Doljak B, Sadaghiani AM, Bogyo M, Kos J. Cathepsin X-mediated beta2 integrin activation results in nanotube outgrowth. *Cell Mol Life Sci.* 2009;66:1126-1134.

106. Saftig P, Klumperman J. Lysosome biogenesis and lysosomal membrane proteins: trafficking meets function. *Nat Rev Mol Cell Biol.* 2009;10:623-635.

107. Lechner AM, Assfalg-Machleidt I, Zahler S, Stoeckelhuber M, Machleidt W, Jochum M, et al. RGD-dependent binding of procathepsin X to integrin alphavbeta3 mediates cell-adhesive properties. *J Biol Chem.* 2006;281:39588-39597.

108. Alblas J, Ulfman L, Hordijk P, Koenderman L. Activation of Rhoa and ROCK are essential for detachment of migrating leukocytes. *Mol Biol Cell.* 2001;12:2137-2145.

109. Mohamed MM, Sloane BF. Cysteine cathepsins: multifunctional enzymes in cancer. *Nat Rev Cancer.* 2006;6:764-775.

110. Sahai E, Marshall CJ. Differing modes of tumour cell invasion have distinct requirements for Rho/ROCK signalling and extracellular proteolysis. *Nat Cell Biol.* 2003;5:711-719.

111. Luzio JP, Pryor PR, Bright NA. Lysosomes: fusion and function. *Nat Rev Mol Cell Biol.* 2007;8:622-632.

112. Obermajer N, Jevnikar Z, Doljak B, Kos J. Role of cysteine cathepsins in matrix degradation and cell signalling. *Connect Tissue Res.* 2008;49:193-196.

113. Colvin RA, Means TK, Diefenbach TJ, Moita LF, Friday RP, Sever S, et al. Synaptotagmin-mediated vesicle fusion regulates cell migration. *Nat Immunol.* 2010;11:495-502.

114. Constantin G, Laudanna C. Leukocyte chemotaxis: from lysosomes to motility. *Nat Immunol.* 2010;11:463-464.

115. Waghray A, Keppler D, Sloane BF, Schuger L, Chen YQ. Analysis of a truncated form of cathepsin H in human prostate tumor cells. *J Biol Chem.* 2002;277:11533-11538.

116. Cavallo-Medved D, Sloane BF. Cell-surface cathepsin B: understanding its functional significance. *Curr Top Dev Biol.* 2003;54:313-341.

117. Harrison JS, Rameshwar P, Chang V, Bandari P. Oxygen saturation in the bone marrow of healthy volunteers. *Blood.* 2002;99:394.

118. Fiegl M, Samudio I, Clise-Dwyer K, Burks JK, Mnjoyan Z, Andreeff M. CXCR4 expression and biologic activity in acute myeloid leukemia are dependent on oxygen partial pressure. *Blood.* 2009;113:1504-1512.

119. Rozhin J, Sameni M, Ziegler G, Sloane BF. Pericellular pH affects distribution and secretion of cathepsin B in malignant cells. *Cancer Res.* 1994;54:6517-6525.

120. Gatenby RA, Gawlinski ET, Gmitro AF, Kaylor B, Gillies RJ. Acid-mediated tumor invasion: a multidisciplinary study. *Cancer Res.* 2006;66:5216-5223.

121. Ishidoh K, Kominami E. Procathepsin L degrades extracellular matrix proteins in the presence of glycosaminoglycans in vitro. *Biochem Biophys Res Commun.* 1995;217:624-631.

122. Almeida PC, Nantes IL, Chagas JR, Rizzi CC, Faljoni-Alario A, Carmona E, et al. Cathepsin B activity regulation. Heparin-like glycosaminogylcans protect human cathepsin B from alkaline pH-induced inactivation. J Biol Chem. 2001;276:944-951.

123. Kafienah W, Brömme D, Buttle DJ, Croucher LJ, Hollander AP. Human cathepsin K cleaves native type I and II collagens at the N-terminal end of the triple helix. *Biochem J.* 1998;331:727-732.

124. Friedrichs B, Tepel C, Reinheckel T, Deussing J, von Figura K, Herzog V, et al. Thyroid functions of mouse cathepsins B, K, and L. *J Clin Invest.* 2003;111:1733-1745.

125. Xia L, Kilb J, Wex H, Li Z, Lipyansky A, Breuil V, et al. Localization of rat cathepsin K in osteoclasts and resorption pits: inhibition of bone resorption and cathepsin K-activity by peptidyl vinyl sulfones. *Biol Chem.* 1999;380:679-687.

126. Wang B, Sun J, Kitamoto S, Yang M, Grubb A, Chapman HA, et al. Cathepsin S controls angiogenesis and tumor growth via matrix-derived angiogenic factors. *J Biol Chem.* 2006;281:6020-6029.

127. Premzl A, Zavasnik-Bergant V, Turk V, Kos J. Intracellular and extracellular cathepsin B facilitate invasion of MCF-10A neoT cells through reconstituted extracellular matrix in vitro. *Exp Cell Res.* 2003;283:206-214.

128. Lerdrup M, Bruun S, Grandal MV, Roepstorff K, Kristensen MM, Hommelgaard AM, et al. Endocytic down-regulation of ErbB2 is stimulated by cleavage of its C-terminus. *Mol Biol Cell.* 2007;18:3656-3666

129. Safaei R, Larson BJ, Cheng TC, Gibson MA, Otani S, Naerdemann W, et al. Abnormal lysosomal trafficking and enhanced exosomal export of cisplatin in drug-resistant human ovarian carcinoma cells. *Mol Cancer Ther.* 2005;4:1595-1604.

## Chapter 3

1. Chomczynski P, Sacchi N. The single-step method of RNA isolation by acid guanidinium thiocyanate-phenol-chloroform extraction: twenty-something years on. *Nat Protoc.* 2006;1:581-585.

2. Lee J, Bogyo M. Development of near-infrared fluorophore (NIRF)-labeled activity-based probes for in vivo imaging of legumain. *ACS Chem Biol.* 2010;5:233-243.

3. Gry M, Rimini R, Strömberg S, Asplund A, Pontén F, Uhlén M, et al. Correlations between RNA and protein expression profiles in 23 human cell lines. *BMC Genomics.* 2009;10:365.

4. Michaud J, Simpson KM, Escher R, Buchet-Poyau K, Beissbarth T, Carmichael C, et al. Integrative analysis of RUNX1 downstream pathways and target genes. *BMC Genomics*. 2008;9:363.

5. Ivanov A, Beers SA, Walshe CA, Honeychurch J, Alduaij W, Cox KL, et al. Monoclonal antibodies directed to CD20 and HLA-DR can elicit homotypic adhesion followed by lysosome-mediated cell death in human lymphoma and leukemia cells. *J Clin Invest.* 2009;119:2143-2159.

## Chapter 4

1. Zalai CV, Kolodziejczyk MD, Pilarski L, Christov A, Nation PN, Lundstrom-Hobman M, et al. Increased circulating monocyte activation in patients with unstable coronary syndromes. *J Am Coll Cardiol.* 2001;38:1340-1347.

2. American Type Culture Collection Standards Development Organization Workgroup ASN-0002. Cell line misidentification: the beginning of the end. *Nat Rev Cancer.* 2010;10:441-448.

3. Hughes P, Marshall D, Reid Y, Parkes H, Gelber C. The costs of using unauthenticated, over-passaged cell lines: how much more data do we need? *Biotechniques.* 2007;43:575, 577-8, 581-582 passim.

## Chapter 5

1. Gaynon PS, Desai AA, Bostrom BC, Hutchinson RJ, Lange BJ, Nachman JB, et al. Early response to therapy and outcome in childhood acute lymphoblastic leukemia: a review. *Cancer.* 1997;80:1717-1726.

2. Uckun FM, Stork L, Seibel N, Sarquis M, Bedros C, Sather H, et al. Residual bone marrow leukemic progenitor cell burden after induction chemotherapy in pediatric patients with acute lymphoblastic leukemia. *Clin Cancer Res.* 2000;6:3123-3130.

3. Galderisi F, Stork L, Li J, Mori M, Mongoue-Tchokote S, Huang J. Flow cytometric chemosensitivity assay as a predictive tool of early clinical response in acute lymphoblastic leukemia. *Pediatr Blood Cancer.* 2009;53:543-550.

4. Cortez MA, Scrideli CA, Yunes JA, Valera ET, Toledo SR, Pavoni-Ferreira PC, et al. mRNA expression profile of multidrug resistance genes in childhood acute lymphoblastic leukemia. Low expression levels associated with a higher risk of toxic death. *Pediatr Blood Cancer.* 2009;53:996-1004.

5. Kidd JG, Sobin LH. The incorporation of l-asparagine-14C by lymphoma 6C3HED cells: its inhibition by guinea pig serum. *Cancer Res.* 1966;26:208-211.

6. Cooney DA, Handschumacher RE. L-asparaginase and L-asparagine metabolism. *Annu Rev Pharmacol.* 1970;10:421-440.

7. Shan J, Lopez MC, Baker HV, Kilberg MS. Expression profiling after activation of the amino acid deprivation response in HepG2 human hepatoma cells. *Physiol Genomics.* 2010 Mar 9 [Epub ahead of print]

8. Asselin BL, Ryan D, Frantz CN, Bernal SD, Leavitt P, Sallan SE, et al. In vitro and in vivo killing of acute lymphoblastic leukemia cells by L-asparaginase. *Cancer Res.* 1989;49:4363-4368.

9. Nandy P, Periclou AP, Avramis VI. The synergism of 6-mercaptopurine plus cytosine arabinoside followed by PEG-asparaginase in human leukemia cell lines (CCRF/CEM/0 and (CCRF/CEM/ara-C/7A) is due to increased cellular apoptosis. *Anticancer Res.* 1998;18:727-737.

10. Panosyan EH, Grigoryan RS, Avramis IA, Seibel NL, Gaynon PS, Siegel SE, et al. Deamination of glutamine is a prerequisite for optimal asparagine deamination by asparaginases in vivo (CCG-1961). *Anticancer Res.* 2004;24:1121-1125.

11. Hernández-Espinosa D, Miñano A, Martínez C, Pérez-Ceballos E, Heras I, Fuster JL, et al. L-asparaginase-induced antithrombin type I deficiency: implications for conformational diseases. *Am J Pathol.* 2006;169:142-153.

12. Kidd JG. Regression of transplanted lymphomas induced in vivo by means of normal guinea pig serum. I. Course of transplanted cancers of various kinds in mice and rats given guinea pig serum, horse serum, or rabbit serum. *J Exp Med.* 1953;98:565-582.

13. Broome JD. Evidence that the L-Asparaginase activity of guinea pig serum is responsible for its antilymphoma effects*. Nature* 1961;191:1114-1115.

14. Old LJ, Boyse EA, Campbell HA, Daria GM. Leukaemia-inhibiting properties and L-asparaginase activity of sera from certain South American rodents. *Nature.* 1963;198:801.

15. Boyse EA, Old LJ, Campbell HA, Mashburn LT. Suppression of murine leukemias by L-asparaginase. Incidence of sensitivity among leukemias of various types: comparative inhibitory activities of guinea pig serum L-asparaginase and Escherichia coli L-asparaginase. *J Exp Med.* 1967;125:17-31.

16. Mashburn LT. Wriston JC Jr. Tumor inhibitory effect of L-asparaginase from Escherichia coli. *Arch Biochem Biophys.* 1964;105:450-452.

17. Oettgen HF, Old LJ, Boyse EA, Campbell HA, Philips FS, Clarkson BD, et al. Inhibition of leukemias in man by L-asparaginase. *Cancer Res.* 1967;27:2619-2631.

18. Tallal L, Tan C, Oettgen H, Wollner N, McCarthy M, Helson L, et al. E. coli L-asparaginase in the treatment of leukemia and solid tumors in 131 children. *Cancer.* 1970;25:306-320.

19. Sutow WW, Garcia F, Starling KA, Williams TE, Lane DM, Gehan EA. L-asparaginase therapy in children with advanced leukemia. The Southwest Cancer Chemotherapy Study Group. *Cancer.* 1971;28:819-824.

20. Jaffe N, Traggis D, Das L, Moloney WC, Hann HW, Kim BS, et al. L-asparaginase in the treatment of neoplastic diseases in children. *Cancer Res.* 1971;31:942-949.

21. Ortega JA, Nesbit ME Jr, Donaldson MH, Hittle RE, Weiner J, Karon M, et al. L-Asparaginase, vincristine, and prednisone for induction of first remission in acute lymphocytic leukemia. *Cancer Res.* 1977;37:535-540.

22. Reaman GH, Ladisch S, Echelberger C, Poplack DG. Improved treatment results in the management of single and multiple relapses of acute lymphoblastic leukemia. *Cancer.* 1980;45:3090-3094.

23. Sallan SE, Hitchcock-Bryan S, Gelber R, Cassady JR, Frei E 3rd, Nathan DG. Influence of intensive asparaginase in the treatment of childhood non-T-cell acute lymphoblastic leukemia. *Cancer Res.* 1983;43:5601-5607.

24. Douer D. Is asparaginase a critical component in the treatment of acute lymphoblastic leukemia? *Best Pract Res Clin Haematol.* 2008;21:647-658.

25. Asselin BL, Kreissman S, Coppola DJ, Bernal SD, Leavitt PR, Gelber RD, et al. Prognostic significance of early response to a single dose of asparaginase in childhood acute lymphoblastic leukemia. *J Pediatr Hematol Oncol.* 1999;21:6-12.

26. Silverman LB, Gelber RD, Dalton VK, Asselin BL, Barr RD, Clavell LA, et al. Improved outcome for children with acute lymphoblastic leukemia: results of Dana-Farber Consortium Protocol 91-01. *Blood.* 2001;97:1211-1218.

27. Pession A, Valsecchi MG, Masera G, Kamps WA, Magyarosy E, Rizzari C, et al. Long-term results of a randomized trial on extended use of high dose L-asparaginase for standard risk childhood acute lymphoblastic leukemia. *J Clin Oncol.* 2005;23:7161-7167.

28. Duval M, Suciu S, Ferster A, Rialland X, Nelken B, Lutz P, et al. Comparison of Escherichia coli-asparaginase with Erwinia-asparaginase in the treatment of childhood lymphoid malignancies: results of a randomized European Organisation for Research and Treatment of Cancer-Children's Leukemia Group phase 3 trial. *Blood.* 2002;99:2734-2739.

29. Capizzi RL. Asparaginase-methotrexate in combination chemotherapy: schedule-dependent differential effects on normal versus neoplastic cells. *Cancer Treat Rep.* 1981;65 Suppl 4:115-121.

30. Ramakers-van Woerden NL, Pieters R, Loonen AH, Hubeek I, van Drunen E, Beverloo HB, et al. TEL/AML1 gene fusion is related to in vitro drug sensitivity for L-asparaginase in childhood acute lymphoblastic leukemia. *Blood.* 2000;96:1094-1099.

31. Prager MD, Bachynsky N. Asparagine synthetase in asparaginase resistant and susceptible mouse lymphomas. *Biochem Biophys Res Commun.* 1968;31:43-47.

32. Haskell CM, Canellos GP. L-asparaginase resistance in human leukemia--asparagine synthetase. *Biochem Pharmacol.* 1969;18:2578-2580.

33. Kiriyama Y, Kubota M, Takimoto T, Kitoh T, Tanizawa A, Akiyama Y, et al. Biochemical characterization of U937 cells resistant to L-asparaginase: the role of asparagine synthetase. *Leukemia.* 1989;3:294-297.

34. Aslanian AM, Fletcher BS, Kilberg MS. Asparagine synthetase expression alone is sufficient to induce L-asparaginase resistance in MOLT-4 human leukaemia cells. *Biochem J.* 2001;357:321-328.

35. Li BS, Gu LJ, Luo CY, Li WS, Jiang LM, Shen SH, et al. The downregulation of asparagine synthetase expression can increase the sensitivity of cells resistant to L-asparaginase. *Leukemia.* 2006;20:2199-2201.

36. Scherf U, Ross DT, Waltham M, Smith LH, Lee JK, Tanabe L, et al. A gene expression database for the molecular pharmacology of cancer. *Nat Genet.* 2000;24:236-244.

37. Stams WA, den Boer ML, Holleman A, Appel IM, Beverloo HB, van Wering ER, et al. Asparagine synthetase expression is linked with L-asparaginase resistance in TEL-AML1-negative but not TEL-AML1-positive pediatric acute lymphoblastic leukemia. *Blood.* 2005;105:4223-4225.

38. Stams WA, den Boer ML, Beverloo HB, Meijerink JP, Stigter RL, van Wering ER, et al. Sensitivity to L-asparaginase is not associated with expression levels of asparagine synthetase in t(12;21)+ pediatric ALL. *Blood.* 2003;101:2743-2747.

39. Appel IM, den Boer ML, Meijerink JP, Veerman AJ, Reniers NC, Pieters R. Up-regulation of asparagine synthetase expression is not linked to the clinical response L-asparaginase in pediatric acute lymphoblastic leukemia. *Blood.* 2006;107:4244-4249.

40. Krejci O, Starkova J, Otova B, Madzo J, Kalinova M, Hrusak O, et al. Upregulation of asparagine synthetase fails to avert cell cycle arrest induced by L-asparaginase in TEL/AML1-positive leukaemic cells. *Leukemia.* 2004;18:434-441.

41. Appel IM, Kazemier KM, Boos J, Lanvers C, Huijmans J, Veerman AJ, et al. Pharmacokinetic, pharmacodynamic and intracellular effects of PEG-

asparaginase in newly diagnosed childhood acute lymphoblastic leukemia: results from a single agent window study. *Leukemia.* 2008;22:1665-1679.

42. Panosyan EH, Seibel NL, Martin-Aragon S, Gaynon PS, Avramis IA, Sather H, et al. Asparaginase antibody and asparaginase activity in children with higher-risk acute lymphoblastic leukemia: Children's Cancer Group Study CCG-1961. *J Pediatr Hematol Oncol.* 2004;26:217-226.

43. Holcenberg J. Optimal asparaginase therapy. *J Pediatr Hematol Oncol.* 2004;26:273-274.

44. Asselin BL, Whitin JC, Coppola DJ, Rupp IP, Sallan SE, Cohen HJ. Comparative pharmacokinetic studies of three asparaginase preparations. *J Clin Oncol.* 1993;11:1780-1786.

45. Vrooman LM, Supko JG, Neuberg DS, Asselin BL, Athale UH, Clavell L, et al. Erwinia asparaginase after allergy to E. coli asparaginase in children with acute lymphoblastic leukemia. *Pediatr Blood Cancer.* 2010;54:199-205.

46. Wang B, Relling MV, Storm MC, Woo MH, Ribeiro R, Pui CH, et al. Evaluation of immunologic crossreaction of antiasparaginase antibodies in acute lymphoblastic leukemia (ALL) and lymphoma patients. *Leukemia.* 2003;17:1583-1588.

47. Moghrabi A, Levy DE, Asselin B, Barr R, Clavell L, Hurwitz C, et al. Results of the Dana-Farber Cancer Institute ALL Consortium Protocol 95-01 for children with acute lymphoblastic leukemia. *Blood.* 2007;109:896-904.

48. Allas S, Sahakian P, Fichtner I, Abribat T. Pharmacokinetics and pharmacodynamics in mice of a pegylated recombinant Erwinia Chrysanthemi-derived L-Asparaginase. *Blood (ASH Annual Meeting Abstracts).* 2009;114: 2033.

49. Allas S, Sahakian P, Fichtner I, Abribat T. Immunogenicity profile in mice of a pegylated recombinant Erwinia Chrysanthemi-derived L-Asparaginase. *Blood (ASH Annual Meeting Abstracts).* 2009;114: 2034.

50. Abshire TC, Pollock BH, Billett AL, Bradley P, Buchanan GR. Weekly polyethylene glycol conjugated L-asparaginase compared with biweekly dosing produces superior induction remission rates in childhood relapsed acute lymphoblastic leukemia: a Pediatric Oncology Group Study. *Blood.* 2000;96:1709-1715.

51. Avramis VI, Sencer S, Periclou AP, Sather H, Bostrom BC, Cohen LJ, et al. A randomized comparison of native Escherichia coli asparaginase and polyethylene glycol conjugated asparaginase for treatment of children with newly diagnosed standard-risk acute lymphoblastic leukemia: a Children's Cancer Group study. *Blood.* 2002;99:1986-1994.

52. Armstrong JK, Hempel G, Koling S, Chan LS, Fisher T, Meiselman HJ, et al. Antibody against poly(ethylene glycol) adversely affects PEG-asparaginase therapy in acute lymphoblastic leukemia patients. *Cancer.* 2007;110:103-111.

53. Caruso V, Iacoviello L, Di Castelnuovo A, Storti S, Mariani G, de Gaetano G, et al. Thrombotic complications in childhood acute lymphoblastic leukemia: a meta-analysis of 17 prospective studies comprising 1752 pediatric patients. *Blood.* 2006;108:2216-2222.

54. Knoderer HM, Robarge J, Flockhart DA. Predicting asparaginase-associated pancreatitis. *Pediatr Blood Cancer.* 2007;49:634-639.

55. Earl M. Incidence and management of asparaginase-associated adverse events in patients with acute lymphoblastic leukemia. *Clin Adv Hematol Oncol.* 2009;7:600-606.

56. Holland J, Fasanello S, Onuma T. Psychiatric symptoms associated with L-asparaginase administration. *J Psychiatr Res.* 1974;10:105-113.

57. Cohen H, Bielorai B, Harats D, Toren A, Pinhas-Hamiel O. Conservative treatment of L-asparaginase-associated lipid abnormalities in children with acute lymphoblastic leukemia. *Pediatr Blood Cancer.* 2010;54:703-706.

58. Vieira Pinheiro JP, Wenner K, Escherich G, Lanvers-Kaminsky C, Würthwein G, Janka-Schaub G, et al. Serum asparaginase activities and asparagine concentrations in the cerebrospinal fluid after a single infusion of 2,500 IU/m(2) PEG asparaginase in children with ALL treated according to protocol COALL-06-97. *Pediatr Blood Cancer.* 2006;46:18-25.

59. Gaynon PS. Childhood acute lymphoblastic leukaemia and relapse. *Br J Haematol.* 2005;131:579-587.

60. Jarrar M, Gaynon PS, Periclou AP, Fu C, Harris RE, Stram D, et al. Asparagine depletion after pegylated E. coli asparaginase treatment and induction outcome in children with acute lymphoblastic leukemia in first bone marrow relapse: a Children's Oncology Group study (CCG-1941). *Pediatr Blood Cancer.* 2006;47:141-146.

61. Riccardi R, Holcenberg JS, Glaubiger DL, Wood JH, Poplack DG. L-asparaginase pharmacokinetics and asparagine levels in cerebrospinal fluid of rhesus monkeys and humans. *Cancer Res.* 1981;41:4554-4558.

62. Appel IM, Pinheiro JP, den Boer ML, Lanvers C, Reniers NC, Boos J, et al. Lack of asparagine depletion in the cerebrospinal fluid after one intravenous dose of PEG-asparaginase: a window study at initial diagnosis of childhood ALL. *Leukemia.* 2003;17:2254-2256.

63. Boos J, Werber G, Ahlke E, Schulze-Westhoff P, Nowak-Göttl U, Würthwein G, et al. Monitoring of asparaginase activity and asparagine levels in children on different asparaginase preparations. *Eur J Cancer.* 1996;32:1544-1550.

64. Pinheiro JP, Boos J. The best way to use asparaginase in childhood acute lymphatic leukaemia--still to be defined? *Br J Haematol.* 2004;125:117-127.

65. Ohnuma T, Holland JF, Freeman A, Sinks LF. Biochemical and pharmacological studies with asparaginase in man. *Cancer Res.* 1970;30:2297-2305.

66. Brueck M, Koerholz D, Nuernberger W, Juergens H, Goebel U, Wahn V. Elimination of L-asparaginase in children treated for acute lymphoblastic leukemia. *Dev Pharmacol Ther.* 1989;12:200-204.

67. Broome JD. Factors which may influence the effectiveness of L-asparaginases as tumor inhibitors. *Br J Cancer.* 1968;22:595-602.

68. Lanvers C, Vieira Pinheiro JP, Hempel G, Wuerthwein G, Boos J. Analytical validation of a microplate reader-based method for the therapeutic drug monitoring of L-asparaginase in human serum. *Anal Biochem.* 2002;309:117-126.

69. Werner A, Röhm KH, Müller HJ. Mapping of B-cell epitopes in E. coli asparaginase II, an enzyme used in leukemia treatment. *Biol Chem*. 2005;386:535-540.

70. Rizzari C, Citterio M, Zucchetti M, Conter V, Chiesa R, Colombini A, et al. A pharmacological study on pegylated asparaginase used in front-line treatment of children with acute lymphoblastic leukemia. *Haematologica.* 2006;91:24-31.

71. Patel N, Krishnan S, Offman MN, Krol M, Moss CX, Leighton C, et al. A dyad of lymphoblastic lysosomal cysteine proteases degrades the antileukemic drug L-asparaginase. *J Clin Invest.* 2009;119:1964-1973.

## Chapter 6

1. Allavena P, Sica A, Solinas G, Porta C, Mantovani A. The inflammatory micro-environment in tumor progression: the role of tumor-associated macrophages. *Crit Rev Oncol Hematol.* 2008;66:1-9.

2. Sica A, Schioppa T, Mantovani A, Allavena P. Tumour-associated macrophages are a distinct M2 polarised population promoting tumour progression: potential targets of anti-cancer therapy. *Eur J Cancer.* 2006;42:717-727.

## Chapter 8

1. Schmittgen TD, Livak KJ. Analyzing real-time PCR data by the comparative C(T) method. *Nat Protoc.* 2008;3:1101-1108.

2. Mach L, Stüwe K, Hagen A, Ballaun C, Glössl J. Proteolytic processing and glycosylation of cathepsin B. The role of the primary structure of the latent precursor and of the carbohydrate moiety for cell-type-specific molecular forms of the enzyme. *Biochem J.* 1992;282:577-582.

3. Mach L, Mort JS, Glössl J. Maturation of human procathepsin B. Proenzyme activation and proteolytic processing of the precursor to the mature proteinase, in vitro, are primarily unimolecular processes. *J Biol Chem.* 1994;269:13030-13035.

4. Johansen HT, Knight CG, Barrett AJ. Colorimetric and fluorimetric microplate assays for legumain and a staining reaction for detection of the enzyme after electrophoresis. *Anal Biochem.* 1999;273:278-283.

5. Loak K, Li DN, Manoury B, Billson J, Morton F, Hewitt E, et al. Novel cell-permeable acyloxymethylketone inhibitors of asparaginyl endopeptidase. *Biol Chem.* 2003;384:1239-1246.

## Supplemental


| | Page |
|---|---|
| Chapter 3 | 260 |
| Chapter 4 | 275 |
| Chapter 5 | 277 |
| Chapter 6 | 278 |

**Supplementary Table S3.1** Details of patient samples assayed for AEP expression by qRT-PCR. UPN numbers represent samples examined for AEP protein expression and ASNase digestion.

| *Subtype* | *Patient initials* | *Sample ID* | *UPN* | *Cytogenetics* |
|---|---|---|---|---|
| **Progenitor-B ALL *ETV6-RUNX1*** | MMi | 42 | | 46, XX; interphase FISH, *ETV6-RUNX1* fusion with loss of *wt ETV6* |
| | EHi | 45 | | Detailed karyotype not available; interphase FISH, *ETV6-RUNX1* fusion |
| | SBi | 77 | | Interphase FISH, *ETV6-RUNX1* fusion |
| | ARa | 87 | | 46, XX (20 metaphases); interphase FISH, variant *ETV6-RUNX1* fusion |
| | JBut | 130 | 1 | 46, XY; interphase FISH, *ETV6-RUNX1* |
| | JMG | 138 | | 46, XY; interphase FISH, *ETV6-RUNX1* |
| | SKh | 153 | | 46,XY, dup(7)(p15p22), t(12;19)(q13;p13); interphase FISH, *ETV6-RUNX1*, additional *RUNX1* copies in 36% cells (of 200) |
| | DBa | 188 | | 47, XY, ?add(2)(p23), add(3)(q34), dup(5)(q31q35), del(7)(p1), ?add(7)(q32), del(10)(q24.1q24.3), add(12)(p13), t(12;21)(p13;q22), add(20)(q13), +(21)/ 47, idem, del(12)(p11.2); interphase FISH, *ETV6-RUNX1* |
| | GKe | 215 | | 46, XX, t(12:21)(p13;q22), del(14)(q23?)/ interphase FISH, *ETV6-RUNX1* fusion |
| | AmZu | F2508 | | 49, X, -Y, +5, add(6)(p25), del(6)(q11-12q23), +del(6)(q11-12q23), +8, ins(9;?)(p13;/), der(9)del(9)(q22q33)ins(9;?)(p13;?), add(11)(p15), -12, t(12;21)(p13;q22), +der(21)t(12;21)(p13;q22), +mar1/ 50, idem, +19/ 50X, -Y, +5, del(6)(q11-12q23), +del(6)(q11-12q23), +?7, +8, ins(9;?)(p13;?), der(9)del(9)(q22q33)ins(9;?)((p13;?), add(11)(p15), -12, t(12;21)(p13;q22), -18, +der(21)t(12;21)(p13;q22), +mar1, +mar2/ 46, XY; interphase FISH, *ETV6-RUNX1*, 2 fusions |

| *Subtype* | *Patient initials* | *Sample ID* | *UPN* | *Cytogenetics* |
|---|---|---|---|---|
| ***ETV6-RUNX1*** | OSa | F2760 | | 46, XY, t(3;12;21)(q2; p13; q21); interphase FISH, *ETV6-RUNX1* fusion, loss of *wt ETV6* allele |
| | OMi | F3175 | | 46, XY, t(12;13)(p13;q12), ?t(12;21)(p13;q22)/46, XY, t(3;17)(p21;q25), ?t(12;21)(p13;q22), ?del(11)(q2?q22) |
| | KTh | F6336 | | Failed G-banded karyotype; interphase FISH, *ETV6-RUNX1* fusion |
| | OM | F6410 | | 47, XY, t(2;7)(P21;q34), add(4)(q31), add(4)(q31), add(9)(q32), add(10)(p11.2), der(12)t(12;21)(p13;q22)?add(12)(p11.2), add(12)(p11.2), t(13;21)(q10;q10), add(16)(p11.2), add(19)(q13), der(21)t(12;21)(p13;q22), +der(21)t(12;21)(p13;q22); interphase FISH, *ETV6-RUNX1* with loss of *wt ETV6* |
| | AZ | F7255 | | 48, XY, del(6)(q11-12q23), +del(6)(q11-12q23), +8, der(9)ins(9;?)(p13;?)del(9)(q22q33), add(11)(p15), der(12)t(9;12)(?;p1?)del(12)(q12q21), der(21)t(12;21)(?;q22)/48, idem, _Y, +der(21)t(12;21)(?;q22)/46, XY; interphase FISH, *ETV6-RUNX*1 fusion |
| | MMu | F7556 | | 47, XY, add(2)(q1), add(5)(q11.2), der(6)(t(6;7)(q22;p13), der(7)add(7)(p1)del(7)(q32q36), -9, add(9)(p2), del(12)(p11.2p13), -13, del(14)(q24q32), -15, +?21, +der(?)t(5;?)(q1:?), +der(?)t(9;?)(q1,?), +mar; interphase FISH, two copies of *ETV6-RUNX1* fusion |
| **Progenitor B ALL High Hyperdiploidy** | SIA | 15 | | 57, XY, +X, +4, +6, +10, +14, +15, +17, +18, +21, +21, mar |
| | EBr | 54 | | 57, XX, +X, +X, +der(1)t(1;?), +4, +6, +10, +14, +17, +18, +21, +21/ 46,XX; interphase FISH negative for sentinel rearrangements |
| | AVe | 59 | | 54 XY, +X, ins(1;?)(q2;?), +6, del(6)(q1q2), +10, +18, +18, +21, +21, +mar; interphase FISH negative for sentinel rearrangements |
| | JWi | 71 | 2 | 57, XY, +X, +4, +4, +6, +9, +10, +14, +17, +18, +21, +21; interphase FISH negative for sentinel rearrangements |

| *Subtype* | *Patient initials* | *Sample ID* | *UPN* | *Cytogenetics* |
|---|---|---|---|---|
| **High Hyperdiploidy** | EWi | 75 | | 59, XX, +X, +2, +4, +6, +8, +9, +10, +12, +17, +?18, +21, +21, +21; interphase FISH negative for sentinel rearrangements |
| | ACh | 106 | | 57, XX, +X, +4, +6, +10, +14, +14, +17, +18, +21, +21, +mar; interphase FISH negative for sentinel rearrangements |
| | FRo | 111 | | 56, XX, +X, dup(1)(q21q42), +4, +6, +10, +14, +17, +18, +21, +2mar/ 4( XX; interphase FISH negative for sentinel rearrangements |
| | ZCh | 131 | | 54-59, XY, +9, +?11, +14, +14, +?17, +?20, +21, +21, +21, +?22, +mar1,+mar2; interphase FISH negative for sentinel rearrangements |
| | AMi | 169 | | 55, XX, +X, +4, +6, +10, +14, +14, +17, +21, +21/46, XX; interphase FISH negative for sentinel rearrangements |
| | JMa | 173 | | 55, XY, +X, +4, +14, +14, +17, +18, +21, +21/46, XY; interphase FISH negative for sentinel rearrangements |
| | ASa | 191 | | 55, XX, +X, +4, +6, +8, +10. +14, +18, +19, ?del(20)(q1?), +21; interphase FISH negative for sentinel rearrangements |
| | BBl | 203 | | 57, XY, +X, +4, +5, +9, +10, +14, +17, +?add(18)(q?11.2), +21c, +mar/ 58, idem, +21/ 59, idem, +11, +21/ 47, XY, +21c; interphase FISH negative for sentinel rearrangements |
| | NKa | F5511 | 3 | 56, XY, +X, +4, +5, +6, +8, +14, +17, +18, +21, +21/ 46, XY; interphase FISH negative for sentinel rearrangements |
| **Progenitor-B ALL** | SDa | 99 | 4 | 46, XX, der(19)t(1;19)(q23;p13)/ 50, idem, +5, +8, +8, +14 |
| ***TCF3-PBX1*** | NAY | 199 | | 46, XX, t(1;19),(q23:p13)/ 44, XX, idem, +8, +8/ 48, XX, -1, +8, der(19) ,t(1:19)(q23;p13), +mar1, +mar2(1)/ 46, XX |
| | LNi | 278 | 6 | 46, XX, der(19)t(1;19)(q23;p13)/46, XX |
| | MMa | F8141 | 5 | 46, XY, t(1:19)(q23;p13)/45, idem, -Y, del(9)(p13-21p24)/46, XY |

| *Subtype* | *Patient initials* | *Sample ID* | *UPN* | *Cytogenetics* |
|---|---|---|---|---|
| ***TCF3-PBX1*** | JAK | F9460 | | 47, XX, t(1;19)(q23;p13), i(7)(q10), der(13)t(1;13)(q12;p11.2), i(21)(q10), +mar |
| **Progenitor-B ALL Normal Karyotype** | — | 25 | | Detailed karyotype not available; interphase FISH negative for sentinel rearrangements; no hidden hyperdiploidy on Multiprobe-I testing |
| | CGe | 36 | | Failed G-banded karyotype; interphase FISH negative for sentinel rearrangements; no hidden hyperdiploidy on Multiprobe-I testing |
| | ASh | 43 | | 46, XY/ minor subclone - 47, XY, +2, add(10)(q24) |
| | AMo | 69 | 11 | 46, XX; interphase FISH negative for sentinel rearrangements |
| | CSw | 118 | | 46, XY; interphase FISH negative for sentinel rearrangements |
| | AMu | 160 | | 46, XX; interphaseFISH: 12p deletion, negative for sentinel fusions |
| **Progenitor-B ALL Miscellaneous** | JHa | 17 | | 46, XY, i(9)(q10); interphase FISH negative for sentinel rearrangements |
| | ACh | 52 | | 46, XY, -1, -2, del(2)(p1p2), -4, -5, der(7)t(1;7)(p13;q2), der(9)t(4;9)(q1;p1), -10, -15, +21, +der(?)t(5;?)(q1;?), +4mar; interphase FISH negative for sentinel rearrangements |
| | JKe | 198 | | 46,XY, i(17)(q10)(2)/ 46, XY, idem, ?dup(7)(p?21), del(13)(q?14,q?22)/ 46, XY, idem, ?dup(7)(p?21), del(13)(q?14q?22), +mar1, +mar2/ 46,XY; interphase FISH negative for sentinel rearrangements |
| | KFr | 204 | | 46, XX, ?del(9)(p?)/ 46,XX, del 9p21; interphase FISH, loss of one p16 allele (9p21 locus), negative for sentinel rearrangements |
| | LFe | 301 | 12 | 46, XX, t(1:9)(q21;p21), ?add(5)(q3); interphase FISH negative for sentinel rearrangements |

| *Subtype* | *Patient initials* | *Sample ID* | *UPN* | *Cytogenetics* |
|---|---|---|---|---|
| **Progenitor-B ALL Hypodiploidy** | ATu | 134 | 7 | 26, X, +Y, +14, +21/ 26, idem, -14, +mar/ 52, idemx2/ 52, idemx2, -14, -14, +mar, +mar/ 46, XY |
| | RSm | 245 | | 37, XY, -2, -3, -4, -7, del(9)(q1~q2q34), -12, -13, der(13)t(13;13)(q34;q12), -15, -16, -17 |
| | AMo | 252 | | 26, X, +14, +18, +21/ 46, XY / 52, idem x 2 |
| **Progenitor-B ALL *BCR-ABL1*** | NAu | 140 | | 46, XY, t(9;22)(q34;q11)/ 45, idem, der(7)t(7;9)(p1?;q1?), -9/ 46, idem, der(7)t(7;9)(p1?;q1?), -9, +der(22)t(9;22)(q34;q11); interphase FISH, BCR-ABL1, deletion of MML (21%), deletion of IgH (26%), deletion of p16 (19%) |
| | AhZu | 184 | | 53, XY, +21, t(9;22)(q34;q11.2); interphase, FISH *BCR-ABL1* fusion |
| | RHu | 193 | | 49, XY, t(9;22)(q34; q11.2), +21 |
| | OMo | 205 | | 46, XY, der(9), del(9)(p13p24)t(9;22)(q34;q11.2), der(22)t(9;22) |
| | SaB | 258 | 8 | 49, XX, +8, t(9;22)(q34;q11.2), +der(22)t(9;22), +mar/ 46, XX |
| | NAl | F8122 | | 46, XY, t(9;22)(q34;q11.2) |
| | TD | ALL2003-4479 | | Detailed karyotype not available; interphase FISH, BCR-ABL1 fusion |
| **Progenitor-B ALL iAMP21** | lAy | 110 | 9 | 46, XX, der(21)idic(21)(q?)iAMP21q/ 46, XX |
| | EYe | 170 | | 46, XY, +mar; interphase FISH, iAMP21 |
| **Progenitor-B ALL Multiple *RUNX1* copies** | KLa | 29 | | 46, XX, -21, +mar1/ 47, idem, +mar2/ 46, XX; interphase FISH, 6 *RUNX1* copies |
| | CDa | 123 | | 46, XY/ 47, XY, ?del(6q), +mar; interphase FISH, 4 *RUNX1* copies |

| *Subtype* | *Patient initials* | *Sample ID* | *UPN* | *Cytogenetics* |
|---|---|---|---|---|
| **Progenitor-B ALL Multiple *RUNX1* copies** | JBus | F5481 | | 49, XY, +X, -10, -11, add(12)(p11.2), +14, del(21)(q22q22)x2, +21, -22, +2 mar/ 49, XY, +X, del(7)(p15p22), -10, -11, add(12)(p11.2), +14, del(21)(q22q22)x2, +21, -22, +2 mar/ 46, XY; interphase FISH, four *RUNX1* copies |
| **Progenitor-B ALL *MLL* rearranged** | DBo | F7901 | 10 | 46, XY, t(4;11)(q21;q23)/ 46, XY |
| | TSe | 183 | | 46, XY, t(4;11)(q21;q23)/ 46,XY |
| | GWi | 237 | | 46, XX, t(4;11)(q21;q23) |
| **Progenitor-T ALL** | KKn | 28 | | 46 XY; interphase FISH negative for sentinel rearrangements |
| | CWO | 57 | | 46, XY, t(6;10)(q2?1/q?11), add(11)(q23), del(12)(p1?2)/ 46, XY; interphase FISH negative for sentinel rearrangements |
| | DLi | 73 | | 46, XX; interphase FISH negative for sentinel rearrangements |
| | LMe | 86 | | 46,XY,del(6)(q)(10); interphase FISH negative for sentinel rearrangements |
| | JTa | 96 | | 46, XY; interphase FISH negative for sentinel rearrangements |
| | PLe | 141 | | Failed G-banded karyotype; interphase FISH negative for sentinel rearrangements; no hidden hyperdiploidy on Multiprobe-I testing |
| | DDo | 150 | | 46, XY, t(1;17)(p13;q11), t(2;11)(q37;q23)/ 46, idem, del(8)(q1?1q1?3), add(9)(q34)/ 46, XY |
| | BMi | 152 | | 46, XY, ?dup(2),(q3?q3?), ?dup(3)(q2?5q2?7), add(5)(p1?5), del(6)(q21q25), add(8)(p2?), del(12)(p11.2),add(17)(p11.2)(20); interphase FISH, 161/250(64%) loss of oneETV6 allele |
| | ASo | 3122 | | 46, XY, add(11)(p1); interphase FISH, t(7;11)(q35; p13) |

| *Subtype* | *Patient initials* | *Sample ID* | *UPN* | *Cytogenetics* |
|---|---|---|---|---|
| **Acute Myeloid Leukaemia** | JNe | 31 | | 46, XY; interphase FISH negative for sentinel rearrangements |
| | GCa | 90 | | 51, XX, +2, ?der(2)t(1;2)(q25;q3?), +10, +13, +15, +22; interphase FISH negative for sentinel rearrangements |
| | Es | 157 | | 46, XY; interphase FISH negative for sentinel rearrangements |
| | JMa | 182 | | AML M7 (dry marrow tap, detailed karyotyping not available) |

**Supplementary Table S3.2** Details of adherent and other suspension cell lines used in experiments

| Cell line | Lineage | Genetic hallmark | Full karyotype |
|---|---|---|---|
| MHH-CALL2 | Human precursor B leukaemia | Hyperdiploidy | Hyperdiploid, 13% polyploidy, modal number 50-52, XX, gain of chromosomes 8, 10, 18, 21 (tetrasomy) |
| 697 | Human precursor B leukaemia | TCF3-PBX1 | Near diploid - 46(45-48) XY, t(1;19)(q23;p13), del(6)(q21) |
| U266 | Human multiple myeloma | 11q13 breakpoint | Complex hypodiploid, modal number 40-46, XY, loss of chromosome 8, 10, 13, gain of chromosome 15, marker +3q27, +7q32, +8q24, +9q34, +10p14, +14p11, +17p11, +18p12, der(22)t(15;22)(q21;q13), t(1;11)(p33;q13), t(4;11)(q?21;q23) |
| RPMI-8402 | Human precursor T leukaemia | SIL-TAL1<br>Also, LMO1-TCRD | Hypotetraploid, modal number 79-91, XXX, loss of chromosomes X, 10, 13, 14, 18, 20, gain of chromosome 3, 15, deletions (6)(q14q22)x2, duplication (4)(q13q23)x2, marker +15p13, t(11;14)(p15;q11)x2, sideline clone with der(1)t(1;9)(p35/36;q11), +13q34 |
| MV4:11 | Human acute monocytic leukaemia | MLL-AF4 | 48(46-48)XY, gains of chromosome 8, 18, 19, loss of chromosome 21, t(4;11)(q21;q23) |
| HL60 | Human acute myeloid leukaemia | Nil specific | Hypotetraploid with hypodiploid sideline, modal number 82-88, XX, deletions of chromosome X, 8, 16, 17, gain of chromosomes 18, 22, markers +6q27x2, +18q21, ins(1;8)(p?31;q24hsr)x2, der(5)t(5;17)(q11;q11)x2, der(9)del(9)(p13)t(9;14)(q?22;q?22)x2, der(14)t(9;14)(q?22;q?22)x2, der(16)t(16;17)(q22;q22)x1-2, - sideline with losses of chromosome 2, 5, 15, deletion (11)(q23.1q23.2) |
| NB4 | Human acute promyelocytic leukaemia | PML-RARA | Hypertriploid, modal number 71-81, XX, loss of chromosomes X, 19, gain of chromosomes 2, 6, 7, 11, 12, 13, 14, 17, 20, markers +14pder(8)t(8;?)(q24;?), der(11) from 3-way intrachromosomal rearrangements, der(12)t(12;?)(p11;?), t(15;17)(q22;q11-12.1), der(19)t(10;19)(q21.1;p13.3)x2 |
| THP-1 | Human acute monocytic leukaemia | MLL-AF9 | Near-tetraploid, modal number 88-96, XY/XXY, loss of chromosomes Y, 8, 13, 19, 22, gain of chromosomes 1, 3, 6, deletions 1q42.2, (6p21)x2-4, markers +1p11, +(12q24)x1-2, +(?18q21), isochromosome 2q, der(9)t(9;11)(p22;q23)i(9)(p10)x2, der(11)t(9;11)(p22;q23)x2, der(13)t(8;13)(p11;p12) |

| | | | |
|---|---|---|---|
| U937 | Human acute monocytic leukaemia | CALM-AF10 | Hypotriploid, modal number 58-69, XXY, loss of chromosomes 2, 4, 6, 9, 20, 21 gain of chromosome 7, markers +9p22, +16q22, +19q13, isochromosome 11q, 12p, der(5)t(1;5)(p22;q35), t(1;12)(q21;p13), , t(10;11)(p14;q23), t(1;5) |
| K562 | Human Chronic Myeloid Leukaemia in myelo-erythroid blast crisis | BCR-ABL1, encoding the e13-a2 fusion transcript | Hypotriploid, modal number 61-68, loss of chromosomes X, 3,13, 18, gain of chromosome 7, deletions (9)(p11/13), Xp22, markers der(14)t(14;?)(p11;?), der(17)t(17;?)(p11/13;?), der(?18)t(15;?18)(q21;?q12); t(9;22)(q34;q11) by FISH |
| HEK293 | Human embryonic kidney fibroblasts | Nil specific | Near-triploid, modal number 64-69, loss of chromosomes 10, 13, 16, 18, 20, gain of chromosomes 1, 6, 21, 22, deletions 1p35, 6q11, inversions (1)(p35q43), markers +(?X)(p22), +(8)(q24), +(13)(p13), +(17)(qter), der(?)t(5;?)(q13;?), isochromosome(5p) |
| PC3 | Human prostate carcinoma | c-myc amplification | Hypotetraploid, modal number 80-90, XX/XXX, loss of chromosomes Y, 1, 2, 4, 5, 8, 10, 12, 13, 15, 16, 17, 18, 22, gain of chromosomes 3, 7, 14, deletion (1)(p34p35), (5)(p1?)x1-2, (9)(p21)x1-2, 17p11, marker +18-21, +1-2 double-minute, +1p?32, +3p1?, +3q13, +(3)(q21)x2, +9(p1?1), +9q34, +12q24, +13p11, +19p13 - sideline with der(3)add(3)(p2?5)add(3q2?), deletion (4)(q2?4q2?8), +7q11, +(8)(p1?) |

**Supplementary Table S3.3** Real-time TaqMan assays: Fluorescent probe details (on-demand reagents from Applied Biosystems)

| *Transcript* | *Product code* | *Target nucleotide sequence and location* |
|---|---|---|
| AEP | Hs 00271599_m1 | CAAAGTCCTGAAGAGTGGCCCCCAG<br>Exon boundary 5 and 6<br>79 bp amplicon |
| β2M | Hs 99999907_m1 | TTAAGTGGGATCGAGACATGTAAGC<br>Exon boundary 2 and 3<br>75 bp amplicon |

Note: Primer sequence details are not available as are deemed proprietary (vide correspondence with Applied Biosystems UK [now part of Life Technologies Corporation]; Inquiry Reference 2-1839759341, dated 14/2/2011)

**Supplementary Table S3.4** Raw Ct values of AEP and β2M transcripts in primary leukaemia samples

| *Sample ID* | *AEP Ct* | *Mean/CV* | *β2M Ct* | *Mean/CV* | *AEP-β2M* |
|---|---|---|---|---|---|
| **Progenitor-B ALL** | | | | | |
| *ETV6-RUNX1* | | | | | |
| | 25.99 | 25.93 | 22.44 | 22.04 | 3.89 |
| AZ_F2508 | 25.95 | 0.3% | 21.77 | 1.6% | |
| | 25.86 | | 21.91 | | |
| OS_F2760 | 29.68 | 29.46 | 23.48 | 23.42 | 6.05 |
| | 29.33 | 0.7% | 23.48 | 0.4% | |
| | 29.38 | | 23.30 | | |
| OM_F3175 | 29.55 | 29.79 | 20.83 | 23.45 | 6.34 |
| | 29.96 | 0.7% | 22.94 | 7.1% | |
| | 29.87 | | 23.97 | | |
| KT_F6336 | 26.17 | 26.53 | 22.48 | 22.47 | 4.07 |
| | 26.68 | 1.2% | 22.39 | 0.3% | |
| | 26.75 | | 22.53 | | |
| AZ_F7255 | 28.26 | 28.24 | 21.99 | 21.84 | 6.39 |
| | 28.20 | 0.1% | 21.82 | 0.6% | |
| | 28.25 | | 21.72 | | |
| 12:21_42 | 25.62 | 25.59 | 19.16 | 19.19 | 6.40 |
| | 25.55 | 4.9% | 19.21 | 0.2% | |
| | 27.84 | | 19.20 | | |
| 12:21_45 | 24.09 | 23.97 | 19.72 | 19.70 | 4.27 |
| | 23.88 | 0.4% | 19.65 | 0.2% | |
| | 23.95 | | 19.73 | | |
| 12:21_77 | 24.30 | 24.29 | 19.31 | 19.29 | 5.00 |
| | 24.28 | 0.1% | 19.19 | 0.5% | |
| | 24.29 | | 19.36 | | |
| 12:21_87 | 24.85 | 25.14 | 18.71 | 18.57 | 6.57 |
| | 25.10 | 1.3% | 18.54 | 0.7% | |
| | 25.48 | | 18.47 | | |
| 12:21_130 | 23.86 | 24.1 | 19.69 | 19.5 | 4.6 |
| | 24.24 | 0.8% | 19.38 | 1.1% | |
| | 24.12 | | 19.28 | | |
| 12:21_138 | 27.20 | 27.25 | 22.79 | 22.83 | 4.41 |
| | 27.23 | 0.2% | 22.85 | 0.2% | |
| | 27.30 | | 22.87 | | |
| 12:21_153 | 25.17 | 25.0 | 19.70 | 19.9 | 5.0 |
| | 24.83 | 0.7% | 20.17 | 1.2% | |
| | 24.89 | | 19.97 | | |
| 12:21_188 | 25.52 | 25.33 | 19.44 | 19.28 | 6.05 |
| | 25.16 | 0.7% | 19.17 | 0.7% | |
| | 25.30 | | 19.23 | | |
| 12:21_215 | 24.96 | 25.0 | 20.24 | 20.2 | 4.8 |
| | 24.94 | 0.1% | 19.99 | 0.7% | |
| | 24.96 | | 20.25 | | |
| MMu_F7556 | 30.70 | 30.49 | 22.82 | 22.82 | 7.68 |
| | 30.36 | 0.60% | 22.79 | 0.1% | |
| | 30.42 | | 22.84 | | |

| *Sample ID* | *AEP Ct* | *Mean/CV* | *β2M Ct* | *Mean/CV* | *AEP-β2M* |
|---|---|---|---|---|---|
| MM_F8141 | 27.59 | 27.54 | 21.54 | 21.50 | 6.04 |
| | 27.47 | 0.22% | 21.46 | 0.2% | |
| | 27.55 | | 21.49 | | |
| *Hyperdiploidy* | | | | | |
| NKa_F5511 | 25.23 | 25.24 | 21.75 | 21.72 | 3.53 |
| | 25.16 | 0.4% | 21.60 | 0.5% | |
| | 25.34 | | 21.80 | | |
| HHD_15 | 24.16 | 24.20 | 18.52 | 18.41 | 5.79 |
| | 24.26 | 0.2% | 18.38 | 0.6% | |
| | 24.18 | | 18.32 | | |
| HHD_54 | 25.41 | 25.48 | 19.96 | 19.72 | 5.76 |
| | 25.50 | 0.2% | 19.56 | 1.1% | |
| | 25.53 | | 19.64 | | |
| HHD_59 | 24.11 | 24.2 | 19.50 | 19.6 | 4.6 |
| | 24.24 | 0.3% | 19.53 | 0.5% | |
| | 24.19 | | 19.67 | | |
| HHD_71 | 26.21 | 26.23 | 21.39 | 21.26 | 4.97 |
| | 26.26 | 0.1% | 21.14 | 0.6% | |
| | 26.22 | | 21.25 | | |
| HHD_75 | 26.42 | 26.38 | 19.88 | 19.89 | 6.50 |
| | 26.35 | 0.1% | 19.90 | 0.04% | |
| | 26.38 | | 19.88 | | |
| HHD_106 | 23.61 | 23.60 | 19.10 | 19.11 | 4.49 |
| | 23.56 | 0.1% | 19.18 | 0.4% | |
| | 23.63 | | 19.04 | | |
| HHD_111 | 24.13 | 24.08 | 18.73 | 18.77 | 5.31 |
| | 24.15 | 0.4% | 18.77 | 0.2% | |
| | 23.97 | | 18.81 | | |
| HHD_131 | 24.23 | 24.22 | 18.96 | 19.01 | 5.21 |
| | 24.29 | 0.3% | 18.95 | 0.5% | |
| | 24.15 | | 19.12 | | |
| HHD_169 | 23.19 | 23.2 | 19.20 | 19.3 | 3.9 |
| | 23.02 | 0.6% | 19.37 | 0.5% | |
| | 23.28 | | 19.36 | | |
| HHD_173 | 23.00 | 22.9 | 19.85 | 19.9 | 3.0 |
| | 22.83 | 0.4% | 19.93 | 0.2% | |
| | 22.96 | | 19.95 | | |
| HHD_191 | 24.89 | 25.07 | 19.19 | 19.29 | 5.77 |
| | 25.17 | 0.6% | 19.23 | 0.8% | |
| | 25.14 | | 19.47 | | |
| HHD_203 | 28.14 | 28.1 | 21.92 | 22.9 | 5.2 |
| | 28.20 | 0.5% | 23.14 | 4.0% | |
| | 27.95 | | 23.71 | | |
| *TCF3-PBX1* | | | | | |
| 1:19_JAK | 27.84 | 27.96 | 22.62 | 22.85 | 5.12 |
| | 28.12 | 0.5% | 23.01 | 0.9% | |
| | 27.94 | | 22.91 | | |
| 1:19_99 | 25.86 | 25.92 | 19.57 | 19.44 | 6.49 |
| | 25.99 | 0.2% | 19.55 | 1.1% | |

| *Sample ID* | *AEP Ct* | *Mean/CV* | *β2M Ct* | *Mean/CV* | *AEP-β2M* |
|---|---|---|---|---|---|
| | 25.92 | | 19.19 | | |
| 1:19_199 | 26.70 | 26.72 | 19.89 | 19.88 | 6.84 |
| | 26.74 | 0.1% | 19.94 | 0.3% | |
| | 26.72 | | 19.82 | | |
| 1:19_278 | 27.01 | 27.1 | 19.96 | 20.0 | 7.0 |
| | 27.00 | 0.4% | 20.14 | 0.5% | |
| | 27.21 | | 19.99 | | |
| *Pre B ALL-Other* | | | | | |
| Other_17 | 25.18 | 25.20 | 17.23 | 17.23 | 7.97 |
| | 25.19 | 0.10% | 17.20 | 0.13% | |
| | 25.22 | | 17.24 | | |
| Other_52 | 22.68 | 22.64 | 19.54 | 19.51 | 3.13 |
| | 22.68 | 0.3% | 19.48 | 0.2% | |
| | 22.56 | | 19.52 | | |
| Other_198 | 26.95 | 26.9 | 21.18 | 21.1 | 5.8 |
| | 26.92 | 0.4% | 20.93 | 0.6% | |
| | 26.73 | | 21.07 | | |
| Other_204 | 25.53 | 26.1 | 19.01 | 20.3 | 5.8 |
| | 26.46 | 1.9% | 20.38 | 0.8% | |
| | 26.30 | | 20.14 | | |
| Other_301 | 23.81 | 23.7 | 18.93 | 18.9 | 4.8 |
| | 23.63 | 0.6% | 18.75 | 0.5% | |
| | 23.52 | | 18.90 | | |
| *Normal Karyotype* | | | | | |
| NK_25 | 26.93 | 27.03 | 18.72 | 18.62 | 8.41 |
| | 26.96 | 0.53% | 18.60 | 0.50% | |
| | 27.19 | | 18.53 | | |
| NK_43 | 27.77 | 27.66 | 18.38 | 18.50 | 9.16 |
| | 27.49 | 0.5% | 18.52 | 0.6% | |
| | 27.72 | | 18.60 | | |
| NK_69 | 26.30 | 26.4 | 20.10 | 20.7 | 5.7 |
| | 26.58 | 0.7% | 20.74 | 2.7% | |
| | 26.24 | | 21.23 | | |
| NK_118 | 26.36 | 26.53 | 19.10 | 19.08 | 7.44 |
| | 26.59 | 0.5% | 19.14 | 0.4% | |
| | 26.63 | | 19.01 | | |
| NK_160 | 24.63 | 24.6 | 19.75 | 20.0 | 4.6 |
| | 24.70 | 0.6% | 20.31 | 1.4% | |
| | 24.42 | | 19.93 | | |
| *High-Risk Pre-B ALL* | | | | | |
| JB_F5481 | 27.93 | 27.81 | 21.79 | 21.95 | 5.86 |
| | 27.61 | 0.62% | 22.10 | 0.7% | |
| | 27.90 | | 21.97 | | |
| DB_F7901 | 26.54 | 27.36 | 23.28 | 22.92 | 4.44 |
| | 27.37 | 2.99% | 22.74 | 1.4% | |
| | 28.18 | | 22.74 | | |
| NA_F8122 | 26.59 | 26.63 | 23.49 | 23.29 | 3.33 |
| | 26.45 | 0.72% | 22.93 | 1.4% | |
| | 26.83 | | 23.47 | | |

| *Sample ID* | *AEP Ct* | *Mean/CV* | *β2M Ct* | *Mean/CV* | *AEP-β2M* |
|---|---|---|---|---|---|
| Ph+_140 | 24.53 | 24.58 | 18.60 | 18.61 | 5.96 |
| | 24.64 | 0.2% | 18.58 | 0.2% | |
| | 24.57 | | 18.66 | | |
| Ph+_184 | 24.47 | 24.46 | 19.85 | 19.77 | 4.69 |
| | 24.42 | 0.1% | 19.69 | 0.4% | |
| | 24.49 | | 19.77 | | |
| Ph+_193 | 22.92 | 22.83 | 19.18 | 19.03 | 3.80 |
| | 22.68 | 0.60% | 18.89 | 0.74% | |
| | 22.90 | | 19.02 | | |
| Ph+_205 | 26.27 | 26.28 | 19.52 | 19.61 | 6.67 |
| | 26.25 | 0.11% | 19.62 | 0.44% | |
| | 26.31 | | 19.69 | | |
| Ph+_258 | 26.40 | 26.32 | 19.05 | 18.94 | 7.38 |
| | 26.25 | 0.3% | 18.88 | 0.5% | |
| | 26.30 | | 18.89 | | |
| MLL_183 | 27.41 | 27.5 | 20.89 | 20.9 | 6.6 |
| | 27.54 | 0.3% | 21.01 | 0.3% | |
| | 27.53 | | 20.90 | | |
| MLL_237 | 27.70 | 28.1 | 20.81 | 20.9 | 7.1 |
| | 28.26 | 1.1% | 20.88 | 0.5% | |
| | 28.19 | | 21.03 | | |
| HypoD_134 | 28.41 | 28.1 | 19.85 | 19.9 | 8.2 |
| | 27.96 | 1.0% | 19.75 | 0.5% | |
| | 27.93 | | 19.97 | | |
| HypoD_245 | 23.11 | 23.2 | 20.00 | 19.9 | 3.2 |
| | 23.15 | 0.3% | 19.84 | 0.4% | |
| | 23.25 | | 19.98 | | |
| HypoD_252 | 23.44 | 23.4 | 20.02 | 20.0 | 3.4 |
| | 23.39 | 0.3% | 19.89 | 0.8% | |
| | 23.52 | | 20.22 | | |
| iAMP21_110 | 23.57 | 23.6 | 20.17 | 20.4 | 3.2 |
| | 23.56 | 0.1% | 20.51 | 0.9% | |
| | 23.60 | | 20.42 | | |
| iAMP21_170 | 23.80 | 23.8 | 21.39 | 21.0 | 2.8 |
| | 23.93 | 0.6% | 20.88 | 1.6% | |
| | 23.65 | | 20.77 | | |
| *RUNX1*amp_29 | 23.88 | 24.0 | 21.24 | 21.2 | 2.8 |
| | 24.01 | 0.6% | 21.26 | 0.1% | |
| | 24.18 | | 21.23 | | |
| *RUNX1*amp_123 | 24.73 | 24.7 | 20.05 | 19.9 | 4.8 |
| | 24.67 | 0.3% | 19.95 | 0.6% | |
| | 24.80 | | 19.82 | | |
| **Progenitor T ALL** | | | | | |
| T_28 | 26.65 | 26.63 | 20.00 | 20.03 | 6.60 |
| | 26.58 | 0.2% | 20.14 | 0.5% | |
| | 26.66 | | 19.95 | | |
| T_57 | 23.90 | 23.8 | 19.41 | 19.6 | 4.2 |
| | 23.57 | 0.7% | 19.56 | 0.8% | |
| | 23.79 | | 19.72 | | |

| *Sample ID* | *AEP Ct* | *Mean/CV* | *β2M Ct* | *Mean/CV* | *AEP-β2M* |
|---|---|---|---|---|---|
| T_73 | 28.38 | 28.27 | 18.68 | 18.90 | 9.37 |
| | 28.22 | 0.3% | 18.62 | 2.3% | |
| | 28.21 | | 19.41 | | |
| T_86 | 28.35 | 28.59 | 18.92 | 19.11 | 9.48 |
| | 28.77 | 0.7% | 19.18 | 0.9% | |
| | 28.64 | | 19.23 | | |
| T_96 | 25.48 | 25.48 | 19.84 | 19.72 | 5.76 |
| | 25.44 | 0.1% | 19.43 | 1.3% | |
| | 25.51 | | 19.89 | | |
| T_141 | 24.95 | 24.9 | 20.83 | 20.8 | 4.1 |
| | 24.86 | 0.3% | 20.75 | 0.2% | |
| | 24.99 | | 20.82 | | |
| T_152 | 24.53 | 25.1 | 15.18 | 19.7 | 5.4 |
| | 25.38 | 2.0% | 19.86 | 1.1% | |
| | 25.40 | | 19.56 | | |
| T_150 | 25.52 | 25.6 | 20.93 | 19.4 | 6.2 |
| | 25.71 | 0.4% | 19.44 | 0.01% | |
| | 25.60 | | 19.44 | | |
| T_3122 | 28.70 | 28.8 | 22.19 | 22.2 | 6.6 |
| | 28.74 | 0.4% | 22.36 | 0.8% | |
| | 28.94 | | 22.03 | | |
| **Acute Myeloid Leukaemia** | | | | | |
| AML_90 | 28.26 | 28.24 | 18.43 | 18.53 | 9.71 |
| | 27.98 | 0.9% | 18.57 | 0.5% | |
| | 28.49 | | 18.60 | | |
| AML_157 | 28.67 | 28.59 | 19.54 | 19.46 | 9.13 |
| | 28.51 | 0.3% | 19.35 | 0.5% | |
| | 28.59 | | 19.50 | | |
| AML_182 | 25.79 | 25.73 | 19.16 | 18.98 | 6.75 |
| | 25.54 | 0.6% | 18.86 | 0.9% | |
| | 25.85 | | 18.90 | | |

**Supplementary Table S3.5** Relative AEP transcript expression and enzyme activity in lymphoid and myeloid cell lines. Note discrepancy in AEP transcript expression and activity in the RPMI-8402 and K562 cell lines (shaded gray)

| Cell line | Relative* normalised AEP RNA expression | Relative* AEP enzyme activity |
|---|---|---|
| HRC57 | 1.0000 | 1.0000 |
| SD1 | 1.6196 | 1.1005 |
| SupB15 | 0.0183 | 0.0185 |
| REH | 0.1914 | 0.0021 |
| 697 | 0.0018 | *BLD* |
| MHH-CALL2 | 0.0086 | — |
| U266 | 0.9480 | 1.5345 |
| RPMI-8402 | 2.4144 | 0.1834 |
| MV4;11 | 0.0024 | 0.0012 |
| HL60 | 0.0542 | *BLD* |
| NB4 | *BLD* | — |
| THP1 | 0.0052 | — |
| U937 | 0.0002 | — |
| K562 | 0.9324 | 0.0120 |

BLD, below limit of detection *Relative to the HRC57 cell line

**Supplementary Table S4.1** Summary of Boyden chamber motility assays in inducible AEP-expressing HEK293 cells.

Lower chamber cell counts (cells/mL) 24 hours after seeding of 8-micron pore Matrigel-coated inserts (1:50 dilution) loaded with $1\times10^5$ cells. AEP.293GS: HEK293 cells stably transfected with the mifepristone (Mfp)-inducible AEP-expressing dual-plasmid GeneSwitch constructs. Mfp-treated: AEP293.GS cells pulsed with mifepristone (10nM) 24 hours prior to assay. Untreated (Mfp-untreated) and ethanol-treated (Vehicle control) AEP.293GS cells served as controls. Experiments 4a and 4b refer to invasion assays performed in two separate plates on the same day.

| | AEP.293 GS cells (cells/mL) | | |
|---|---|---|---|
| | Mfp-treated | Mfp-untreated | Vehicle control |
| Experiment 1 | 160 | 20 | — |
| | 100 | 40 | |
| | 100 | 100 | |
| | 60 | 100 | |
| | 200 | 220 | |
| | 280 | 80 | |
| Experiment 2 | 180 | 80 | — |
| | 120 | 20 | |
| | 140 | 20 | |
| | 220 | 120 | |
| | 60 | 100 | |
| | 120 | 240 | |
| Experiment 3 | 80 | 80 | 100 |
| | 80 | 40 | 40 |
| | 100 | 80 | 40 |
| | 80 | — | — |
| | 120 | — | — |
| | 80 | — | — |
| Experiment 4a | 190 | 294 | 415 |
| | 138 | 156 | 138 |
| | 398 | 121 | 138 |
| | 242 | — | — |
| | 346 | — | — |
| | 208 | — | — |
| Experiment 4b | 208 | 208 | 156 |
| | 225 | 69 | 68 |
| | 35 | 346 | 173 |
| | 52 | — | — |
| | 242 | — | — |
| | 761 | — | — |
| Experiment 5 | 383 | 17 | — |
| | 156 | 35 | |
| | 190 | 52 | |
| | 138 | 17 | |
| | 121 | — | |
| | 86 | — | |

Table
Summary of Boyden chamber motility assays in enforced AEP-expressing HEK293 cells

Lower chamber cell counts (cells/mL) 24 hours after seeding uncoated 8-micron pore inserts with $1\times10^5$ cells. AEP.293, Enforced AEP-expressing HEK293 cells; EV.293: Mock transfected isogenic controls; PC3: human prostate adenocarcinoma cell line as positive control

| | Lower chamber cell counts (cells/mL) | | |
|---|---|---|---|
| | AEP293 | EV293 | PC3 |
| Expt 1 | 700 | 540 | 1560 |
| | 740 | 800 | 1800 |
| | 1040 | | 2640 |
| Expt 2 | 420 | 240 | 1400 |
| | 500 | 500 | 1520 |
| | 700 | 540 | 1520 |
| | 740 | 600 | 1560 |
| | 820 | 660 | 1560 |
| | 860 | 660 | 1580 |
| Expt 3 | 649 | 1272 | — |
| | 519 | 1160 | |
| | 960 | 1168 | |
| | 908 | | |

**Supplementary Table S4.2** Parallel proliferation and migration studies on enforced AEP-expressing HEK293 cells.

Serial cell counts of stably transfected AEP-expressing (AEP.293) and mock-transfected (EV.293) HEK293 cells seeded in parallel in 6-well plates and in 24-well Boyden chamber assays using 8-micron pore uncoated inserts).

| | AEP.293 | | EV.293 | |
|---|---|---|---|---|
| Hours after seeding | Cells/mL | Migration (Cells/mL) | Cells/mL | Migration (Cells/mL) |
| 12h | 1500000 | 740 | 1500000 | 1800 |
| | 1497000 | 920 | 1548000 | 1120 |
| | 1365000 | 980 | 1302000 | 1820 |
| 24h | 1300000 | 960 | 1199000 | 1140 |
| | 940800 | 860 | 980000 | 1420 |
| | 1212000 | 800 | 861600 | 2020 |
| 60h | 1570000 | 1320 | 1887000 | 1680 |
| | 1608000 | 1080 | 1992000 | 1700 |
| | 2006000 | 1740 | 2184000 | 1760 |
| 80h | 1750000 | 1660 | 2311000 | 2000 |
| | 1523000 | 1100 | 2258000 | 1400 |
| | *3397000* | 1740 | 2230000 | 2200 |
| 100h | 3151000 | 1140 | 2342000 | 1780 |
| | 3235000 | 1260 | 2231000 | 1920 |
| | 2587000 | 1220 | 2000000 | 1760 |
| 135h | — | 2880 | — | 2280 |
| | | 2120 | | 1680 |
| | | 1800 | | 2620 |

The italicised value is probably an erroneous readout.

**Supplementary Figure S5.1** Both AEP and CTSB cleave to inactivate ASNase

Residual ASNase activity estimated 3 hours after incubation with purified recombinant human AEP or CTSB (lower panel). ASNase activity was assessed using a proprietary chromogen substrate-cleavage assay kit (Medac Asparaginase Activity Test; schematic, upper panel) [70].

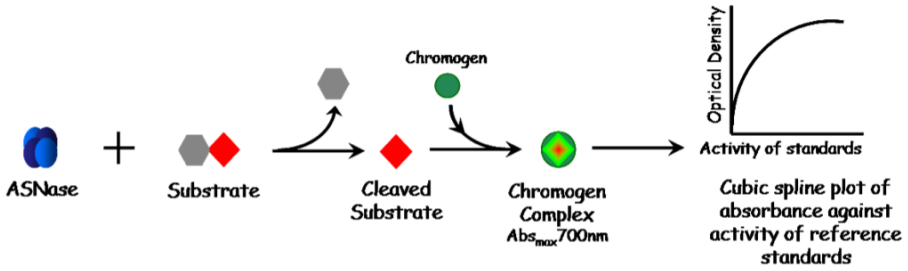


| Residual ASNase activity (%) after protease incubation | Assay 1 | Assay 2 | Assay 3 | Mean |
|---|---|---|---|---|
| AEP | 39 | 42 | 51 | 44 |
| CTSB | 23 | 25 | 30 | 26 |

**Supplementary Figure S5.2** In non AEP-expressing REH cells, a papain family cathepsin degrades ASNase

ASNase immunoblot of digests of ASNase (2μg) incubated (12-16 hours) with REH whole cell lysates pretreated with the AEP inhibitor MV026630 (AEPi), a protease inhibitor cocktail (PIC) or its individual components, leupeptin, pepstatin, AEBSF, bestatin and aprotinin. Lysate pretreatment with PIC or leupeptin alone prevented ASNase degradation.

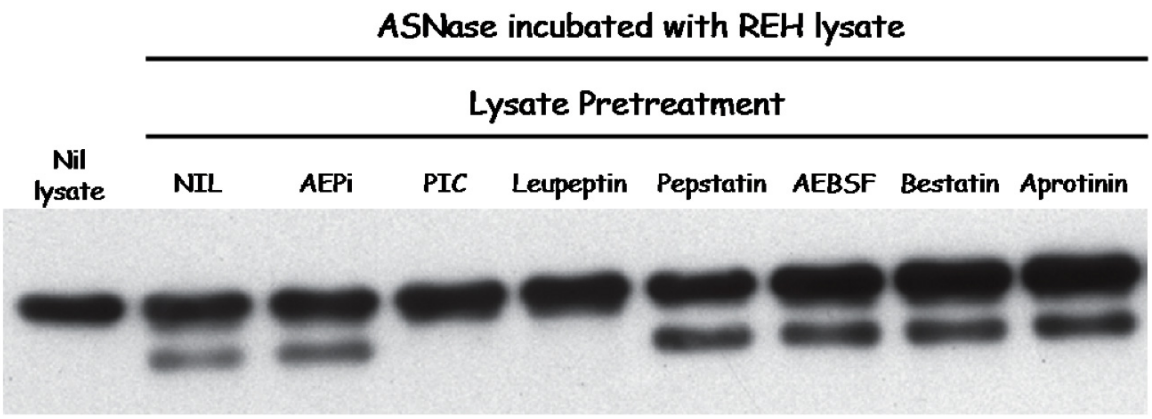

**Supplementary Figure S5.3** Singly or in combination, Cathepsin B and AEP alone in primary lymphoblasts cleave ASNase

ASNase immunoblots following 24-hour incubation of ASNase (2-4μg) with whole cell lysates of primary lymphoblasts (UPN1-12) in acid citrate digestion buffer. The profile of ASNase cleavage inhibition is directly determined by blast expression of CTSB and AEP (inset, summary table of AEP and CTSB immunoblot expression)

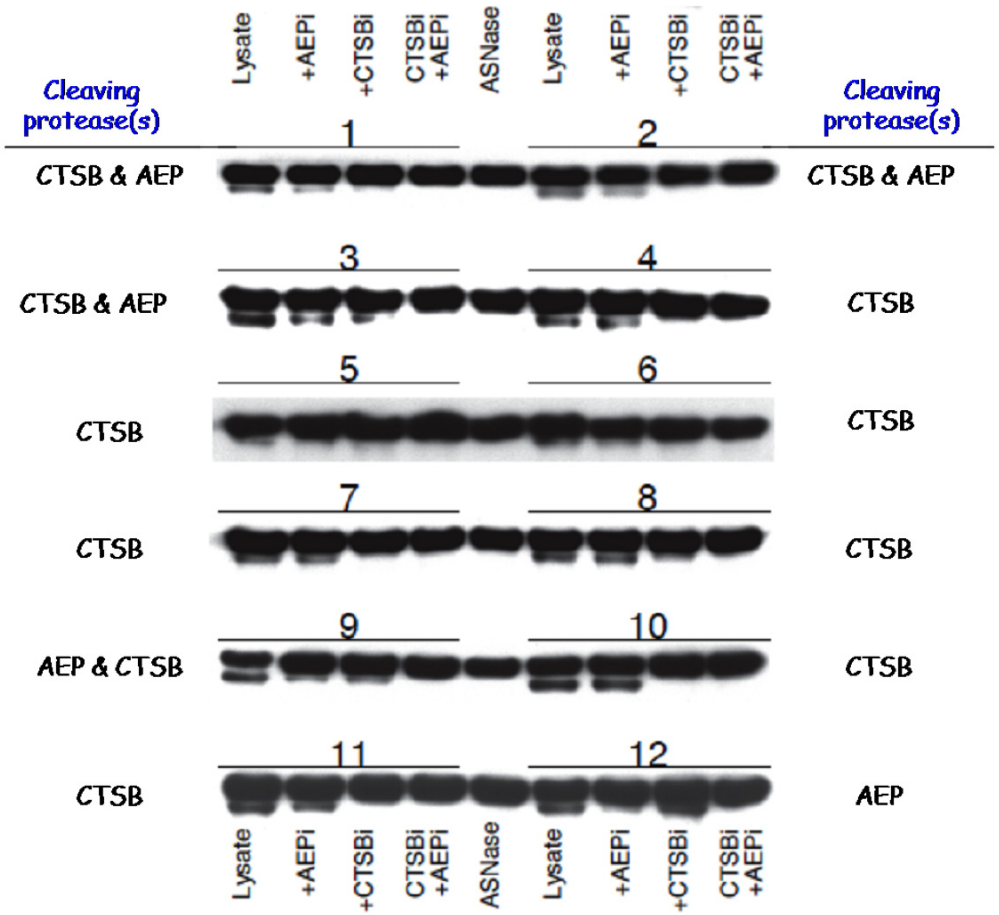


| UPN | AEP expression | CTSB expression |
|---|---|---|
| 1 | PreproAEP | Yes |
| 2 | Yes | Yes |
| 3 | Yes | Yes |
| 4 | — | Yes |
| 5 | — | Yes |
| 6 | — | Yes |
| 7 | — | Yes |
| 8 | — | Yes |
| 9 | Yes | Weak |
| 10 | — | Yes |
| 11 | — | Yes |
| 12 | Yes | — |

**Supplementary Table S6.1** Method outline for continuous coupled spectrophotometry estimation of glutaminase activity of native and variant ASNase recombinants (method adapted from various sources; reagents from Sigma-Aldrich)

| Reaction | Reaction components | Assay condition | Reaction product |
|---|---|---|---|
| **Reaction Step 1**<br>Test sample (0.5 mg/mL) + L-Glutamine (final, 20mM); no sample blank included | Sodium acetate pH 5.0 | 1 mL, microfuge format; 37°C, 60min | Hydrolysis of L-Glutamine to L-Glutamate (and ammonia) |
| **Reaction Step 2**<br>Aliquot from Reaction step 1 + L-Glutamate dehydrogenase (L-GDH) | Tris-EDTA pH 9.0; hydrazine hydrate to scavenge α-ketoglutarate and maintain unidirectionality of reaction; adenine diphosphate to stabilise L-GDH | 48-well format, 500μL volume; room temperature, 40 minutes. Baseline absorbance measured pre- L-GDH | Redox reaction to generate α-ketoglutarate and β-NAD |
| **Reaction standard**<br>Ten-point L-Glutamate standard 0-500μM | As above | As above | As above |
| **Readout**<br>β-NAD, absorbance at 340nm | | Minute-by-minute reading until plateau (20 minutes) | |
| **Optimisation steps**<br>L-Glutamine concentration | Final concentration range from 2 to 50mM | L-Glutamine 20mM optimal | |
| Volume from Reaction Step 1 to be used in Reaction Step 2 | 15 to 250μL volumes | To ensure absorbance within middle part of L-Glutamate standard curve | |
| *E. coli* L-Glutaminase enzyme as positive test control | Activity range from 20-200mU | Strength adjusted to linear part of standard curve, 100mU optimal | |
| **Estimation of glutaminase activity of test sample (U/mg)** | Calculated from the following variables: blank-corrected increase in absorbance (β-NAD generation), reaction volume in Step 1 (1mL); reaction volume from Step 1 used in Step 2; test sample quantity (0.5 mg); assay time (60 minutes) and molar absorption coefficient of β-NAD (6.22) | | |

# Appendix A–D

## Appendix A

Culture Characteristics of B-lineage leukaemic and lymphoblastoid cell lines

| Features | SD1 | SupB15 | REH | HRC57 |
|---|---|---|---|---|
| Type | B cell precursor ALL | B cell precursor ALL | B cell precursor ALL | Mature normal B lymphoblastoid |
| Genetic subtype | BCR-ABL1, p190 | BCR-ABL1, p190 | ETV6-RUNX1 | Normal |
| Origin | Woman with Ph+ ALL, peripheral blood at diagnosis | 9-year boy with Ph+ALL, bone marrow at second relapse | 15-year North African girl, *ETV6-RUNX*1 ALL, peripheral blood, first relapse | Not available |
| Karyotype | Near-tetraploid clone with two balanced Ph+ translocations | Pseudodiploid karyotype 46XY, t(9;22)(q34;q11), der(1)t(1;1)(p11;q31), add(3)(q2?7), der(4)t(1;4)(p11;q35), , add(10)(q25), ?del(14)(q23q31), der(16)t(9;16)(q11;p13) | 45-47X, -X, del (3)(p21p22), t(4:12;21;16)(q32;p13;q22;q24), inv(12)(p13q22), t(5;12)(q31;p1?2), +der(16)t(4;12;21;16), +21[cp10]; ETV6-RUNX1 fusion by FISH, 2 additional ETV6 signals | Diploid |
| Growth medium | RPMI 1640, 10% FBS | RPMI 1640, 10% FBS | RPMI 1640, 10% FBS | RPMI 1640, 10% FBS |
| Morphology in culture | Highly pleomorphic, loosely clumping ovoid cells associated with microvesicles in culture | Uniform single round cells, loosely adherent to base of culture flask | Uniform small single round cells, small loose clumps when overgrown | Pleomorphic loosely clumping ovoid cells |
| Doubling time | 28-32 hours | 60-72 hours | 60-72 hours | 24-48 hours |
| Seeding and passage cell density | $1 \cdot 10^6$ cells/mL | $1 \times 10^6$ cells/mL | $1 \times 10^6$ cells/mL at seeding, $2 \times 10^6$ /mL at passage | $1 \times 10^6$ cells/mL |
| EBV transformation | Yes | No | No | Yes |
| Cryopreservation | RPMI 1640, 10% DMSO, 20% FBS at 10-20×$10^6$ cells/cryovial | RPMI 1640, 10% DMSO, 20% FBS at 10-20×$10^6$ cells/cryovial | RPMI 1640, 10% DMSO, 20% FBS at 10-20×$10^6$ cells/cryovial | RPMI 1640, 10% DMSO, 20% FBS at 10-20×$10^6$ cells/cryovial |
| Mycoplasma | Negative (monthly tests) | Negative (monthly tests) | Negative (monthly tests) | Negative (monthly tests) |
| Source | CRUK Central Cell Services | DSMZ (German collection of cell cultures) | CRUK Central Cell Services | CRUK Central Cell Services |

## Appendix B

### AEP transcript nucleotide sequence NCBI accession RefSeq NM_005606.5

The 2040-nucleotide (nt) transcript corresponds to location 93170154-93215012 on the minus strand of the genomic AEP sequence (NC_000014.8) and is one of eleven (well annotated, 7) alternative transcripts, all of which encode the same protein. Alternating font colours demarcate exons (n=14). Underlined nucleotide sequences indicate forward (continuous line) and reverse (dashed line) sequencing primers. Boxed sequences enclose the coding segment (1302 nt). The grey-highlighted nucleotide sequence refers to the exon-spanning (exon boundaries 5 and 6) target sequence for the FRET-labelled AEP Taqman probe. Yellow highlights indicate nucleotides with known non-synonymous coding polymorphisms.

```
1     gcacagtggc ccttaagcga ggagcggcgg cgcccgcagc aatcacagca gtgccgacgt
61    cgtgggtgtt tggtgtgagg ctgcgagccg ccgcgagttc tcacggtccc gccggcgcca
121   ccaccgcggt cactcaccgc cgccgccgcc accactgcca ccacggtcgc ctgccacagg
181   tgtctgcaat tgaactccaa ggtgcagaat ggtttggaaa gtagctgtat tcctcagtgt
241   ggccctgggc attggtgccg ttcctataga tgatcctgaa gatggaggca agcactgggt
301   ggtgatcgtg gcaggttcaa atggctggta taattatagg caccaggcag acgcgtgcca
361   tgcctaccag atcattcacc gcaatgggat tcctgacgaa cagatcgttg tgatgatgta
421   cgatgacatt gcttactctg aagacaatcc cactccagga attgtgatca acaggcccaa
481   tggcacagat gtctatcagg gagtcccgaa ggactacact ggagaggatg ttaccccaca
541   aaatttcctt gctgtgttga gaggcgatgc agaagcagtg aagggcatag gatccggcaa
601   agtcctgaag agtggccccc aggatcacgt gttcatttac ttcactgacc atggatctac
661   tggaatactg gtttttccca atgaagatct tcatgtaaag gacctgaatg agaccatcca
721   ttacatgtac aaacacaaaa tgtaccgaaa gatggtgttc tacattgaag cctgtgagtc
781   tgggtccatg atgaaccacc tgccggataa catcaatgtt tatgcaacta ctgctgccaa
841   ccccagagag tcgtcctacg cctgttacta tgatgagaag aggtccacgt acctgggggа
901   ctggtacagc gtcaactgga tggaagattc ggacgtggaa gatctgacta aagagaccct
961   gcacaagcag taccacctgg taaaatcgca caccaacacc agccacgtca tgcagtatgg
1021  aaacaaaaca atctccacca tgaaagtgat gcagtttcag ggtatgaaac gcaaagccag
1081  ttctcccgtc cccctacctc cagtcacaca ccttgacctc acccccagcc ctgatgtgcc
1141  tctcaccatc atgaaaagga aactgatgaa caccaatgat ctggaggagt ccaggcagct
1201  cacggaggag atccagcggc atctggatgc caggcacctc attgagaagt cagtgcgtaa
1261  gatcgtctcc ttgctggcag cgtccgaggc tgaggtggag cagctcctgt ccgagagagc
1321  cccgctcacg gggcacagct gctacccaga ggccctgctg cacttccgga cccactgctt
1381  caactggcac tcccccacgt acgagtatgc gttgagacat ttgtacgtgc tggtcaacct
1441  ttgtgagaag ccgtatccgc ttcacaggat aaaattgtcc atggaccacg tgtgccttgg
1501  tcactactga agagctgcct cctggaagct tttccaagtg tgagcgcccc accgactgtg
1561  tgctgatcag agactggaga ggtggagtga gaagtctccg ctgctcgggc cctcctgggg
1621  agcccccgct ccagggctcg ctccaggacc ttcttcacaa gatgacttgc tcgctgttac
1681  ctgcttcccc agtcttttct gaaaaactac aaattagggt gggaaaagct ctgtattgag
1741  aagggtcata tttgctttct aggaggtttg ttgttttgcc tgttagtttt gaggagcagg
1801  aagctcatgg gggcttctgt agcccctctc aaaaggagtc tttattctga gaatttgaag
1861  ctgaaacctc tttaaatctt cagaatgatt ttattgaaga gggccgcaag ccccaaatgg
1921  aaaactgttt ttagaaaata tgatgatttt tgattgcttt tgtatttaat tctgcaggtg
1981  ttcaagtctt aaaaaataaa gatttataac agaacccaaa aaaaaaaaaa aaaaaaaaaa
```

## Appendix C

### AEP prepropeptide amino acid sequence (433 amino acids, UniProtKB/Swiss-Prot accession Q99538)

The highlighted sequences represent the sequentially cleaved N- and C-terminal segments in the maturing peptide. The 1-17 amino acid signal peptide sequence resides within the N-terminal cleaved segment. The H148 and C189 residues (underlined, in red boldface) define the His-Cys catalytic dyad within the His-Gly-spacer-Ala-Cys catalytic motif. Yellow highlights indicate polymorphic amino acid residues.

```
1    MVWKVAVFLS VALGIGAVPI DDPEDGGKHW VVIVAGSNGW YNYRHQADAC
51   HAYQIIHRNG IPDEQIVVMM YDDIAYSEDN PTPGIVINRP NGTDVYQGVP
101  KDYTGEDVTP QNFLAVLRGD AEAVKGIGSG KVLKSGPQDH VFIYFTDHGS
151  TGILVFPNED LHVKDLNETI HYMYKHKMYR KMVFYIEACE SGSMMNHLPD
201  NINVYATTAA NPRESSYACY YDEKRSTYLG DWYSVNWMED SDVEDLTKET
251  LHKQYHLVKS HTNTSHVMQY GNKTISTMKV MQFQGMKRKA SSPVPLPPVT
301  HLDLTPSPDV PLTIMKRKLM NTNDLEESRQ LTEEIQRHLD ARHLIEKSVR
351  KIVSLLAASE AEVEQLLSER APLTGHSCYP EALLHFRTHC FNWHSPTYEY
401  ALRHLYVLVN LCEKPYPLHR IKLSMDHVCL GHY
```

## Appendix D

**Primary ALL bone marrow cells: AEP transcript and protein expression and ASNase digestion profile**

| Patient | Relative AEP RNA expression* | Relative AEP enzyme activity** | Immunoblotting | | ASNase digestion inhibition | | |
|---|---|---|---|---|---|---|---|
| | | | AEP | CTSB heavy chain | AEP*i* only | CTSB*i* only | AEP*i* & CTSB*i* |
| UPN1 | 1.06 | 0.378 | Prepropeptide | Yes | — | — | Yes |
| UPN2 | 0.54 | 1.817 | Yes | Yes | — | — | Yes |
| UPN3 | 2.12 | 1.261 | Yes | Yes | — | — | Yes |
| UPN4 | 0.30 | 0.283 | No | Yes | — | Yes | — |
| UPN5 | 0.37 | 0.141 | No | Yes | — | Yes | — |
| UPN6 | 0.20 | 0.054 | No | Yes | — | Yes | — |
| UPN7 | 0.09 | 0.259 | No | Yes | — | Yes | — |
| UPN8 | 0.16 | 0.531 | No | Yes | — | Yes | — |
| UPN9 | 2.83 | 1.063 | Yes | Yes | — | — | Yes |
| UPN10 | 1.13 | 0.023 | No | Yes | — | Yes | — |
| UPN11 | 0.51 | 0.161 | No | Yes | — | Yes | — |
| UPN12 | 0.94 | 2.513 | Yes | No | Yes | — | — |

* β2M transcript expression as reference, HRC57 expression as calibrator ** Normalised to HRC57 AEP activity AEP*i*, whole cell lysates pre-treated with the AEP inhibitor MV026630; CTSB*i* whole cell lysates pre-treated with the CTSB inhibitor CA-074Me

## Publications in the course of this study

1. Patel N, Krishnan S, Offman MN, Krol M, Moss CX, Leighton C, van Delft FW, Holland M, Liu J, Alexander S, Dempsey C, Ariffin H, Essink M, Eden TO, Watts C, Bates PA, Saha V. A dyad of lymphoblastic lysosomal cysteine proteases degrades the antileukemic drug L-asparaginase. *J Clin Invest.* 2009;119:1964-1973.

2. Krishnan S, Wade R, Moorman AV, Mitchell C, Kinsey SE, Eden TO, Parker C, Vora A, Richards S, Saha V. Temporal changes in the incidence and pattern of central nervous system relapses in children with acute lymphoblastic leukaemia treated on four consecutive Medical Research Council trials, 1985-2001. *Leukemia.* 2010;24:450-459.